Faster-Than-Nyquist communication systems : from single-carrier to multi-carrier signaling

Titouan Petitpied

université de BORDEAUX

THALES

Thèse en vue de l'obtention du diplôme de Doctorat

École doctorale Sciences Physiques et de l'Ingénieur
Spécialités Automatique, Productique, Signal & Image, Ingenierie Cognitique
Préparée au Laboratoire de l'Intégration du Matériau au Système

TITOUAN PETITPIED

Faster-Than-Nyquist Communications: From Single-Carrier to Multi-Carrier Signaling

---

Soutenue le 18 juin 2021
Devant la commission d'examen formée de :

CHARLY POULLIAT	Professeur des Universités Toulouse INP, France	Président
CATHERINE DOUILLARD	Professeure des Universités IMT Atlantique, France	Rapportrice
GIULIO COLAVOLPE	Professeur des Universités Université de Parme, Italie	Rapporteur
DAMIEN ROQUE	Professeur des Universités ISAE-SUPAERO, France	Examinateur
GUILLAUME FERRÉ	Maître de Conférence HDR Bordeaux INP, France	Directeur de thèse
ROMAIN TAJAN	Maître de Conférence Bordeaux INP, France	Encadrant académique
SYLVAIN TRAVERSO	Docteur – Spécialiste THALES THALES, France	Encadrant industriel
PASCAL CHEVALIER	Professeur du CNAM – Expert THALES THALES, France	Encadrant industriel

Version du manuscrit pour une édition en ligne

—

Thèse réalisée avec le Laboratoire de l'**Intégration du Matériau au Système** (IMS) de Bordeaux, au sein de l'équipe **SPECTRAL** du groupe **Signal et Image**.

Université de Bordeaux, Laboratoire IMS
UMR 5218
351 Cours de la Libération
Bâtiment A31
F-33400 TALENCE Cedex

—

Thèse réalisée en contrat CIFRE avec **Thales**,
au sein du service WaveForm Design (WFD) du département Hardware Technologies, Tools & Engineering (HTE)

Thales SIX GTS FRANCE SAS
4 Avenue des Louvresses
92230 Gennevilliers

À ma fiancée.

Remerciements

Je tiens à remercier mes directeur et encadrant de thèse Guillaume Ferré et Romain Tajan de l'Université de Bordeaux pour leur accompagnement bienveillant, collaboration, partage et suivi au cours de ce travail, et plus généralement le long de mes années d'étude.

Je remercie vivement Pascal Chevalier et Sylvain Traverso qui m'ont accueilli, entouré, guidé et ont su me transmettre de précieuses connaissances au sein de Thales.

Je tiens aussi à exprimer ma reconnaissance au laboratoire IMS et à l'école doctorale SPI de l'Université de Bordeaux qui m'a aceuilli pour cette thèse.

J'exprime également toute ma gratitude au service *WaveForm Design* de Thales dirigé par Jean-Luc Perron qui m'a permis d'effectuer cette thèse, et m'a offert un environnement de travail irréprochable.

Par ailleurs, je témoigne toute ma reconnaissance à mon employeur actuel Semtech, et plus particulièrement à Frantz Prianon qui m'a permis de finaliser ce travail dans de bonnes conditions.

Je souhaite par ailleurs remercier Baptiste Laporte-Fauret avec qui j'ai pu partager des expériences, anecdotes et moments forts durant ce travail.

Enfin, je suis reconnaissant envers ma famille pour son soutien, et plus spécialement envers ma fiancée Andréa pour sa patience et son dévouement.

Résumé de la Thèse

Titre : Communications Faster-Than-Nyquist : Des liaisons mono-porteuse Aux liaisons multi-porteuses

Mot-clés : Faster-Than-Nyquist (FTN), FTN Multi-Porteuses, FTN Circulairement convolué, FTN Linéairement Convolué, Peak-to-Average Power Ratio (PAPR), Instantaneous-to-Average Power Ratio (IAPR), Factorisation Graphique (FG), Interférence Entre Symboles (IES), Interférence Entre Porteuses (IEP), Égalisation, Turbo-égalisation, Expectation Propagation (EP), Bahl-Cocke-Jelinek-Raviv (BCJR), Minimum Mean Square Error (MMSE), Linéaire au Sens Large (LSL).

Résumé : Les liaisons FTN ont été formellement proposées pour la première fois en 1975 pour augmenter l'efficacité spectrale des communications. En effet, J. Mazo a mis en exergue une sous-utilisation des ressources temps/fréquence lorsque l'on emploie une communication Nyquist sur un canal à Bruit Additif Blanc Gaussien (BABG), sous réserve de disposer d'un récepteur optimal en réception, particulièrement complexe. Il a alors été prouvé qu'un gain en débit de 25 % est possible en augmentant le débit symbole, sans dégradation du Taux d'Erreurs Binaire (TEB). Le facteur de compression $\tau = 0.802$ associé a cette augmentation des débits est communément appelé *borne de Mazo*. Cependant, la contrainte de complexité calculatoire étant trop forte, la technique a été mise de côté jusqu'au début des années 2000, après la découverte des procédés de turbo-égalisation ainsi qu'une capacité calculatoire plus importante dont disposent les appareils communicants. C'est dans ce mouvement de regain d'intérêt pour les communications FTN que s'inscrit cette thèse de doctorat.

Afin d'évaluer l'intérêt pratique des communications FTN, nous avons souhaité intégrer des contraintes multiples provenant de différents éléments d'une chaîne de communication. Au-delà de l'augmentation de l'efficacité spectrale proposée par le FTN, nous nous sommes intéressés à l'efficacité énergétique et la complexité calculatoire en réception pour rendre possible un traitement temps-réel. La contrainte énergétique a été comprise au travers d'une approche multi-critères qui s'intéresse à l'amplificateur de puissance de l'émetteur, car il s'agit du principal élément responsable de la consommation énergétique. L'intérêt de la technique du FTN pour augmenter l'efficacité spectrale est justifié au travers d'une analyse de capacité. En effet, on peut démontrer que l'efficacité spectrale atteignable par des schémas FTN est plus élevée que pour les schémas Nyquist dès lors que le facteur de retombée du filtre est non nul. Nous proposons ensuite une nouvelle métrique de comparaison des communications. Cette métrique a pour objectif

de pénaliser les formes d'onde à fort PAPR car elles nécessitent un recul important par rapport à la puissance de saturation de l'amplificateur de puissance. Or, c'est justement cette puissance de saturation qui détermine l'énergie effectivement consommée. Cette pénalisation permet donc d'évaluer l'intérêt du FTN plus efficacement. Les comparaisons effectuées démontrent que le FTN à une tendance à réduire le PAPR des communications pour une efficacité spectrale cible. Cette métrique a ainsi été utilisée tout au long de la thèse pour évaluer l'intérêt du FTN d'un point de vue multi-critères.

Suite aux premières études sur le FTN, des auteurs ont étendu les résultats à d'autres filtres de Nyquist et des constellations plus riches, et avec du codage canal. Pour cela, des récepteurs optimaux ont été envisagés sur canal à BABG et montrent une nouvelle fois, dans un contexte plus large, une sous-utilisation des ressources au prix d'un traitement complexe en réception. En effet, pour récupérer l'information des symboles en présence d'IES, les traitements mettent en jeu un algorithme de Viterbi ou BCJR pour optimiser le critère du Maximum de Vraisemblance (MV) ou Maximum A Posteriori (MAP). Suite à cela, des solutions à complexité réduite ont été étudiées.

Afin de proposer des traitements utilisables en temps-réel, il a été envisagé d'utiliser des approximations de l'algorithme BCJR (RS-BCJR, M*-BCJR). Néanmoins, leur complexité reste exponentielle avec l'ordre de la constellation, et ne permet donc pas d'atteindre les efficacités spectrales souhaitées. Des approches par filtrage comme le MMSE ont donc été envisagées, que ce soit par traitement temporel ou fréquentiel (FD-MMSE). Ces solutions ont l'intérêt de nécessiter une faible complexité, indépendante de la constellation. Cette méconnaissance de la distribution des symboles entraîne cependant une perte d'information qui ne permet pas au récepteur de rivaliser avec les approches MV ou MAP en terme de TEB. Ainsi, pour des efficacité spectrales élevées, il n'existait pas de solution de traitement de l'IES générée par le FTN, qui soit à la fois efficace et à faible complexité.

Une des contributions principales de cette thèse porte donc sur la conception et le développement de récepteurs permettant de combler ces lacunes. Pour cela, nous avons étudié le concept d'EP et adoptons une approche visuelle fondée sur la FG afin de présenter de façon didactique ce formalisme. L'algorithme régissant le récepteur est alors obtenu en calculant les messages échangés au travers du graphe, et dépend de plusieurs hypothèses initiales pour leur calcul. En effet, il convient tout d'abord de choisir une famille de distribution contraignant les messages, ainsi qu'un ordonnancement de ces messages. Ces choix conduisent à différents algorithmes, certains ayant déjà été proposés pour l'égalisation d'un canal sélectif en fréquence. Nous avons par la suite introduit de nouvelles familles de distributions donnant lieu à des récepteurs LSL. Par ailleurs, nous avons combiné un modèle d'émission CCFTN avec une famille particulière de distributions gaussiennes pour laquelle toute la matrice de covariance de la distribution des symboles est contrainte à être proportionnelle à la matrice identité. Ces deux hypothèses donnent lieu à un traitement pouvant être effectué dans le domaine fréquentiel sans préfixe cyclique, de façon efficace et offrant des performances très compétitives. Les différents récepteurs développés pour le FTN se trouvent être complémentaires, atteignant de hautes efficacités spectrales et nécessitant des complexités différentes. Par ailleurs, quelque soit le récepteur EP utilisé, les communications FTN peuvent alors proposer des gains en rapport signal à bruit très

significatifs par rapport aux communications Nyquist. Ce gain vient notamment d'un schéma itératif entre un égaliseur MMSE, et un bloc que nous appelons *Constellation Matcher* en charge de réaligner l'estimée d'un symbole en sortie de filtrage avec la constellation. Cette prise en compte de la constellation fait que les récepteurs EP sont à mi-chemin entre les approches MAP et MMSE. Ils combinent alors la faible complexité du filtrage, et l'importante capacité de traitement de l'IES des récepteurs MAP. De plus, ces gains sont d'autant plus importants que l'efficacité spectrale visée est élevée (jusqu'à 5 bits/s/Hz).

À la suite de cela, il a été envisagé de complexifier le modèle du canal en considérant une communication avec des trajets multiples. Pour cela, la technique du FTN a été étendue au contexte multi-porteuses, faisant apparaître une compression fréquentielle générant de l'IEP en plus de l'IES. Cette compression temps/fréquence permet théoriquement un doublement de l'efficacité spectrale par rapport aux communications orthogonales pour des faibles constellations (BPSK, QPSK). Le modèle couramment utilisé pour le MFTN dans la littérature est donc présenté, ainsi que les récepteurs existants. Afin de limiter la complexité en réception, il est couramment envisagé de traiter de façon disjointe l'IES et l'IEP. Les premières études ont alors mis en place un algorithme de BCJR pour traiter l'IES, après avoir utilisé une suppression successive de l'interférence pour traiter l'IEP. Dans un souci de limiter la complexité, il a ensuite été envisagé d'égaliser l'IES à l'aide de traitements MMSE par filtrage en temps, puis en fréquence. Cependant, l'inconvénient de l'égalisation fréquentielle tient du fait qu'elle nécessite l'introduction du préfixe cyclique pour circulariser la convolution au récepteur. Nous avons donc proposé un nouveau modèle de mise en forme du signal MFTN, fondé sur une double circularité à l'émission. Ceci permet notamment de s'affranchir du préfixe cyclique, et offre également l'avantage d'être mis en œvre en fréquence à l'émission pour diminuer la complexité. Au récepteur, le signal est ensuite traité en fréquence au travers du récepteur EP, similaire à celui proposé pour les communications mono-porteuse. Le schéma résultant offre des performances supérieures aux récepteurs à faible complexité existants. Avec le codage canal utilisé, on retrouve alors la possibilité de doubler l'efficacité spectrale avec une constellation QPSK. Pour les constellations plus riches (jusqu'à la 256-QAM), le récepteur proposé permet également une augmentation significative de la compression temps/fréquence sans dégradation du TEB. Ainsi, le schéma proposé offre des gains importants par rapport aux communications orthogonales multi-porteuses.

Enfin, les schéma mono et multi-porteuses développés sont comparés aux schémas orthogonaux en présence de canal sélectif en fréquence. Pour cela, nous utilisons un canal Proakis B, particulièrement sélectif. Nous montrons alors que le schéma MFTN est plus performant qu'un schéma multi-porteuses orthogonal. De même, le schéma FTN mono-porteuse se trouve être plus performant que le schéma Nyquist. Il apparaît finalement que le MFTN n'est pas aussi efficace du point de vue multi-critères que la communication mono-porteuse FTN. Cependant, l'écart tend à diminuer avec l'augmentation de l'efficacité spectrale. Par ailleurs, ces résultats sont obtenus sous des hypothèses bien précises de modèle de canal, de codage et de filtre utilisés. Il serait alors intéressant de poursuivre l'étude en généralisant les conclusions à des modèles plus réalistes, en intégrant des contraintes opérationnelles telles que la synchronisation temps/fréquence, et en combinant les récepteurs proposés avec des filtres optimisés.

Abstract of the Thesis

Title: Faster-Than-Nyquist Communications: From Single-Carrier to Multi-Carrier Signaling

Keywords: Faster-Than-Nyquist (FTN), Multi-Carrier Faster-Than-Nyquist (MFTN), Circularly Convolved FTN (CCFTN), Linearly Convolved FTN (LCFTN), Peak-to-Average Power Ratio (PAPR), Instantaneous-to-Average Power Ratio (IAPR), Factor Graph (FG), Inter-Symbol Interference (ISI), Inter-Carrier Interference (ICI), Equalization, Turbo-equalization, Expectation Propagation (EP), Bahl-Cocke-Jelinek-Raviv (BCJR), Minimum Mean Square Error (MMSE), Widely Linear (WL).

Abstract: This thesis is a multi-criteria study of the Faster-Than-Nyquist (FTN) technique. We first consider the context of single-carrier communications without propagation channel. We assume two types of FTN signal shaping: the linear FTN classically studied, and the circular FTN which has the advantage of simplifying the filtering process that can be performed in the frequency domain. Under these assumptions, we define different criteria of interest: spectral efficiency, energy efficiency through the Peak-to-Average Power Ratio (PAPR), computational complexity of the reception algorithms. Then we show that the potential of FTN is higher than the one of Nyquist communications because it allows the PAPR to be optimized. However, FTN signaling is not currently used because of the computational complexity required by the reception algorithms for Inter-Symbol Interference (ISI) processing. Indeed, Minimum Mean-Square-Error (MMSE) filtering approaches offer substantial gains at low spectral efficiency, but there is a need to switch to Maximum A Posteriori (MAP) detectors, which are more efficient in terms of error rate when the ISI is too powerful. However, these MAP approaches require computational complexity that is prohibitively high for rich constellations. Thus, we are interested in passing message algorithms to reduce the computational cost of interference processing. To do so, we propose to use Expectation Propagation (EP) which aims at filtering the ISI just like MMSE algorithms, while constraining the constellation of symbols. This constraint is imposed by a processing block called "Constellation Matcher" which is responsible for realigning the MMSE estimate of the symbols with the known constellation. Hence, an iterative symbol processing appears between a filter and this Constellation Matcher block. In order to extend the capabilities of the EP to FTN signals, we propose different distributions families in which EP messages are exchanged. We study three families that give rise to the time-domain EP processing for the most classical family, the frequency-domain EP processing subject to the use of the circular shaping of the FTN, and the Widely Linear (WL) approach which processes separately the I and Q parts of the

received signal. These different EP receivers for FTN are then used in the multi-criteria study and we show SNR gains up to 8 dB compared to Nyquist communications, while limiting the computational complexity. The different types of EP receivers then allow a trade-off between computational complexity and error rate. The last application framework of this study is the multi-carrier context of the FTN signaling. Given the benefits of EP approaches for the multi-criteria study, we adapt these algorithms to the multi-carrier case and show significant gains compared to the literature, but also compared to Nyquist communications.

Table of Contents

List of Figures

List of Tables

Abbreviations

AMP	Approximate Message Passing
AWGN	Additive White Gaussian Noise
BCJR	Bahl Cocke Jelinek Raviv
BER	Binary Error Rate
BPSK	Binary PSK
CCDF	Complementary Cumulative Distribution Function
CCFTN	Circularly Convolved FTN
CPM	Continuous Phase Modulation
DFE	Decision Feedback Equalization
DFT	Discrete FT
EP	Expectation Propagation
ESNR	Effective SNR
FD	Frequency-Domain
FER	Frame Error Rate
FFT	Fast FT
FG	Factor Graph
FIR	Finite Impulse Response
FN	Factor Node
FT	Fourier Transform
FTN	Faster-Than-Nyquist
IAPR	Instantaneous-to-average Power Ratio
IC	Interference Cancellation
ICI	Inter-Carrier Interference
iid	independant and identically distributed
IOTA	Isotropic Orthogonal Transform Algorithm

ISI	Inter-Symbol Interference
LCFTN	Linearly Convolved FTN
LLR	Log Likelihood Ratio
MAP	Maximum A Posteriori
MFB	Matched-Filter Bound
MFTN	Multi-Carrier FTN
ML	Maximum Likelihood
MMSE	Minimum MSE
MSE	Mean-Square Error
OFDM	Orthogonal Frequency-Division Multiplexing
OTFS	Orthogonal Time Frequency and Space
PAM	Pulse-Amplitude Modulation
PAPR	Peak-to-Average Power Ratio
pmf	probability mass function
PSD	Power Spectral Density
QAM	Quadrature Amplitude Modulation
QPSK	Quadrature PSK
RC	Raised-Cosine
rRC	root-RC
RS-BCJR	Reduce State BCJR
RSC	Recursive Systematic Code
SER	Symbol Error Rate
SLC	Shamai Laroia Conjecture
SNR	Signal-to-Noise Ratio
SO	Second Order
VN	Variable Node
WL	Widely-Linear
WMF	Whitening Matched Filter

Definitions

Column vectors are represented using lowercase bold letters while matrices are written with uppercase bold characters. For any vector $\mathbf{a}$ with length N_a, the scalar a_i, $i \in [1, N_a]$ corresponds to its ith element and $\mathbf{a}_{i:j}$ denotes the subset of $\mathbf{a}$ from a_i to a_j ($i \leq j$). Similarly, the element of a matrix $\mathbf{A}$ at position (i, j) is referred by $(\mathbf{A})_{i,j}$. Moreover, $\mathbf{A}^T$ denotes the transpose matrix of $\mathbf{A}$ and $\mathbf{A}^\dagger$ its transpose conjugate. $\mathbf{e}_n \triangleq [0 \ldots 0\ 1\ 0 \ldots 0]^T$ refers to the vector having 1 at position n.

For a multivariate distribution, $p(\mathbf{a})$ represents the joint distribution while $p(a_i)$ stands for the ith marginal distribution. Note that $p(a_i)$ can be a probability density function (pdf) if a_i lies in a continuous set $\mathcal{A}$ or a probability mass function (pmf) if $\mathcal{A}$ is a discrete set. The expectation operator is defined as $\mathbb{E}_p[a_i] \triangleq \sum_{a_i \in \mathcal{A}} a_i \cdot p(a_i)$ if $p(a_i)$ is a pmf or $\mathbb{E}_p[a_i] \triangleq \int a_i \cdot p(a_i)\, \mathrm{d}a_i$ if $p(a_i)$ is a pdf. Similarly, the variance operator is defined as $\mathbb{V}_p[a_i] \triangleq \sum_{a \in \mathcal{A}} |a_i|^2 \cdot p(a_i) - |\mathbb{E}_p[a_i]|^2$ or $\mathbb{V}_p[a_i] \triangleq \int |a_i|^2 \cdot p(a_i)\, \mathrm{d}a_i - |\mathbb{E}_p[a_i]|^2$. The operator $\propto$ stands for a proportionality link between two quantities. Furthermore, if p is the distribution of the random variable a_i, and q is an integrable positive function, we write $p(a_i) \propto q(a_i)$ which should be understood as: $p(a_i) = \lambda_q^{-1} q(a_i)$ where $\lambda_q = \int q(a_i)\, \mathrm{d}a_i$ if $\mathcal{A}$ is a continuous set or $\lambda_q = \sum_{a_i \in \mathcal{A}} q(a_i)$ if $\mathcal{A}$ is a discrete set.

The set of the Second Order (SO) circular multivariate complex Gaussian distributions is denoted by $\mathcal{N}_\mathrm{C}$. An element of $\mathcal{N}_\mathrm{C}$ is a complex multivariate distribution denoted by $\mathcal{N}_\mathrm{C}(\mathbf{s} : \boldsymbol{\mu}, \mathbf{V}) \propto \exp(-(\mathbf{s} - \boldsymbol{\mu})^\dagger \mathbf{V}^{-1} (\mathbf{s} - \boldsymbol{\mu}))$ with mean $\boldsymbol{\mu} = \mathbb{E}[\mathbf{s}]$ and covariance matrix $\mathbf{V} = \mathbb{V}[\mathbf{s}]$. Moreover, we extend the family $\mathcal{N}_\mathrm{C}$ to form $\mathcal{N}_\mathrm{NC}$ the subset of the SO non-circular multivariate complex Gaussian distributions with independent real (I) and imaginary (Q) parts. We denote an element of $\mathcal{N}_\mathrm{NC}$: $\mathcal{N}_\mathrm{NC}(\mathbf{s} : \boldsymbol{\mu}, \mathbf{V}_I, \mathbf{V}_Q) = \mathcal{N}_\mathrm{R}(\mathbf{s}_I : \boldsymbol{\mu}_I, \mathbf{V}_I) \mathcal{N}_\mathrm{R}(\mathbf{s}_Q : \boldsymbol{\mu}_Q, \mathbf{V}_Q)$ with the random vectors $\mathbf{s} = \mathbf{s}_I + j\mathbf{s}_Q$ and $\boldsymbol{\mu} = \boldsymbol{\mu}_I + j\boldsymbol{\mu}_Q$, $\mathbf{s}_I, \mathbf{s}_Q, \boldsymbol{\mu}_I, \boldsymbol{\mu}_Q \in \mathbb{R}^N$ of N elements, $\mathbf{V}_I$ represents the covariance matrix of $\mathbf{s}_I$, $\mathbf{V}_Q$ the covariance matrix of $\mathbf{s}_Q$. The function $\mathcal{N}_\mathrm{R}(\mathbf{s}_I : \boldsymbol{\mu}_I, \mathbf{V}_I) \propto \exp(-\frac{1}{2}(\mathbf{s}_I - \boldsymbol{\mu}_I)^\dagger \mathbf{V}_I^{-1} (\mathbf{s}_I - \boldsymbol{\mu}_I))$ characterizes a Gaussian distribution of a real random variable and similarly for $\mathcal{N}_\mathrm{R}(\mathbf{s}_Q : \boldsymbol{\mu}_Q, \mathbf{V}_Q)$. For the sake of simplicity, we assimilate in the following the circularity of a random variable to the SO circularity.

Notations

Variables

- N_b: number of information bits
- N_c: number of channel coded bits
- N_s: number of transmitted symbols
- N_v: number of channel paths
- N_w: window semi-length
- R: channel code-rate
- T: orthogonality time of $h(t)$
- β: excess bandwidth factor of $h(t)$
- W: bandwidth of $h(t)$
- τ: FTN time compression factor
- ν: frequency compression parameter
- F: frequency space between two adjacent sub-carriers
- Ω: frequency overlap between the sub-carriers
- T_s: symbol time
- L: truncation parameter of $h(t)$ yielding $h(t) = 0$ for $t \notin [-LT, LT]$
- L_τ: truncation parameter of $h(t)$ yielding $h(t) = 0$ for $t \notin [-L_\tau T_s, L_\tau T_s]$
- $N_{\bar{x}}$: length of $\bar{\mathbf{x}}$
- $N_{\dot{x}}$: length of $\dot{\mathbf{x}}$
- N_x: length of $\mathbf{x}$
- N_0: PSD of $w(t)$
- N_r: length of $\mathbf{r}$

- C: Shannon capacity
- η: achievable spectral efficiency
- ρ: spectral efficiency
- IAPR(θ): backoff ensuring a saturation probability θ for $x(t)$
- P_{sat}: saturation power of the PA
- P_x: average power of $x(t)$
- E_b: useful bits average energy
- $\mathcal{I}$: number of EP iterations
- T_e: sampling-time

Time-continuous Signals

- $h(t)$: shaping filter
- $H(f)$: FT of $h(t)$
- $\bar{x}(t)$: LCFTN transmitted signal
- $\dot{h}(t)$: periodized shaping filter with period $N_s T_s$
- $\dot{H}(f)$: FT of $\dot{h}(t)$
- $\gamma(t)$: unitary low-pass filter
- $\Gamma(f)$: FT of $\gamma(t)$
- $\dot{x}(t)$: CCFTN transmitted signal
- $v(t)$: propagation channel filter
- $V(f)$: FT of $v(t)$
- $w(t)$: AWGN noise
- $W(f)$: FT of $w(t)$
- $h'(t)$: matched filter
- $g(t)$: global filter
- $G(f)$: FT of $g(t)$
- $r(t)$: received signal

- $p(t)$: pulse shape of the MFTN model
- $p_l(t)$: pulse shape of the MFTN model lth sub-carrier
- $P(f)$: FT of $p(t)$
- $P_l(f)$: FT of $p_l(t)$
- $\Gamma(f)$: FT of $\gamma(t)$
- $\dot{p}(t)$: periodized pulse shape of the MFTN model
- $\dot{p}_l(t)$: periodized pulse shape of the MFTN model lth sub-carrier
- $\dot{x}(t)$: transmit signal of the circular MFTN model
- $\ddot{x}(t)$: transmit signal of the doubly-circular MFTN model
- $\ddot{r}(t)$: received signal of the doubly-circular MFTN model

Vectors

- $\mathbf{b}$: information bit sequence
- $\mathbf{c}$: channel coded bit sequence
- $\mathbf{d}$: interleaved channel coded bit sequence
- $\mathbf{s}$: transmitted symbol sequence
- $\mathbf{s}_l$: lth sub-carrier of $\mathbf{s}$
- $\vec{\mathbf{s}}$: rotated signal $\mathbf{s}$
- $\vec{\mathbf{s}}_l$: lth sub-carrier of $\vec{\mathbf{s}}$
- $\bar{\mathbf{x}}$: LCFTN transmitted signal
- $\dot{\mathbf{x}}$: CCFTN transmitted signal
- $\hat{\mathbf{s}}$: FT of $\mathbf{s}$
- $\mathbf{w}$: filtered and sampled AWGN noise
- $\mathbf{r}$: filtered and sampled received signal
- $\mathbf{y}$: received signal after matched filter and down-sampling
- $\vec{\mathbf{y}}$: rotated signal $\mathbf{y}$
- $\vec{\mathbf{y}}_l$: lth sub-carrier of $\vec{\mathbf{y}}$

- $\mathbf{w}'$: matched filtered noise
- $\vec{\mathbf{w}}'$: rotated matched filtered noise
- $\vec{\mathbf{z}}_l$: rotated signal $\vec{\mathbf{y}}$ after IC for ICI
- $\vec{\mathbf{w}}$: rotated filtered and sampled noise
- $\ddot{\mathbf{x}}$: transmit signal of the doubly-circular MFTN model
- $\ddot{\mathbf{r}}$: filtered and sampled received signal of the doubly-circular MFTN model
- $\mathbf{d}_n$: sub-vector of $\mathbf{d}$ which bits correspond to the nth symbol s_n
- $\hat{\mathbf{y}}$: DFT of $\mathbf{y}$
- $\hat{\mathbf{s}}$: DFT of $\mathbf{s}$
- $\hat{\ddot{\mathbf{x}}}$: DFT of $\ddot{\mathbf{x}}$
- L^a: prior LLRs of the symbol-stage process
- L^e: extrinsic LLRs of the symbol-stage process

Matrices

- Π: permutation matrix of the interleaver
- $\mathbf{U}$: up-sampling matrix with a factor 2
- $\mathbf{H}$: convolution matrix of $h(t)$
- $\dot{\mathbf{H}}$: circulant matrix associated to $\dot{h}(t)$
- $\mathbf{F}_N$: normalized DFT matrix of size $(N \times N)$
- $\hat{\dot{\mathbf{H}}}$: DFT of $\mathbf{H}$
- $\mathbf{V}$: convolution matrix of $v(t)$
- $\mathbf{D}$: down-sampling matrix
- $\mathbf{G}$: convolution matrix of the aliased Nyquist filter $g(t)$
- $\mathbf{G}_{l',l}$: sub-matrix of $\mathbf{G}$ representing the interference of the transmit sub-carrier l to the received sub-carrier l'
- $\mathbf{W}$: window matrix
- $\mathbf{V}$: channel filter convolution matrix
- $\mathbf{P}$: MFTN pulse shape convolution matrix

- $\mathbf{R}$: matrix for the symbols rotation
- $\mathbf{\Sigma}$: MMSE inverse matrix
- $\ddot{\mathbf{P}}$: doubly-circular convolution matrix associated to $p(t)$
- $\ddot{\mathbf{P}}_l$: doubly-circular convolution matrix associated to $p_l(t)$
- $\ddot{\mathbf{G}}$: doubly-circular convolution matrix associated to the global filter $g(t)$
- $\ddot{\mathbf{G}}_{l',l}$: sub-matrix of $\ddot{\mathbf{G}}$ representing the interference of the transmit sub-carrier l to the received sub-carrier l'
- $\hat{\mathbf{\Sigma}}$: DFT of $\mathbf{\Sigma}$
- $\hat{\mathbf{G}}$: DFT of $\ddot{\mathbf{G}}$
- $\hat{\ddot{\mathbf{P}}}$: DFT of $\ddot{\mathbf{P}}$

Functions & Operators

- $\mathcal{C}$: channel code
- $\mathcal{M}$: digital modulation (same notation as the symbols' constellation)
- $\mathcal{F}(\cdot)$: time-continuous Fourier Transform
- $\star$: convolution product
- $\delta(t)$: Dirac delta function
- $\delta(t)$: Kronecker delta function

Sets

- $\mathbb{F}_2 = \{0, 1\}$: binary set
- $\mathcal{M}$: symbols' constellation (same notation as the digital modulation)
- $\mathcal{N}_{\mathrm{C}}$: set of Gaussian distributions of circular complex random variables
- $\mathcal{N}_{\mathrm{NC}}$: set of Gaussian distributions of SO non-circular complex random variables without I/Q cross-correlations
- $\mathcal{N}_{\mathrm{R}}$: set of Gaussian distributions of real-valued random variables

Introduction

The development of digital communications is in constant progress, pushed by the user needs and the plurality of their applications. From the first analogical telegraph system to the actual standards embodied by the 5th generation of mobile communications, decades of scientific researches gave rise to optimized waveforms for a constrained environment. The time and frequency domains are more and more exploited requiring the next solutions to propose higher spectral efficiencies. Moreover, the communicating devices require a real-time and low complexity processing at receiver with high decoding performance. Finally, the mobility offered by mobile communications comes with high constraints on the power efficiency. In order to optimize the energy consumption, waveforms characterized by low Peak-to-Average Power Ratio (PAPR) are favored.

The multi-factorial context yielded H. Nyquist to propose a century ago a type of signaling which symbol-rate is bounded by the bandwidth occupancy [Nyq24]. For non-frequency selective channels, this allows an easy processing at receiver and is referred as Nyquist signaling. Hence, some decades ago in 1973, J. Salz proposed to overcome such a limitation [Sal73]. This new concept suffers from deterministic and invariant Inter-Symbol Interference (ISI) at receiver because the symbol-rate is higher than the Nyquist rate. Nevertheless, J. Mazo proved in 1975 [Maz75] that the induced ISI does not affect the Bit Error Rate (BER) up to a compression rate of 25 % if it is processed by a Maximum Likelihood (ML) receiver when using a Binary PSK (BPSK) modulation and cardinal sine shaping filter. This counter-intuitive and promising result is now referred as the Mazo bound. Furthermore, this technique taking benefit of the compression factor as a supplementary freedom degree is named Faster-Than-Nyquist (FTN) signaling.

More recently, Rusek and Anderson [RA09a], as well as Colavolpe [Col11] showed that for a given performance level, FTN communications achieve higher information rates than Nyquist ones. Some papers also extended the first results of Mazo to higher constellation orders, other shaping filters and turbo-equalization schemes [PAR08; AR07; LG03] since their introduction in 1995 [Dou+95b]. The ML receiver minimizing the Frame Error Rate (FER) with the Viterbi algorithm [Vit67a; For73] has been replaced by the Soft Output Viterbi Algorithm [HH89], or even by the Bahl Cocke Jelinek Raviv (BCJR) algorithm [Bah+74] which optimizes the symbol-wise Maximum A Posteriori (MAP) criterion and minimizes the Symbol Error Rate (SER) when considering channel coding. However, the spectral efficiency increase comes with an exponential complexity growth of such types of receivers.

Various reception strategies for reducing the state space of the BCJR algorithm have been proposed: Reduce State BCJR (RS-BCJR), M-BCJR or M*-BCJR [CFR01; RLP07; Fra+02; FA97; FM76], where M is related to the number of considered states.

However, these approximations come with Signal-to-Noise Ratio (SNR) loss especially for high modulation orders. Alternatively, linear Minimum MSE (MMSE) receivers with Interference Cancellation (IC) have been studied, in time domain [JY04; Yu+14] to tackle the equalization problem while considering prior information. Frequency-Domain (FD) equalization operating with a lower-complexity has also been studied in [Sug13] and [TPB16] which developed a Circularly Convolved FTN (CCFTN) for avoiding any cyclic prefix by performing a circular shaping filtering at the transmitter. While being less complex than MAP based receivers, MMSE based receivers also offer poor performance when increasing the spectral efficiency due to their lack of knowledge about the constellation.

In order to combine the benefits of both the MAP and MMSE receivers, more recent studies propose iterative algorithms based on the concept of turbo-equalization. Instead of solving the joint problem of symbol processing and bit decoding, the groundbreaking paper [Dou+95b] separates this process in two sub-processes exchanging information iteratively. On a similar way, other works apply the emerging technique of Expectation Propagation (EP) [MP01] to ISI processing. Indeed, the concept of EP can be employed to approximate optimal MAP receivers by assuming Gaussianly distributed symbol information. It yields a low complexity iterative receiver [SA11] called EP-MMSE by [SMFO15; San+18], recently enhanced by the EP-MMSE-DFE of [Şa+18]. The EP concept can be illustrated as a message passing algorithm using a factor graph formalism [KFL01; Şa+18]. Nevertheless, most of available EP receivers have been developed in a context of Nyquist signaling with frequency selective channels and then are not directly suitable for FTN signaling. The use of EP algorithm for FTN signaling in turbo-equalization has been proposed in [Wu+17] but they only use it for approximating the prior information from the decoder which amounts to performing a classical turbo-equalization scheme operating with a MMSE equalizer [TSK02].

Finally, by increasing the communication data rate, the propagation channels become more and more frequency selective. In order to tackle this problem, actual standards make use of multi-carrier signaling for by-passing a complex equalization. This led us to extend the previous results, by building a new doubly-circular Multi-Carrier FTN (MFTN) model allowing a low-complexity processing at reception. From this formalism, we adapted the concept of EP to estimate and mitigate the induced interference, composed of ISI as well as Inter-Carrier Interference (ICI) coming from adjacent sub-carriers. The proposed transceiver is able to target very high spectral efficiencies with MFTN signaling. Its performance are finally compared to single-carrier FTN signaling and orthogonal schemes in the presence of a multipaths propogation channel.

Beyond the spectral efficiency increase, some studies take advantage of the perfect ISI knowledge from the receiver and apply precoding at the transmitter's level to FTN signaling [Cha+15; Jan+17; Wan+17]. However, this is known to damage the transmitted signal's spectral containment while increasing the PAPR, which yet can be lowered by non-precoded FTN signaling [Le+14; Luc+16; Pet+18]. Moreover, the compression factor of FTN signaling can also be used to lower the PAPR of Nyquist signaling [Luc+16]. Nevertheless, few multi-criteria studies taking into account both transmitter and receiver constraints exist in the literature. For this reason, we propose to evaluate the overall benefit of FTN signaling with a metric presented in the thesis.

This thesis is organized as follows. Chapter I is dedicated to a brief historical reminder until nowadays leading FTN signaling to be a trendy topic of research. First, we present how H. Nyquist developed a criteria allowing a low-complexity receiver deprived of ISI when considering an Additive White Gaussian Noise (AWGN) channel. Very soon, J. Mazo proved that such a criteria limits the spectral efficiency [Maz75] and he proposed to use the FTN in the 70's. Hence, various receiver strategies have been considered in order to propose realistic ISI processing algorithm in terms of computational complexity. In chapter II we present the main single-carrier FTN receivers of the literature, after recalling the mathematical system model of FTN signaling. Despite the numerous papers about FTN receivers which performance are mainly evaluated through one particular criterion (FER, BER, PAPR...), we still do not know whether, for a given high spectral efficiency and a reasonable complexity, it always exists a combination of FTN parameters (compression factor, shaping filter, constellation) achieving a lower error rate than its Nyquist counterpart. Consequently, the question raised by the interest of FTN signaling operating with reasonable complexity receivers and achieving high spectral efficiencies without increasing the PAPR and maintaining good spectral containment is still open [ARO13]. In other words, FTN signaling has not been yet attested to be a serious candidate for future waveforms [AMJ14] compared to Nyquist signaling. This multi-criteria analysis of single-carrier FTN signaling is conducted in chapter III. Then, we propose to fill the previously mentioned gap by showing that for high spectral efficiency and under complexity constraints, FTN signaling may still be better than Nyquist communications. The solution we propose involves the emerging technique of EP which is presented in chapter IV. Finally, this technique is extended in chapter V to a multi-carrier context, after developing a new doubly-circular MFTN system model allowing a low-complexity processing at reception. The proposed single-carrier and multi-carrier are finally evaluated through a multi-criteria comparison in the presence of a multipaths propagation channel.

List of publications

Journal papers

[HCP19] Sonja Hiltunen, Pascal Chevalier, and Titouan Petitpied. "New insights into time synchronization of MIMO systems without and with interference". In: *Signal Processing* 161 (2019), pp. 180–194. ISSN: 0165-1684. DOI: https://doi.org/10.1016/j.sigpro.2019.03.001. URL: https://www.sciencedirect.com/science/article/pii/S016516841930088X.

[Pet+21] T. Petitpied, R. Tajan, P. Chevalier, S. Traverso, and G. Ferré. "Circular Faster-Than-Nyquist Signaling For high Spectral Efficiencies: Optimized EP-based receivers". In: *IEEE Transactions on Communications* (2021).

Patents

[Pet+19b] Titouan Petitpied, Sylvain Traverso, Pascal Chevalier, Romain Tajan, and Guillaume Ferré. "Procédé et Système pour Décoder des Communications au-delà de la cadence de Nyquist". Pat. FR072373 (France). Dec. 2019. URL: https://hal.archives-ouvertes.fr/hal-02463321.

International conferences

[Pet+18] T. Petitpied, S. Traverso, P. Chevalier, R. Tajan, and G. Ferré. "Multi-criteria Performance Analysis of Faster Than Nyquist Signaling". In: *2018 25th International Conference on Telecommunications (ICT)*. June 2018, pp. 42–46.

[Pet+19] T. Petitpied, R. Tajan, G. Ferré, P. Chevalier, and S. Traverso. "A New Widely Linear Equalizer Based on Expectation Propagation for Faster-Than-Nyquist". In: *2019 IEEE Global Communications Conference (GLOBECOM)*. 2019, pp. 1–6. DOI: 10.1109/GLOBECOM38437.2019.9014275.

[Pet+20] T. Petitpied, R. Tajan, P. Chevalier, G. Ferré, and S. Traverso. "A Frequency-Domain EP-based Receiver for Faster-Than-Nyquist Signaling". In: *2020 IEEE 21st International Workshop on Signal Processing Advances in Wireless Communications (SPAWC)*. 2020, pp. 1–5. DOI: 10.1109/SPAWC48557.2020.9154339.

National conferences

[Pet+19a] Titouan Petitpied, Romain Tajan, Guillaume Ferré, Pascal Chevalier, and Sylvain Traverso. "Algorithme d'égalisation fractionnée fondé sur l'EP-MMSE-DFE". In: *GRETSI. XXVIIème Colloque francophone de traitement du signal et des images*. Lille, France, Aug. 2019. URL: https://hal.archives-ouvertes.fr/hal-02463307.

Chapter I

From Nyquist to Faster-Than-Nyquist Signaling

Outline

The 19th was a phase of industrialization and saw the Technological Revolution which carried on until the early 20th century. It is marked in the occidental countries by the development of standardization, a growing population, the globalized production pushed by the means of transportation, but also the first telecommunication technologies. These progresses were allowed by a change of paradigm, we acknowledged that Science serves the technological progress. Pushed by those developments, and following the World War I of the early 20th century, we understood that rapid exchange of information is furthermore essential for succeeding against the enemy. We did not mistake given the crucial role played by Enigma some years later. In this context, the Bell Telephone Laboratories are founded in 1925 where H. Nyquist, among others, was able to develop the first theoretical concepts of Telegraph signaling.

A Nyquist Signaling

The first point of interest of Nyquist, was to increase the rate of information (called *intelligence* before the paper [Har28] of Hartley who introduced the Information Theory in 1928) by means of coding and signal shaping. From this consideration, he suggested to use shaping filters rectangular in the time-domain for Telegram transmissions in 1924 [Nyq24]. Indeed, he highlights that such a simple filter does not induce *interference*, adversely to any arbitrary band-limited filter. The cardinal sine Power Spectral Density (PSD) of such a rectangular filter constitutes a drawback for a wireless communication in terms of bandwidth containment. Consequently, its paper illustrates for the first time the adversity between quantity of interference, and frequency occupancy: "the greatest amount of currents of higher frequencies [...], the poorest from the standpoint of interference" [Nyq24]. Note that, in this paper, the notion of *interference* is not the same as the ISI for two reasons:

1. Nyquist does not consider any matched filter at receiver,
2. he defines as an interference the overlapping area between two successive shaped symbols instead of considering the sampled filter coefficients at the symbol-time.

The idea of the spectral efficiency maximization, i.e. bandwidth reduction and data rate increase, remains today a special area of interest and constitutes the first elements of our multi-criteria analysis.

Some years later in 1928, Nyquist went much further by introducing multiple aspects of a communication described hereafter [Nyq28]. First, he mentioned the idea of practical implementation for equalization: "While signal shaping and equalizing are equivalent it does not follow that they are equally practicable" [Nyq28]. At that time, the communication technologies were mainly composed of analog processing which is obviously not the case nowadays. However, the idea of practicable implementation remains an actual constraint and is now limited by the computational complexity of the processes which constitutes the second criterion of our analysis.

Secondly, Nyquist defined precisely the concept of interference: the term *inter-symbol interference* was already introduced but Nyquist preferred naming it *characteristic interference*. He also noted that such an undesirable term in the communication is "closely related to characteristic distortion", where the *characteristic distortion* stands for an uncorrelated noise coming from the electronic components today modeled by an AWGN.

Then, Nyquist introduced the sampling operation and the importance of limiting numerically the interference only for the signal sampled at the symbol-time: "No notice will be taken of the wave at any other point in the time unit, and consequently deformations of the wave at other points will not matter". This important concept in fact relaxes the problem of limiting the interference corresponding to the ISI. Indeed, the only optimal solution for limiting the interference while maximizing the information rate was, before that, to use a rectangle filter. After this finding, we moved to a whole filter family satisfying this criterion named the *Nyquist filters*.

Finally, always in the same paper [Nyq28], Nyquist defined what is called today the Nyquist frequency, corresponding to the half of the signaling speed under the constraint of limiting the ISI: "a frequency range numerically equal to the speed of signaling is necessary". He proved that the data rate increases proportionally with the bandwidth occupancy.

Consequently, Nyquist proposed to maximize the received signal's power after matched filter and down-sampling. He also showed the necessity of using the Nyquist filters in order to limit the ISI mainly because of the inability of performing an analog equalization. Actually, such a reason does not hold anymore and the technique of FTN signaling could arise.

B Genesis of Faster-Than-Nyquist signaling

The concept of FTN signaling has first been published in a short letter by Donald W. Tufts in 1968 [Tuf68] who mentioned the idea of transmitting "any finite number of data elements at rates faster than the Nyquist rate". Such a suggestion has never been explored until a pessimistic paper published by J. Salz in 1973 [Sal73].

B.1 Nyquist signaling for MSE minimization

The previously mentioned paper [Sal73] showed that Nyquist signaling offers always better performance in terms of Mean-Square Error (MSE) compared to FTN signaling at fixed spectral efficiency with Pulse-Amplitude Modulation (PAM) constellations over an AWGN channel, even when considering Decision Feedback Equalization (DFE) with perfect decisions. Note that no channel coding was introduced in the waveform and these results can be easily extended to any Quadrature Amplitude Modulation (QAM) constellations. Hence, this study gave a preliminary negative answer about the interest of

FTN signaling because, at that time, most of the considered reception techniques where performed with MMSE-based strategies which perform filtering operations with a limited complexity. Consequently, Salz demonstrated mathematically the interest of the Nyquist criterion: it optimizes the MSE at fixed spectral efficiency. However, as its name suggests, the MSE does not consider the estimate distributions, i.e. the symbols constellation.

While J. Salz conducted a study based on MSE optimization, a new algorithm developed by A. Viterbi in 1967 [Vit67b] allowed new types of estimation problems to be handled with limited computational complexities. Indeed, A. Viterbi developed an algorithm which reduces the set of sequences to explore when solving a ML estimation. To do so, the proposed solution takes benefit of the finite memory length of the filter applied to the symbols. Such a ML problem is detailed in [For73] and amounts to evaluate the more likely sequence from the observation signal. Consequently and conversely to the MMSE criterion, the ML strategy takes into account the symbols constellation. In order to apply the Viterbi algorithm, an element of the signal of interest needs to be formed by a combination of its neighboring elements. Hence, the convolution effect of a Nyquist filter at a rate higher than the Nyquist rate falls within the scope of this algorithm.

B.2 The Mazo bound

The introduction of the Viterbi algorithm shed a new light on ML problems and G. Forney saw its potential for signals suffering from ISI [For72] in 1972, closely followed by G. Ungerboeck [Ung74] in 1974. More precisely, G. Forney and G. Ungerboeck proposed two different theoretical approaches yielding distinct implementations with similar complexity and same performance. However, these two types of ML receivers are not equivalent anymore when developing sub-optimal ML-based receivers [RLP07; RCS15], as detailed in Sec. B.

In this context, J. E. Mazo in 1975 [Maz75] introduced the term of FTN signaling and demonstrated the first unexpected and optimistic result of this technique. Indeed, he showed that compressing the symbol-time by a factor down to $\tau = 0.802$ does not reduce the minimum inter-sequence distance when considering a BPSK constellation with a time-domain cardinal sine Nyquist filter. In other words, the resulting FTN signal increases the spectral efficiency by $\tau^{-1} - 1 \approx 25\%$ without damaging the error rate, if the ISI is handled by a Viterbi algorithm in a channel with high SNR. This counter-intuitive result gave a particular place to FTN signaling and the factor $\tau = 0.802$ was named the "Mazo bound". Nevertheless, almost fifteen years of silence on the FTN technique followed this conceptual starting point.

Later on, some studies tried to mathematically compute and extend the Mazo bound to other constellations such as D. Hajela [Haj90] in 1990 and to other filters as C.K. Wang [CL91] in 1995. Indeed, the cardinal sine filter is not usable for practical implementations as it comes with an infinite PAPR. But the difficulty of this problem and the required computational complexity of the receiver did not allow any performance simulations until 2003 [LG03]. These first operational results have been enabled by turbo reception techniques developed in 1995 and approaching the Shannon capacity.

C Shannon Capacity & Turbo receivers

Following the technical works of Nyquist and theoretical studies of H. Hartley on Information Theory, C. Shannon proposed a general formalism under a theory of communication in 1948 [Sha48]. This new subject area gathers mathematics for measuring, electronic for operational systems and statistics to anticipate every situation. In its study, C. Shannon formalized the conception of a communication system. Moreover, he detailed and exploited the concept of *Entropy* as a measure of information before introducing the notion of *Capacity* which measures the maximum achievable information rate when communicating over a noisy channel. However, this theoretical bound remained unreachable in practice during decades because it assumes a Gaussian distribution of the symbols.

Simultaneously to the theoretical studies for FTN signaling, a research team composed of C. Berrou, A. Glavieux and P. Thitimajshima proposed an unprecedented method for channel coding and decoding [BGT93]. This new class of codes are named Turbo-Codes and approach the Shannon Capacity for the first time. At reception, a turbo-decoder is based on an iterative exchange of information between two decoders, each taking benefit of different coded bits. This principle of iterative information exchange has then been applied to channel equalization two years later [Dou+95a] by C. Douillard, M Jézéquel, C. Berrou, A. Picart, P. Didier and A. Glavieux. Those major findings allowed a joint decoding and channel equalization under computational complexity constraints. They had a major impact on the field of digital communications, and also renewed the interest of FTN signaling.

D Practical benefits of FTN systems

Compared to Nyquist signaling, the FTN technique offers the compression factor τ as a supplementary degree of freedom for a waveform design. Hence, we can wonder if this supplementary setting allows practical benefits for operational communications.

D. Liveris proposed the first performance simulations of a FTN signaling communication with Raised-Cosine (RC) filters and a BPSK modulation [LG03]. To do so, he assumed both uncoded and channel coded schemes. The ISI is processed by a Viterbi-based algorithm with soft output for channel coding, combined with an iterative decoder. He pointed out the complexity of this reception technique, and confirmed the theoretical studies previously lead by J. Mazo.

On the following chapter, we present the mathematical derivation and a state of the art of single-carrier FTN signaling. We recall the background yielding Linear MMSE and BCJR algorithms developed to process the ISI of FTN signaling [TSK02; Bah+74; Rus07]. Moreover, sub-optimal receivers of the literature able to achieve higher spectral efficiencies are also presented before proposing new receivers dedicated to FTN signaling.

Chapter II

Single-Carrier Faster-Than-Nyquist Signaling

Outline

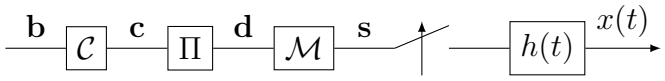

Figure II.1: System model of a FTN transmitter

This chapter presents a state-of-the-art of ISI processing for single-carrier FTN signaling. A FTN system model is presented in Sec. A assuming two types of FTN signaling with different properties. The characteristic of FTN holds in the introduction of the time compression factor τ applied to the symbol-time. This compression allows increasing the symbol-rate without changing the communication bandwidth of Nyquist signaling. Sec. B shows that the side-effect of the time compression factor is to generate ISI after matched-filtering and down-sampling. In order to address this issue, an iterative joint decoding and equalization process is considered at the receiver. For the symbol-stage processing, BCJR-based as well as MMSE-based strategies are detailed, offering different error rate and complexity trade-offs.

A System model

This section is devoted to the mathematical definition of a baseband FTN communication. A channel code is supposed in sub-Sec. A.1 and two ways of performing the FTN modulation are presented. Those two methods are referred to as Linearly Convolved FTN (LCFTN) in sub-Sec. A.3 for the linear convolution of the symbol sequence with the shaping filter, while CCFTN in sub-Sec. A.4 operates a frequency-domain circular convolution. A comparison between the two types of FTN signaling is then conducted in sub-Sec. A.5, before introducing the AWGN channel model in sub-Sec. A.6.

A.1 Bit stream processing

We suppose a general communication chain in which the transmitter depicted in Fig. II.1 generates N_b information bits stored in the random vector $\mathbf{b} = [b_1, b_2, ..., b_{N_b}]^T$. The elements of $\mathbf{b}$ are supposed to be independant and identically distributed (iid) as well as uniformly distributed within the field $\mathbb{F}_2 = \{0, 1\}$. If considering any channel code $\mathcal{C}$ with associated rate R, then the resulting coded bits are given by $\mathbf{c} = \mathcal{C}(\mathbf{b})$ composed of $N_c = N_b R^{-1}$ elements. Those bits are interleaved with a permutation matrix Π resulting in the interleaved coded bits $\mathbf{d} = \Pi\mathbf{c}$.

The resulting random bits are then mapped into a complex constellation $\mathcal{M}$. To do so, we define the linear modulation forming one complex symbol from each group of $\log_2 |\mathcal{M}|$ bits. Hence, the resulting random symbol vector $\mathbf{s} = [s_1, s_2, ..., s_{N_s}]^T = \mathcal{M}(\mathbf{d})$ is composed of $N_s = \frac{N_c}{\log_2 |\mathcal{M}|}$ elements. In the following, we will assume a normalized and centered constellation yielding $\mathbb{E}[s_n] = 0$ and $\mathbb{E}|s_n|^2 = 1$ and we denote E_b the useful bit energy.

A.2 The Nyquist criterion

In order to control the spectrum of the communication, the symbol sequence is convolved with a continuous-time shaping filter $h(t)$. This filter is supposed to be a square-root-Nyquist filter, as it ensures the following time-domain Nyquist criterion:

$$\exists T > 0 : g(t) \sum_{n \in \mathbb{Z}} \delta(t - nT) = g(0)\delta(t) \tag{II.1}$$

where $\delta(t)$ is the Dirac delta function, $g(t) = (h \star h')(t)$ is called the Nyquist filter with $h'(t) = h^*(-t)$ the matched filter. The smallest T value satisfying the criteria of (II.1) is named the *orthogonality time* associated to the filter $g(t)$ (or $h(t)$). From (II.1), one can derive the equivalent frequency-domain Nyquist condition expressed as follows:

$$\exists T > 0 : \sum_{k \in \mathbb{Z}} G\left(f - \frac{k}{T}\right) = g(0)T \tag{II.2}$$

where $G(f) = \mathcal{F}(g(t)) = |H(f)|^2$ is the Fourier Transform (FT) of the filter $g(t)$ and $H(f)$ is the FT of $h(t)$.

A direct consequence of (II.2) is that the bandwidth of a Nyquist communication for a band-limited filter $g(t)$ is necessarily equal or wider than the symbol-rate T^{-1}. Hence, the draw-back of the Nyquist criterion is to limit the achievable information rate D_b in bits/s as we have: $D_b \leq \log_2 |\mathcal{M}| W$. From this observation, we call *rolloff* or *excess bandwidth* the factor denoted by $\beta \geq 0$ satisfying $\beta = TW - 1$. In this thesis, we restrict the Nyquist filters family to the symmetric and real filters whose excess bandwidth factor is limited as follows: $\beta \in [0, 1]$. Furthermore, for $\beta = 0$ the filter $h(t)$ as well as $g(t)$ coincide to a cardinal sine. In this particular case, one can show that the inverse of the orthogonality time of a Nyquist filter $g(t)$ also corresponds to its -3 dB bandwidth. For the particular case of a cardinal sine filter RC(0), T^{-1} represents the full bandwidth. An illustration of the considered RC Nyquist filters is depicted in Fig. II.2 in time domain and Fig. II.3 in frequency domain. In the following we consider that $h(t)$ is normalized, i.e. $\int |H(f)|^2 \, \mathrm{d}f = g(0) = 1$.

The different rolloff filters are useful when designing a communication. At fixed symbol-rate, while filters with low rolloff limit the spectral occupation, filters with high rolloff are more tolerant to a timing synchronization offset and can be preferred to minimize the PAPR. Whichever the rolloff is, we present two different approaches for shaping the symbols by the filter $h(t)$: the Linearly and Circularly Convolved FTN, denoted respectively by LCFTN and CCFTN. While LCFTN is generally used in the literature, we show in the following chapters some benefits brought by CCFTN for frequency-domain receiver processing. Hence, both the filtering methods are detailed hereafter.

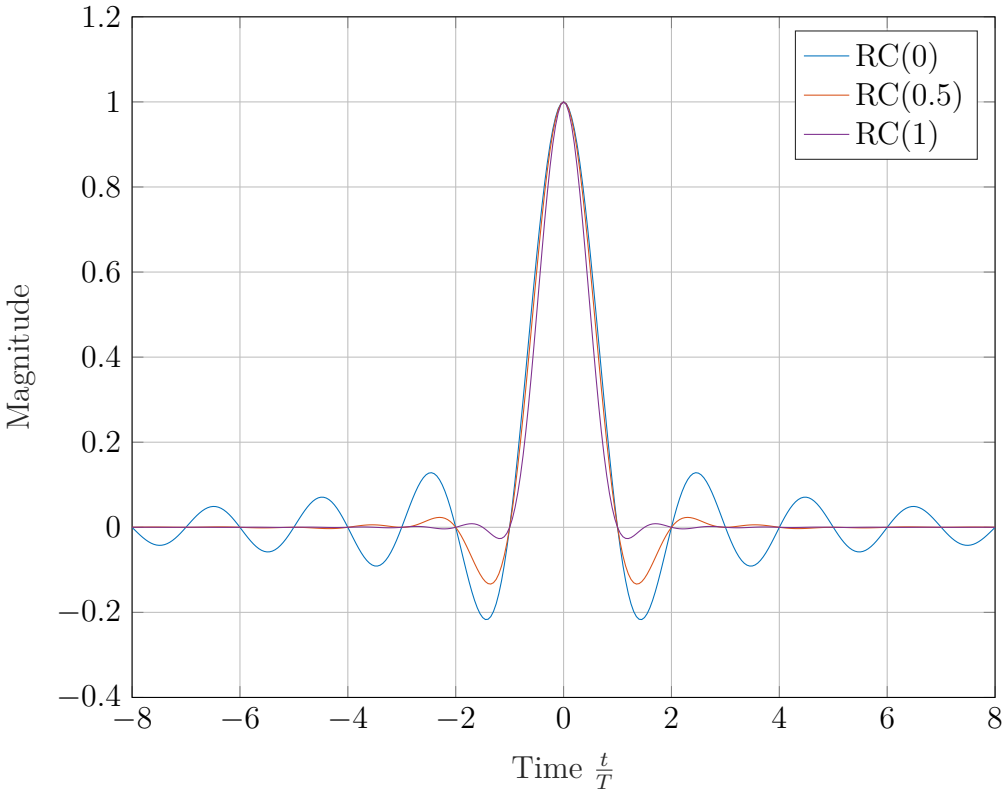

Figure II.2: Nyquist filters for different excess bandwidth factors in time domain

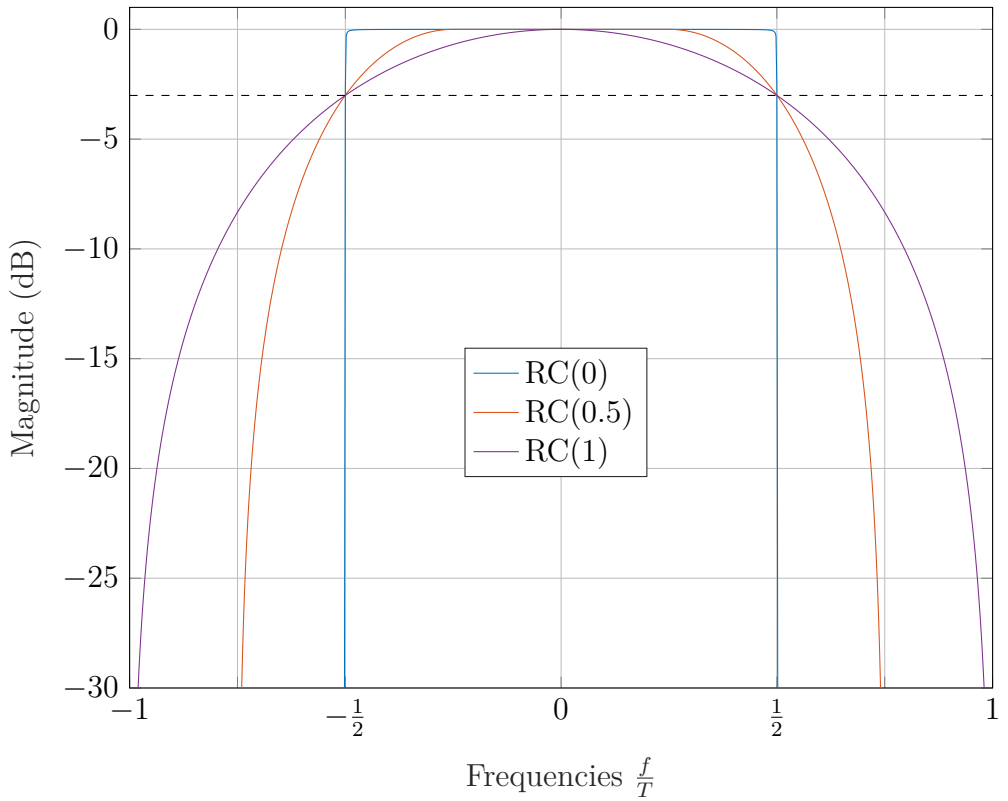

Figure II.3: Nyquist filters for different excess bandwidth factors in frequency domain

A.3 Linearly Convolved Faster-Than-Nyquist

The filtering operation of the symbols composing the vector $\mathbf{s}$ is generally performed by a linear convolution [Maz75]. We propose to call this model LCFTN. Hence, the continuous-time transmitted signal is given by:

$$\bar{x}(t) = \sum_{n=0}^{N_s-1} s_{n+1} h(t - nT_s) \tag{II.3}$$

where $T_s = \tau T$ represents the symbol duration, and $\tau \in (0, 1]$ is the FTN time compression factor. For $\tau = 1$, the Nyquist criterion (II.1) or (II.2) is ensured and the reception is not affected by ISI if correctly processed (see sub-Sec. B.1).

We propose to represent equivalently the signal $\bar{x}(t)$ over the bandwidth W with a discrete-time formalism. To do so, we assume that:

1. the bandwidth of $\bar{x}(t)$ coincide with the bandwidth of $h(t)$[1].
2. the time support of $\bar{x}(t)$ is limited.

The first assumption comes from the Nyquist-Shannon sampling theorem giving that we need to represent $\bar{x}(t)$ with a sampling-rate equal or wider than W. One can verify that an over-sampling rate of 2 yielding a sampling-time of $\frac{T_s}{2}$ meets this condition $\forall \beta \in [0, 1]$ and $\forall \tau \in (0, 1]$ as we have:

$$\frac{2}{T_s} \geq W \iff \tau(1 + \beta) \leq 2 \tag{II.4}$$

The second assumption can be satisfied if the shaping filter is a Finite Impulse Response (FIR) filter as proposed by [Tra16], i.e. $\exists L > 0 : h(t) = 0$ for $t \notin [-LT, LT]$ or $t \notin [-L_\tau T_s, L_\tau T_s]$ where $L_\tau = \frac{L}{\tau}$. However, we generally use root-RC (rRC) filters which concentrate most of their energy around $t = 0$ (see Fig. II.2). In practice, they are truncated for some $L > 0$, but this can damage the spectral bandwidth occupancy especially for low values of L and β. Fig. II.4 shows this effect in terms of out-of-band energy when truncating a rRC filter. Filters with low rolloff values require long impulse response coming with high memory usage and latency. As an example, the DVB-S2X standard for satellite communications implements rolloff factors down to $\beta = 0.05$ [ETS]. This strong constraint could be relaxed by means of FTN signaling at the price of ISI to process at reception [Luc+16].

Hence, the signal $\bar{x}(t)$ defined in (II.3) is equivalent to the discrete signal $\bar{\mathbf{x}} = [\bar{x}_1, \bar{x}_2, ..., \bar{x}_{N_x}]^T$ where $N_{\bar{x}} = 2(N_s + L_\tau)$ and $\bar{x}_i = \bar{x}\left((i - 1 - 2L_\tau)\frac{T_s}{2}\right)$. It is important that L_τ depends on τ in order to ensure that the time support of $h(t)$ remains the same

[1] This hypothesis tends to be true for large values of N_s and iid symbols

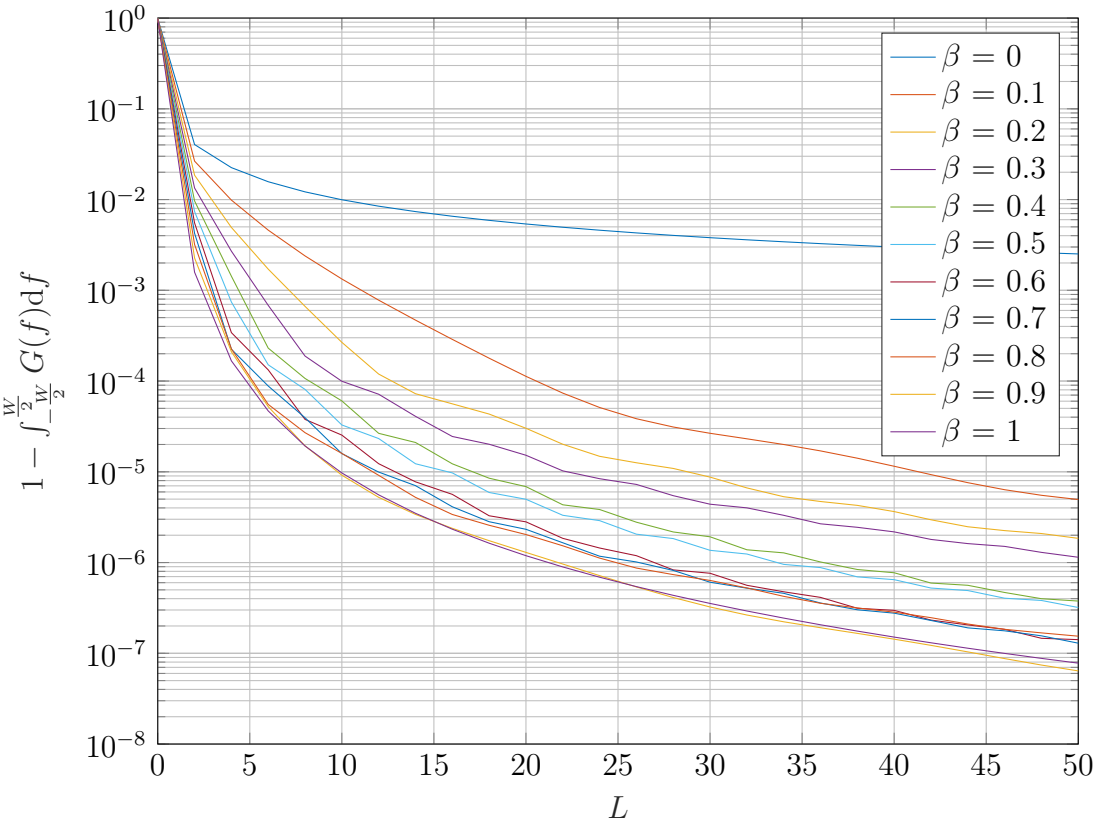

Figure II.4: Out-of-band energy ratio against the truncation setting for RC filters

regardless of the value of τ. With a matrix formalism, we have:

$$\bar{\mathbf{x}} = \mathbf{HUs} \tag{II.5}$$

where $\mathbf{U}$ represents the $(2N_s \times N_s)$ up-sampling matrix by a factor 2 defined as:

$$\mathbf{U} = \begin{pmatrix} 1 & 0 & 0 & \dots & 0 \\ 0 & 0 & 0 & \dots & 0 \\ 0 & 1 & 0 & \dots & 0 \\ 0 & 0 & 0 & \dots & 0 \\ \vdots & \vdots & & & \vdots \\ 0 & 0 & 0 & \dots & 0 \\ 0 & 0 & 0 & \dots & 1 \\ 0 & 0 & 0 & \dots & 0 \end{pmatrix} \tag{II.6}$$

yielding $\mathbf{Us} = [s_1, 0, s_2, 0, ..., s_{N_s}, 0]$ and $\mathbf{H}$ is the $(N_{\bar{x}} \times 2N_s)$ convolution matrix associated

to the filter $h(t)$ sampled at time $\frac{T_s}{2}$:

$$\mathbf{H} = \begin{pmatrix} h(L_\tau T_s) & 0 & \dots & \dots & \dots & \dots & 0 \\ h(L_\tau T_s - \frac{T_s}{2}) & h(L_\tau T_s) & 0 & \dots & \dots & \dots & 0 \\ \vdots & & \ddots & 0 & \dots & \dots & 0 \\ h(-L_\tau T_s) & h(-L_\tau T_s + \frac{T_s}{2}) & \dots & h(L_\tau T_s) & 0 & \dots & 0 \\ 0 & h(-L_\tau T_s) & & & \ddots & \ddots & 0 \\ 0 & 0 & \ddots & & & \ddots & 0 \\ 0 & \ddots & \ddots & \ddots & & & h(L_\tau T_s) \\ \vdots & \ddots & \ddots & \ddots & \ddots & & \vdots \\ 0 & \dots & \dots & \dots & 0 & h(-L_\tau T_s) & h(-L_\tau T_s + \frac{T_s}{2}) \\ 0 & \dots & \dots & \dots & 0 & 0 & h(-L_\tau T_s) \end{pmatrix} \tag{II.7}$$

The matrix $\mathbf{H}$ is rectangular and Toeplitz. In the following, we will use equivalently (II.3) and (II.5) for referring to the LCFTN transmitted signal.

Fig. II.5 and Fig. II.6 depict the signals considering a BPSK modulation and a Nyquist filter RC(0.5) for both Nyquist and FTN signaling. The colored signals corresponds the different filters associated to each symbol. The main problematic about FTN signaling appears clearly: for a given communication bandwidth fixed by the filter, the FTN signal offers a higher data-rate. However, this potential interest of the FTN technique has to be balanced: at reception, the signal suffers from ISI after matched-filter. This ISI has to be handled by a receiver strategy as presented in Sec. B.

A.4 Circularly Convolved Faster-Than-Nyquist

A different way of filtering the symbols has been proposed in [TPB16] referred as CCFTN. It consists in performing a circular convolution between the symbol sequence $\mathbf{s}$ and the filter $h(t)$. A circular convolution is obtained by convolving two functions, after periodizing them. It results in a periodic function, but we keep only one period being the useful information we transmit and the period length is chosen to be the sequence length $N_s T_s$. Such a convolution of periodized signals can equivalently be performed in the frequency domain by multiplying the discrete signals' spectra. In that case, the frequency discretization step corresponds to the inverse period $\frac{1}{N_s T_s}$. We first present the time-domain circular convolution using continuous-time signals, before presenting the equivalent discrete frequency approach with a matrix formalism.

We define the periodized filter $\dot{h}(t)$ for transmitting a sequence of N_s symbols as

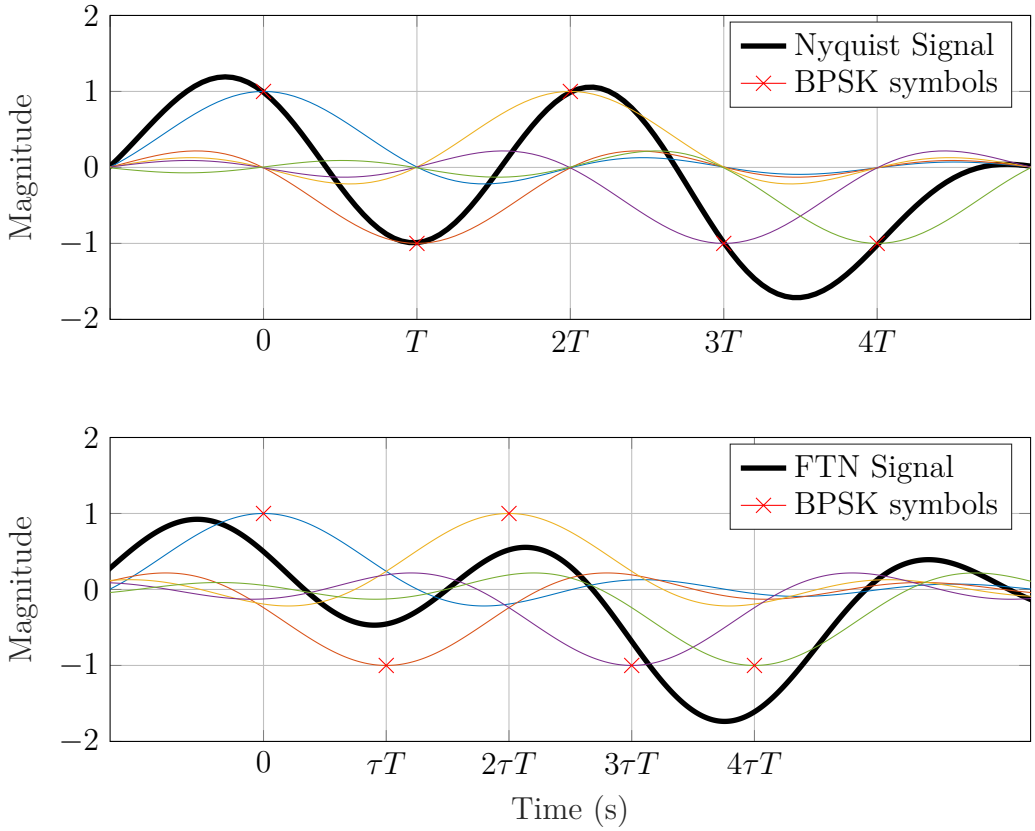

Figure II.5: Nyquist (top) and FTN $\tau = 0.8$ (bottom) time-domain signal

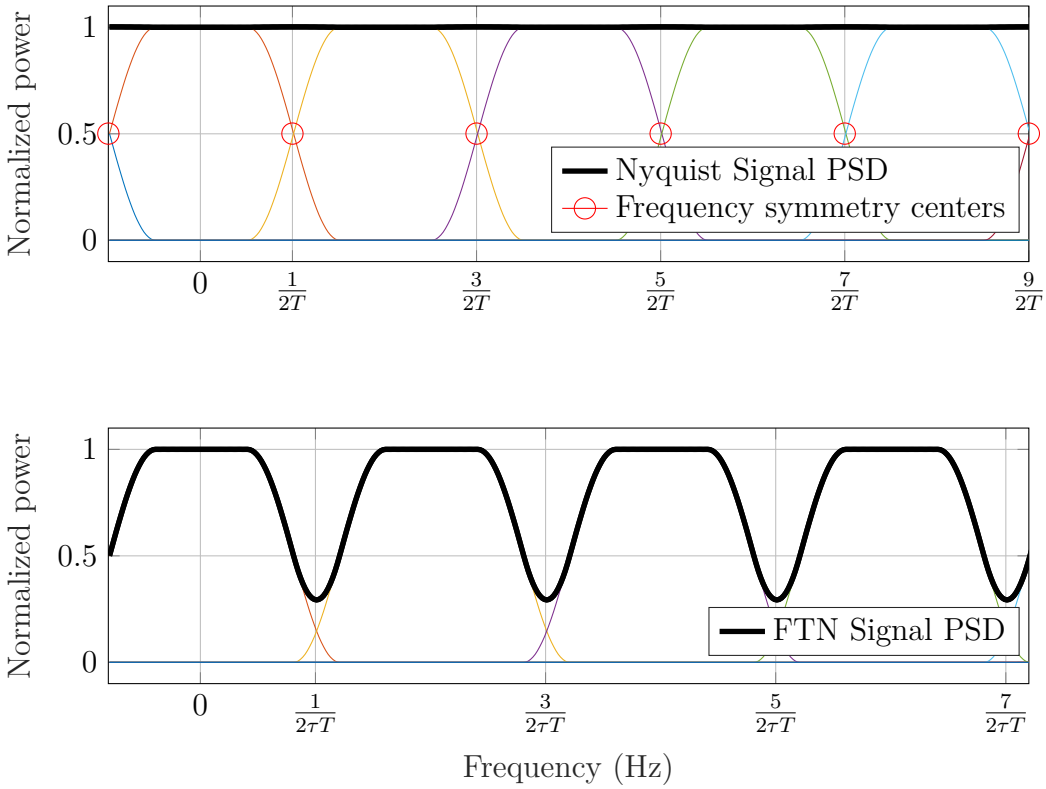

Figure II.6: Nyquist (top) and FTN $\tau = 0.8$ (bottom) frequency-domain signal

follows:

$$\dot{h}(t) = \sum_{m\in\mathbb{Z}} h(t - mN_sT_s) \tag{II.8}$$

The filter $\dot{h}(t)$ is then periodic with period the sequence duration N_sT_s. Note that (II.8) can be written in the frequency-domain to show that $h(t)$ and $\dot{h}(t)$ share the same Fourier coefficients at frequencies $\{\frac{m}{N_sT_s}\}_{m\in\mathbb{Z}}$, up to a scaling factor, as we have:

$$\dot{H}(f) = \frac{1}{N_sT_s} \sum_{m\in\mathbb{Z}} H\left(\frac{m}{N_sT_s}\right) \delta\left(f - \frac{m}{N_sT_s}\right) \tag{II.9}$$

where $\dot{H}(f)$ corresponds to the FT of $\dot{h}(t)$. In order to use a matrix formalism, we define the $(2N_s \times 2N_s)$ convolution matrix $\dot{\mathbf{H}}$ representing a period of $\dot{h}(t)$ at a sampling-time $\frac{T_s}{2}$. Such a matrix is expressed by:

$$(\dot{\mathbf{H}})_{a,b} = \dot{h}\left((b-a)\frac{T_s}{2}\right) \tag{II.10}$$

where $a, b \in [\![1, 2N_s]\!]$. Moreover, shifting by any $c \in \mathbb{Z}$ the two indices (a, b) does not change the value of the matrix element with shifted indices (modulo the matrix size $2N_s$). Indeed, defining $a' = [(a + c - 1) \mod 2N_s] + 1$ and $b' = [(b + c - 1) \mod 2N_s] + 1$, we have:

$$\begin{aligned}(\dot{\mathbf{H}})_{a',b'} &= \dot{h}\left(([(b + c - 1) \mod 2N_s] - [(a + c - 1) \mod 2N_s])\frac{T_s}{2}\right) \\ &= \dot{h}\left(((b + c - 1) - (a + c - 1))\frac{T_s}{2}\right) \\ &= (\dot{\mathbf{H}})_{a,b}\end{aligned}$$

where the second equality is due to the N_sT_s-periodicity of $\dot{h}(t)$. Hence, $(\dot{\mathbf{H}})_{a,b}$ is invariant by shifting the indices modulo $2N_s$, proving that $\dot{\mathbf{H}}$ is not only Toeplitz but also circulant. This is in fact a direct consequence of the *circular* convolution.

The filtering operation is then applied to the symbol sequence at the sampling-rate to form the discrete-time transmitted sequence $\dot{\mathbf{x}}$:

$$\dot{\mathbf{x}} = \dot{\mathbf{H}}\mathbf{U}\mathbf{s} \tag{II.11}$$

However, it is possible to lower the computational complexity of $\dot{\mathbf{x}}$ using the Discrete FT (DFT). To do so, we define the unitary $(N \times N)$ DFT Matrix $\mathbf{F}_N$ as follows:

$$(\mathbf{F}_N)_{a,b} = \frac{1}{\sqrt{N}} \mathrm{e}^{-j2\pi\frac{(a-1)(b-1)}{N}} \; \forall a, b \in [\![1, N]\!] \tag{II.12}$$

The vectors composing $\mathbf{F}_N$ are known to form a basis diagonalizing any circulant matrix. Hence, we rewrite the CCFTN transmitted sequence as follows:

$$\dot{\mathbf{x}} = \mathbf{F}_{2N_s}^{\dagger} \hat{\dot{\mathbf{H}}} \hat{\mathbf{s}}' \tag{II.13}$$

having $\hat{\dot{\mathbf{H}}} = \mathbf{F}_{2N_s}\dot{\mathbf{H}}\mathbf{F}_{2N_s}^{\dagger}$ the DFT of $\dot{\mathbf{H}}$. The matrix $\dot{\mathbf{H}}$ being circulant, $\hat{\dot{\mathbf{H}}}$ is then diagonal and can be expressed as: $(\hat{\dot{\mathbf{H}}})_{a,a} = H\left(T_s^{-1}\left(1 + \frac{a-1}{N_s} \bmod 2\right) - T_s^{-1}\right)$, and $\hat{\mathbf{s}}' = \mathbf{F}_{2N_s}\mathbf{U}\mathbf{s}$. The vector $\mathbf{s}'$ is the DFT of the up-sampled sequence by a factor 2. From the FT properties, we know that such a the time-domain up-sampling is equivalent to a frequency-domain duplication. More precisely, we note $\hat{\mathbf{s}} = \mathbf{F}_{N_s}\mathbf{s}$ the DFT of the symbol sequence $\mathbf{s}$ and we have:

$$\hat{\mathbf{s}}' = \mathbf{F}_{2N_s}\mathbf{U}\mathbf{s} = \begin{pmatrix} \hat{\mathbf{s}} \\ \hat{\mathbf{s}} \end{pmatrix} \tag{II.14}$$

Hence, the computation complexity of $\hat{\mathbf{s}}$ reduces to $O(N_s \log_2 N_s)$ the complexity of a N_s-long DFT.

The computational complexity benefits come from two tricks:

- the application of $\mathbf{F}_N$ or $\mathbf{F}_N^{\dagger}$ to a vector or a circulant matrix can be performed in $O(N\log(N))$ using the Fast FT (FFT) algorithm,
- the product $\hat{\dot{\mathbf{H}}}\hat{\mathbf{s}}'$ in (II.13) can be performed in $O(N_s)$ because $\hat{\dot{\mathbf{H}}}$ is diagonal.

Consequently, the sequence $\dot{\mathbf{x}}$ can be efficiently computed with a complexity $O(N_s \log(N_s))$ using the definition of (II.13).

Finally, we need to form a continuous-time vector $\dot{x}(t)$ from the discrete sequence $\dot{\mathbf{x}}$. The frequency spectrum of these two signals are required to coincide over the bandwidth $\frac{2}{T_s}$. Hence, we use an ideal and unitary low-pass filter $\gamma(t)$ which FT is defined as follows:

$$\Gamma(f) = \begin{cases} \frac{T_s}{2} & \text{if } f \in [-\frac{1}{T_s}; \frac{1}{T_s}] \\ 0 & \text{else} \end{cases} \tag{II.15}$$

and we obtain the continuous-time transmitted signal:

$$\dot{x}(t) = \sum_{m=0}^{2N_s-1} \dot{x}_{m+1}\Gamma\left(t - m\frac{T_s}{2}\right) \tag{II.16}$$

$$= \sum_{n=0}^{N_s-1} s_{m+1}\dot{h}(t - mT_s) \tag{II.17}$$

where the $(m+1)$ component of $\dot{\mathbf{x}}$ satisfies $\dot{x}_{m+1} = \dot{x}\left(m\frac{T_s}{2}\right)$. Note that any low-pass filter which replicas frequency shifted by $\frac{2m}{T_s}, m \in \mathbb{Z}$ form an orthonormal basis could have been used instead of $\gamma(t)$. The candidate filters for $\gamma(t)$ coincide with the Nyquist filters with orthogonality time $\frac{2}{T_s}$.

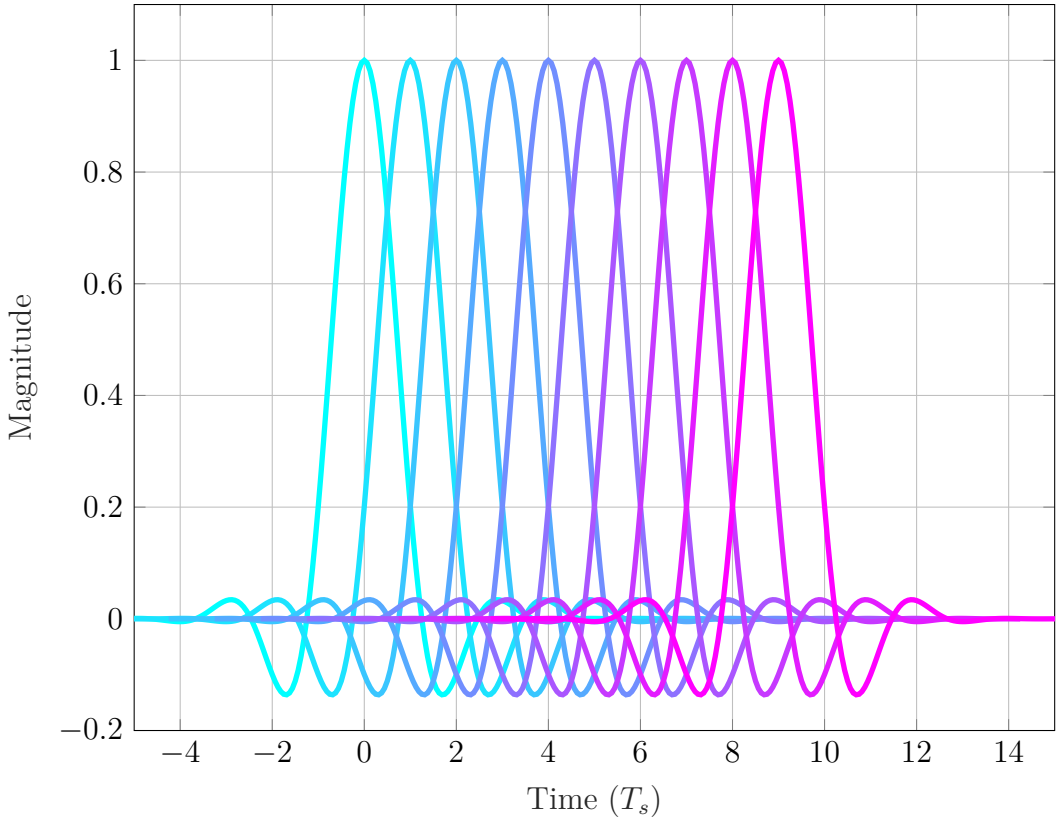

Figure II.7: Nyquist filters of LFTN signaling with $\tau = 0.8$ and $\beta = 0.5$

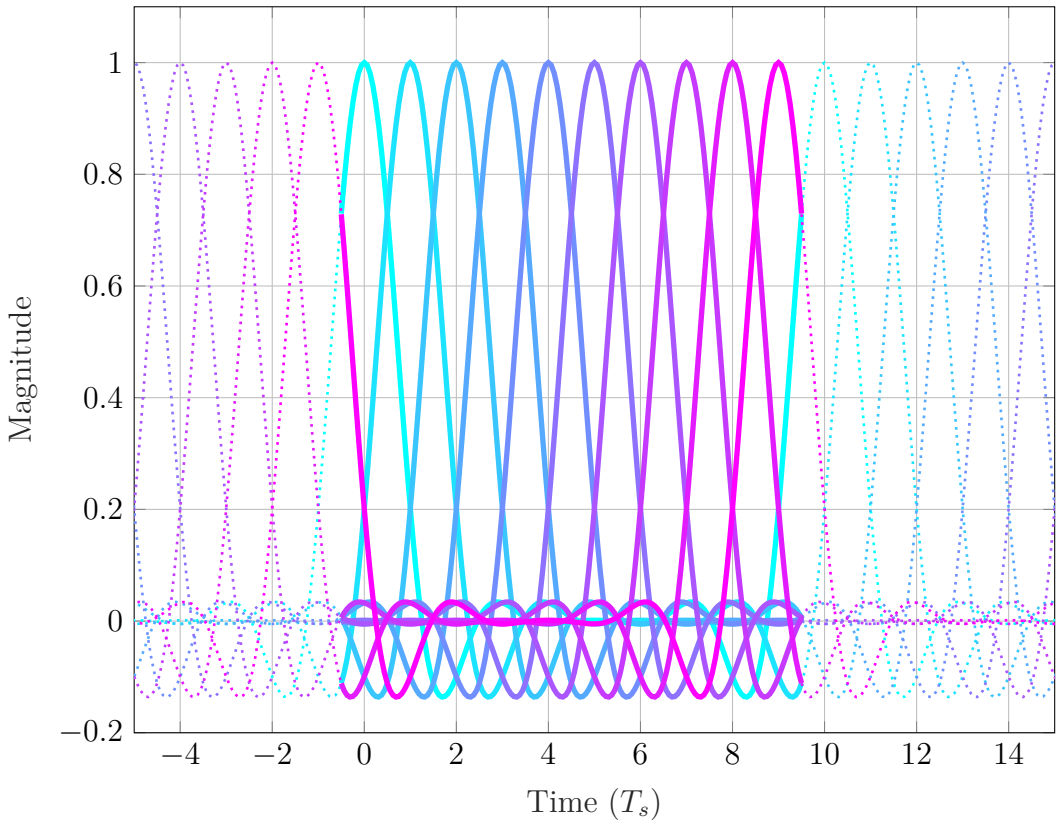

Figure II.8: Nyquist filters of CCFTN signaling with $\tau = 0.8$ and $\beta = 0.5$

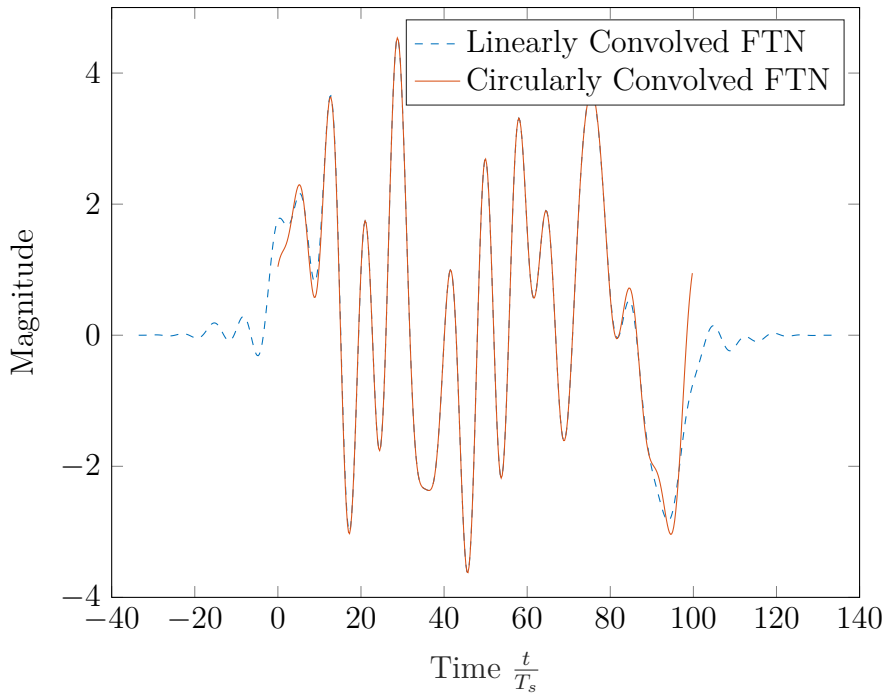

Figure II.9: Transmitted signals in a frame of $N_s = 100$ symbols considering a BPSK modulation shaped with a cardinal sine filter and $\tau = 0.3$

A.5 Comparison between LCFTN and CCFTN

Fig. II.7 and Fig. II.8 show a comparison between LCFTN and CCFTN filters associated to $N_s = 10$ symbols for $\tau = 0.8$. For CCFTN, dotted lines stand for the periodic shaping filters, while plain lines corresponds to filters on the time support of interest. Regarding the ISI, the firsts and lasts symbols of the CCFTN signal defined in (II.16) strongly interfere because of the filters replicas, as if they were neighboring symbols. However, apart from the transmitted signal edges, the transmitted signal using CCFTN coincide with the LCFTN technique. This difference is illustrated in Fig. II.9 where we show that CCFTN offers latency savings as well as a spectral efficiency gains because the time support of the transmitted signal is smaller. However, this benefit comes at the price of spectrum damages due to the strong transitions at the beginning and the ending CCFTN frame. In practice, these transitions can be smoothened by windowing.

On the computational complexity side, CCFTN offers some advantages because the filtering can be applied in the frequency-domain without approximation. In addition to the computational complexity aspects, the interest of CCFTN lies in the circulant structure of $\hat{\mathbf{H}}$ which can be exploited by FD-based receiver processing for example. A similar result can be obtained by adding a cyclic prefix to the LCFTN waveform as in [Sug13] in the same way as Orthogonal Frequency-Division Multiplexing (OFDM). However, this cyclic prefix damages the spectral efficiency and CCFTN should be preferred.

In the following, we note $x(t)$, $\mathbf{x}$ and N_x standing for either $\bar{x}(t)$, $\bar{\mathbf{x}}$ and $N_{\bar{x}}$ when considering LCFTN, or $\dot{x}(t)$, $\dot{\mathbf{x}}$ and $N_{\dot{x}} = 2N_s$ for CCFTN signaling. Moreover, we will

use the general term of FTN signaling for either LCFTN or CCFTN signaling.

A.6 Ideal model of a wireless communication propagation channel

In this thesis, we focus on propagation channels supposed to be time-invariant compared to a sequence duration. In the following and up to the end of Chap. IV, we suppose an ideal AWGN propagation channel without multipath. This model considers a random noise gathering some undesired impacts of the analog components involved in the communication. This AWGN component denoted by $w(t)$ is supposed to be complex, circular and centered with PSD $\mathbb{E}|W(f)|^2 = N_0$ where $W(f)$ is the FT of $w(t)$.

The received signal after the channel model is then defined as follows:

$$r(t) = x(t) + w(t) \tag{II.18}$$

We can also use a matrix formalism equivalent to the definition of $r(t)$ over the communication time and frequency supports. To do so, we define the discrete-time received vector $\mathbf{r} = [r_1, r_2, ..., r_{N_r}]^T$ where $r_m = (r \star \gamma)\left(m\frac{T_s}{2}\right)$ yielding:

$$\mathbf{r} = \mathbf{x} + \mathbf{w} \tag{II.19}$$

where $\mathbf{w} = [w_1, w_2, ..., w_{N_r}]^T$ having $w_m = (w \star \gamma)\left(m\frac{T_s}{2}\right)$ and $N_r = N_x$. The filter $\gamma(t)$ applied to $r(t)$ is used to preserve the noise whiteness and energy over the communication bandwidth. Moreover, one can show that a noise component of the vector $\mathbf{w}$ follows $w_m \sim \mathcal{N}_{\mathrm{C}}(0, \sigma_w^2)$ where $\sigma_w^2 = N_0$ and we have $\mathbb{E}[w_m w_{m'}^*] = 0$ if $m \neq m'$. This noise damages the transmitted signal, and the vector $\mathbf{r}$ has to be properly processed to retrieve the information as presented in next section.

B Introduction to different demodulation strategies

The main contributions in the literature of FTN signaling focus on the receiver. Indeed, Nyquist signaling avoids ISI at reception after matched-filtering and down-sampling at time $T_s = T$ but FTN does not benefit from this advantage as presented in sub-Sec B.1. Another difficulty comes from the sampled noise after matched-filtering which looses its whiteness. In order to overcome these issues, different strategies are considered in the following sub-sections.

B.1 Nyquist receiver applied to FTN

The optimal symbol-level Nyquist receiver consists in different operations depicted in Fig. II.10. The first one is the filtering process by the matched-filter $h'(t)$ which aims

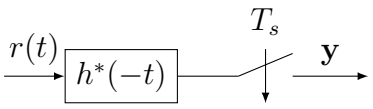

Figure II.10: Nyquist receiver

at maximizing the SNR after down-sampling. This filter is followed by a down-sampling operation at the symbol-rate before estimating the symbols. Hence, the resulting sequence $\mathbf{y} = [y_1, y_2, ..., y_{N_s}]^T$ where $y_{n+1} = (h' \star r \star \gamma)(nT_s)$ is defined as follows:

$$\mathbf{y} = \mathbf{D}\mathbf{H}^\dagger\mathbf{r} \tag{II.20}$$

where $\mathbf{H}^\dagger$ is the convolution matrix associated to the matched-filter $h'(t)$ and $\mathbf{D} = \mathbf{U}^\dagger$ is the $(N_s \times 2N_s)$ down-sampling matrix by a factor 2. Consequently, we have:

$$\mathbf{y} = \mathbf{G}\mathbf{s} + \mathbf{w}' \tag{II.21}$$

where $\mathbf{w}' = \mathbf{D}\mathbf{H}^\dagger\mathbf{w}$ is the down-sampled matched-filtered noise defined by $w'_{n+1} = (h' \star w \star \gamma)(nT_s)$ and we have:

$$\mathbf{G} = \mathbf{D}\mathbf{H}^\dagger\mathbf{H}\mathbf{U} \tag{II.22}$$

represents the $(N_s \times N_s)$ convolution matrix of the sampled Nyquist filter $g(t)$ expressed as $(\mathbf{G})_{a,b} = g\left((b-a)T_s\right)$.

In the particular case of Nyquist signaling, we notice that $\mathbf{G} = \mathbf{I}_{N_s}$ because $g(nT_s) = \delta_n$ with δ_n the Kronecker delta function. Moreover, the down-sampled noise $\mathbf{w}'$ in the signal $\mathbf{y}$ remains white and its PSD $\Gamma_{w'}(f)$ is expressed as follows:

$$\Gamma_{w'}(f) = \frac{N_0}{T_s}\sum_{k\in\mathbb{Z}} G\left(f - \frac{k}{T_s}\right) \tag{II.23}$$

$$= N_0 \text{ only for } \tau = 1 \tag{II.24}$$

Hence, if no channel coding is considered, the optimal Nyquist receiver returning the estimated symbols $\hat{\mathbf{s}} = [\hat{s}_1, \hat{s}_2, ..., \hat{s}_{N_s}]^T$ is the following:

$$\hat{s}_n = \underset{s_n\in\mathcal{M}}{\operatorname{argmin}} |y_n - s_n|^2 \tag{II.25}$$

However, if considering FTN signaling, an element y_n of the signal $\mathbf{y}$ can be decomposed as follows:

$$y_n = s_n + \sum_{\substack{m=1\\m\neq n}}^{N_s} g\left((m-n)T_s\right)s_m + w'_n \tag{II.26}$$

where the term $\sum_{\substack{m=1\\m\neq n}}^{N_s} g\left((m-n)T_s\right)s_m$ is called the ISI and the noise term w'_n is no longer white as expressed in (II.23) and depicted in Fig. II.6. Moreover, the interference power contained in the signal $\mathbf{y}$ does not change much for LCFTN or CCFTN. This is depicted in Fig. II.11. Indeed, the ISI contribution is the same unless at the edges of the signal $\mathbf{y}$.

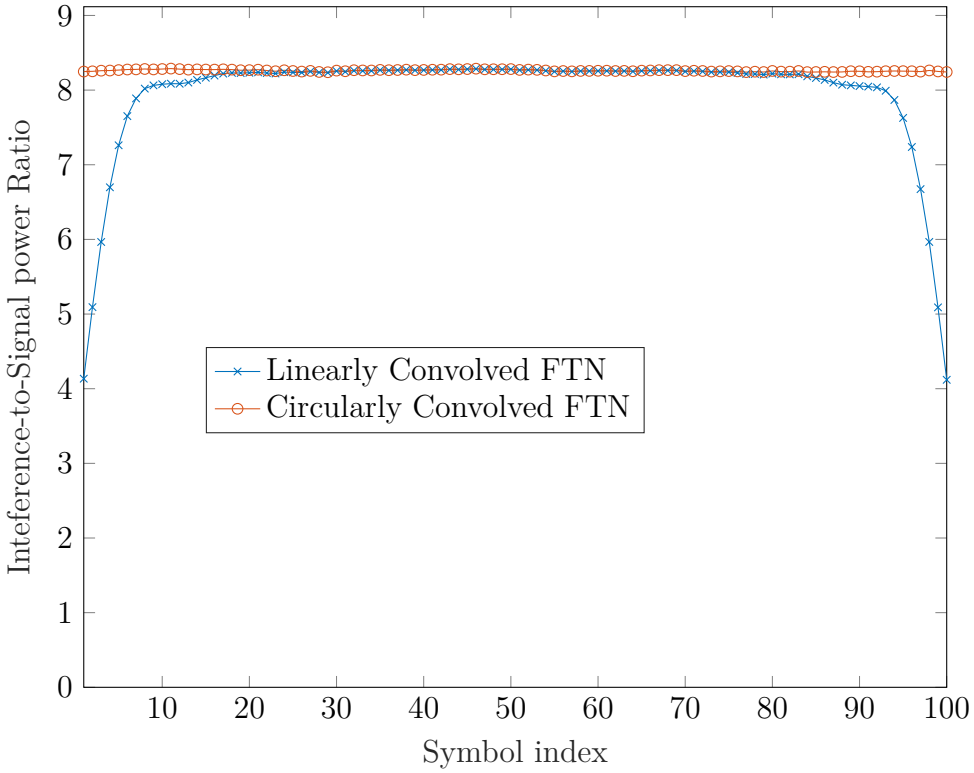

Figure II.11: Interference power against the symbol position within the frame of $N_s = 100$ symbols considering a BPSK modulation shaped by a RC($\beta = 0.3$) filter and $\tau = 0.1$

The first (resp. last) symbol of LCFTN signaling is only subject to future (resp. past) ISI and then it is corrupted by a twice less powerful interference. For large frames, the two types of FTN signaling are almost equivalently interfered.

Consequently, the correlation of w'_n and the ISI term are not addressed by the Nyquist estimator (II.25). Hence, specific strategies have been developed as detailed in the following.

B.2 Iterative joint equalization and decoding for bit-wise MAP estimation

Since the encouraging work of J. Mazo [Maz75; ML88] represented in Fig. II.12 for uncoded communications, FTN signaling has been considered as a candidate waveform for future communication standards [CL91]. Different rolloff values and constellations have also been explored [LG03; Rus07]. By extension, for a given rolloff β, we call the *Mazo bound* the lowest value of τ yielding no SNR loss when the ISI is processed by a MAP receiver. In the following, we focus on block estimations meaning that we suppose the whole received signal $\mathbf{r}$ to be known as well as the noise PSD N_0 which needs to be estimated in practical implementations. Moreover, the modulation, the shaping filter and any kind of waveforms parameters are also supposed to be known.

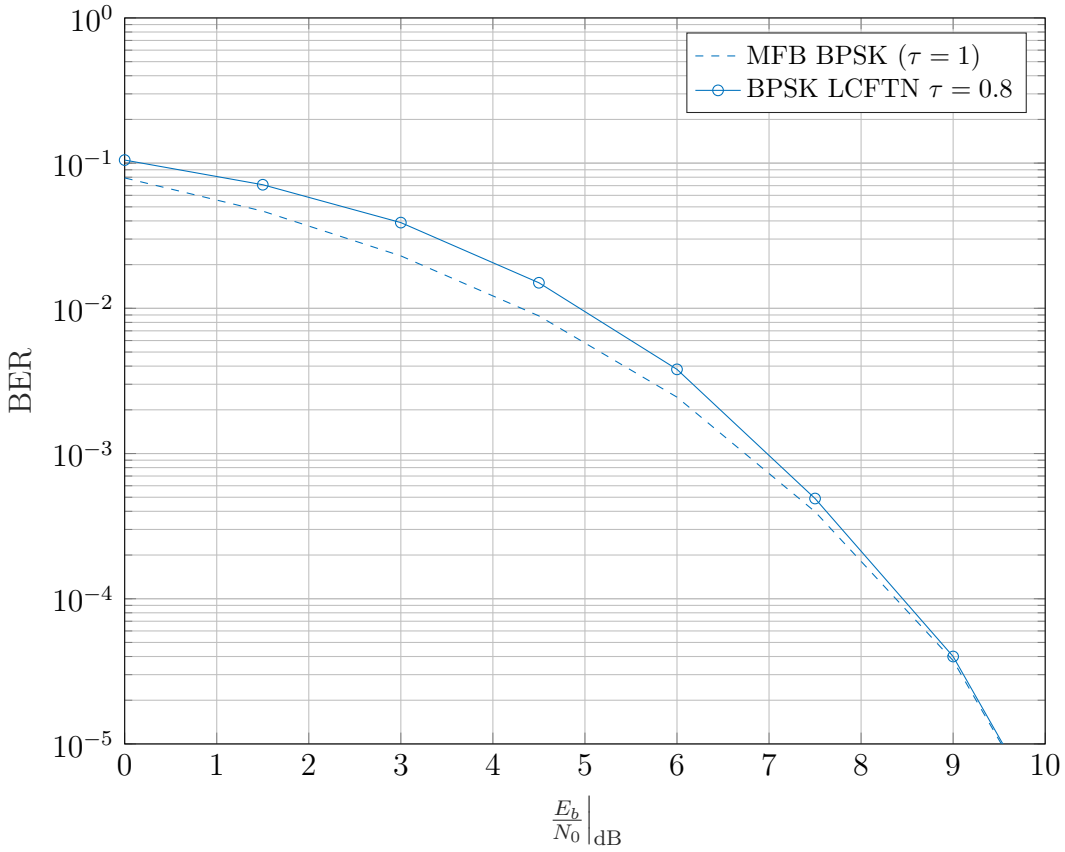

Figure II.12: The Mazo bound: FTN signaling achieves a 25% higher spectral efficiency without BER loss at high SNR with BPSK symbols shaped with a RC(0) filter processed by a ML receiver

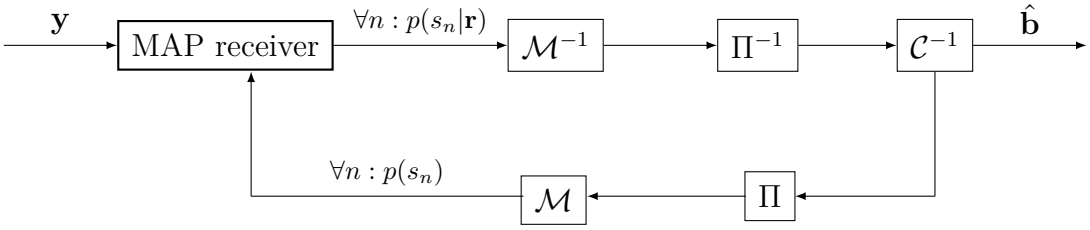

Figure II.13: Turbo-equalization receiver

In order to make the communication reliable, channel coding is generally considered with FTN signaling [Rus07; PAR08; PA12]. Hence, a joint equalization and decoding receiver with iterative processing referred as turbo-equalization [Dou+95a; TKS02; LGL01] can be considered. This type of iterative receivers depicted in Fig. II.13 allows huge computational complexity savings compared to the optimal joint receiver, while offering good performance and convergence properties [TKS02; TS11].

The MAP estimation of the sequence $\mathbf{b}$ aims at taking the following decision:

$$\hat{\mathbf{b}} = \underset{\mathbf{b}\in\mathbb{F}_2^{N_b}}{\operatorname{argmax}}\, p(\mathbf{b}|\mathbf{r}) \tag{II.27}$$

where the posterior probability mass function (pmf) $p(\mathbf{b}|\mathbf{r})$ can be written:

$$p(\mathbf{b}|\mathbf{r}) \propto p(\mathbf{r}|\mathbf{s})p(\mathbf{s}|\mathbf{d})p(\mathbf{d}|\mathbf{b})p(\mathbf{b}) \tag{II.28}$$

$$\propto p(\mathbf{r}|\mathbf{s}) \prod_{n=1}^{N_s} p(s_n|\mathbf{d}_n)p(\mathbf{d}_n|\mathbf{b})p(\mathbf{b}) \tag{II.29}$$

where $\mathbf{d}_n$ corresponds to the elements of the coded bits $\mathbf{d}$ mapped to the symbol s_n.

The pmf $p(\mathbf{d}|\mathbf{b})$ is computed by means of an interleaver and a BCJR algorithm whose complexity depends on the considered code. The symbol estimation process exchanges a sequence of Log Likelihood Ratio (LLR) with a decoder representing the Bernoulli distribution of the N_c coded bits $\mathbf{d}$. These LLRs coming from the decoder are denoted $\mathbf{L}^a$ and are converted by the *Soft-Mapper* into distributions on the symbols:

$$p(s_n) \approx p(s_n|\mathbf{d}_n)p(\mathbf{d}_n) \tag{II.30}$$

Conversely, the *Soft-Demapper* translates the symbol posterior distribution $p(s_n|\mathbf{r})$ into LLRs on the coded bits denoted by $\mathbf{L}^e$ assuming:

$$p(s_n|\mathbf{r}) \approx p(\mathbf{r}|\mathbf{s}_n)p(s_n) \tag{II.31}$$

A LLR of the mth bit of $\mathbf{d}$ is defined as follows:

$$L_m = \log \frac{p(d_m = 0|\mathbf{r})}{p(d_m = 1|\mathbf{r})} \tag{II.32}$$

where L_m represents the mth component of $\mathbf{L}^a$ or $\mathbf{L}^e$.

Soft-Mapper

The prior pmf $p(s_n), s_n \in \mathcal{M}$ of the nth symbol can be derived from the decoder LLRs $\mathbf{L}^a = [L_1^a, ..., L_{N_c}^a]^T$:

$$p(s_n) \propto \prod_{i=1}^{n_b} e^{-\mathcal{D}_i(s_n) L^a_{n \cdot n_b + i}}, s_n \in \mathcal{M} \tag{II.33}$$

where $\mathcal{D}_i(s_n)$ represents the ith bit of the symbol s_n.

Soft-Demapper

The Soft-Demapper is in charge of computing the LLRs from a given symbol posterior distribution $p(s_n|\mathbf{r})$. The posterior LLRs $\mathbf{L}^p = [L_1^p, ..., L_{N_c}^p]^T$ are then given by:

$$L_m^p = \log \frac{\sum_{s_n \in \mathcal{M}: \mathcal{D}_i(s_n)=0} p(s_n|\mathbf{r})}{\sum_{s_n \in \mathcal{M}: \mathcal{D}_i(s_n)=1} p(s_n|\mathbf{r})} \text{ where } m = n \cdot n_b + i, 1 \leq i \leq n_b \tag{II.34}$$

Once $\mathbf{L}^p$ is computed, the Soft-Demapper returns an extrinsic information $\mathbf{L}^e = \mathbf{L}^p - \mathbf{L}^a$ for removing any correlation with respect to the prior information.

In the following, we focus on the posterior distribution $p(s_n|\mathbf{r})$ of the transmitted symbols.

B.3 Posterior estimation with BCJR

In order to compute the posterior pmf $p(s_n|\mathbf{r})$, a BCJR algorithm has been proposed by [CB05]. To do so, we rewrite the posterior pmf expression yielding:

$$p(s_n|\mathbf{r}) \propto p(s_n) p(\mathbf{r}|s_n) \propto \sum_{\mathbf{s}_{\sim n} \in \mathcal{M}^{N_s - 1}} p(\mathbf{r}|\mathbf{s}) \prod_{i=1}^{N_s} p(s_i) \tag{II.35}$$

where we used the approximation $p(\mathbf{s}) = \prod_{i=1}^{N_s} p(s_i)$. The AWGN channel assumption gives the following derivation proposed by Ungerboeck for its Viterbi algorithm [Ung74]:

$$p(\mathbf{r}|\mathbf{s}) = \mathcal{N}_{\mathrm{C}}(\mathbf{r} : \mathbf{HUs}, \sigma_w^2) \tag{II.36}$$

$$\propto \prod_{n=1}^{N_s} \exp\left(\frac{2 s_n}{\sigma_w^2}\left(y_n - \frac{g_0 s_n^*}{2} - \sum_{l=1}^{L_\tau} g_l s_{n-l}\right)\right) \tag{II.37}$$

where LCFTN signaling is considered and we supposed that $s_n = 0$ for $n < 1$. The likelihood expression (II.37) is called the Ungerboeck model [Ung74]. It should be noted that the optimization is performed on the received signal $\mathbf{r}$ before any processing at reception. Nevertheless, (II.37) involves the elements of the received signal after matched-filtering and down-sampling $\mathbf{y}$.

Another alternative consists in filtering the received signal $\mathbf{r}$ by a Whitening Matched Filter (WMF) yielding the so-called Forney model [For72]. Both models have been extensively used in the literature. However, when FTN signaling is considered, such a WMF does not always exist especially when targeting high spectral efficiencies. Indeed, as soon as $\tau < (1+\beta)^{-1}$ the filter $g(t)$ has ranges of *zeros* in its spectrum and the matrix $\mathbf{G}$ turns out to be hardly invertible and the WMF is not stable. For this reason, we focus on the Ungerboeck model in this thesis. It should be noted that some manipulations can be used to approximate the WMF [Rus07].

Using the supposedly finite memory length of the Nyquist filter, the posterior pmf $p(s_n|\mathbf{r})$ can be computed:

$$p(s_n|\mathbf{r}) = \sum_{\sigma_n,\sigma_{n+1}} \alpha_n(\sigma_n)\gamma_n(\sigma_n,\sigma_{n+1})\beta_{n+1}(\sigma_{n+1}) \tag{II.38}$$

where $\sigma_n = [s_{n-2L_\tau}, s_{n-2L_\tau+1}, ..., s_{n-1}]^T$ characterizes a trellis state, $\alpha_n(\sigma_n)$ is the forward metric and $\beta_n(\sigma_n)$ the backward metric. These metrics can be efficiently computed in a recursive way [CFR01; CB05]:

$$\alpha_n(\sigma_n) = \sum_{\sigma_{n-1}} \alpha_{n-1}(\sigma_{n-1})\gamma_{n-1}(\sigma_{n-1},\sigma_n) \tag{II.39}$$

$$\beta_n(\sigma_{n+1}) = \sum_{\sigma_n} \beta_{n+1}(\sigma_{n+1})\gamma_n(\sigma_n,\sigma_{n+1}) \tag{II.40}$$

$$\gamma_n(\sigma_{n-1},\sigma_n) = p(s_n)\exp\left(\frac{2s_n}{N_0}\left(y_n - \frac{g_0 s_n^*}{2} - \sum_{l=1}^{L_\tau} g_l s_{n-l}\right)\right) \tag{II.41}$$

The computation of the BCJR metrics is then efficient as it takes benefit of the finite memory of the filter $g(t)$ truncated to $\pm 2L_\tau T_s$. Indeed, for each symbol index n, their exists $|\mathcal{M}|^{2L_\tau}$ different states σ_n and then $|\mathcal{M}|^{2L_\tau}$ metrics $\alpha_n(\sigma_n)$ and $\beta_n(\sigma_n)$. Then, the computation of $p(s_n|\mathbf{r})$ requires $|\mathcal{M}|$th more branch metrics to compute. Consequently, the resulting algorithm requires $|\mathcal{M}|^{2L_\tau+1}$ branch metric computations for each transmitted symbol.

B.4 Posterior estimation with Widely-Linear BP for FTN signaling with QAM modulations

A simple way to reduce the BCJR complexity consists in using a Widely-Linear (WL) BCJR [PC95] expressing the posterior pmf as follows:

$$p(s_n|\mathbf{r}) = p(s_{n,I}|\mathbf{r}_I)p(s_{n,Q}|\mathbf{r}_Q) \tag{II.42}$$

where the indices I (resp. Q) refer to the real (resp. imaginary) part of its associated vector. However, (II.42) only holds for QAM constellations and for real-valued Nyquist filters. Indeed, these two conditions guarantee the independence between the real and imaginary parts of a symbol s_n. It does not hold for any complex channel filter for instance. The computation of $p(s_{n,I}|\mathbf{r}_I)$ or $p(s_{n,I}|\mathbf{r}_I)$ amounts to considering a PAM constellation

with $\sqrt{|\mathcal{M}|}$ symbols. Hence, the BCJR computation of a LCFTN communication with a QAM constellation can be handled in $2|\mathcal{M}|^{L_\tau}$ branch metric computations per transmitted symbol. This drastically simpler yet optimal alternative has been presented in [CF14].

Apart from this optimal proposition, some BCJR approximations have been proposed to limit the exponential computation complexity. They are detailed in the following.

B.5 Approximate Posterior estimation algorithms

In order to reduce the computational complexity, the firstly proposed sub-optimal BCJR algorithms are the M-BCJR and T-BCJR algorithms [FA97]. The main idea consists in keeping a limited number of states for every symbol to estimate. However, they differ in their state discrimination strategies.

The T-BCJR keeps only the metrics $\alpha_n(\sigma_n)$ and $\beta_n(\sigma_n)$ higher than a given threshold, and sets to 0 the others. The advantage of the T-BCJR come from its very simple approach which, however, does not guaranty any complexity nor memory consumption for practical implementation because the number of kept metrics $\alpha_n(\sigma_n)$ and $\beta_n(\sigma_n)$ can be arbitrarily high. In order to overcome this issue, the M-BCJR only keeps M remaining states corresponding to the higher metrics. In terms of implementation, this algorithm then operates at fixed complexity, at the price of a partial sort of the metrics. This algorithm is known to offer a good performance-complexity trade-off.

Apart from these strategies, the RS-BCJR does not limit the number of states but rather reduces the states space [CFR01]. To do so, the states σ_n are reduced to a given number of components μ. Moreover, the branch metric computation needs to preserve its expression and hence determines the missing symbols $s_{n-2L_\tau}, s_{n-2L_\tau+1}, ..., s_{n-\mu-1}$ by taking anticipated decisions for each survivor state. The resulting algorithm also offers good convergence properties and is easier to implement compared to the M-BCJR.

Nowadays, the M*-BCJR which combines both the RS-BCJR and the M-BCJR is a reference for BCJR-based algorithms [SC05]. It consists in keeping a reduced number of survivors as the M-BCJR, but the non-survivor states are merged with survivor ones, rather than nullified as in the RS-BCJR and M-BCJR. To do so, each non-survivor path is redirected to a given state and the metrics are summed up. Then arises the question of the state merging strategy, which is fully explored in [AR07]. Note that other BCJR-based algorithms not presented here have been proposed in combination with channel shortening as in [RP12].

Hence, these approximate-based BCJR offer the ability to estimate the ISI while controlling the computational complexity. Even though the value of M or μ can be arbitrarily low, the complexity is still intractable for rich constellations. For this reason, we explore in the following sub-section MMSE-based techniques for iterative decoding.

B.6 Time-domain MMSE equalization with prior information

The concept of turbo-equalization with a Viterbi-based algorithm handling the ISI has been proposed for the first time in [Dou+95a]. Nevertheless, we can consider a MMSE equalizer for the symbol-level processing stage which aims at minimizing the MSE criterion expressed as follows:

$$\forall n \in [\![1, N_s]\!] : \hat{s}_n = \mathbf{q}_n^\dagger \mathbf{r} + p_n \text{ with } (\mathbf{q}_n, p_n) = \underset{(\mathbf{q},p)}{\operatorname{argmin}}\, v_n^{\tilde{\Psi}} \tag{II.43}$$

where $v_n^{\tilde{\Psi}} = \mathbb{E}|s^{\tilde{\Psi}} - s|^2$ represents the MSE of the estimate $s_n^{\tilde{\Psi}} = \mathbf{q}^\dagger \mathbf{r} + p$ of s_n, having $\mathbf{q}_n$ a filter and p_n a scalar. Moreover, we suppose having a Gaussian prior information on the symbols $\mathbf{s}$:

$$\forall n \in [\![1, N_s]\!] : p(s_n) = \mathcal{N}_{\mathrm{C}}(s_n : s_n^\Phi, v_n^\Phi) \tag{II.44}$$

where s_n^Φ represents the prior soft estimation of s_n and v_n^Φ its MSE.

The optimization (II.43) yields [TSK02]:

$$\mathbf{q}_n = v_n^\Phi \mathbf{f}_n^\dagger \mathbf{D}\mathbf{H}^\dagger \tag{II.45}$$

$$p_n = s_n^\Phi + v_n^\Phi \mathbf{f}_n^\dagger \mathbf{G}\mathbf{s}^\Phi \tag{II.46}$$

where $\mathbf{f}_n = \mathbf{\Sigma}^{-1}\mathbf{e}_n$ represents the MMSE filter, $\mathbf{\Sigma} = \mathbf{G}\mathbf{V}^\Phi + \sigma_w^2 \mathbf{I}_{N_s}$ the MMSE matrix and $\mathbf{V}^\Phi = \mathrm{diag}([v_1^\Phi, v_2^\Phi, ..., v_{N_s}^\Phi])$ the prior covariance matrix. Injecting the analytical expression of $\mathbf{q}_n$ and p_n into the definition of $s_n^{\tilde{\Psi}}$ yields:

$$s_n^{\tilde{\Psi}} = s_n^\Phi + v_n^\Phi \mathbf{f}_n^\dagger (\mathbf{y} - \mathbf{G}\mathbf{s}^\Phi) \tag{II.47}$$

It should be noted that we retrieve the expression of the received signal after matched filtering and up-sampling $\mathbf{y}$ as well as the aliased Nyquist filter $\mathbf{G}$. The resulting posterior MSE $v_n^{\tilde{\Psi}}$ is given by:

$$v_n^{\tilde{\Psi}} = v_n^\Phi (1 - v_n^\Phi \xi_n) \tag{II.48}$$

where $\xi_n = \mathbf{f}_n \mathbf{G} \mathbf{e}_n$.

The MMSE equalization can be used for both LCFTN and CCFTN, its complexity is majored by the filtering operation in (II.47). To solve this issue, different approaches detailed hereafter can be considered.

For LCFTN signaling, the filtering complexity can be lowered by assuming that most of the energy of s_n is contained within $\mathbf{y}_n = \mathbf{W}_n \mathbf{y} = [y_{n-N_w}, y_{n-N_w+1}, ..., y_{n+N_w}]^T$ where N_w is a trade-off value between the complexity and the equalizer performance, and $\mathbf{W}_n =$ is a $((2N_w + 1) \times N_s)$ window matrix defined as:

$$\mathbf{W}_n = \begin{pmatrix} \mathbf{0}_{n-1-N_w} \\ \mathbf{I}_{2N_w+1} \\ \mathbf{0}_{N_s-n-N_w} \end{pmatrix} \tag{II.49}$$

The estimation of s_n becomes the same as given (II.47) where we replace $\mathbf{y}$ by $\mathbf{y}_n$ and the $(N_s \times N_s)$ matrix $\mathbf{G}$ by the $((2N_w+1) \times N_s)$ matrix $\mathbf{G}_n = \mathbf{W}_n\mathbf{G}$. It follows that $\mathbf{\Sigma}$ becomes $\mathbf{\Sigma}_n \approx \mathbf{G}_n\mathbf{V}_n^{\Phi} + \sigma_w^2\mathbf{I}_{2N_w+1}$ which is now a $((2N_w+1) \times (2N_w+1))$ matrix as well as $\mathbf{V}_n^{\Phi} = \mathbf{W}_n\mathbf{V}^{\Phi}$, and the filter $\mathbf{f}_n = \mathbf{\Sigma}_n^{-1}\mathbf{e}_{N_w+1}$ has $2N_w+1$ coefficients. We will not detail the approximation leading to $\mathbf{\Sigma}_n$ because it goes beyond the scope of this thesis.

A frequency-domain approximation for LFTN signaling has also been proposed by [Sug13] based on a frequency-domain filtering to reduce the complexity. This approximation results on small performance losses but it requires a cyclic prefix known to damage the spectral efficiency. In order to remove the cyclic prefix constraint, [TPB16] proposed to use the CCFTN shaping method yielding the equalizer presented hereafter.

B.7 Frequency-domain MMSE equalization with prior information for CCFTN

The frequency-domain approach denoted FD-MMSE requires to approximate the prior MSE by their average value (II.46):

$$v_n^{\Phi} \approx v^{\Phi} \tag{II.50}$$

where $v^{\Phi} = N_s^{-1}\sum_n v_n^{\Phi}$ is the averaged prior MSE. Injecting this approximated prior MSE into the expressions of $s_n^{\tilde{\Psi}}$ and $v_n^{\tilde{\Psi}}$ yields:

$$s_n^{\tilde{\Psi}} = s_n^{\Phi} + v^{\Phi}\mathbf{f}_n^{\dagger}(\mathbf{y} - \mathbf{G}\mathbf{s}^{\Phi}) \tag{II.51}$$

$$v^{\tilde{\Psi}} = v^{\Phi}(1 - v^{\Phi}\xi) \tag{II.52}$$

where $\xi = \mathbf{f}_1\mathbf{G}\mathbf{e}_1$ and $v^{\tilde{\Psi}}$ do not depend on n anymore, having $\mathbf{\Sigma} = v^{\Phi}\mathbf{G} + \sigma_w^2\mathbf{I}_{N_s}$.

The frequency-domain equalization then arises naturally: the approximate estimation $s_n^{\tilde{\Psi}}$ can be re-written as follows:

$$s_n^{\tilde{\Psi}} = s_n^{\Phi} + v^{\Phi}\mathbf{e}_n^{\dagger}\mathbf{F}_{N_s}^{\dagger}\hat{\mathbf{\Sigma}}^{-1}(\hat{\mathbf{y}} - \hat{\mathbf{G}}\hat{\mathbf{s}}^{\Phi}) \tag{II.53}$$

where we replace all the v_n^{Φ} by v^{Φ} yielding $\hat{\mathbf{\Sigma}} = \mathbf{F}_{N_s}\mathbf{\Sigma}\mathbf{F}_{N_s}^{\dagger}$ the DFT of $\mathbf{\Sigma}$ to be diagonal, the vector $\hat{\mathbf{y}} = \mathbf{F}_{N_s}\mathbf{y}$ represents the frequency-domain received signal after matched filtering and up-sampling, and $\hat{\mathbf{s}} = \mathbf{F}_{N_s}\mathbf{s}$ is the DFT of the prior soft estimates. The complexity reduction comes from the diagonal structure of both $\hat{\mathbf{\Sigma}}$ and $\hat{\mathbf{G}}$ because $\mathbf{\Sigma}$ and $\mathbf{G}$ are circulant matrices when using CCFTN and the approximation (II.50). Hence, the computational complexity of $s_n^{\tilde{\Psi}}$ is majored by the FFT complexity performed in $O(N_s\log_2(N_s))$.

Consequently, both the time-domain and frequency-domain MMSE equalizers operate without knowledge on the constellation. This is a major difference compared to BCJR techniques. It results in algorithms performing a linear filter whose complexity does not depend on the constellation. The FD-MMSE approach goes further in the complexity reduction by performing a DFT at the price of small performance losses. Hence,

MMSE equalizers operate even with high order constellations, but their performance are promptly outperformed in case of severe ISI.

Based on these existing receivers of the literature, we propose in the following chapter a first contribution consisting in a multi-criteria analysis of single-carrier FTN signaling.

Chapter III

Faster-Than-Nyquist Signaling: A multi-criteria Analysis

Outline

This chapter is devoted to a multi-criteria analysis of FTN signaling with receivers of the literature. First, in Sec. A the different criteria involved in the comparison are presented, taking into account both transmitter and receiver constraints such as the spectral efficiency, the energy efficiency at transmission through the PAPR, but also the computational complexity. The analysis of these different criteria reveals significant difference between Nyquist and FTN signaling. For instance, FTN signaling can be used to improve the overall link budget of the communication. Therefore, the question raised by the interest of FTN signaling on a multi-criteria basis is not simple.

In order to evaluate the overall performance while taking benefits of FTN signaling improvements, we introduce a metric we call Effective SNR (ESNR). Then, we compare different FTN and Nyquist communications at fixed spectral efficiency using this metric with and without channel coding in Sec. B. The results have been published in a conference paper [Pet+18] and reveal a great interest to use FTN rather than Nyquist signaling when considering an AWGN channel model, up to a spectral efficiency of 2.5 bits/s/Hz. Higher spectral efficiencies are addressed further, in chapter IV with channel coding.

A Criteria of interest

In this section we detail the different criteria for the multi-criteria analysis of FTN signaling. The criteria are the following:

- spectral efficiency in sub-Sec A.1: in order to fairly evaluate the interest of FTN against Nyquist signaling, we present comparisons at fixed spectral efficiency. For this reason, we focus on the achievable spectral efficiency of a FTN communication and compare with Nyquist signaling.
- energy efficiency in sub-Sec A.2: the transmitter dedicates most of its energy to the power amplifier. Furthermore, the power amplifier efficiency is mostly determined by the PAPR of the communication which depends on the compression factor τ, among other parameters. This yielded us to develop a metric called ESNR aiming at penalizing waveforms with high PAPR.
- computational complexity in sub-Sec A.3: in order to be embedded in real devices, the receiver handling the ISI in real-time has stringent complexity constraints.

These different criteria are used further in the multi-criteria comparisons of Sec. B.

A.1 Achievable Spectral efficiency of FTN signaling

In this sub-section, we focus on the achievable spectral efficiency without transmission errors as described by C. Shannon [Sha48], which can be reached using gaussianly distributed symbols. This general model is then particularized to a FTN communication

by constraining the shaping filter. Then, we restrict the symbols distribution to the discrete set of the constellation using the Shamai Laroia Conjecture (SLC). This yields us to highlight the interest of the FTN technique in terms of spectral efficiency compared to Nyquist signaling.

Optimal communication: the Shannon capacity

The Shannon capacity represents the higher data-rate for an errorless communication of bandwidth W over an AWGN channel. This capacity does not presuppose any particular modulation, channel coding, constellation nor symbols correlation. In other words, the capacity quantifies the achievable spectral efficiency assuming optimally modulated bits for an errorless communication. One way to achieve the capacity C expressed as follows would be to assume Gaussian iid symbols [Sha48]:

$$C = W \log_2 \left(1 + \frac{P_x}{N_0 W}\right) \text{ in bits/s} \tag{III.1}$$

This bound can also be expressed in bits/s/Hz as a spectral efficiency $\eta_1 = \frac{C}{W}$. We use the letter η here to characterize the achievable spectral efficiency bound of an errorless communication, while the spectral efficiency of a practical communication scheme is denoted hereafter ρ. Indeed, the achievable spectral efficiency is limited by operational considerations: the shaping filters, symbol-rates, application to FTN and Nyquist signaling, constrained symbol distributions and channel codes. In the following, we present this step-by-step analysis of the achievable spectral efficiency for both FTN and Nyquist signaling.

Constrained filter: the generalized Shannon capacity

Consider the case of a particular shaping or deterministic and time invariant channel filter $h(t)$ with frequency spectrum $H(f)$ over the bandwidth W instead of a constant magnitude. Assuming that the filter is normalized, i.e. $\int_{-\frac{W}{2}}^{\frac{W}{2}} |H(f)|^2 \, \mathrm{d}f = 1$, the expression of the capacity generalizes to:

$$\eta_2 = \frac{1}{W} \int_{-\frac{W}{2}}^{\frac{W}{2}} \log_2 \left(1 + \frac{P_x}{N_0} G(f)\right) \, \mathrm{d}f \tag{III.2}$$

where $G(f) = |H(f)|^2$.

In practice, samples of information called *symbols* are transmitted at a discrete time T_s. The derivation of the achievable spectral efficiency under this assumption is addressed hereafter.

Constrained symbol-rate: the constrained capacity

We assume now a transmission of an infinite sequence of iid symbols separated by T_s through the filter $h(t)$ of bandwidth W. The resulting ISI after matched-filtering and up-sampling yields the information η_3 obtained by replacing $G(f)$ by its folded version:

$$\eta_3 = \frac{1}{W}\int_{-\frac{1}{2T_s}}^{\frac{1}{2T_s}} \log_2\left(1+\frac{P_x}{N_0}\sum_{k\in\mathbb{Z}} G\left(f-\frac{k}{T_s}\right)\right)\,\mathrm{d}f \tag{III.3}$$

and η_3 is necessarily limited by the less constrained spectral efficiency η_2, itself lower than η_1 for the same reason. Hence, we obtain:

$$\eta_3 \leq \eta_2 \leq \eta_1 \tag{III.4}$$

where the right inequality can also be obtained using the Jensen inequality with the concave function $\log_2(1+\cdot)$. F. Rusek carried out the main results on capacity under the term *Constrained Capacity* [RA07] for FTN signaling presented in the following.

Achievable spectral efficiency of Nyquist and FTN signaling

In FTN signaling, the achievable spectral efficiency η_{FTN} has the same expression as η_3 with a filter $G(f)$ chosen to be a Nyquist filter with orthogonality time $T = \frac{1+\beta}{W}, \beta \in [0,1]$, and the symbol duration is assumed to be smaller that the orthogonality time: $T_s = \tau T, \tau \in (0,1]$. Under these considerations, (III.4) yields:

$$\forall(\tau,\beta) : \eta_{\mathrm{FTN}} \leq \eta_2 \leq \log_2\left(1+\frac{P_x}{N_0 W}\right) \tag{III.5}$$

Moreover, Nyquist signaling being a particular case of FTN signaling, its spectral efficiency η_{Ny} is obtained from (III.5) considering the case $\tau = 1$. $G(f)$ being a Nyquist filter, we have $\sum_{k\in\mathbb{Z}} G(f-\frac{k}{T_s}) = T_s = T$ and η_{FTN} reduces to:

$$\eta_{\mathrm{Ny}} = (1+\beta)^{-1}\log_2\left(1+\frac{P_x(1+\beta)}{N_0 W}\right) \tag{III.6}$$

and (III.5) becomes:

$$\forall\beta : \eta_{\mathrm{Ny}} \leq \eta_2 \leq \log_2\left(1+\frac{P_x}{N_0 W}\right) \tag{III.7}$$

Note that if $g(t)$ is a RC(0), the three terms are equal: $\eta_{\mathrm{Ny}} = \log_2\left(1+\frac{P_x}{N_0 W}\right)$.

From the inequalities (III.5) and (III.7), we know that the achievable spectral efficiencies η_{FTN} and η_{Ny} are limited by the same quantity given in η_2 with $G(f)$ a Nyquist filter. However, we do not have any order relation between η_{FTN} and η_{Ny} at this point.

If $g(t)$ is not a cardinal sine RC(0), it has been demonstrated in [RA09a] that FTN signaling can achieve higher spectral efficiencies than Nyquist signaling:

$$\exists \tau < 1 : \eta_{\text{FTN}} > \eta_{\text{Ny}} \tag{III.8}$$

and particularly for $\tau = (1+\beta)^{-1}$ which in fact maximizes η_{FTN}. This can be shown by the left inequality of (III.5) becoming an equality for $\tau = (1+\beta)^{-1}$. Indeed, the compression $\tau = (1+\beta)^{-1}$ is the limit for which *zeros* appear in the aliased Nyquist filter PSD. Hence, the expression $\sum_{k\in\mathbb{Z}} G\left(f - \frac{k}{T_s}\right)$ of (III.3) can be replaced by $G(f)$ yielding $\eta_{\text{FTN}} = \eta_2$.

To sum-up, we have the following inequalities:

$$\forall \beta > 0, \exists \tau < 1 : \eta_{\text{Ny}} < \eta_{\text{FTN}} \leq \log_2\left(1 + \frac{P_x}{N_0 W}\right) \tag{III.9}$$

This expression is very meaningful because it suggests that:

- there is always a FTN compression factor τ for which FTN signaling achieves a higher spectral efficiency than Nyquist signaling,
- constraining the shaping filter decreases the achievable spectral efficiency of Nyquist signaling, this is not necessarily the case for FTN.

In the following, we call SNR the following ratio:

$$\text{SNR} = \frac{P_x}{N_0 W} \tag{III.10}$$

The evolution of η_{FTN} and η_{Ny} against the SNR is illustrated in Fig. III.1 for different RC filters and $\tau = 0.5$. The spectral efficiency gain provided by FTN signaling achieves $\eta_1 = \log_2\left(1 + \frac{P_x}{N_0 W}\right)$ and growths with the SNR. For $\beta = 1$, the spectral efficiency of FTN signaling approaches 3 bits/s/Hz while Nyquist signaling achieves 2.2 bits/s/Hz for a SNR of 10 dB. On the SNR, FTN signaling achieves 2.2 bits/s/Hz at 7 dB and then performs 3 dB better than Nyquist signaling.

Fig. III.2 is obtained considering a fixed SNR set to 10 dB for different values of τ. At fixed rolloff (i.e. at fixed color), the difference between the plain and dashed lines corresponds to the achievable spectral efficiency gain brought by FTN signaling, growing with the time compression. This gain is maximized for $\tau = (1+\beta)^{-1}$. Moreover, a FTN communication with $\tau = 0.5$ and RC(0.3) is shown to reach the same achievable spectral efficiency as a Nyquist communication with $\beta = 1$.

These results show the gain brought by FTN signaling on the achievable spectral efficiency compared to Nyquist signaling. It offers an additional parameter for the waveform design which can be tuned depending on the considered filter. The value $\tau = (1+\beta)^{-1}$ achieves the higher spectral efficiency. However, the concept of achievable spectral efficiency remains a theoretical bound reachable by gaussianly distributed symbols for in-

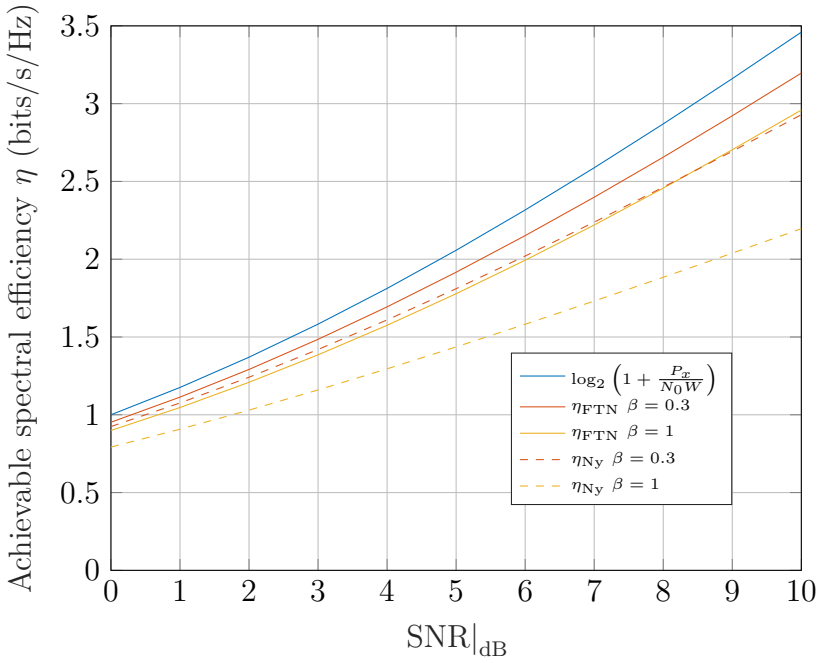

Figure III.1: Spectral efficiency against the SNR for $\tau = 0.5$, RC filters

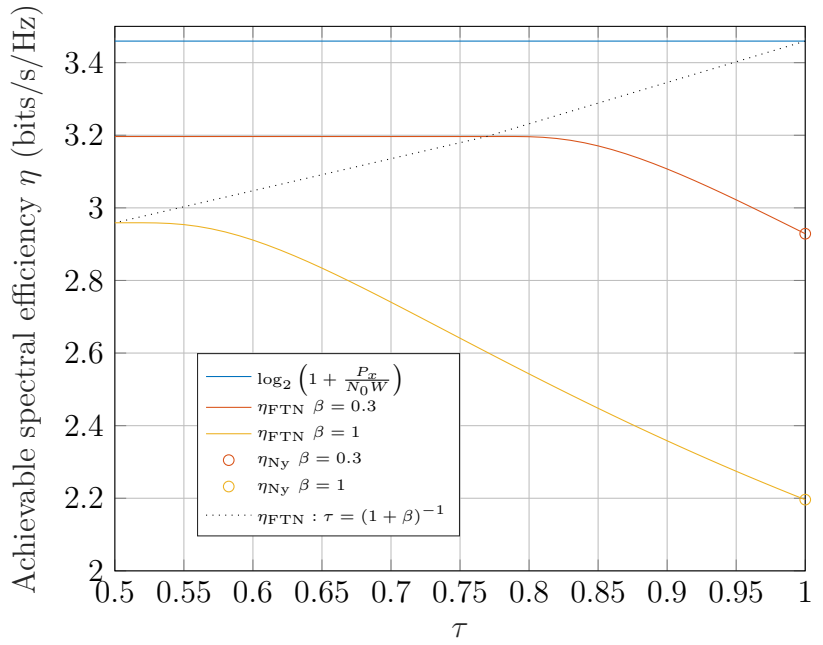

Figure III.2: Spectral efficiency against τ at SNR = 10 dB, RC filters

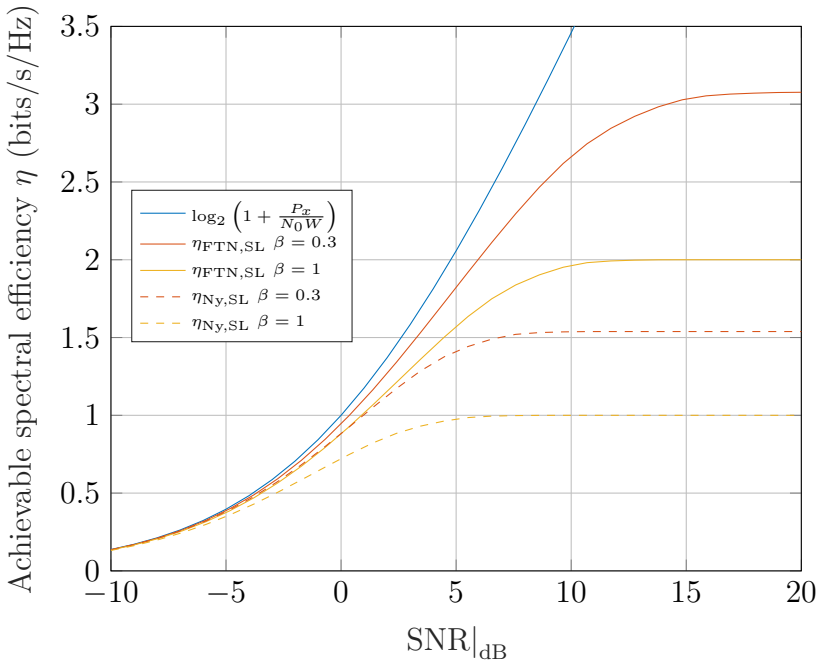

Figure III.3: Spectral efficiency against the SNR for $\tau = 0.5$, RC filters and a QPSK

stance. In practice, the symbols are distributed in a discrete set. Hence, we propose to go further by evaluating the impact of the symbols distribution on the spectral efficiency.

Constrained symbols distribution

For practical implementations, we assume a linear modulation of symbols distributed in a finite complex alphabet called *constellation*. This supplementary constraint makes the spectral efficiency analysis more difficult. Indeed, there exists no analytical expression of the achievable spectral efficiency for a given constellation.

Fortunately, Shamai Laroia proposed in [SL96] a good and easy to compute conjecture of the highest spectral efficiency at fixed constellation. In fact, this SLC does not bound the spectral efficiency but it represents a good approximation, especially at high SNR. We can compute its expression for FTN signaling, we note the resulting spectral efficiencies $\eta_{\text{FTN,SL}}$ for FTN and $\eta_{\text{Ny,SL}}$ for Nyquist signaling.

The SLC spectral efficiencies are depicted in Fig. III.3 and III.4 considering a Quadrature PSK (QPSK) constellation. The results are very different compared to the previous comments with gaussianly distributed symbols. First, the spectral efficiency appears clearly to be bounded at high SNR, this is a direct consequence of the constellation discretization. We can only transmit a finite number of information bits at each symbol-rate. Moreover, at high SNR we have: $\eta_{\text{FTN,SLC}} = \tau^{-1}\eta_{\text{Ny,SLC}}$ where $\eta_{\text{FTN,SLC}}$ and $\eta_{\text{Ny,SLC}}$ are computed with the same rolloff. In other words, with an optimal channel code, FTN signaling increases the symbol-rate by the factor τ without transmission error at high SNR.

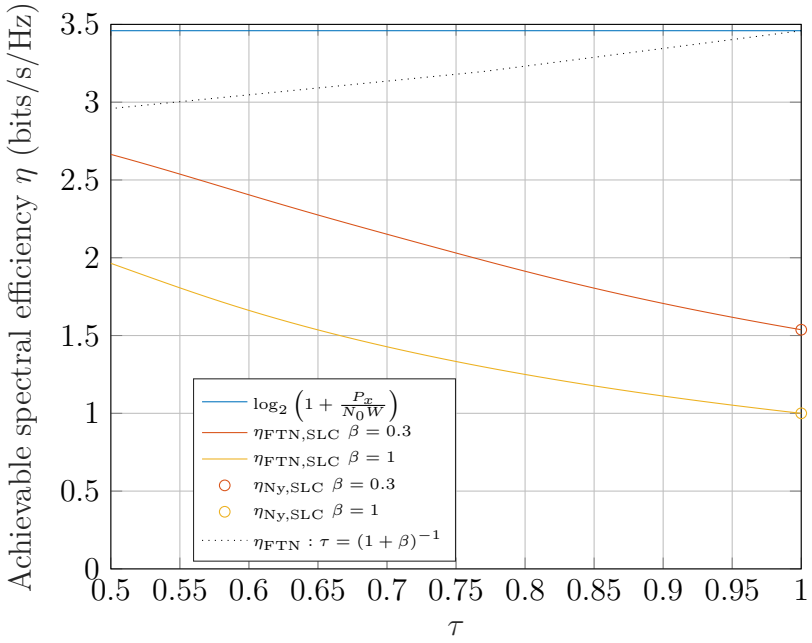

Figure III.4: Spectral efficiency against τ at SNR = 10 dB, RC filters and a QPSK

Although these results suggest high benefits in favor of FTN signaling, it should be noted that the SLC is an approximation rather than a real bound for the achievable spectral efficiency. Hence, more accurate simulations can be performed assuming practical low-complexity receivers adapted to the considered channel: see [BFC09] for AWGN channel assumption, but also [Pie+13] for the case of nonlinear satellite channels and [CF14] for the case of nonlinear optical channels. Conclusion is that, under the assumption of considering low-complexity receivers and discrete constellations, values of τ lower than $(1+\beta)^{-1}$ allow even higher achievable spectral efficiencies than Nyquist signaling.

More recently, [Jan+17] showed that using a particular linear precoding combined with a rRC(β) shaping filter is equivalent to leaving out the pre-coding if the shaping is performed with a new rRC(β') filter where $\beta' = \tau(1+\beta) - 1$. In this case, the received filter is then matched to the new rRC(β') and the equalization process can be adapted accordingly. Nevertheless, using directly this new filter instead of performing linear pre-coding implies a more difficult timing synchronization process. Furthermore, the newly defined filter rRC(β') has a lower rolloff $\beta' \leq \beta$ yielding a larger time support requiring more taps for a given out-of-band power leakage. Hence, FTN signaling with rRC(β) with linear pre-coding should be preferred and achieves the same spectral efficiency than a Nyquist signaling scheme with a rRC(β') shaping filter (for $\tau \geq (1+\beta)^{-1}$). Consequently, FTN signaling not only compensate the excess-bandwidth loss, but also improves the spectral efficiency if $\tau < (1+\beta)^{-1}$ compared to Nyquist signaling.

Hence, FTN signaling appears to be a very promising technique on the spectral efficiency point of view. However, at this point, we assumed an optimal communication coding scheme. We propose now to work with a given channel code and study its impact on the spectral efficiency.

Constrained coding: comparisons at fixed spectral efficiency

For a given code with coderate R, a FTN communication achieves a useful bit-rate of $\frac{R\log_2|\mathcal{M}|}{T_s}$ over the communication bandwidth $W = \frac{1+\beta}{T}$. Hence, the spectral efficiency defined as the ratio between those two quantities is expressed as:

$$\rho = \frac{R\log_2|\mathcal{M}|}{T_s}\frac{T}{1+\beta} = \frac{R\log_2|\mathcal{M}|}{\tau(1+\beta)} \tag{III.11}$$

In fact, the definition of ρ reveals the challenge of FTN signaling: it offers a supplementary freedom degree with the compression factor τ. This additional parameter can compensate a higher rolloff β or a lower constellation order $\log_2|\mathcal{M}|$ than Nyquist signaling to achieve a same spectral efficiency. Hence, at fixed channel code, spectral efficiency ρ and constellation, FTN signaling can decrease the rolloff β of Nyquist signaling while compensating with τ. This can help minimizing the PAPR in single-carrier signaling for instance (see sub-Sec. A.2). Another way of fixing the spectral efficiency ρ with FTN signaling is to decrease the constellation order $\log_2|\mathcal{M}|$ and compensate with τ. This spreads out the constellation elements, while suffering from ISI produced by $\tau < 1$.

The comparison between Nyquist and FTN signaling at fixed bandwidth and spectral efficiency is scarcely considered in the literature. In the following, we evaluate the performance of FTN and Nyquist signaling with different values of R, $|\mathcal{M}|$, β and τ allowing to achieve a same spectral efficiency ρ.

This analysis yields encouraging conclusions because FTN signaling achieves higher spectral efficiencies than Nyquist signaling at fixed SNR. Also, the SLC shows that constraining the constellation drastically limits the achievable spectral efficiency. However, this assumption is necessary for energy efficiency purposes of the transmitter as detailed hereafter.

A.2 PAPR & IAPR for energy efficiency

The energy efficiency at the transmitter side is an important point of interest for embedded devices. Furthermore, the power amplifier at transmitter plays a major role but spends about 70 % of the overall energy. Generally, its consumption mainly depends on its output saturation power P_{sat} regardless of the transmitted instantaneous power $|x(t)|^2$. Nevertheless, power amplifiers saturate over a given power, which damages the signal's spectrum and decreases the demodulation performance at reception. In order to avoid this saturation at transmission, the average power P_x has to be penalized by a factor called the *output backoff*. This effect is represented in Fig. III.5 where the non linear power amplifier response has been modeled with the commonly used Rapp model [Rap91]. We can observe that the power amplifier characteristic function can be decomposed in three regimes:

- the linear regime: the output power is proportional to the input power.

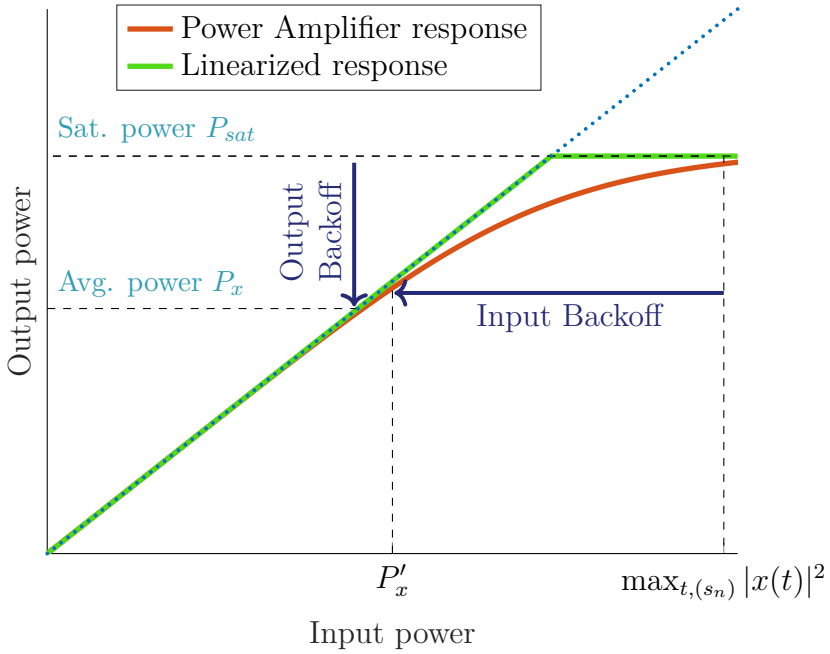

Figure III.5: Power amplifier power response and backoff

- the compression regime: the output power is not proportional anymore to the input power. This regime can be linearized with pre-distorsion techniques if knowing the transfer function. We make this assumption in the following.
- the saturation regime: the output power is P_{sat} whatever the input power value above a given input power threshold.

The instantaneous power $|x(t)|^2$ of a transmitted signal is a continuous-time wide-sense first-order cyclostationary random process with period T_s and a function depending on the modulation, the transmitted sequence, and the shaping filter. With FTN signaling, the time-compression factor τ also plays a major role as presented hereafter. For the sake of simplicity, we generally omit the channel code dependency for backoff analysis, i.e. we assume iid symbols. We suppose an infinite number of transmitted symbols: $N_s \longrightarrow +\infty$ and we consider the instantaneous power $|x(t)|^2$ in the stationary regime by omitting the edge effects of the shaping filter operation. Hence, as shown in Chap. II, we can assume that both LCFTN and CCFTN generate signals with similar instantaneous power statistics. In the following, we present how the output backoff value is determined.

Peak-to-Average Power Ratio

In order to evaluate the required output backoff for a communication, we are interesting in characterizing the waveform dependent PAPR defined as follows [GP93]:

$$\text{PAPR} = \max_{t,(s_n)} \frac{|x(t)|^2}{P_x} \tag{III.12}$$

For a given transmitted signal, the PAPR corresponds to the required input backoff to avoid any saturation on the transmitted signal $x(t)$.

Hence, the PAPR has a negative impact on the budget as it decreases the effective energy from the consumed energy. In order to tackle this problem, Continuous Phase Modulation (CPM) waveforms are interesting for their PAPR of 0 dB when the energy consumption is a critical aspect of the targeted application. However, this type of signaling goes beyond the scope of this thesis. Other studies devoted to FTN signaling also propose to reduce the PAPR of FTN signaling [Cai+19; Liu+18].

The PAPR is not usually considered as it is for practical applications. Indeed, the maximum power of a waveform $\max_{t,(s_n)_n} |x(t)|^2$ could be scarcely achieved by the instantaneous power. Hence, instead of ensuring no saturation, we prefer controlling the probability $\theta \in [0, 1]$ of the instantaneous input power to exceed a given threshold γP_x. This problem is addressed in the following.

Instantaneous-to-Average Power Ratio

The Complementary Cumulative Distribution Function (CCDF) $\tilde{\Upsilon}_x(t, \gamma)$ of the Instantaneous-to-average Power Ratio (IAPR) is defined by [Med+17] as follows:

$$\tilde{\Upsilon}_x(t, \gamma) = \mathbb{P}\left(\frac{|x(t)|^2}{P_x} > \gamma\right) \tag{III.13}$$

where the probability set corresponds to the possible bit sequences for a given compression factor τ and RC filter $h(t)$ characterized by its rolloff β. The time dependency of $\Upsilon_x(t, \gamma)$ does not suit our needs, more precisely, we define $\Upsilon_x(\gamma)$ as the timing ratio for which $|x(t)|^2$ is higher than a threshold γP_x. This can be formalized as follows:

$$\Upsilon_x(\gamma) = \lim_{T_0 \to +\infty} \frac{1}{T_0} \int_{\frac{T_0}{2}}^{\frac{T_0}{2}} \mathbb{1}(|x(t)|^2 > \gamma P_x) \mathrm{d}t \tag{III.14}$$

where $\mathbb{1}(|x(t)|^2 > \gamma P_x)$ equals 1 if $|x(t)|^2 > \gamma P_x$ and 0 else. We show in App. A that $\Upsilon_x(\gamma)$ corresponds to the averaged IAPR CCDF over a cyclostationarity period:

$$\Upsilon_x(\gamma) = \frac{1}{T_s} \int_0^{T_s} \tilde{\Upsilon}_x(t, \gamma) \mathrm{d}t \tag{III.15}$$

From this definition, we define the IAPR of $x(t)$ associated to the probability θ as:

$$\mathrm{IAPR}(\theta) = \min\{\gamma : \Upsilon(\gamma) \leq \theta\} \tag{III.16}$$

It follows that an output backoff set to $\mathrm{IAPR}(\theta)$ ensures a saturation probability of θ for the transmitted signal $x(t)$. Note that this holds for low values of θ ($< 10^{-2}$) which ensures that the input backoff is similar to the output backoff as presented in Tab. III.1. A graphical representation of $\Upsilon(\gamma)$ and $\mathrm{IAPR}(\theta)$ is given in Fig. III.6. It should be noted

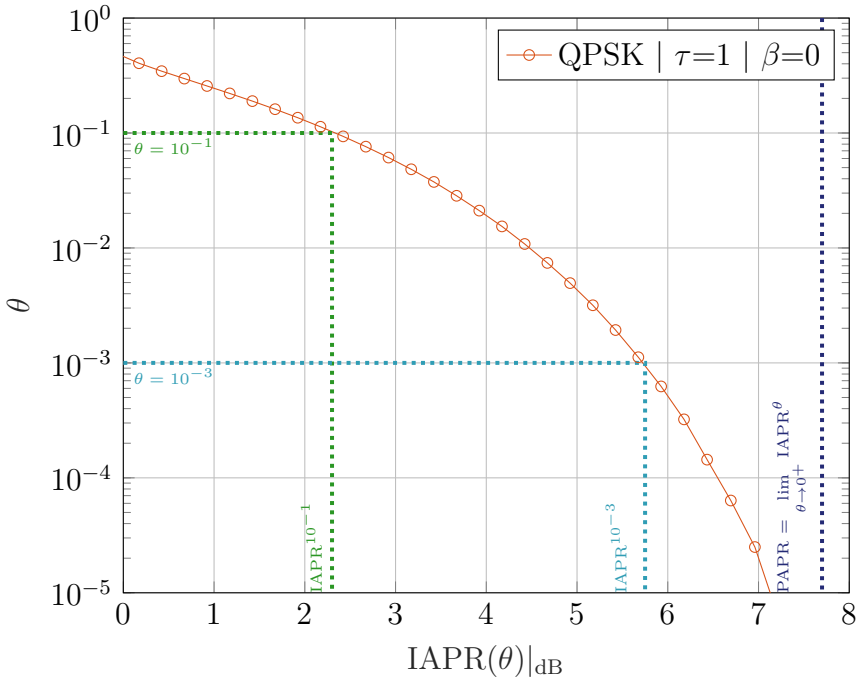

Figure III.6: IAPR CCDF for a QPSK Nyquist signal shaped with a cardinal sine filter

that the IAPR is linked to the PAPR as we have:

$$\text{PAPR} = \lim_{\theta \to 0^+} \text{IAPR}(\theta) \tag{III.17}$$

The average power of $x(t)$ ensuring a saturation probability of θ is also related to the effective power required by the signal transmission P_{sat}:

$$P_x = \frac{P_{sat}}{\text{IAPR}(\theta)} \tag{III.18}$$

where θ is a trade-off parameter between the energy efficiency and the distortion of $x(t)$ due to its saturation. In Fig. III.7 and Fig. III.8 we assume a Nyquist QPSK signal $x(t)$ passing through a power amplifier with a perfectly linear regime up to a saturation power $P_{sat}|_{\text{dB}} = \text{IBO}|_{\text{dB}} + P_x|_{\text{dB}}$ where the input backoff denoted IBO is set to a given value. It results in a saturated signal with a lower average power P'_x, and the output backoff OBO can then been measured as: $\text{OBO}|_{\text{dB}} = P_{sat}|_{\text{dB}} - P'_x|_{\text{dB}}$. The considered backoff values and saturation probabilities θ are given in Tab. III.1 where we can see that the input and output backoffs are similar for low saturation probabilities. Consequently, in the following we assimilate the input to the output backoff, and we assume that $P_x = P'_x$. Furthermore, we observe that the distortion causes an error rate deterioration but also damages the transmitted signal PSD.

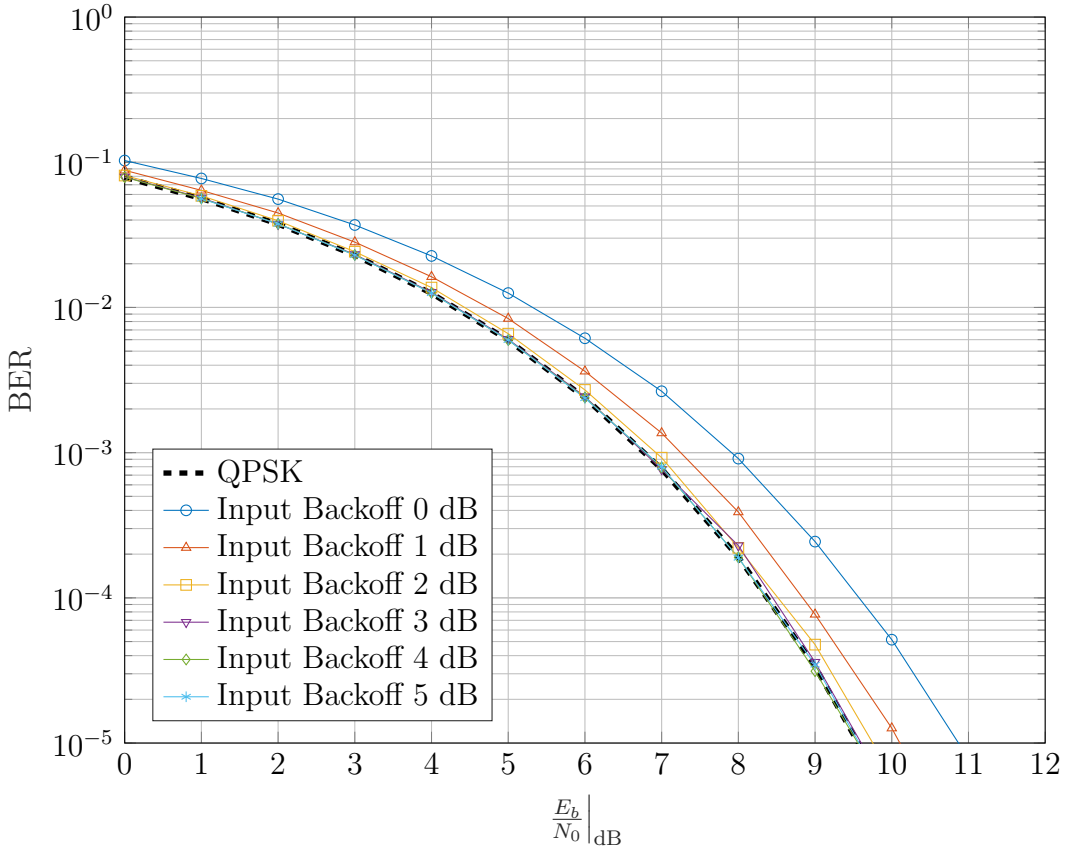

Figure III.7: BER of a QPSK Nyquist comm. with a rRC(0.3) for different input backoffs

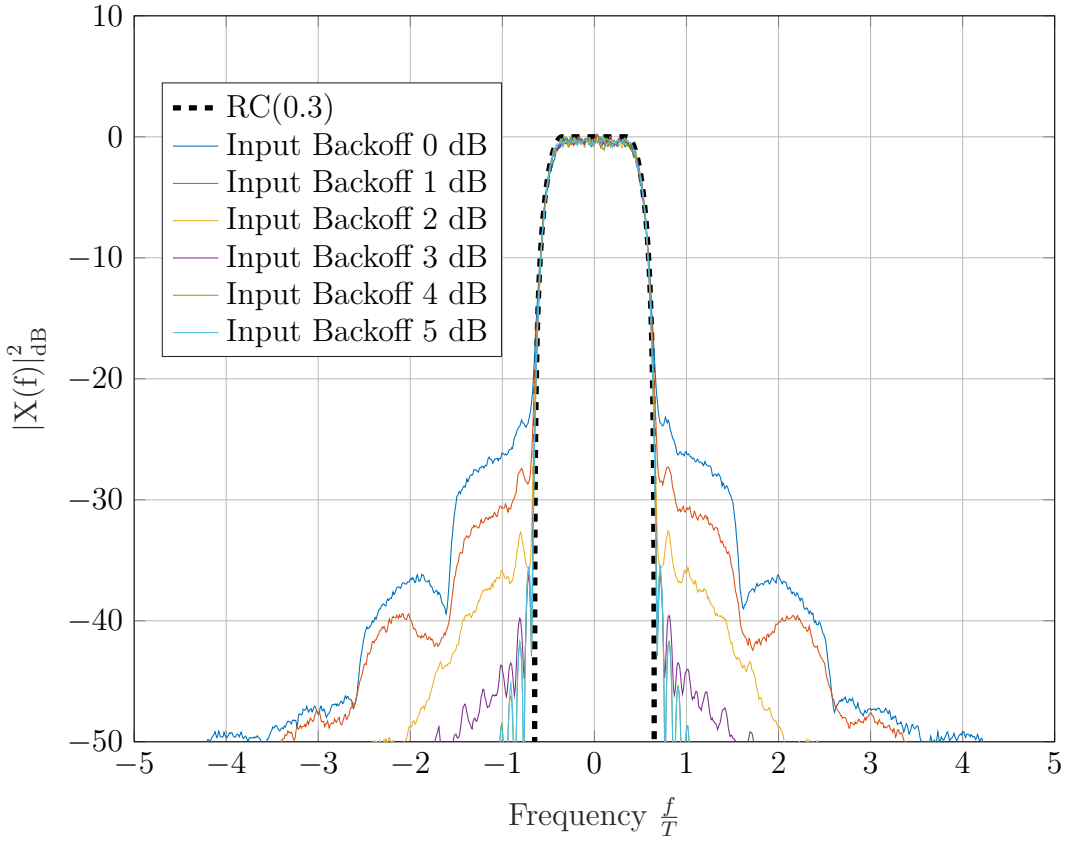

Figure III.8: Periodogram of a QPSK Nyquist signal with a rRC(0.3) for different input backoffs

Table III.1: Backoffs of QPSK Nyquist with a rRC(0.3) for different values of θ

Input Backoff	0 dB	1 dB	2 dB	3 dB	4 dB	5 dB
Output Backoff	0.87 dB	1.35 dB	2.09 dB	3.01 dB	4.00 dB	5.00 dB
Sat. proba. θ	$5 \cdot 10^{-1}$	$3 \cdot 10^{-1}$	$9 \cdot 10^{-2}$	$2 \cdot 10^{-2}$	$6 \cdot 10^{-4}$	$< 10^{-5}$

Effective SNR

In order to evaluate the performance of the proposed reception techniques, error rates are usually represented as a function of the received SNR. The received SNR is defined as the ratio between the received signal's power and the white Gaussian noise power over the bandwidth W:

$$\text{SNR} = \frac{P_x}{N_0 W} = \frac{E_b}{N_0}\rho \tag{III.19}$$

where the average power is given by:

$$P_x = \frac{1}{T_s}\int_0^{T_s} \mathbb{E}|x(t)|^2 \mathrm{d}t \tag{III.20}$$

$$= \frac{E_b R \log_2 |\mathcal{M}|}{T_s} \tag{III.21}$$

assuming that $g(0) = 1$. The relation (III.19) shows that, for a fixed spectral efficiency ρ, comparing error rates as a function of the received SNR is equivalent to representing against $\frac{E_b}{N_0}$.

In order to fairly compare different waveforms, we propose to take into account the energy efficiency of their transmitted signal. The idea is to assimilate the effective power of the communication to the saturation power, instead of the signal's average power. Indeed, for a given power amplifier, a waveform requiring a higher backoff will need to decrease its average power resulting in a lower effective SNR. For this reason, the effectively consumed energy does not depends on P_x but rather on P_{sat}. To do so, we replace P_x in (III.19) by the saturation power P_{sat} in the expression (III.19) of the SNR. This yields a metric we propose to call the *ESNR* defined as follows:

$$\text{ESNR} = \frac{P_{sat}}{N_0 W} = \text{IAPR}(\theta) \cdot \text{SNR} \tag{III.22}$$

where we used (III.18) to recover the expression involving the SNR. Hence, the ESNR amounts to penalizing the commonly used SNR metric by the IAPR(θ) of the waveform. Up to the author knowledge, the definition we propose for the ESNR formalized from our definition of IAPR(θ) has never been used to represent error rates. Note that similar metrics have been proposed as in [Pie+13].

Hence, the ESNR metric enables to take into account the link budget as well as the energy consumption of a communication. Moreover, it offers a comparison of different

Table III.2: Real-valued multiplications of the proposed receivers for one symbol, and their ability to be symbol level parallelized

Receiver	Number of multiplications	parallel.
FD-MMSE-IC	$8\log_2(N_s) + 3\lvert\mathcal{M}\rvert + 4$	yes
MMSE-IC	$8\log_2(2N_w + 1) + 8N_w^2 + 16N_w + 3\lvert\mathcal{M}\rvert + 8$	yes
RS-BCJR	$2^{\log_2\lvert\mathcal{M}\rvert\mu}(\mu + 3 \times 2^{\log_2\lvert\mathcal{M}\rvert})$	no
M*-BCJR	$3\lvert\mathcal{M}\rvert 2^{\log_2\lvert\mathcal{M}\rvert}$	no

waveforms for a given power amplifier. At reception, the major constraint is to limit the computational complexity of the signal's processing. This requirement is addressed in the following sub-section.

A.3 Computational complexity

The receiver of a digital communication has strong complexity constraints because it performs a real-time processing of the information. The interest of FTN signaling is then conditioned by the overall performance, including the complexity efficiency. In practice, such a complexity evaluation is difficult as it highly depends on the targeted application, the implementation, the ability for parallelism. In the following, we assimilate the complexity of a receiver to its number of multiplication given in Tab. III.2. We also provide the ability of each receiver to be symbol level parallelized which yet does not impact the complexity, but could be decisive in real-time applications as the parallelization allows a lower latency.

In the following, we present Nyquist and FTN signaling error rate comparisons at fixed spectral efficiencies using the proposed ESNR metric.

B Multi-criteria evaluation of FTN signaling

This section is devoted to multi-criteria comparisons between FTN and Nyquist signaling. We conduct IAPR comparisons for different rolloff values and compression factors at fixed spectral efficiencies. But also, we show that the cases with $\tau = 1$ are never the optimal choices in terms of the IAPR metric. Moreover, we know since the work of Mazo that choosing $\tau < 1$ does not necessarily induce SNR losses. This suggests an interest for FTN signaling at fixed spectral efficiency.

In order to go further, we propose in a second sub-section to take into account the performance of the different waveforms considering both the SNR and the IAPR metrics. This is possible by comparing the performance against the previously introduced ESNR metric. To do so we consider commonly used receivers of the literature described

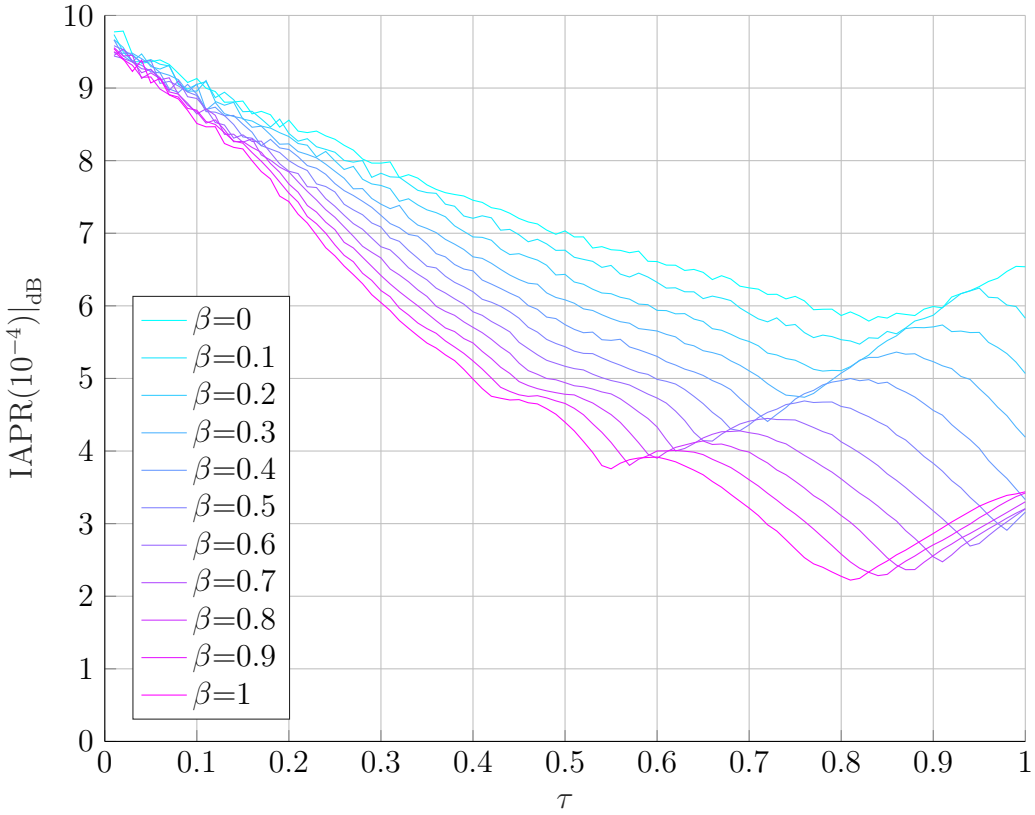

Figure III.9: IAPR(10^{-4}) of a QPSK with rRC filters $L_\tau = 30$ for different values of τ and β

in Chap. II. This second analysis corroborates the same hypothesis: FTN signaling has more potential than Nyquist signaling at fixed spectral efficiency.

B.1 IAPR of FTN Signaling

The IAPR metrics are computed assuming a low saturation probability of $\theta = 10^{-4}$ and rRC filters truncated to $L = 30$. As represented in Fig. III.8, these values have almost no impact on the transmitted signal spectrum.

The resulting IAPR(10^{-4}) for different values of τ and α are represented in Fig. III.9 considering a QPSK constellation. We do not consider here other constellation orders, but the trends remain the same. The Nyquist cases maintain competitive IAPR but do not always achieve minimal values. This is especially true for low and high excess bandwidth factors. Indeed, the compression factor of $\tau = 0.8$ generally optimizes the IAPR while achieving a 20% spectral efficiency increase compared to Nyquist signaling. The IAPR gain can go up to 1 dB for $\beta = 1$.

At fixed spectral efficiency, FTN signaling can also optimize the IAPR at the price of ISI [Luc+16]. This is illustrated in Fig. III.10 for $\rho = 2$ bits/s/Hz and Fig. III.11 for $\rho = 3$ bits/s/Hz where the rolloff factor β is determined by the corresponding values of

ρ, τ and $\log_2 |M|$. Several observations can be made:

- PSK modulations offer 2 dB better IAPR compared to QAM ones, even for FTN signaling (unless for BPSK and QPSK).
- the combinations which optimizes the IAPR are scarcely achieved by Nyquist signaling but rather by FTN signaling. They provide up to 0.5 dB gain at $\rho = 2$ bits/s/Hz (see the 8-PSK/8-QAM of Fig. III.10) and 0.8 dB at $\rho = 3$ bits/s/Hz (see the 32-PSK/32-QAM of Fig. III.11). However, these moderated gains are not the most profitable ones as they assume high order constellations which perform worst in terms of SNR. Consequently, we will rather focus on lower order constellations offering higher gains while targeting the same spectral efficiencies as explained in the following point.
- At fixed spectral efficiency and modulation, FTN signaling can decrease by 2 dB the IAPR compared to Nyquist signaling (see the QPSK of Fig. III.10, and the 8-PSK/8-QAM of Fig. III.11). This is particularly interesting for combinations of τ and β above the Mazo bound, which is the case here. Indeed, these waveforms are not penalized by SNR losses if the ISI is handled by a ML detector.

It appears clearly that Nyquist signaling is never the best way to improve the IAPR as FTN signaling allows several dB gains. This makes the FTN technique a serious candidature for satellite communication standards for instance, where the very high constraint on the rolloff in DVB-S2X could be relaxed by slightly compressing the symbols as claimed in [Pie+13]. These optimistic results have yet to be combined with SNR performance in order to draw a multi-criteria conclusion of its potential interest. This is conducted in sub-Sec. B.2 for uncoded signaling and sub-Sec. B.3 with channel coding.

B.2 Error rate using the Effective SNR for uncoded signaling

This sub-section constitutes the main contribution of the following paper [Pet+18]. As a first step, we consider uncoded communications evaluated through the Binary Error Rate (BER) at reception using both the SNR and ESNR metrics. In order to reveal the potential of FTN signaling, we do not limit the computational complexity. Hence, the ISI is handled by a Viterbi algorithm which optimizes the ML criterion.

The resulting BER are represented in Fig. III.12 against SNR and in Fig. III.13 against ESNR for $\rho = 2$ bits/s/Hz. For each constellation order, the FTN compression factor chosen is the one which best minimizes the BER against ESNR. The SNR representation shows no gain brought by FTN signaling because it introduces ISI and is always outperformed by its Nyquist counterpart. However, when considering the IAPR through the ESNR representation, FTN signaling appears to perform 1.3 dB better than Nyquist signaling. Moreover, this conclusion holds for any constellation order.

Fig. III.14 and III.15 illustrate similar comparisons for a higher spectral efficiency set to $\rho = 2.5$ bits/s/Hz. For such a spectral efficiency, the poorest constellation achieved

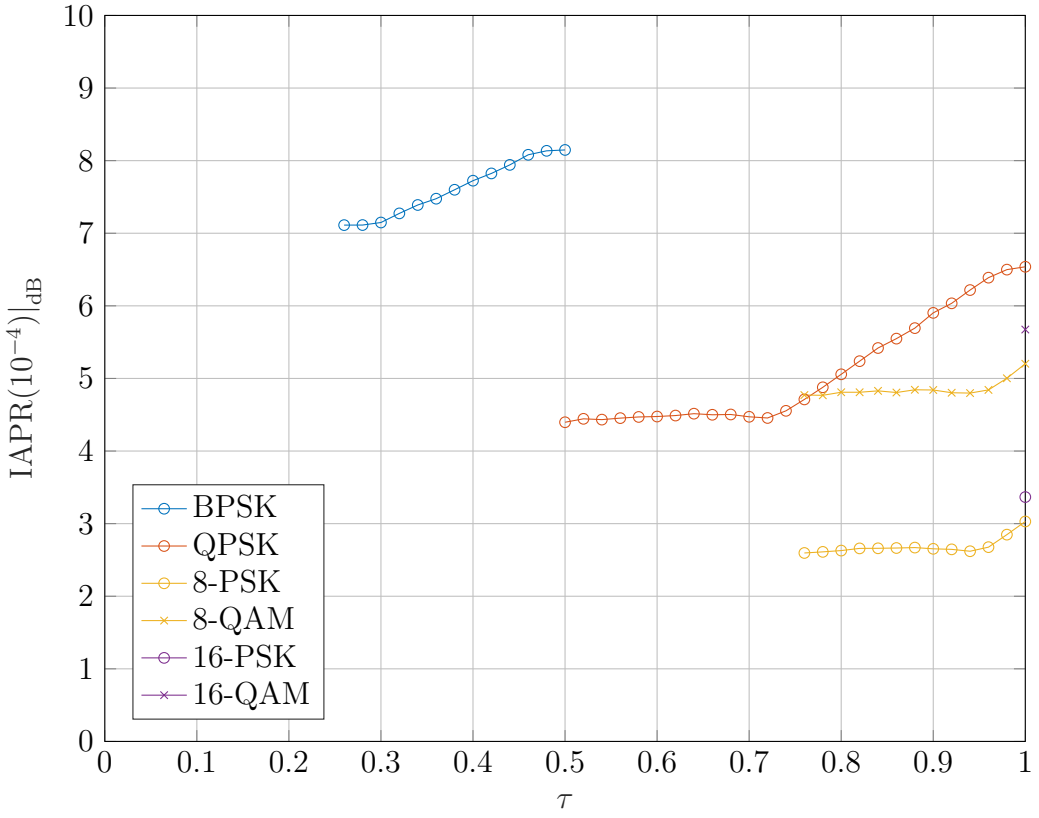

Figure III.10: IAPR(θ) against τ for different constellations achieving $\rho = 2$ bits/s/Hz

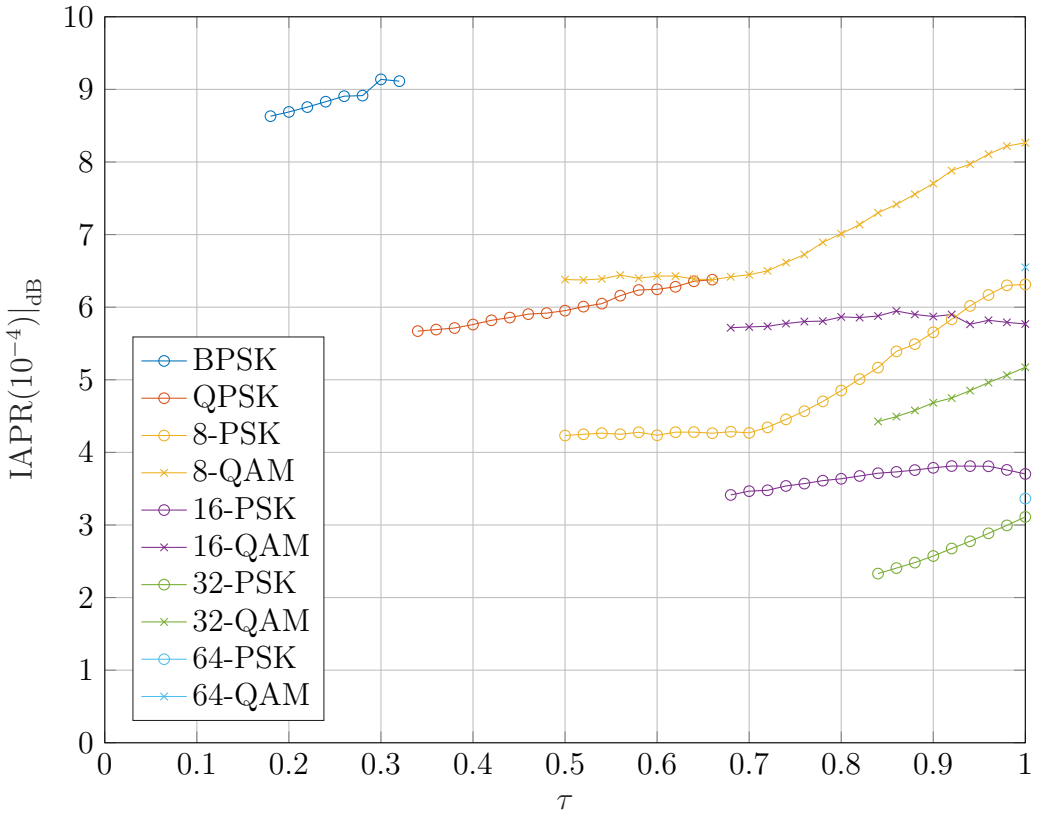

Figure III.11: IAPR(θ) against τ for different constellations achieving $\rho = 3$ bits/s/Hz

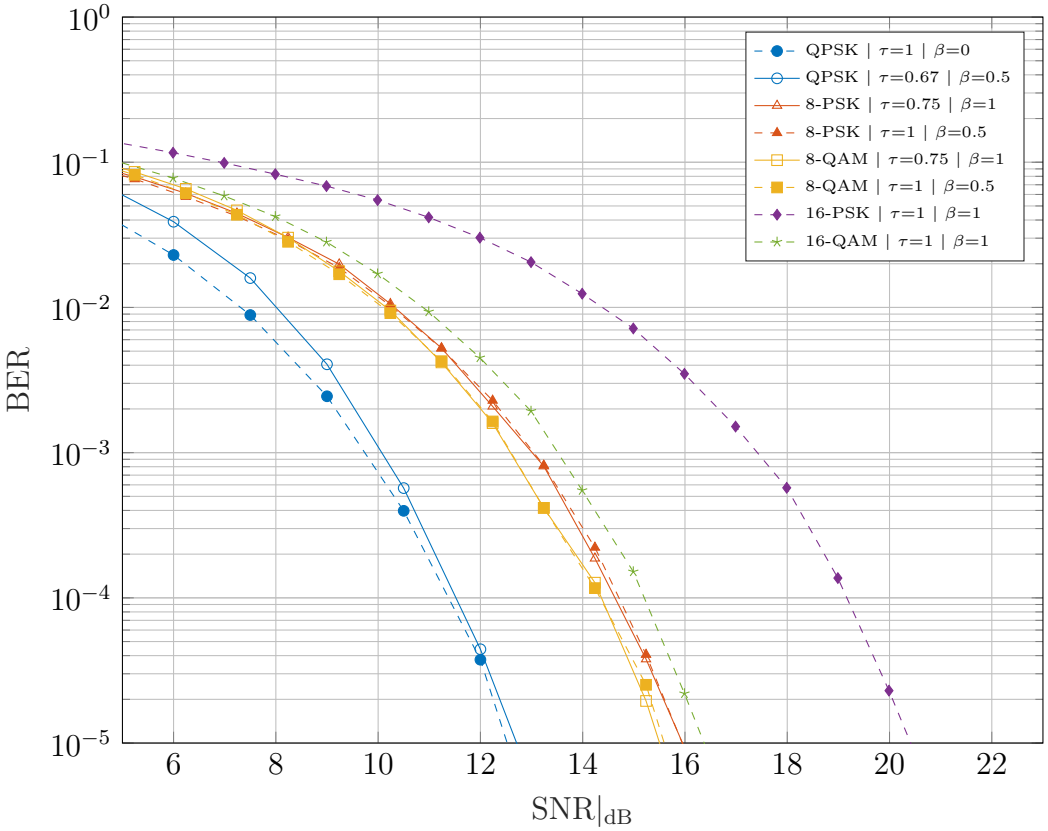

Figure III.12: BER against SNR for different FTN (solid) and Nyquist (dashed) waveforms achieving $\rho = 2$ bits/s/Hz

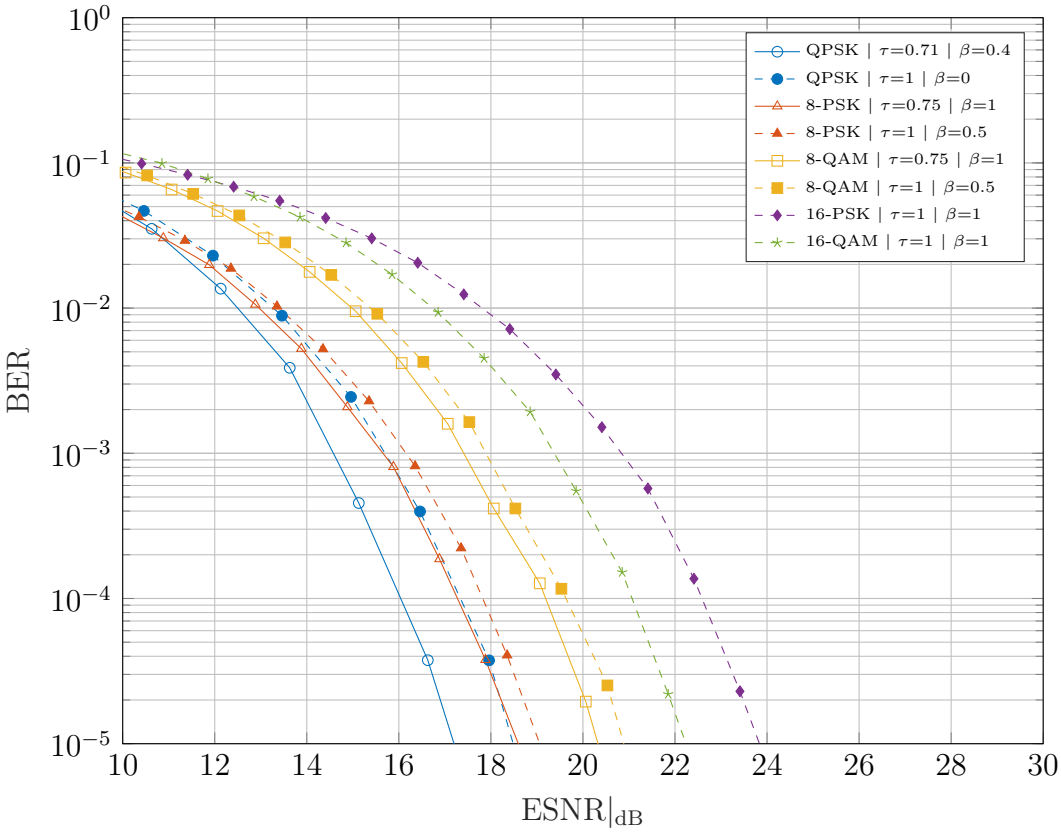

Figure III.13: BER against ESNR for different FTN (solid) and Nyquist (dashed) waveforms achieving $\rho = 2$ bits/s/Hz

Table III.3: Gain using FTN rather than Nyquist signaling for BER $= 10^{-4}$ and $\theta = 10^{-4}$ processed by a ML receiver

	Spectral efficiency (bits/s/Hz)			
	1.5	2	2.5	3
$(\log_2 \lvert\mathcal{M}\rvert, \tau, \beta)$	(2, 0.67, 1)	(2, 0.67, 0.5)	(2, 0.8, 0)	(2, 0.67, 0)
SNR gain	0 dB	0 dB	2.8 dB	1.2 dB
ESNR gain	0.4 dB	1.3 dB	2.5 dB	1.9 dB

by Nyquist signaling are 8-PSK and 8-QAM. For this reason, its is outperformed with a QPSK FTN communication by almost 3 dB, even using a SNR comparison. When considering the ESNR representation, the IAPR contribution yields a total gain of 2.5 dB.

Further spectral efficiencies have been considered and the SNR and ESNR gains are summed-up in Tab. III.3. It appears that high spectral efficiencies benefit to FTN signaling with a SNR comparison. However, when considering the ESNR, FTN signaling always offer significant gains compared to Nyquist signaling, up to 2.5 dB for $\rho = 2.5$ bits/s/Hz.

Finally, it should be recalled that we obtained these conclusions with a high complexity ML receiver. When considering an MMSE equalization, low gains are brought by FTN signaling without channel coding. Hence, we present in the following sub-section channel coded results with MMSE-based strategies for turbo-equalization.

B.3 Error rate using the Effective SNR for channel coded signaling

We suppose a communication composed of $N_b = 8192$ information bits coded with a $(7, 5)_8$ convolutional Recursive Systematic Code (RSC) with coderate $R = \frac{1}{2}$. The considered modulations are a QPSK and a 8-PSK for FTN and Nyquist signaling due to their low IAPR and BER. The shaping operation is performed with a rRC filter which rolloff values are adjusted to fit the targeted spectral efficiencies. At receiver, we perform a FD-MMSE turbo-equalizer with 8 iterations [TSK02].

A spectral efficiency of $\rho = 1$ bits/s/Hz has been considered, and the corresponding IAPR values are given in III.10. We represented in Fig. III.16 the error rates for Nyquist signaling and the best FTN communications using the SNR metric and in Fig. III.17 using the ESNR one. From the SNR representation, it appears clearly that the FD-MMSE equalizer combined with the decoder removes the ISI. The ESNR representation shows a gain of 1 dB provided by FTN signaling compared to Nyquist signaling. The best performing combination is a QPSK modulation with $\tau = 0.7$ and $\beta = 0.4$.

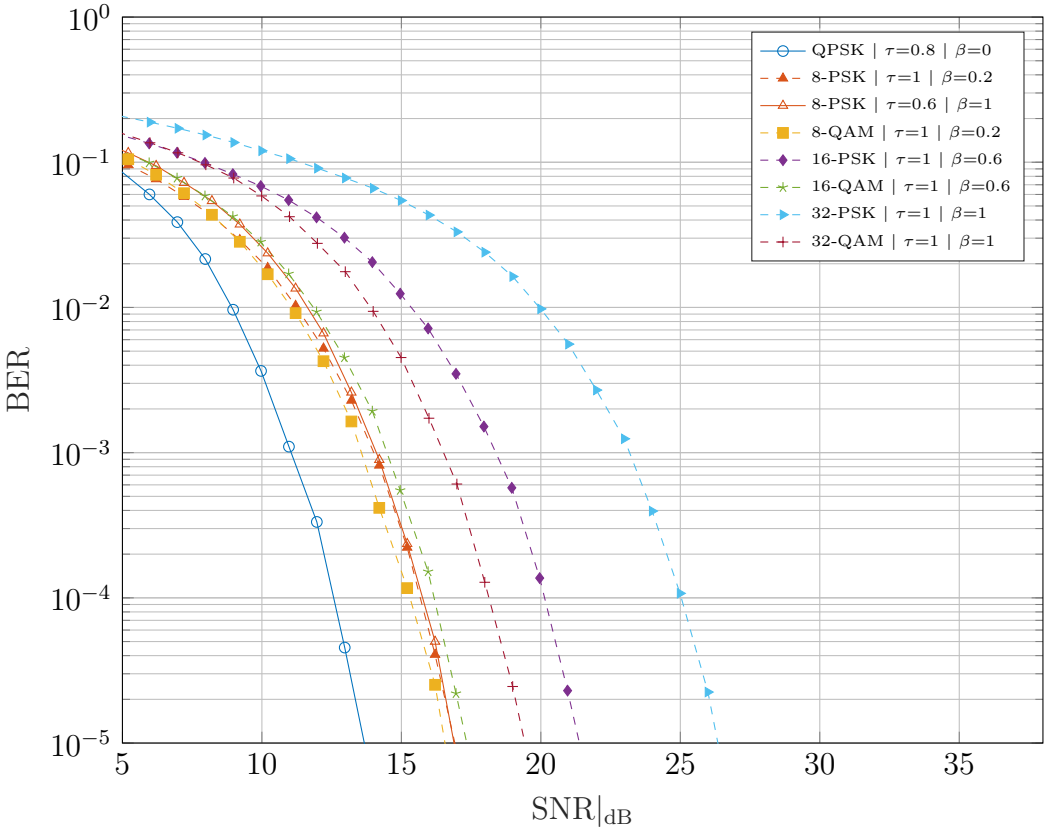

Figure III.14: BER against SNR for different FTN (solid) and Nyquist (dashed) waveforms achieving $\rho = 2.5$ bits/s/Hz

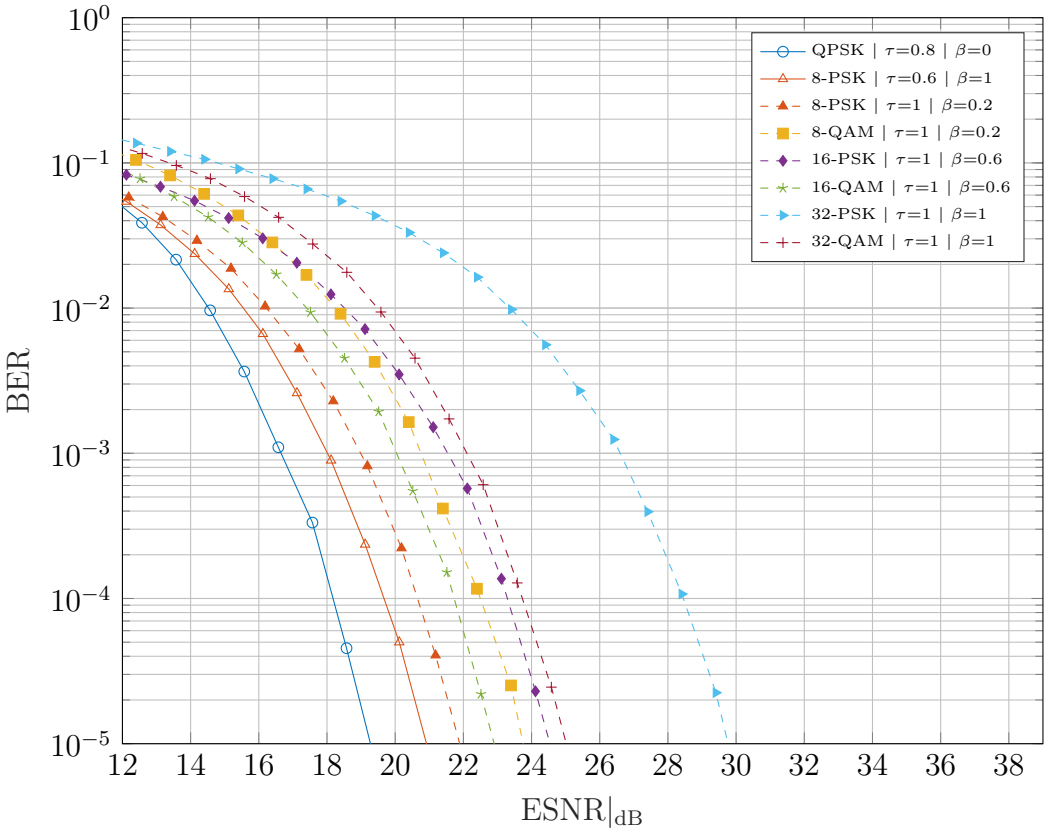

Figure III.15: BER against ESNR for different FTN (solid) and Nyquist (dashed) waveforms achieving $\rho = 2.5$ bits/s/Hz

Similar comparisons are provided for $\rho = 1.5$ bits/s/Hz in Fig. III.17 and III.17 using $\tau = \frac{2}{3}$ for both the FTN communications. No Nyquist QPSK modulation can achieve such a spectral efficiency. Hence, the SNR gain goes up to 2 dB while the ESNR gain outperforms Nyquist signaling by almost 2.5 dB.

C Conclusion

FTN signaling can offer significant ESNR gains with channel coding up to 2 bits/s/Hz. For higher spectral efficiencies, the MMSE based equalizers cannot handle the ISI anymore and BCJR based receivers are necessary. However, for such high spectral efficiencies, BCJR algorithms are intractable and cannot be implemented. Therefore, there is a need to explore new reception strategies able to process the ISI coming from FTN signaling, while keeping strong constraints on the computational complexity. This is addressed in next chapter by means of a message-passing algorithm called *Expectation Propagation*.

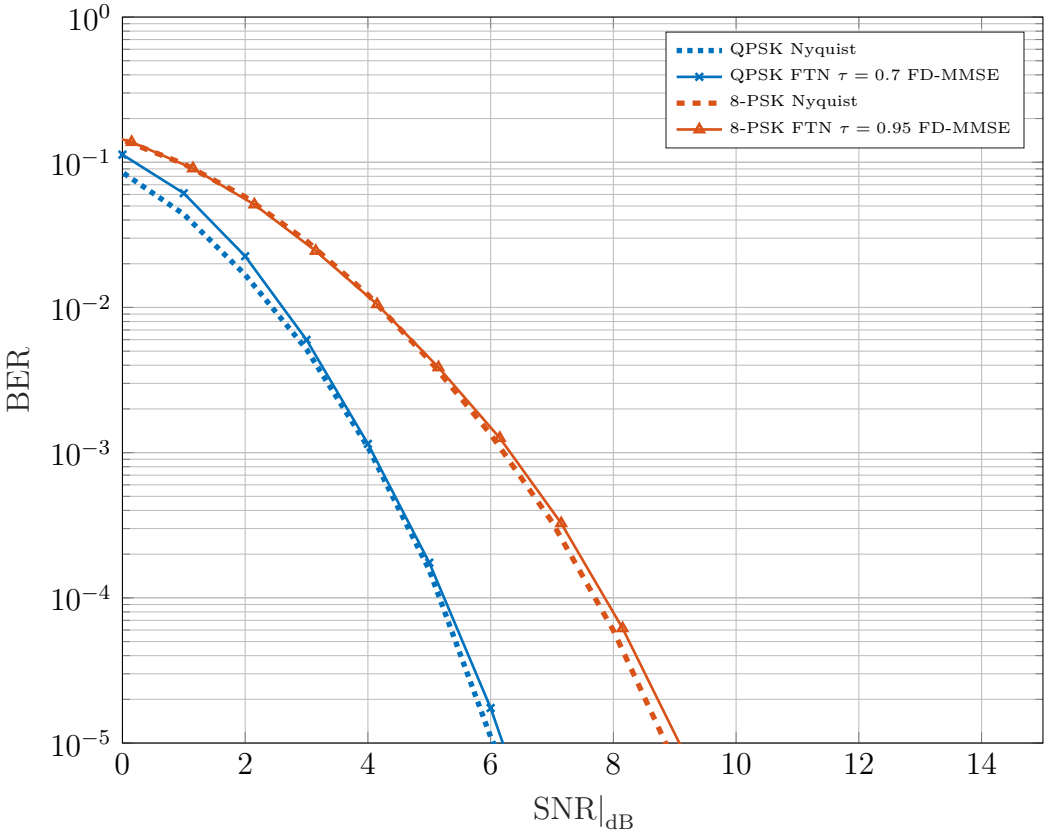

Figure III.16: BER against SNR for different FTN (solid) and Nyquist (dashed) waveforms achieving $\rho = 1$ bits/s/Hz

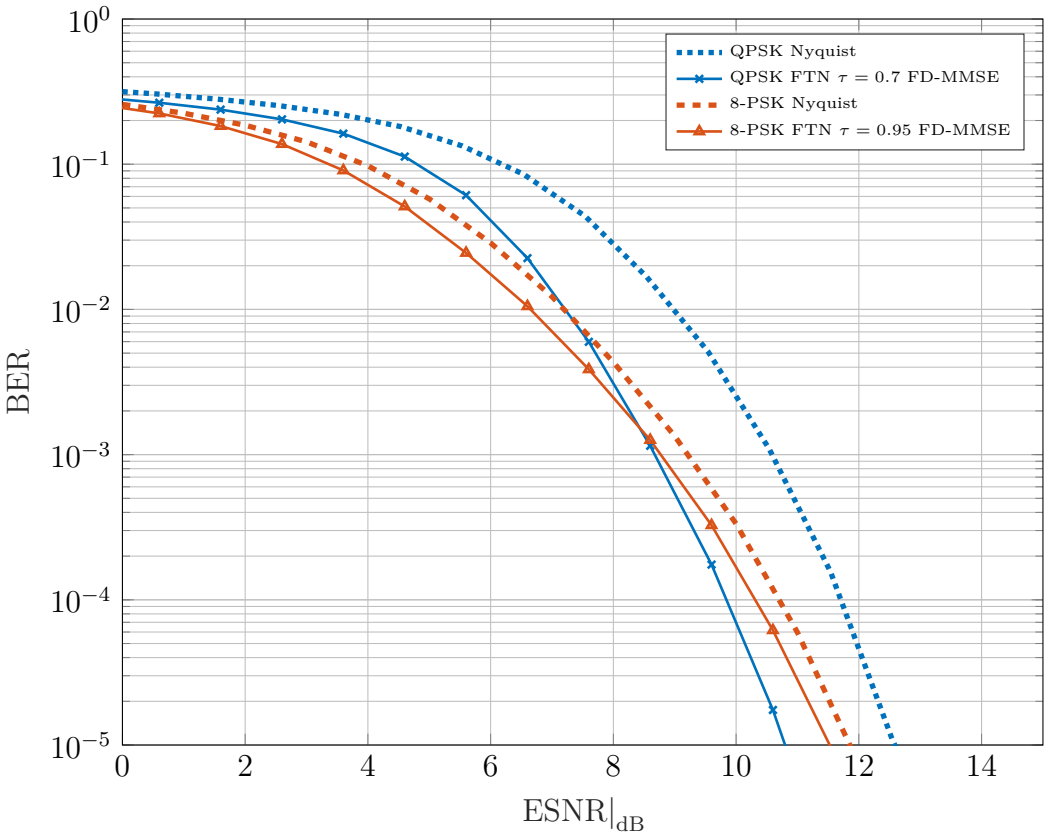

Figure III.17: BER against ESNR for different FTN (solid) and Nyquist (dashed) waveforms achieving $\rho = 1$ bits/s/Hz

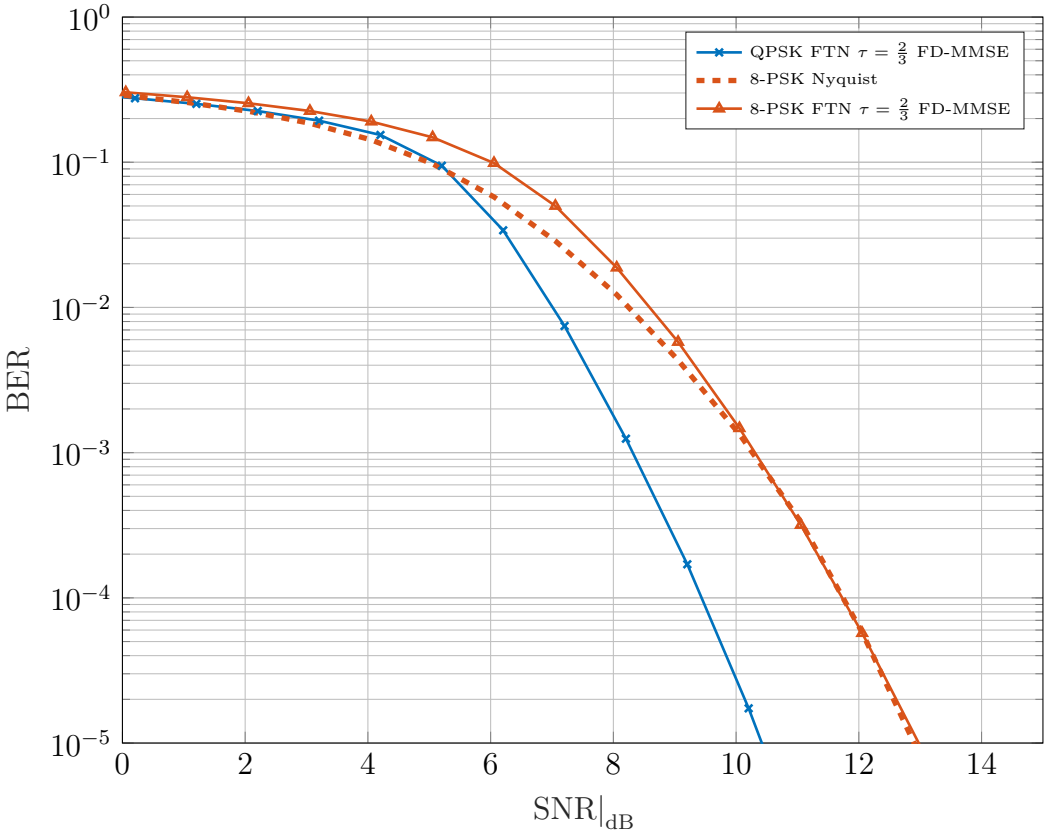

Figure III.18: BER against SNR for different FTN (solid) and Nyquist (dashed) waveforms achieving $\rho = 1.5$ bits/s/Hz

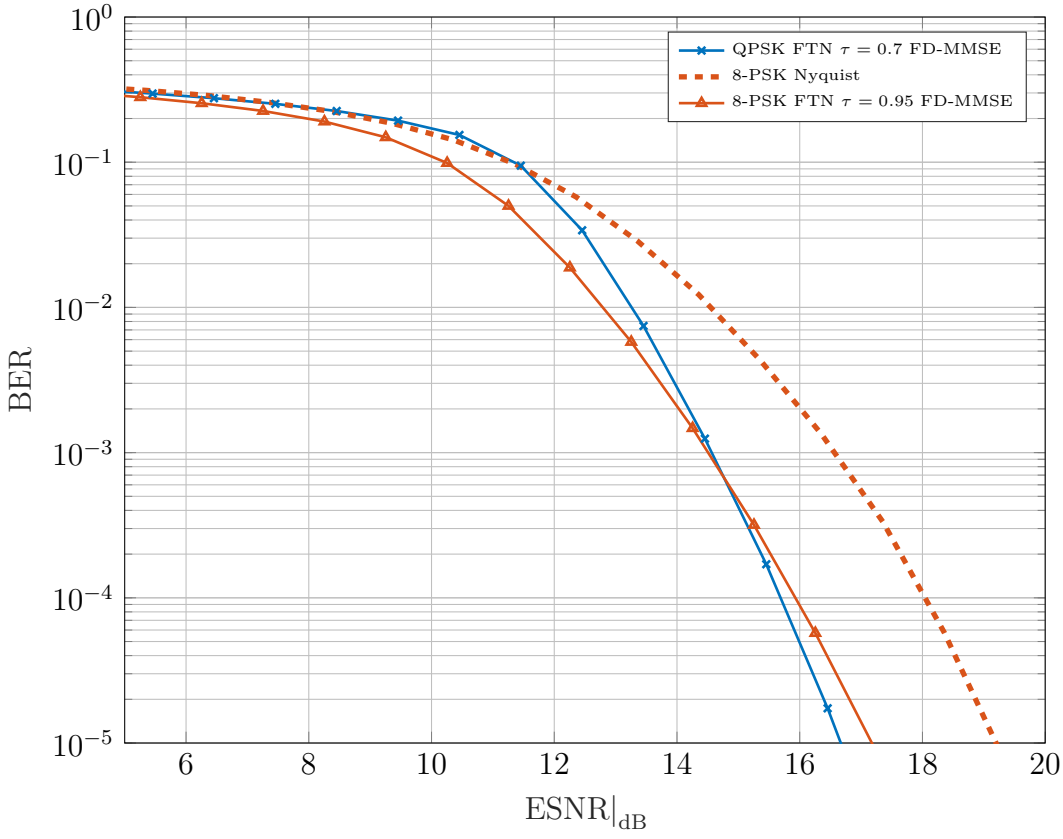

Figure III.19: BER against ESNR for different FTN (solid) and Nyquist (dashed) waveforms achieving $\rho = 1.5$ bits/s/Hz

Chapter IV

Expectation Propagation for Faster-Than-Nyquist Signaling

Outline

This chapter is devoted to a new class of receivers we developed to process the ISI induced by FTN signaling at reception. Its content was partly patented [Pet+19b] and published in two conference papers [Pet+19; Pet+20] as well as a journal paper [Pet+21]. The proposed receivers are based on an iterative message passing formalism called EP [MP01] which finds its applications in various fields. The concept of EP can be employed to approximate optimal MAP receivers by assuming Gaussianly distributed symbol information. It can be illustrated as a message passing algorithm using a Factor Graph (FG) formalism [KFL01; Şa+18]. It yields a low complexity iterative receiver [SA11] combining the benefits of both the MAP and MMSE receivers, called EP-MMSE by [SMFO15; San+18], recently enhanced by the EP-MMSE-DFE of [Şa+18]. Nevertheless, most of available EP receivers have been developed in a context of Nyquist signaling with frequency selective channels and then are not directly suitable for FTN signaling. The use of EP algorithm for FTN signaling in turbo-equalization has been proposed in [Wu+17] but they only approximate the prior information from the decoder which amounts to performing a classical turbo-equalization scheme operating with a MMSE equalizer [TSK02].

In order to adapt and extend these receivers to FTN signaling, we change in the EP process the message scheduling as in [Şa+18] and the Gaussian distributions family generating unprecedented EP-based receivers for FTN:

1. we propose a new family of non-circular Gaussian distributions, taking into account the potential non-circularity of soft decisions on the symbols giving rise to WL receivers [PC95; XCW09],
2. we use a Gaussian family which consists in considering Gaussian distributions whose covariance matrices are restricted to be proportional to the identity.

Combining this second family with the circulant hypothesis of our CCFTN model allows an optimal FD-EP based receiver with unprecedented performance while remaining very competitive from the computational complexity point of view, even for high spectral efficiencies ($\geq$ 3 bits/s/Hz). Moreover, the first WL generalization yields a new WL-EP receiver achieving 5 bits/s/Hz with more than 6 dB gain on the SNR compared to Nyquist signaling. As a summary, the contributions of the chapter are the following:

1. we provide a didactic approach of the EP technique and a common framework for all our EP-based receivers for FTN signaling.
2. we consider three different Gaussian families combined with different types of scheduling. This yields distinct algorithms: EP, EP-DFE, WL-EP, WL-EP-DFE, FD-EP which we partially published in [Pet+19] and in [Pet+20].
3. we use a circular shaping filter at transmission as proposed by [TPB16] for MMSE-IC. Combined with a particular Gaussian family yields the FD-EP receiver benefiting from an efficiency FD implementation.

4. the resulting receivers reach 5 bits/s/Hz with a limited complexity and almost no performance loss. This has never been achieved with FTN signaling, up to our knowledge.

Sec. A presents a didactic rethinking of the EP technique leading to the well-known EP receivers of [SMFO15; San+18; Şa+18] adapted to CFTN signaling and considering the noise coloration after matched filtering. In Sec. B, we propose to explore all the potential of EP for FTN signaling by changing the scheduling and the considered Gaussian family. Finally, comparisons with existing FTN receivers of the literature and with Nyquist communications in Sec. C enlighten the great interest of the proposed EP-based FTN receivers for different spectral efficiencies. To the best of our knowledge, the overall performance of our receivers have never been achieved at high spectral efficiencies and definitely proves the interest of FTN compared to Nyquist signaling.

A Symbol-wise posterior distribution: from BP to EP

The first part of this section shows that the symbol-wise posterior distribution $p(s_n|\mathbf{r})$ can be computed using the BP algorithm on the FG given in Fig. IV.1. From this optimal but computationally complex procedure, a lower complexity message passing strategy called EP is presented in the second part of this section.

A.1 Principle of Belief Propagation

In order to address the computation of $p(s_n|\mathbf{r})$, the dependencies between hidden variables are revealed by expressing $p(s_n|\mathbf{r})$ as the nth marginal distribution of $p(\mathbf{s}|\mathbf{r})$. Furthermore, using the Bayes formula and the symbols independence yields:

$$p(s_n|\mathbf{r}) = \frac{p(s_n)}{p(\mathbf{r})} p(\mathbf{r}|s_n) = p(\mathbf{r})^{-1} \sum_{\mathbf{s}_{\sim n} \in \mathcal{M}^{N_s-1}} p(\mathbf{r}|\mathbf{s}) \prod_{i=1}^{N_s} p(s_i) \tag{IV.1}$$

where $\mathbf{s}_{\sim n} \triangleq [\mathbf{s}_{1:n-1}, \mathbf{s}_{n+1:N_s}]^T$ refers to the vector $\mathbf{s}$ deprived of s_n. The expression of the posterior distribution of s_n given in (IV.1) involves the prior distribution $p(s_n)$ but also the likelihood $p(\mathbf{r}|s_n) \propto \frac{p(s_n|\mathbf{r})}{p(s_n)}$.

The joint distribution which is marginalized in (IV.1) can be represented as the FG given in Fig. IV.1, where the Variable Node (VN) illustrated by the circles, represent the symbols $s_1, ..., s_{N_s}$ while the Factor Node (FN) represent either $p(\mathbf{r}|\mathbf{s})$, or $p(s_1), ..., p(s_{N_s})$. Next, an edge from a FN p to a VN s_i exists if and only if s_i appears in the expression of p [KFL01]. In our case, the top FN $p(\mathbf{r}|\mathbf{s})$ covers all the different VNs $s_1, ..., s_{N_s}$ whereas a bottom FN $p(s_n)$ is only connected to the VN s_n. The nth marginal can then be computed using the belief propagation algorithm where FNs exchange *extrinsic*

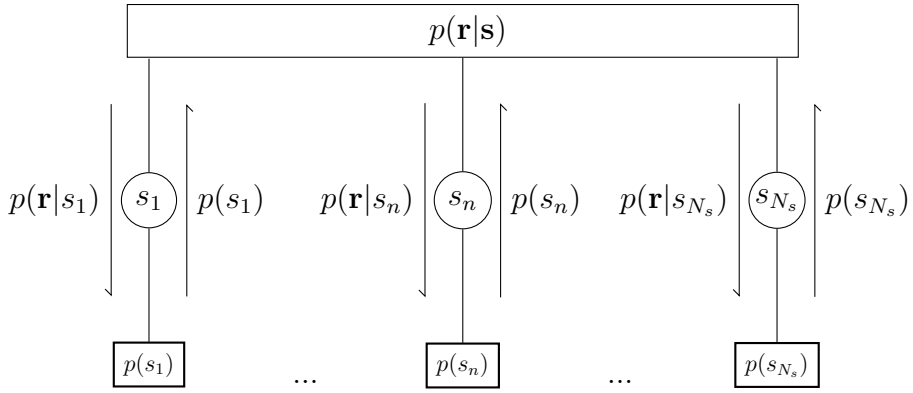

Figure IV.1: Factor graph of IV.1 under BP algorithm

distributions or *messages* given by the output or posterior distribution deprived of (or divided by) its incoming message called *prior*. This allows avoiding a self-confirmation effect by removing correlation with respect to its prior information. Consequently, the extrinsic information of a FN is a message becoming the prior information of another FN linked to it. For more details, the reader is invited to read [KFL01] where a detailed explanation of both the message passing process and the FG representation are provided.

The posterior distribution (IV.1) is computed at the VN s_n using the BP algorithm described hereafter:

1. Every bottom FN delivers an upward message to the top FN representing the pmf $p(s_i)$ where we suppose that $p(s_i) > 0$ for each s_i lying in $\mathcal{M}$.
2. Knowing the different $p(s_i)$ and $\mathbf{r}$, the top FN evaluates the likelihood distribution $p(\mathbf{r}|s_n)$ using (IV.1) with $|\mathcal{M}|^{N_s-1}$ products for every $n \in [\![1, N_s]\!]$.

Finally, the posterior distribution on the VN s_n is given by (IV.1) using its incoming messages $p(\mathbf{r}|s_n)$ and $p(s_n)$. It should be noted that no more iterations between the FNs are required for the messages to converge.

Consequently, without any further assumptions on $\mathbf{H}$, the BP algorithm requires $N_s|\mathcal{M}|^{N_s}$ products which is overly complex. In the particular case where $\mathbf{H}$ represents a convolution channel matrix with $(2L_\tau + 1)$ paths, such a complexity can be reduced to $O(|\mathcal{M}|^{2L_\tau} + 1)$ with a BCJR algorithm [Bah+74] without any approximation. In both cases, the computation complexity of the MAP symbol estimations still remains exponential with respect to the constellation order. Hence, when considering high spectral efficiency schemes with rich constellations, lower complexity strategies have to be explored. The EP technique has been developed to solve this issue as explained in next section.

A.2 Principle of Expectation Propagation

The EP principle is based on an iterative message passing method which can be applied to the same FG as for the BP technique, except that messages are enforced to

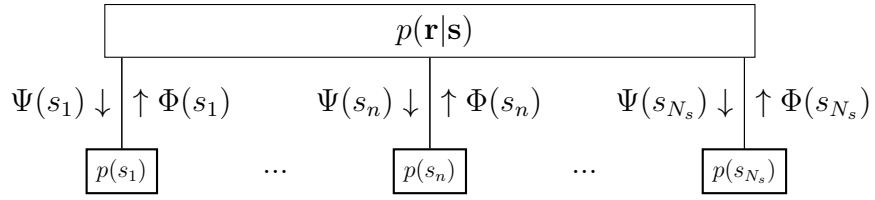

Figure IV.2: Schematic of the EP problem decomposition

represent circular complex Gaussian pdfs. Hence, while the BP technique exchanges the true pmf of the symbols, the EP process propagates approximated pdfs that will be iteratively refined. The FG of BP in Fig. IV.1 should then be slightly adapted by replacing the BP messages by the EP ones depicted in Fig. IV.2. In particular, the upward messages $\Phi_l(s_i)$ (resp. downward messages $\Psi_l(s_i)$) at iteration l are the Gaussian pdfs approximating $p(s_i)$ (resp. $p(\mathbf{r}|s_i)$) given by:

$$\Phi_l(s_n) \triangleq \mathcal{N}_{\mathrm{C}}(s_n : s_n^{\Phi_l}, v_n^{\Phi_l}) \propto \frac{\tilde{\Phi}_l(s_n)}{\Psi_l(s_n)} = \frac{\mathcal{N}_{\mathrm{C}}(s_n : s_n^{\tilde{\Phi}_l}, v_n^{\tilde{\Phi}_l})}{\mathcal{N}_{\mathrm{C}}(s_n : s_n^{\Psi_l}, v_n^{\Psi_l})} \tag{IV.2}$$

$$\Psi_l(s_n) \triangleq \mathcal{N}_{\mathrm{C}}(s_n : s_n^{\Psi_l}, v_n^{\Psi_l}) \propto \frac{\tilde{\Psi}_l(s_n)}{\Phi_{l-1}(s_n)} = \frac{\mathcal{N}_{\mathrm{C}}(s_n : s_n^{\tilde{\Psi}_l}, v_n^{\tilde{\Psi}_l})}{\mathcal{N}_{\mathrm{C}}(s_n : s_n^{\Phi_{l-1}}, v_n^{\Phi_{l-1}})} \tag{IV.3}$$

where:

- $\tilde{\Phi}_l(s_n)$: the posterior Gaussian pdf of s_n of the bottom FN at iteration l,
- $\Phi_l(s_n)$: the extrinsic Gaussian pdf of s_n of the bottom FN at iteration l,
- $\tilde{\Psi}_l(s_n)$: the posterior Gaussian pdf of s_n of the top FN at iteration l,
- $\Psi_l(s_n)$: the extrinsic Gaussian pdf of s_n of the top FN at iteration l.

In order to enforce the messages to be Gaussian pdfs, exact posterior distributions of each FN are projected on the chosen Gaussian family. This projection can be considered as a Gaussian approximation where only the two first moments of the true distribution are kept as depicted in Fig. IV.3. In practice, the approximate posterior distribution of the bottom FN is given by $\tilde{\Phi}_l(s_n) = \mathcal{N}_{\mathrm{C}}(s_n : s_n^{\tilde{\Phi}_l}, v_n^{\tilde{\Phi}_l})$ having: $s_n^{\tilde{\Phi}_l} = \mathbb{E}_{\tilde{\phi}_l}[s_n]$ and $v_n^{\tilde{\Phi}_l} = \mathbb{V}_{\tilde{\phi}_l}[s_n]$ where $\tilde{\phi}_l(s_n)$ is the true posterior distribution before projection. Similarly, $\tilde{\Psi}_l(s_n) = \mathcal{N}_{\mathrm{C}}(s_n : s_n^{\tilde{\Psi}_l}, v_n^{\tilde{\Psi}_l})$ is the Gaussian projection of the exact distribution $\tilde{\psi}_l(s_n)$ where $s_n^{\tilde{\Psi}_l} = \mathbb{E}_{\tilde{\psi}_l}[s_n]$ and $v_n^{\tilde{\Psi}_l} = \mathbb{V}_{\tilde{\psi}_l}[s_n]$. Such a Gaussian approximation imposed by the EP technique can be seen as a reduction of the number of moments.

As we will show in the next subsections, the messages representing extrinsic pdfs in (IV.2) and (IV.3) are directly Gaussian pdfs and their moments $s_n^{\Phi_l}, v_n^{\Phi_l}$ (resp. $s_n^{\Psi_l}, v_n^{\Psi_l}$) are easy to compute. More precisely, we present in the following the computation of the downward messages $\Psi_l(s_n)$ before introducing the upward ones $\Phi_l(s_n)$.

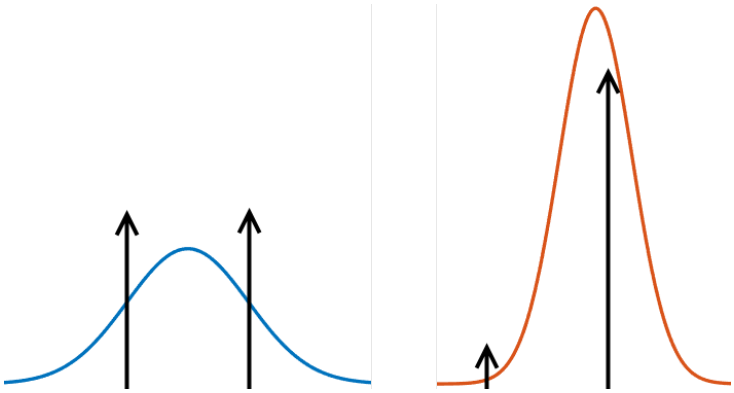

Figure IV.3: Gaussian projection with moment-matching of a pmf on a BPSK and uniform (left) or unbalanced (right) probabilities

Computation of $\Psi_l(s_n)$ at top FN

The downward message $\Psi_l(s_n)$ is obtained by computing the posterior distribution as in BP technique, assuming however that the upward messages $\Phi_{l-1}(s_i)$ are Gaussian pdfs instead of the true pmfs $p(s_i)$. Consequently, the posterior distribution $\tilde{\Psi}_l(s_n)$ does not coincide anymore with $p(s_n|\mathbf{r})$. Also, since $\Phi_{l-1}(s_i)$ are pdfs, the summation $\sum_{\mathbf{s}_{\sim n}}$ in (IV.1) is replaced by the following continuous integration over $\mathbf{s}_{\sim n}$

$$\tilde{\Psi}_l(s_n) \propto \int_{\mathbf{s}_{\sim n}} p(\mathbf{r}|\mathbf{s}) \prod_{i=1}^{N_s} \Phi_{l-1}(s_i)\, \mathrm{d}\mathbf{s}_{\sim n} \tag{IV.4}$$

The main advantage of (IV.4) compared to (IV.1) is that the posterior distribution $\tilde{\Psi}_l(s_n)$ can now be computed analytically. Indeed, since $\mathbf{H}$ is deterministic, we have $p(\mathbf{r}|\mathbf{s}) = \mathcal{N}_{\mathrm{C}}(\mathbf{r} : \mathbf{Hs}, \sigma_w^2 \mathbf{I}_{2N_s})$. Some developments detailed in App. C lead to $\tilde{\Psi}_l(s_n) = \mathcal{N}_{\mathrm{C}}(s_n : s_n^{\tilde{\Psi}_l}, v_n^{\tilde{\Psi}_l})$ with:

$$\begin{cases} s_n^{\tilde{\Psi}_l} = s_n^{\Phi_{l-1}} + v_n^{\Phi_{l-1}} \mathbf{f}_{n,l}^{\dagger} (\mathbf{y} - \mathbf{G}\mathbf{s}^{\Phi_{l-1}}) & \text{(IV.5a)} \\ v_n^{\tilde{\Psi}_l} = v_n^{\Phi_{l-1}} (1 - v_n^{\Phi_{l-1}} \xi_{n,l}) & \text{(IV.5b)} \end{cases}$$

where $\mathbf{f}_{n,l} = \mathbf{\Sigma}_l^{-1} \mathbf{e}_n$, $\xi_{n,l} = \mathbf{f}_{n,l}^{\dagger} \mathbf{G} \mathbf{e}_n$ and $\mathbf{\Sigma}_l = \mathbf{G}\mathbf{V}^{\Phi_{l-1}} + \sigma_w^2 \mathbf{I}_{N_s}$ using $\mathbf{G} = \mathbf{D}\mathbf{H}^{\dagger}\mathbf{H}\mathbf{U}$. The vector $\mathbf{y} = \mathbf{D}\mathbf{H}^{\dagger}\mathbf{r}$ represents the received signal after matched filtering and down-sampling, and the matrix $\mathbf{G}$ corresponds to the circulant convolution matrix of the aliased Nyquist filter. This posterior estimation $s_n^{\tilde{\Psi}_l}$ of the EP technique can be interpreted as a well known linear MMSE-IC equalizer [TSK02] which is a *biased* estimator of s_n [Şa+18].

The extrinsic Gaussian pdf $\Psi_l(s_n) \propto \frac{\tilde{\Psi}_l(s_n)}{\Phi_{l-1}(s_n)}$ returned to the bottom FN is then obtained by Gaussian division, leading to the Gaussian distribution $\Psi_l(s_n) = \mathcal{N}_{\mathrm{C}}(s_n :$

$s_n^{\Psi_l}, v_n^{\Psi_l}$) where:

$$\begin{cases} s_n^{\Psi_l} = \dfrac{s_n^{\tilde{\Psi}_l} v_n^{\Phi_{l-1}} - s_n^{\Phi_{l-1}} v_n^{\tilde{\Psi}_l}}{v_n^{\Phi_{l-1}} - v_n^{\tilde{\Psi}_l}} = s_n^{\Phi_{l-1}} + \xi_{n,l}^{-1} \mathbf{f}_{n,l}^{\dagger} (\mathbf{y} - \mathbf{G}\mathbf{s}^{\Phi_{l-1}}) & \text{(IV.6a)} \\ v_n^{\Psi_l} = \dfrac{v_n^{\Phi_{l-1}} v^{\tilde{\Psi}_l}}{v_n^{\Phi_{l-1}} - v_n^{\tilde{\Psi}_l}} = \xi_{n,l}^{-1} - v_n^{\Phi_{l-1}} & \text{(IV.6b)} \end{cases}$$

This extrinsic estimation of s_n also corresponds to the *unbiased* MMSE-IC equalizer output $s_n^{\Psi_l}$ with MSE $v_n^{\Psi_l}$. Note that the computation of $\mathbf{y} - \mathbf{G}\mathbf{s}^{\Phi_{l-1}}$ in (IV.6a) can be computed in the FD for complexity savings. Nevertheless, the main complexity challenge of the MMSE-IC relies on the computation of the inverse matrix $\mathbf{\Sigma}_l^{-1}$ because $\mathbf{\Sigma}_l$ is not circulant and then cannot be easily invertible in the FD at this point.

Remark

At the initial step, we have $\mathbf{s}^{\Phi_0} = \mathbf{0}_{N_s}$, $\mathbf{V}_n^{\Phi_0} = \mathbf{I}_{N_s}$ and (IV.6) amounts to performing a linear MMSE without IC:

$$\begin{cases} s_n^{\Psi_1} = \xi_{n,1}^{-1} \mathbf{f}_{n,1}^{\dagger} \mathbf{y} \\ v_n^{\Psi_1} = \xi_{n,1}^{-1} - 1 \end{cases} \quad \text{(IV.7)}$$

At convergence after $\mathcal{I}$ iterations and assuming the perfect prior information $\mathbf{s}^{\Phi_{\mathcal{I}}} = \mathbf{s}$ and $\mathbf{V}^{\Phi_{\mathcal{I}}} = \epsilon \mathbf{I}_{N_s}$ where $\epsilon \to 0^+$, the linear MMSE-IC equalizer yields:

$$\begin{cases} s_n^{\Psi_{\mathcal{I}+1}} = s_n + w_n' \\ v_n^{\Psi_{\mathcal{I}+1}} = \sigma_w^2 \end{cases} \quad \text{(IV.8)}$$

where w_n' is the up-sampled matched filtered noise, a circular and centered AWGN. Still at convergence, $(v_n^{\Psi_{\mathcal{I}+1}})^{-1}$ represents the SNR. Such a result can be useful for evaluating the performance of the equalizer given that it corresponds to a theoretical bound assuming a perfect ISI cancellation in the equalization process. It is usually called the Matched-Filter Bound (MFB) (see the chapter "Equalization" of [LM12] on page 448) and we make use of this model in our simulations.

Following the top FN processing, the EP receiver computes the bottom FN $p(s_n)$ derived in next sub-section. It results in a less usual operation making the specificity of the EP processing that we call a Constellation Matcher[1]. It aims at bringing the constellation knowledge to the equalization process.

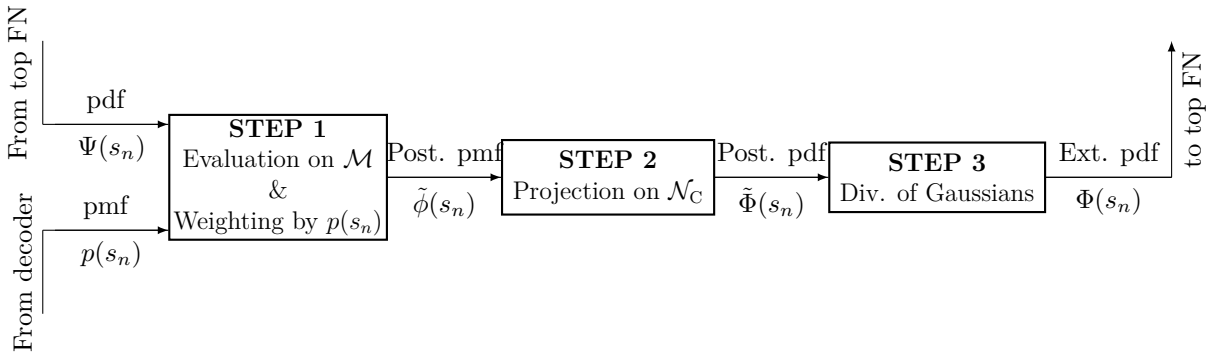

Figure IV.4: Constellation Matcher inner operations

Computation of $\Phi_l(s_n)$ at bottom FN

As for the top FN, the true posterior pmf $\tilde{\phi}_l(s_n)$ is given by the product between the bottom FN pmf $p(s_n)$ and the downward message $\Psi_l(s_n)$ coming from the top FN evaluated at each element of the constellation:

$$\begin{aligned}\tilde{\phi}_l(s_n) &\propto p(s_n)\Psi_l(s_n) \\ &\propto p(s_n)\mathcal{N}_{\mathrm{C}}(s_n : s_n^{\Psi_l}, v_n^{\Psi_l}),\ s_n \in \mathcal{M}\end{aligned} \tag{IV.9}$$

The value of $p(s_n)$ allows the EP receiver to be linked to a decoder to form an iterative turbo-receiver. At the first turbo-iteration or if no channel coding is considered, we have $p(s_n) = \frac{1}{|\mathcal{M}|}, \forall s_n \in \mathcal{M}$.

In order to enforce the posterior to be Gaussian, EP performs a Gaussian approximation of $\tilde{\phi}_l(s_n)$ by moment matching. Thus, the moments of $\tilde{\Phi}_l(s_n)$ are obtained by the ones of the true posterior pmf $\tilde{\phi}_l(s_n)$:

$$\begin{cases} s_n^{\tilde{\Phi}_l} = \mathbb{E}_{\tilde{\phi}_l}[s_n] = \sum\limits_{s_n \in \mathcal{M}} s_n \cdot \tilde{\phi}_l(s_n) & \text{(IV.10a)} \\ v_n^{\tilde{\Phi}_l} = \mathbb{V}_{\tilde{\phi}_l}[s_n] = \sum\limits_{s_n \in \mathcal{M}} |s_n|^2 \cdot \tilde{\phi}_l(s_n) - |s_n^{\tilde{\Phi}_l}|^2 & \text{(IV.10b)} \end{cases}$$

The final step consists in a Gaussian division in order to retrieve the extrinsic pdf $\Phi_l(s_n)$ of (IV.2):

$$\Phi_l(s_n) = \mathcal{N}_{\mathrm{C}}(s_n : s_n^{\Phi_l}, v_n^{\Phi_l}) \text{ where } \begin{cases} s_n^{\Phi_l} = \dfrac{s_n^{\tilde{\Phi}_l} v_n^{\Psi_l} - s_n^{\Psi_l} v_n^{\tilde{\Phi}_l}}{v_n^{\Psi_l} - v_n^{\tilde{\Phi}_l}} & \text{(IV.11a)} \\ v_n^{\Phi_l} = \dfrac{v_n^{\Psi_l} v_n^{\tilde{\Phi}_l}}{v_n^{\Psi_l} - v_n^{\tilde{\Phi}_l}} & \text{(IV.11b)} \end{cases}$$

[1]It should be noted that the Constellation Matcher is sometimes considered as a demapper [SA11]. We prefer to consider a complete separation between the demapper and the Constellation Matcher given that the demapper computes bit distributions whereas the Constellation Matcher stays at the symbol-level.

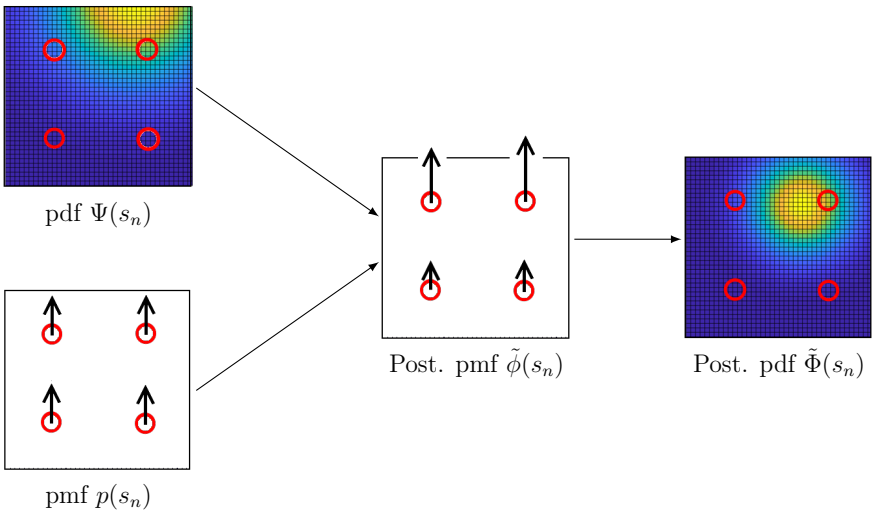

Figure IV.5: Constellation Matcher inner distribution: illustration with a QPSK

In practice, the computation of the extrinsic variance $v_n^{\Phi_l}$ could result in a negative value. This phenomenon appears generally at convergence, when the prior distribution $\Psi_l(s_n)$ is already a good estimation of s_n. Consequently, a common way of ensuring the positivity of the distribution's variance sent to the equalizer is to return the posterior pdf $\tilde{\Phi}_l(s_n)$ instead of the extrinsic one when $v_n^{\Phi_l}$ is negative.

Consequently, by evaluating the pdf $\Psi_l(s_n)$ at each element of $\mathcal{M}$ in (IV.9), the bottom FN brings the knowledge of the symbols alphabet to the equalization process. As depicted in Fig. IV.4, it combines the equalizer's message with the initial information and realigns the estimation of s_n with respect to $\mathcal{M}$. Indeed, we observe on Fig. IV.5 that even if the MMSE estimation $s_n^{\Psi_l}$ is far from the constellation, the bottom FN ensures the refined posterior estimate to lie inside the convex shape delimited by the constellation elements. Indeed, $s_n^{\tilde{\Phi}_l}$ is defined as a barycenter of positive weights $\tilde{\phi}_l(s_n)$ over the constellation $\mathcal{M}$.

The next section is devoted to our contribution based on the framework of EP. Up to now, we computed the messages exchanged in the FG considering circular Gaussian pdfs. In the following, we schedule differently the message computation, and we also change the Gaussian distribution family. Each Gaussian distribution combined with a specific scheduling yields a distinct receiver. Based on this principle, we developed new receivers for FTN presented hereafter.

B Proposed FTN receivers based on Expectation Propagation

This section corresponds to the main contribution of the chapter. It consists in the development and optimization of receivers for FTN based on EP. Our receiver propositions

are the following:

- we focus on the message scheduling in sub-Sec. B.1 combined with the commonly used Gaussian family of the previous section. This yields two new receivers for FTN: the EP and EP-DFE,
- we consider in sub-Sec. B.2 a particular subset of the non-circular Gaussian family yielding new WL receivers [PC95] only valid for FTN. Depending on the scheduling considered, this particular family results in two unprecedented receivers: WL-EP and WL-EP-DFE for FTN,
- we change in sub-Sec. B.3 the Gaussian family and restrict the family to Gaussian pdfs with identity covariance matrix. Combined with CCFTN, this specific family allows a low-complexity FD processing of the MMSE-IC equalizer without requiring any cyclic prefix. Hence, we propose to call this unprecedented receiver FD-EP.

B.1 Scheduling strategy: EP and EP-DFE receivers for FTN

For solving the complex posterior estimation problem, the EP technique exchanges messages between the top and bottom FNs playing complementary roles and computing approximate extrinsic information. The computation of those exchanged messages may be scheduled by two different procedures, giving rise to two different receivers called respectively EP and EP-DFE receivers [Pet+19].

Both the MMSE-IC equalizer of the top FN and the Constellation Matcher of the bottom FN are to be performed for each symbol index $n \in [\![1, N_s]\!]$ at each iteration l until convergence. In other words, we iterate over n fixing l, but one may wonder whether iterating over l fixing n may be better. More precisely, until here, the MMSE equalizer is implemented over the whole sequence followed by the Constellation Matcher for each symbol. Then, we run this double process again, and iterating over l results in a block algorithm we propose to call EP algorithm instead of EP-MMSE algorithm as in [SMFO15; San+18] because it is theoretically closer to the MAP estimator than the MMSE equalizer as detailed in Sec. A.

Let us now consider the case where we iterate over l before iterating over n. For instance, after the processing of s_1 by the MMSE-IC equalizer at iteration l, the Constellation Matcher may also act on s_1 at this iteration to generate an output which will be processed by the MMSE-IC equalizer at iteration l to process s_2. This scheduling is usually referred as EP-DFE processing. More generally, for computing $\Psi_l(s_n)$, the last refinements of s_i available is $\Phi_l(s_i)$ for $i < n$ and $\Phi_{l-1}(s_i)$ for $i \geq n$. This amounts to computing $s_n^{\Psi_l}$ using $\mathbf{s}^{\Phi_{l-1},\mathrm{DFE}} = [s_{1:n-1}^{\Phi_l}, s_{n:N_s}^{\Phi_{l-1}}]^T$ and similarly for $\mathbf{v}^{\Phi_{l-1},\mathrm{DFE}} = [v_{1:n-1}^{\Phi_l}, v_{n:N_s}^{\Phi_{l-1}}]^T$ in (IV.6). A graphical explanation of the two types of scheduling as well as the message passing of their equalization step is depicted in Fig. IV.6 for EP and Fig. IV.7 for EP-DFE respectively. In this second case, the scheduling leads to the EP-DFE receiver in reference to [Şa+18] which refers it as EP-MMSE-DFE. Note that this receiver do not work with

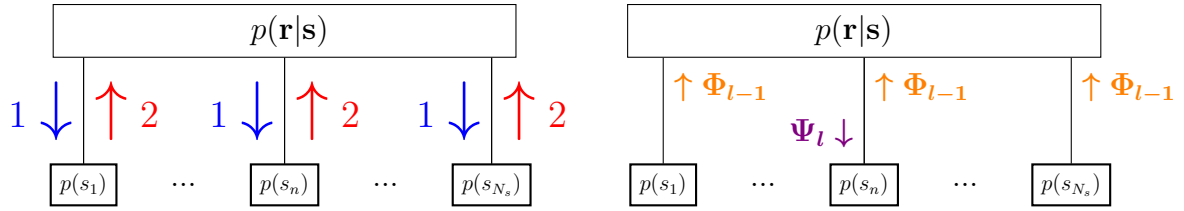

Figure IV.6: Scheduling of EP (left) and (right) message passing for computing a downward message $\Psi_l(s_n)$

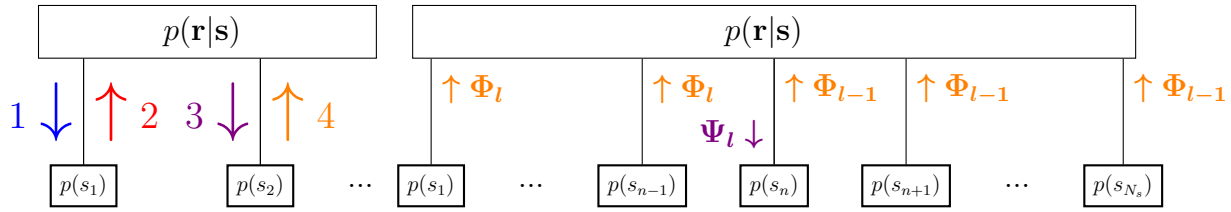

Figure IV.7: Scheduling of EP-DFE (left) and message passing for computing a downward message $\Psi_l(s_n)$ (right)

the same kind of feedback as the common MMSE-DFE equalizer, see the introduction of [Şa+18] for an overview of the different types of DFE.

Algorithm 1 EP and EP-DFE receivers

Require: $\mathbf{r}, \mathbf{H}, \forall n : p(s_n)$
  $\forall n : s_n^{\Phi_0} = \sum_{s_n} s_n \cdot p(s_n)$ and $v_n^{\Phi_0} = \sum_{s_n} |s_n|^2 \cdot p(s_n) - |s_n^{\Phi_0}|^2$
  for $l = 1, ..., \mathcal{I}+1$ **do**
    for $n = 1, ..., N_s$ **do**
      $s_n^{\Psi_l}, v_n^{\Psi_l} \leftarrow$ (IV.6), using $\mathbf{s}^{\Phi_{l-1},\mathrm{DFE}}, \mathbf{v}^{\Phi_{l-1},\mathrm{DFE}}$ instead of $\mathbf{s}^{\Phi_{l-1}}, \mathbf{v}^{\Phi_{l-1}}$ for EP-DFE
      $s_n^{\tilde{\Phi}_l}, v_n^{\tilde{\Phi}_l} \leftarrow$ (IV.10)
      if $v_n^{\Psi_l} - v_n^{\tilde{\Phi}_l} < \gamma \Leftarrow$ convergence reached (We set $\gamma = 10^{-6}$ in our simulations) **then**
        $s_n^{\Phi_l}, v_n^{\Phi_l} \leftarrow [s_n^{\tilde{\Phi}_l}, v_n^{\tilde{\Phi}_l}$ or $s_n^{\Psi_l}, v_n^{\Psi_l}]$
      else
        $s_n^{\Phi_l}, v_n^{\Phi_l} \leftarrow$ (IV.11)
      end if
    end for
  end for
  return $\forall n : \tilde{\phi}_{\mathcal{I}+1}(s_n)$

Alg. 1 depicts an implementation of both the EP and EP-DFE receivers where the output $\tilde{\phi}_{\mathcal{I}+1}(s_n)$ corresponds to the approximation of $p(s_n|\mathbf{r})$. We detail in the following different Gaussian families aiming at optimizing the trade-off between complexity and performance of EP-based receivers.

B.2 EP with non-circular Gaussian distributions: WL-EP and WL-EP-DFE receivers for FTN

Up to now, messages in EP receivers have been enforced to belong to the set of SO circular complex Gaussian distributions $\mathcal{N}_{\mathrm{C}}$. However, the MSE characterizing the I and Q parts of a complex estimate have no reason to be equal. Hence, instead of $\mathcal{N}_{\mathrm{C}}$, we consider a subset of non-circular Gaussian distributions characterized by:

$$\mathcal{N}_{\mathrm{NC}}\left(s_n : s, v_I, v_Q\right) \triangleq \mathcal{N}_{\mathrm{R}}(s_{n,I} : s_I, v_I)\mathcal{N}_{\mathrm{R}}\left(s_{n,Q} : s_Q, v_Q\right) \tag{IV.12}$$

where $s_n = s_{n,I} + j s_{n,Q}$, $s \triangleq \mathbb{E}[s_n] = s_I + j s_Q$, $v_I \triangleq \mathbb{E}\left[s_{n,I}^2\right] - s_I^2$ and $v_Q \triangleq \mathbb{E}\left[s_{n,Q}^2\right] - s_Q^2$. v_I characterizes the variance of the real part of s_n, while v_Q denotes the variance of its imaginary part. Based on this new distribution assumption, the equalizer and Constellation Matcher equations must be updated as in [Pet+19].

Equalizer update based on the new non-circular distribution assumption

The shaping filter $h(t)$ is real valued and so is the matrix $\mathbf{G} = \mathbf{D}\mathbf{H}^{\dagger}\mathbf{H}\mathbf{U}$. Therefore, one can show that working with distributions in the family $\mathcal{N}_{\mathrm{NC}}$ leads to the following WL equalizer which do not apply the same filters to the I and Q parts of the received signal [Pet+19]:

$$\begin{cases} s_n^{\Psi_l} & = s_n^{\Phi_{l-1}} + \xi_{n,l,I}^{-1}\tilde{\mathbf{f}}_{n,l,I}^{\dagger}\left(\mathbf{y}_I - \mathbf{G}\mathbf{s}_I^{\Phi_{l-1}}\right) + j\xi_{n,l,Q}^{-1}\tilde{\mathbf{f}}_{n,l,Q}^{\dagger}\left(\mathbf{y}_Q - \mathbf{G}\mathbf{s}_Q^{\Phi_{l-1}}\right) \\ v_{n,I/Q}^{\Psi_l} & = \xi_{n,l,I/Q}^{-1} - v_{n,I/Q}^{\Phi_{l-1}} \end{cases} \tag{IV.13}$$

where $\xi_{n,l,I/Q} = \mathbf{f}_{n,l,I/Q}^{\dagger}\mathbf{G}\mathbf{e}_n$ having the MMSE filters $\mathbf{f}_{n,l,I/Q} = (\mathbf{G}\mathbf{V}_{I/Q}^{\Phi_{l-1}} + \frac{\sigma_w^2}{2}\mathbf{I}_{N_s})^{-1}\mathbf{e}_n$ and $\mathbf{V}_{I/Q}^{\Phi_{l-1}} = \mathrm{diag}([v_{I/Q}^{1,\Phi_{l-1}}, v_{I/Q}^{2,\Phi_{l-1}}, ..., v_{I/Q}^{N_s,\Phi_{l-1}}]^T)$ using the notation I/Q meaning that the given expression is defined twice: once using the character I and the other one with Q. Hence, the WL equalizer is slightly modified from its circular version and requires twice more matrix inversions.

Constellation Matcher update based on the non-circular distribution assumption

The Constellation Matcher can then be expressed as follows:

$$\begin{cases} s_{n,I/Q}^{\tilde{\Phi}_l} & = \sum_{s_{n,I/Q} \in \mathcal{M}_{I/Q}} s_{n,I/Q} \cdot \phi_l(s_{n,I/Q}) \\ v_{n,I/Q}^{\tilde{\Phi}_l} & = \sum_{s_{n,I/Q} \in \mathcal{M}_{I/Q}} |s_{n,I/Q}| \cdot \phi_l(s_{n,I/Q}) - |s_{n,I/Q}^{\tilde{\Phi}_l}|^2 \end{cases} \tag{IV.14}$$

where $s_n^{\tilde{\Phi}_l} = s_{n,I}^{\tilde{\Phi}_l} + j s_{n,Q}^{\tilde{\Phi}_l}$ and $\mathcal{M}_{I/Q} = \{s_{I/Q} : s \in \mathcal{M}\}$.

The expression of the Constellation Matcher does not change much from the circular receiver. The main difference is that I and Q parts must be computed separately.

Moreover, if considering square or rectangular QAM constellations, processing separately I and Q parts leads to a simpler Constellation Matcher. Indeed, in these cases exploring independently $\mathcal{M}_I$ and $\mathcal{M}_Q$ is quicker than exploring the complete alphabet $\mathcal{M}$.

Discussion: This WL equalization extension can be applied on the EP receiver with or without DFE. Nevertheless, we must note that equation (IV.13) is not valid in the general case of a communication with a complex frequency selective channel since the I and Q parts of the MMSE-IC cannot be processed separately anymore. As a generalization of the circular EP process, it offers a better model fitting at the price of a slight computational overhead. Consequently, it comes with enhanced performance as presented in sub-Sec. B.3.

B.3 EP receiver with equal variance circular Gaussian distributions: FD-EP receiver for CCFTN

In the previous EP-based receivers, the MMSE-IC equalization step performed at the top FN is quite complex due to the inversion of the matrix $\mathbf{\Sigma}_l = \mathbf{G}\mathbf{V}^{\Phi_{l-1}} + \sigma_w^2\mathbf{I}_{N_s}$. In order to simplify such a computation, we propose an alternative consisting in changing the considered Gaussian family.

More precisely, we assume now that the messages $\Phi_l(s_n)$ (respectively $\Psi_l(s_n)$) have a common variance parameter as in [Pet+20]. Hence, $\forall n \in [\![1, N_s]\!]$, we will consider that $v_n^{\Phi_l} = v^{\Phi_l}$ (resp. $v_n^{\Psi_l} = v^{\Psi_l}$). This amounts to considering the messages $\Phi_l(\mathbf{s}) = \prod_{n=1}^{N_s}\Phi_l(s_n)$ and $\Psi_l(\mathbf{s}) = \prod_{n=1}^{N_s}\Psi_l(s_n)$ representing circular multivariate complex Gaussian distribution with $\mathbf{V}^{\Phi_l} = v^{\Phi_l}\mathbf{I}_{N_s}$ and $\mathbf{V}^{\Psi_l} = v^{\Psi_l}\mathbf{I}_{N_s}$. Again, under this new assumption, the equalizer and the Constellation Matcher must be updated. Furthermore, the CCFTN model is considered for this section.

MMSE-IC equalizer

Under the previous assumptions, the MMSE-IC equalizer of (IV.6) becomes:

$$\begin{cases} s_n^{\Psi_l} = s_n^{\Phi_{l-1}} + \xi_l^{-1}\mathbf{e}_n^\dagger\mathbf{\Sigma}_l^{-1}(\mathbf{y} - \mathbf{G}\mathbf{s}^{\Phi_{l-1}}) & \text{(IV.15a)} \\ v^{\Psi_l} = \xi_l^{-1} - v^{\Phi_{l-1}} & \text{(IV.15b)} \end{cases}$$

where $\xi_l = (\mathbf{\Sigma}_l^{-1}\mathbf{G})_{1,1}$ does not depend on n anymore, having $\mathbf{\Sigma}_l = v^{\Phi_{l-1}}\mathbf{G} + \sigma_w^2\mathbf{I}_{N_s}$. Moreover, the CCFTN model yields a circulant matrix $\mathbf{G}$, and $\hat{\mathbf{G}} = \mathbf{F}\mathbf{G}\mathbf{F}^\dagger$ is a diagonal matrix as well as $\hat{\mathbf{\Sigma}}_l = \mathbf{F}\mathbf{\Sigma}_l\mathbf{F}^\dagger = v^{\Phi_{l-1}}\hat{\mathbf{G}} + \sigma_w^2\mathbf{I}_{N_s}$. Hence, we obtain: $\xi_l = \sum_{k=1}^{N_s}(\hat{\mathbf{G}})_{k,k}/(v^{\Phi_{l-1}}(\hat{\mathbf{G}})_{k,k} + \sigma_w^2)$ and (IV.6) can be computed in the FD as follows:

$$\begin{cases} \mathbf{s}^{\Psi_l} = \mathbf{s}^{\Phi_{l-1}} + \xi_l^{-1}\mathbf{F}^\dagger\hat{\mathbf{\Sigma}}_l^{-1}(\hat{\mathbf{y}} - \hat{\mathbf{G}}\hat{\mathbf{s}}^{\Phi_{l-1}}) & \text{(IV.16a)} \\ v^{\Psi_l} = \xi_l^{-1} - v^{\Phi_{l-1}} & \text{(IV.16b)} \end{cases}$$

where $\hat{\mathbf{y}} = \mathbf{F}\mathbf{y}$ represents the FD received signal after matched filtering and down-sampling, and $\hat{\mathbf{s}}^{\Phi_{l-1}} = \mathbf{F}\mathbf{s}^{\Phi_{l-1}}$ is the DFT of $\mathbf{s}^{\Phi_{l-1}}$.

Constellation Matcher

For computing the Constellation Matcher message, we first need to introduce the projection of EP messages in the precise case of the Gaussian family we consider. This derivation is detailed in App. B and leads to averaging the posterior variance terms. Hence, (IV.10) becomes:

$$\begin{cases} s_n^{\tilde{\Phi}_l} = \sum\limits_{s_n \in \mathcal{M}} s_n \cdot \tilde{\phi}_l(s_n) & \text{(IV.17a)} \\ v^{\tilde{\Phi}_l} = \dfrac{1}{N_s} \sum\limits_{n=1}^{N_s} \left(\sum\limits_{s_n \in \mathcal{M}} |s_n|^2 \cdot \tilde{\phi}_l(s_n) - |s_n^{\tilde{\Phi}_l}|^2 \right) & \text{(IV.17b)} \end{cases}$$

and the resulting extrinsic distribution is given by:

$$\Phi_l(s_n) = \mathcal{N}_{\mathrm{C}}(s_n : s_n^{\Phi_l}, v_n^{\Phi_l}) \text{ where } \begin{cases} s_n^{\Phi_l} = \dfrac{s_n^{\tilde{\Phi}_l} v^{\Psi_l} - s_n^{\Psi_l} v^{\tilde{\Phi}_l}}{v^{\Psi_l} - v^{\tilde{\Phi}_l}} & \text{(IV.18a)} \\ v^{\Phi_l} = \dfrac{v^{\Psi_l} v^{\tilde{\Phi}_l}}{v^{\Psi_l} - v^{\tilde{\Phi}_l}} & \text{(IV.18b)} \end{cases}$$

Such a Gaussian division only requires one computation for the variance term instead of N_s for the time-domain EP receivers.

Discussion: The proposed family restriction yields significant complexity reductions. More particularly, the FD computation of (IV.16) is much more simpler than the one performed in the time domain as it can be efficiently computed in $O(N_s \log_2(N_s))$ for the whole symbol sequence. Note that such an efficient result has been obtained without any approximation and needs both the CCFTN model and the particular Gaussian family with covariance matrices proportional to $\mathbf{I}_{N_s}$. With LCFTN signaling, a similar result could be obtained by introducing a cyclic prefix of length the shaping filter delay as in [Sug13], but it would have damaged the spectral efficiency. However, this more constrained distribution family will need more inner EP iterations to converge, and the complexity reduction has to be balanced with the overall complexity and performance trade-off at convergence. We propose to call the resulting receiver FD-EP as it allows a FD processing for the equalizer.

The following section evaluates the performance of the proposed receivers and draws a comparison with existing techniques under computational complexity constraints.

C Simulation results and comparisons

In order to enlighten the relevance of the proposed receivers, we evaluate the performance of the latter in comparison with both the reference receivers of the literature and the best Nyquist receivers for several values of spectral efficiencies and under complexity constraints. The reference receivers of the literature correspond to the well-known MMSE-IC equalizer of [TSK02], the FD-MMSE-IC of [TPB16], but also BCJR based receivers such as the RS-BCJR of [CFR01] and the M*-BCJR of [RLP07]. We did consider other message passing algorithms based on Approximate Message Passing (AMP) which turns out to have a similar implementation with our EP-based receivers. These receivers are presented at the end of this section in sub-Section C.3. Numerical complexities of the considered receivers is first evaluated before the BER performance analysis.

C.1 Receivers computational complexity

For MMSE-IC and EP based receivers, the computational complexity is dominated by the MMSE filtering operation of (IV.6). From this consideration, we propose to parameterize the MMSE filter length with $2N_w + 1$ coefficients using the method presented in sub-Sec B.6 yielding a complexity per symbol in $O((2N_w + 1)^2)$. Considering the RS-BCJR, its complexity is tuned by the memory length μ, while the factor M of the M*-BCJR is related to the retained states number. Note that we did not considered channel shortening as proposed in [RP12] to optimize the performance of BCJR-based algorithms at fixed complexity.

In the following, we assimilate the receivers complexity to their number of multiplications. The overall EP equalizer's operations are presented in Tab. IV.1. Note that the newly proposed non-circular generalization, which is only valid in FTN signaling with AWGN channel, comes with a small computational increase given that the MMSE filters have to be computed twice. Moreover, depending on the scheduling that we consider for the EP process, the symbol's equalization can be parallelized. More specifically, the MMSE-IC equalization operation using (IV.5b) can be performed in parallel for $n \in [\![1, N_s]\!]$. However, if considering the DFE extension, the equalization of a symbol s_n in (IV.5b) depends on the equalization of $s_1, ..., s_{n-1}$ which prevents from equalizing the whole sequence in parallel. Moreover, the DFE extension comes with a significant complexity growth. Finally, the WL generalization only requires a slight computational complexity increase, with depends on the value of $2N_w + 1$.

C.2 BER analysis for a given complexity and fixed spectral efficiencies

In order to compare the performance of the receivers listed in Tab. IV.1, we use a standard (7,5) convolutional code with rate $R = \frac{1}{2}$. Monte-Carlo simulations have been performed considering $N_b = 4096$ information bits mapped in Gray coding for each

Table IV.1: Real-valued multiplications of the proposed receivers for one symbol, and their ability to be symbol level parallelized

Receiver	Number of multiplications	parallel.
FD-MMSE-IC	$8\log_2(N_s) + 3\lvert\mathcal{M}\rvert + 4$	yes
MMSE-IC	$8\log_2(2N_w+1) + 8N_w^2 + 16N_w + 3\lvert\mathcal{M}\rvert + 8$	yes
RS-BCJR	$2^{\log_2\lvert\mathcal{M}\rvert\mu}(\mu + 3\times 2^{\log_2\lvert\mathcal{M}\rvert})$	no
M*-BCJR	$3\lvert\mathcal{M}\rvert 2^{\log_2\lvert\mathcal{M}\rvert}$	no
Proposed EP	$(\mathcal{I}+1)(8N_w^2 + 8\log_2(N_s) + 12N_w + 3\lvert\mathcal{M}\rvert + 10)$	yes
Proposed WL-EP	$(\mathcal{I}+1)(16N_w^2 + 8\log_2(N_s) + 24N_w + 4\lvert\mathcal{M}\rvert + 12)$	yes
Proposed EP-DFE	$(\mathcal{I}+1)(16N_w^2 + 8N_s\log_2(N_s) + 24N_w + 3\lvert\mathcal{M}\rvert + 12)$	no
Proposed WL-EP-DFE	$(\mathcal{I}+1)(32N_w^2 + 8N_s\log_2(N_s) + 40N_w + 4\lvert\mathcal{M}\rvert + 16)$	no
Proposed FD-EP	$(\mathcal{I}+1)(8\log_2(N_s) + 3\lvert\mathcal{M}\rvert + 4)$	yes

modulation. The shaping filter is a rRC filter with rolloff $\beta = 0.3$. The compression factors are set depending on the targeted spectral efficiency, and we chose not to consider values below $\tau = 0.5$ to limit the ISI. We compare the different receivers at fixed spectral efficiencies, from $\rho = 2.3$ bits/s/Hz (moderate) to $\rho = 5$ bits/s/Hz (very high). Such high spectral efficiencies are scarcely achieved in the literature with FTN signaling.

MMSE-IC and EP receivers are evaluated at fixed spectral efficiencies with LCFTN using a window filter parameter set to $N_w = 7$ symbols, unless the FD-MMSE and FD-EP which assume the CCFTN model. As far as possible, the receivers of the literature are tuned to have a same order of magnitude in terms of computational complexity compared to the proposed EP-based receivers whose complexities are presented in Tab. IV.1. Also, the FTN signaling performance simulations are compared to the associated MFB which is represented by the Nyquist communication with the same modulation achieving a spectral efficiency of $\rho_{\text{MFB}} = \rho\tau$. The number of EP iterations for EP receivers goes from $\mathcal{I} = 0$ to $\mathcal{I} = 1$ or $\mathcal{I} = 3$ depending on the spectral efficiency. Finally, the results have been obtained after 8 turbo-iterations with the decoder, and we clipped the LLRs to 8 for avoiding very confident probabilities [San+17].

Moderate spectral efficiency

We use a 8-PSK modulation and FTN signaling achieving $\rho \approx 2.3$ bits/s/Hz with $\tau = \frac{1}{2}$, and we compare it with a 64-QAM Nyquist achieving a similar spectral efficiency. Fig. IV.8 shows, for several FTN receivers (FD-MMSE-IC, MMSE-IC, RS-BCJR, M-BCJR, EP, FD-EP, WL-EP, EP-DFE-WL-EP-DFE) and for the best Nyquist scheme, the BER as a function of $\frac{E_b}{N_0}$ at $\rho = 2.3$ bits/s/Hz.

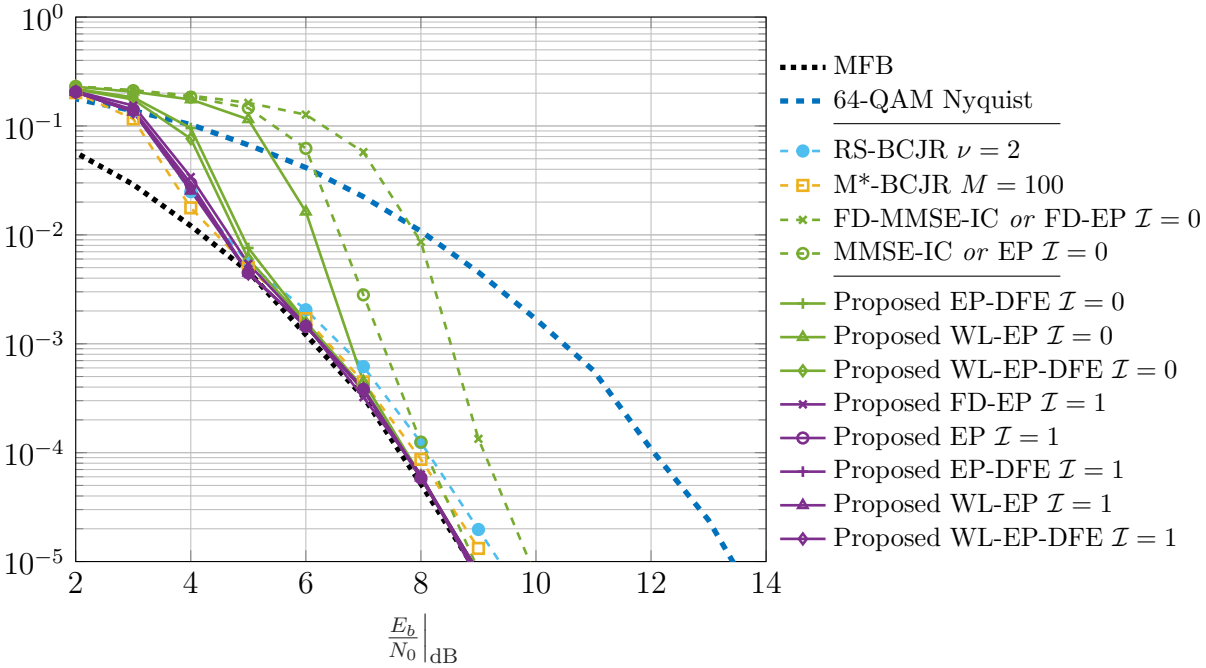

Figure IV.8: BER as a function of $\frac{E_b}{N_0}$ for several FTN receivers and the best Nyquist scheme at $\rho = 2.3$ bits/s/Hz

The FD-MMSE-IC of [TPB16] is equivalent to the FD-EP for $\mathcal{I} = 0$ and requires a lower complexity compared to the MMSE-IC. It achieves 1 dB less than its MFB then does not completely tackle the effect of the ISI. Similarly, the classical MMSE-IC equalizer of [TSK02] coincides with the EP by setting $\mathcal{I} = 0$ and performs 4 dB better than a 64-QAM Nyquist communication with same spectral efficiency for a BER of 10^{-5} while requiring a moderate complexity. The convergence can be quicker with our proposed WL extension (WL-EP), the DFE scheduling (EP-DFE), or both (WL-EP-DFE). When no EP iterations are considered, BCJR-based receivers perform better. However, by allowing EP iterations, the proposed receivers are very competitive, especially FD-EP which has a lower complexity.

High spectral efficiency

We propose here to use a 16-QAM modulation leading to a spectral efficiency of $\rho = 3$ bits/s/Hz for the compression factor $\tau = \frac{1}{2}$. Hence, the proposed receiver performance are compared to a 64-QAM Nyquist signaling with same spectral efficiency. Fig. IV.9 shows, for several FTN receivers and for the best Nyquist scheme, the BER as a function of $\frac{E_b}{N_0}$ at $\rho = 3$ bits/s/Hz. Moreover, due to their intractable complexities, BCJR based receivers are omitted. Also, given the complexity growth coming with the DFE extension for negligible gains at convergence, we do not consider the EP-DFE receiver.

The considered reception techniques of the literature are not able to handle the ISI nor to compete with Nyquist signaling. The WL extension allows a slight SNR benefit of 1 dB without iterations. Nevertheless, EP receivers offer significant enhancements

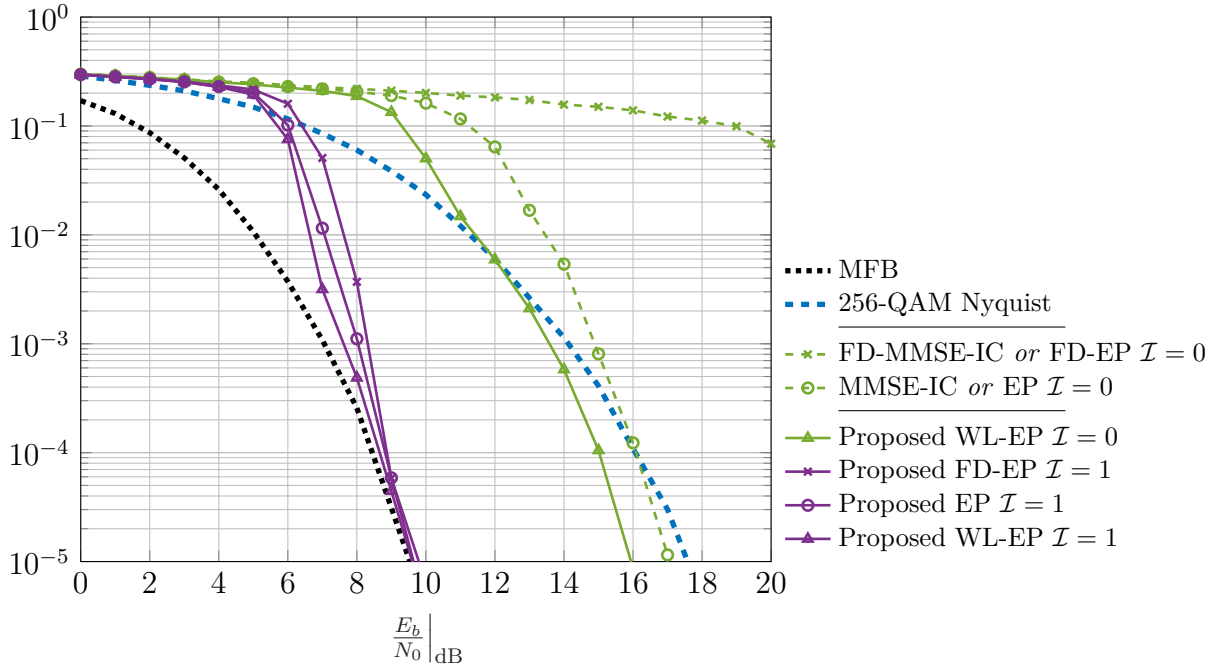

Figure IV.9: BER as a function of $\frac{E_b}{N_0}$ for several FTN receivers and the best Nyquist scheme at $\rho = 3$ bits/s/Hz

when considering EP iterations in a high spectral efficiency scheme. In any case, all the proposed EP based receivers for FTN signaling almost achieve the MFB leading to 8 dB gain compared to Nyquist signaling for a BER of 10^{-5}. Up to the authors knowledge, this new result for FTN signaling has never been achieved for such a spectral efficiency. Moreover, the FD-EP receiver completely removes the ISI and hence should be preferred due to its limited computational complexity.

Very high spectral efficiency

We consider a spectral efficiency of $\rho = 5$ bits/s/Hz. This is obtained by choosing a 2048-QAM constellation with a rRC $\beta = 0.1$ filter for a Nyquist link, and setting $\tau = 0.6$ with a 256-QAM constellation for FTN signaling and a rRC $\beta = 0.3$ filter. Moreover, due to their intractable complexities, BCJR based receivers are omitted.

Fig. IV.10 reveals that the MMSE-IC and FD-MMSE-IC equalizers do not decode at all in the considered region of $\frac{E_b}{N_0}$ while the proposed WL-EP allows performing significantly better especially for a small number of iterations at the cost of a slight complexity increase. Moreover, at such a spectral efficiency, the low complexity FD-EP receiver is not able to remove the ISI. Once again, such a spectral efficiency of 5 bits/s/Hz has never been considered with single-carrier signaling and the interest of FTN is now clearly demonstrated at such a spectral efficiency with EP reception techniques. The gain in SNR is higher than 6 dB for a BER of 10^{-5}.

In the following, we consider other strategies based on different message passing

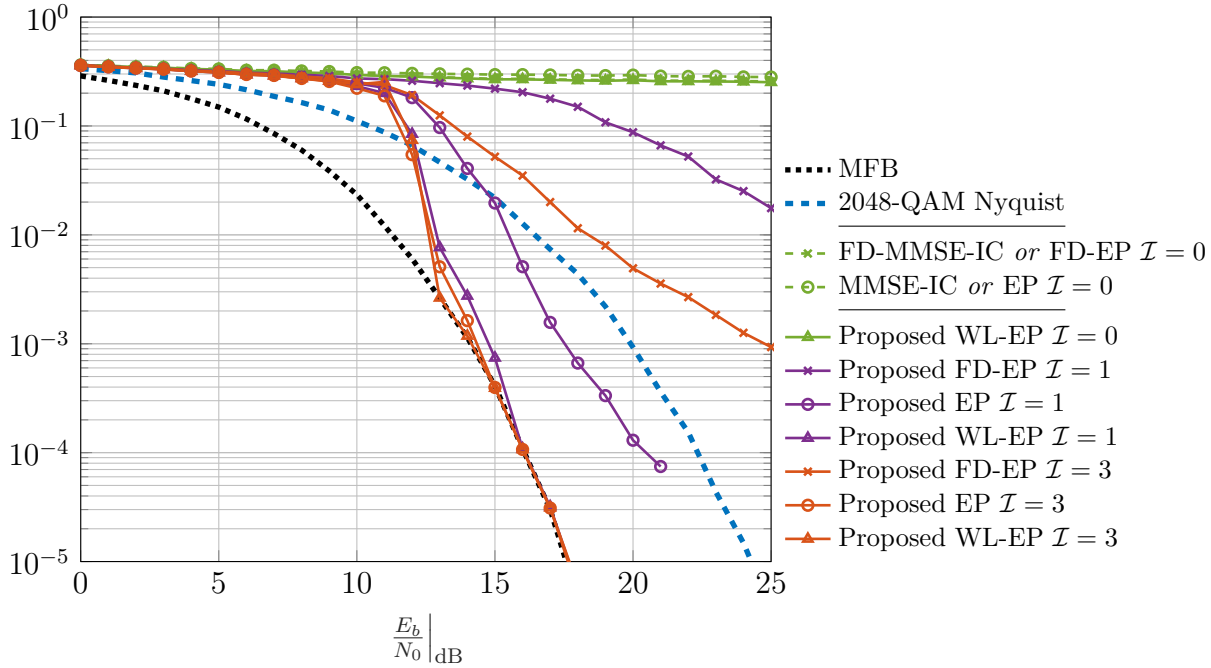

Figure IV.10: BER as a function of $\frac{E_b}{N_0}$ for several FTN receivers and the best Nyquist scheme at $\rho = 5$ bits/s/Hz

algorithms applied to our CCFTN system model.

C.3 EP-based receivers compared to other message passing algorithms

Following the emergence of the machine learning, a consequent number of message passing methods have been studied. We propose to recall the most important ones, and put them in relation with the EP-based receivers for developed for FTN signaling.

Following the complexity issue of BP, AMP has been proposed in [DMM09]. It consists in applying first an arbitrary denoising function computing a denoised soft estimate of a symbol as well as its MSE, from a prior symbol distribution. For instance, the unbiased MMSE estimate used in EP falls within the scope of such a denoising function. In that case, AMP then performs a similar Constellation Matcher as EP, but does not return an extrinsic distribution. Instead of that, it replaces the extrinsic mean and variance of the Constellation Matcher extrinsic distribution:

$$\begin{aligned}\mathbf{V}^{\Phi_l} &= \mathbf{V}^{\tilde{\Phi}_l} \\ \mathbf{s}^{\Phi_l} &= \mathbf{s}^{\tilde{\Phi}_l} - \xi_l \mathbf{V}^{\tilde{\Phi}_l}(\mathbf{s}^{\Psi_l} - \mathbf{s}^{\tilde{\Phi}_{l-1}})\end{aligned}$$

We see that the posterior variance is returned instead of the extrinsic one, while the extrinsic symbol estimate is replaced by the posterior one deprived of the correction term $\xi_l \mathbf{V}^{\tilde{\Phi}_l}(\mathbf{s}^{\Psi_l} - \mathbf{s}^{\tilde{\Phi}_{l-1}})$. This term barely removes the prior information in order to

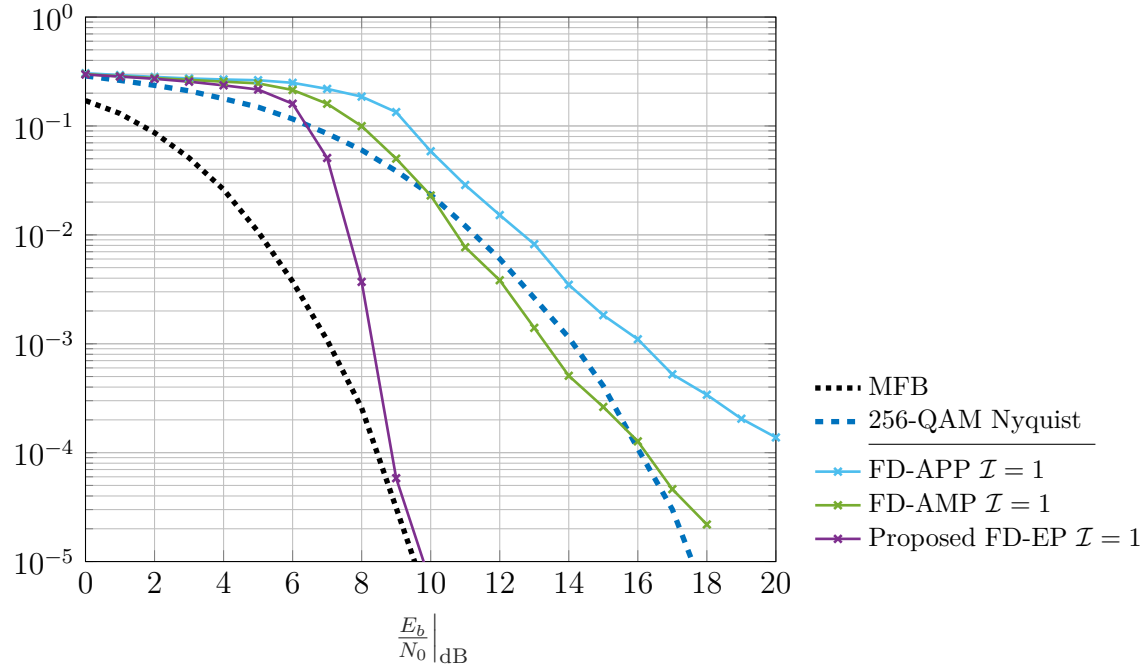

Figure IV.11: BER as a function of $\frac{E_b}{N_0}$ for several message passing receivers and the best Nyquist scheme at $\rho = 3$ bits/s/Hz

minimize the correlation between the input and the output of the Constellation Matcher. Compared to EP, it offers the guaranty of returning positive variances $\mathbf{V}^{\Phi_l}$. The rest of the implementation remains the same as EP. We propose to call the AMP algorithm for CCFTN signaling FD-AMP when considering the same Gaussian family as our FD-EP.

One can see a very close relation between the extrinsic version used by AMP and the posterior distribution of the Constellation Matcher. Indeed, up to the correction term on the mean vector, the Constellation Matcher returns its posterior distribution:

$$\mathbf{V}^{\Phi_l} = \mathbf{V}^{\tilde{\Phi}_l}$$
$$\mathbf{s}^{\Phi_l} = \mathbf{s}^{\tilde{\Phi}_l}$$

The strategy does not handle the correlation between the Constellation Matcher input and output. We call the resulting receiver FD-APP when using the same Gaussian family as our FD-EP.

An extension to AMP has been proposed by [RSF19] under the term AMP. It assumes a FG with vector variable nodes which, therefore, cannot be applied to our FG. However, an equivalent factorization can be considered as in [Pet+20] for our system model. It yields an FD-EP receiver which turns out to be exactly the same as the VAMP algorithm. We prefer the name FD-EP given that EP can be applied to a wider set of FGs.

Fig. IV.11 shows a comparison between the three FD receivers for the high spectral efficiency configuration described in the journal proposal. We clearly see the superiority

of the EP solution. Indeed, the FD-APP does not remove the correlation between its prior an extrinsic distribution. The FD-AMP handles this correlation and then performs better, but does not use a Gaussian division as EP. Hence, the Gaussian division – also called *Onsager correction* [RSF19] – seems to be preferable, even if it does not guaranty the positivity of the extrinsic variance. Note that those conclusions remain the same for different constellations, Gaussian families, scheduling and ISI.

Several damping methods have been proposed in the literature to enhance the convergence of EP. We mainly focused on the following strategy proposed in [Min+05]:

$$x_{n,\text{damped}}^{\Phi_l} = v_n^{\Phi_l}\left[\frac{(1-\alpha)x_n^{\Phi_l}}{v_n^{\Phi_l}} + \frac{\alpha x_{n,\text{damped}}^{\Phi_{l-1}}}{v_{n,\text{damped}}^{\Phi_{l-1}}}\right]$$
$$v_{n,\text{damped}}^{\Phi_l} = \left[\frac{1-\alpha}{v_n^{\Phi_l}} + \frac{\alpha}{v_{n,\text{damped}}^{\Phi_{l-1}}}\right]^{-1}$$

where $\alpha \in [0,1]$ is a damping factor which can vary along the iteration index l. However, we did not observed any major improvement, but rather some small benefits for particular combinations of τ, α, l at the price of a slower convergence. Hence, we preferred removing this damping strategy and we replaced it by clipping (i.e. upper and lower bounding) the LLRs exchanged with the decoder as proposed by [San+17]. Moreover, EP does not always guaranty the positivity of the extrinsic variance, especially at the output of the Constellation Matcher when computing $\mathbf{v}_n^{\tilde{\Phi}_l}$. The case of a negative variance often arises at convergence, and then we chose to replace the extrinsic distribution by the posterior one as detailed in Alg. 1.

C.4 Synthesis of simulation results at fixed spectral efficiencies and computational complexity

As a summary, the reception technique to prefer depends on the targeted spectral efficiency. The best performing receivers are given in Tab. IV.2 associated to their SNR and ESNR gain brought by FTN compared to Nyquist signaling. The ESNR is measured by penalizing the SNR with the IAPR for a saturation probability set to $\theta = 10^{-4}$. For spectral efficiencies below 2.3 bits/s/Hz, the existing BCJR based and (FD-)MMSE-IC receivers perform well with FTN signaling, and EP based receivers do not need any EP iteration to achieve the MFB. At moderate spectral efficiency, the DFE extension allows a quicker convergence at fixed complexity since we do not need to iterate. At 3 bits/s/Hz, EP iterations are necessary for FTN signaling to converge toward the MFB, and the FD-EP offers the best trade-off by lowering the complexity. Finally, for very high spectral efficiencies up to 5 bits/s/Hz, time domain reception techniques are the only way to almost handle the ISI at the price of more turbo-iterations. The WL generalization allows a quicker convergence and represents the best solution.

In any case, if we can afford some complexity to implement a turbo-equalization scheme at reception, FTN signaling is more profitable than Nyquist signaling over an

Table IV.2: SNR and ESNR gain of FTN compared to Nyquist signaling of the best performing receiver for different spectral efficiencies

Spectral Efficiency	Receiver	Processing Domain	SNR gain	ESNR gain
2.3 bits/s/Hz	EP-DFE $\mathcal{I} = 0$	Time	3.4 dB	4.0 dB
3 bits/s/Hz	FD-EP $\mathcal{I} = 1$	Frequency	8.1 dB	7.0 dB
5 bits/s/Hz	WL-DFE $\mathcal{I} = 3$	Time	6.9 dB	6.4 dB

AWGN channel. This holds whatever the targeted spectral efficiency with the operational considerations we used: channel code, MMSE filter length, symbol sequence length, etc... Nevertheless, these unprecedented results for high spectral efficiencies reveals the potential of FTN signaling and is achievable by the mean of EP based receivers for FTN signaling.

D Conclusion

The concept of EP receiver definitely allows FTN signaling to be a serious candidate for future communication standards. Indeed, EP enables approaching a MAP solution while remaining computationally affordable especially for high spectral efficiencies. By making use of different existing scheduling with and without DFE, and adapting the resulting algorithms to our system model, we benefit from limited computation complexity. Also, our WL extension enabled by the real-valued nature of the Nyquist filter results in a best model fitting. We finally introduced a FD-EP solution operating with a very limited complexity.

While classical receivers do not allow FTN to achieve its MFB at spectral efficiency above 2.3 bits/s/Hz, our EP based receivers clearly outperforms them by bringing FTN up to 5 bits/s/Hz with almost no performance deterioration with respect to the MFB. Also, we showed that the DFE extension is relevant for moderate spectral efficiencies but it does not perform better while requiring more complexity for higher spectral efficiencies. Furthermore, while the FD-EP should be preferred for high spectral efficiencies due to its low complexity, the proposed WL generalization appears to be profitable for reaching very high spectral efficiencies. These unprecedented results demonstrate the benefit of FTN compared to Nyquist signaling even for high spectral efficiencies.

At this point, we considered an ideal AWGN channel model which characterizes particular applications such as satellite communications for instance. In order to handle a frequency selectivity induced by a multipath channel, we explore in the following chapter the extension of FTN to multi-carrier signaling.

Chapter V

Multi-Carrier FTN and Frequency selective Channels

Outline

The interest of EP for handling ISI induced by FTN signaling has been motivated in the previous chapters over an AWGN propagation channel model. The need to extend these previous results to more complex channel models appears naturally; this is the aim of the chapter.

We start by showing that single-carrier FTN signaling studied so far shows some limits in the presence of strong frequency selectivity induced by the propagation channel. In order to facilitate the channel equalization, MFTN signaling has been proposed in the previous years. Its interest lies in the control we have on the interference induced by the shaping filters, in a similar way as for single-carrier FTN signaling. Moreover, we can use different filters and tune the frequency space separating them in order to enhance the spectral efficiency at the price of some ICI if the sub-carriers are chosen to be not orthogonal. For this reason, MFTN signaling could be a promising candidate for future standards in a complex environment. Consequently, we adapt the system model and develop a low complexity receiver based on EP. This yields a new doubly-circular MFTN system model combined with a FD-EP receiver adapted to this waveform. The resulting model is able to target spectral efficiencies unachieved so far, while maintaining a low processing complexity. The content presented in this chapter will be shortly submitted for publication in a journal paper.

A Motivation of Multi-Carrier FTN signaling

This section shows the limitations of single-carrier FTN signaling in presence of a multipath propagation channel. We first derive the model of a frequency-selective channel over the communication bandwidth. The resulting ISI combines both the FTN and the channel effects. Provided that the selectivity is sufficient, this interference becomes too severe to be properly handled by the EP receivers. Consequently, in this setup, FTN often yields poorer performance than Nyquist signaling.

A.1 Propagation channel of a wireless communication

We focus on propagation channels considered as time-invariant compared to the sequence duration. The modelization of a channel should represent all the effects of a wireless communication between two antennas. Depending on the environment of the communication, the transmitted waves are diffracted, reflected or refracted. Moreover, the different paths yield different delays at reception, each associated to an amplitude tending to decrease when the delay increases. Consequently, the modelization of a channel composed of N_v paths is a (linear) convolution of a causal filter $v(t)$ whose impulse response is defined as follows:

$$v(t) = \sum_{n=1}^{N_v} \alpha_n \delta(t - t_n) \tag{V.1}$$

where any path $n \in [\![1, N_v]\!]$ is characterized by its delay $t_n \geq 0$ and complex amplitude α_n. Without loss of generality, the channel filter $v(t)$ is shifted by the shortest path delay and we assume that the delays are ordered according to their indices yielding $t_1 = 0$, $|\alpha_1| > 0$ and $\forall n \in [\![1, N_v - 1]\!] : t_n < t_{n+1}$.

Moreover, we consider a random noise gathering some undesired impacts of the analog components involved in the communication. This AWGN component denoted $w(t)$ is supposed to be complex, circular and centered with PSD $\mathbb{E}|W(f)|^2 = N_0$ where $W(f)$ is the FT of $w(t)$.

The received signal after the channel model is then defined as follows:

$$r(t) = (x \star v)(t) + w(t) \tag{V.2}$$

We can also use a matrix formalism equivalent to the definition of $r(t)$ over the communication frequency supports. To do so, we define the discrete-time received vector $\mathbf{r} = [r_1, r_2, ..., r_{N_r}]^T$ sampled at rate T_e^{-1} over its time support as in [MOP94] where $r_m = (r \star \gamma)(mT_e)$ yielding:

$$\mathbf{r} = \mathbf{VPUx} + \mathbf{w} \tag{V.3}$$

with $\mathbf{w} = [w_1, w_2, ..., w_{N_r}]^T$ having $w_m = (w \star \gamma)(mT_e)$, and $\mathbf{V}$ is the $(N_r \times N_x)$ convolution matrix associated to $v(t)$ sampled at rate T_e^{-1} over its time support, where $N_r = N_x + \left\lceil \frac{t_{N_v}}{T_e} \right\rceil$. The filter $\gamma(t)$ applied to $r(t)$ is used to preserve the noise whiteness and energy within the communication bandwidth. Moreover, one can show that a noise component of the vector $\mathbf{w}$ follows $w_m \sim \mathcal{N}_{\mathbb{C}}(0, \sigma_w^2)$ where $\sigma_w^2 = N_0$ and we have $\mathbb{E}[w_m w_{m'}^*] = 0$ if $m \neq m'$.

A.2 Limitations of Single-Carrier FTN signaling with Frequency selective Channels

We propose to evaluate FTN signaling in presence of a deterministic and invariant multipath channel. To do so, we assume that the communication is performed over a theoretical frequency-selective Proakis C channel $v_C(t)$ composed of five paths separated by T. Hence, the impulse response of $v_C(t)$ is expressed as follows:

$$v_C(t) = \frac{1}{\sqrt{19}} \left(\delta(t - 2T) + 2\delta(t - T) + 3\delta(t) + 2\delta(t + T) + \delta(t + 2T)\right) \tag{V.4}$$

The frequency response $|V_C(f)|^2$ of this channel is represented in Fig. V.1.

The global filter now defined as $g(t) = (h \star v_C)(t)$ is sampled every symbol duration $T_s = \tau T$ to obtain the matrix $\mathbf{G}$ representing the aliased Nyquist filter. For this reason, the more we compress in FTN signaling with a low value of τ, the longer is the ISI induced by the propagation channel. Hence, the T_s-sampled delay spread is higher by a factor τ^{-1} in FTN signaling compared to Nyquist signaling. For this reason, the resulting ISI is more powerful and so FTN signaling is more sensitive to a multipath channel.

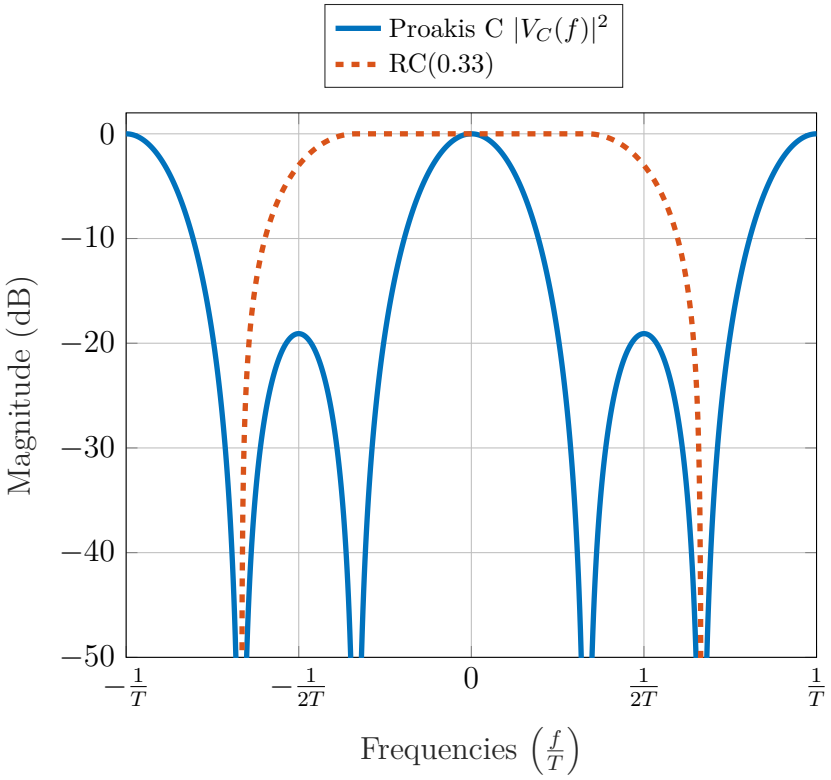

Figure V.1: Frequency response of the channel $v_C(t)$ and RC(0.33) filter

We concentrate on the EP receivers developed in Chap. IV applied to the global filter $g(t)$ grouping both the Nyquist filter and the frequency-selective channel impulse responses. From this observation, the EP receivers are naturally extended when the channel filter is invariant, deterministic and known from the receiver. Moreover, we recall that the WL extension we proposed for EP receivers does not hold in the general case of a complex channel. For this reason, such an extension is voluntarily omitted in the following.

We evaluated in Fig. V.2 the performance of the FD-EP receiver with both CCFTN and Nyquist signaling at a fixed spectral efficiency of 1.5 bits/s/Hz and a given rolloff $\beta = 0.33$. Such a spectral efficiency is achieved by a QPSK FTN waveform setting $\tau = 0.5$ and a 16-QAM Nyquist communication. In Fig. V.2, $N_b = 4096$ information bits are encoded using a $(7, 5)_8$ convolutional code with rate $R = \frac{1}{2}$. At reception, we perform 8 turbo-iterations and 3 EP iterations. Although we showed in Chap. IV that EP is able to handle strong interference, the global ISI is here to severe to be properly mitigated by this receiver. Indeed, the QPSK FTN communication performs worse than the 16-QAM Nyquist alternative, and losses 8 dB from its MFB. Consequently, in a multipath context with high frequency selectivity, the Nyquist communication can achieve similar or better performance than FTN signaling. Therefore, we propose to extend the EP receivers we developed to multi-carrier FTN communications in order to overcome the channel propagation frequency selectivity.

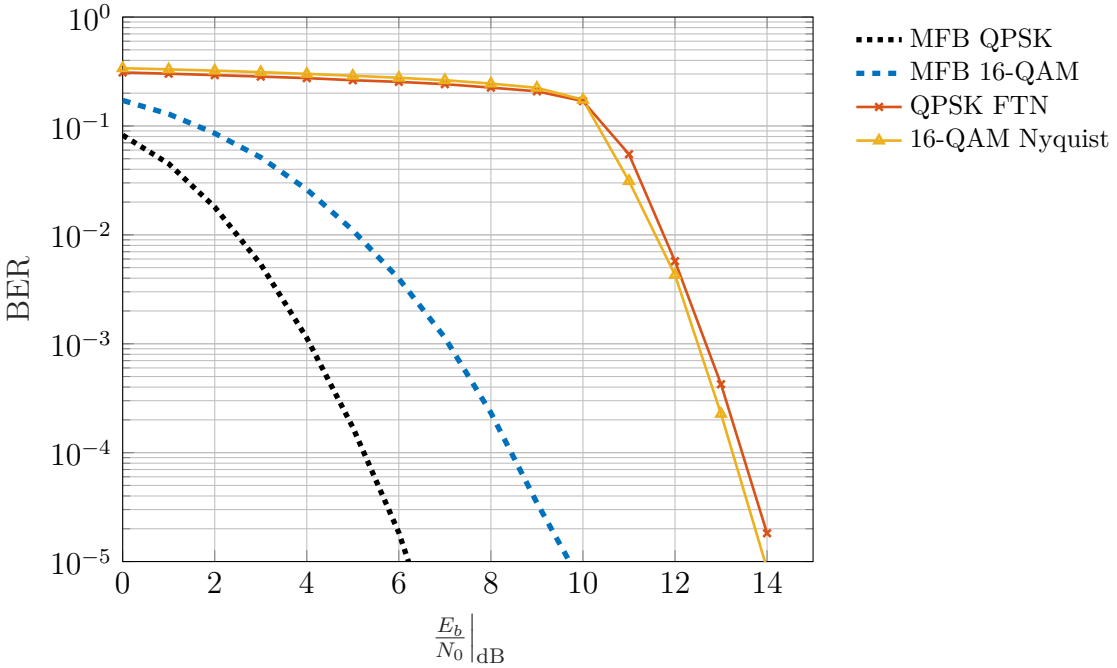

Figure V.2: BER of FTN $\tau = 0.5$ and Nyquist communications achieving 1.5 bits/s/Hz over the channel $v_C(t)$ processed by the FD-EP receiver

B Multi-Carrier FTN signaling for Frequency selective Channels

We saw that severe ISI coming from the channel combined with FTN signaling approaches the EP receivers limits. For this reason, MFTN signaling has been proposed to simplify the equalization step. This concept is based on transmitting the symbols over different sub-carriers, on which the channel can be considered as relatively flat in the frequency domain. The shaping filters, as well as the time and frequency separations can then be tuned to limit the induced interference while achieving high spectral efficiencies.

We start this section by developing the background of MFTN signaling, before presenting a classical MFTN transmitter and the existing receivers of the literature. After that, we propose a new doubly-circular MFTN system model combined with a low complexity EP-based receiver able to target high spectral efficiencies.

B.1 Background of Multi-Carrier FTN signaling

The actual standards of communications faced the frequency selectivity issue of the propagation channel coming with high data rates. While channel equalization was implemented in 3G, new standards such as DVB-T, 4G, 5G and WiFi use multi-carrier signaling to handle the multipath effect of the channel. This technique aims at carrying multiple data in parallel on closely spaced sub-carriers. The frequency space F between

two adjacent sub-carriers, the symbol's constellation and the prototype filter $p(t)$ of each sub-carrier are chosen to optimize different criteria such as the spectral efficiency, the time and frequency localization, the PAPR, the ease of synchronization and the capacity of interference processing. If there are enough sub-carriers over the communication bandwidth, the channel filter perceived by each sub-carrier turns out to be frequency flat. Moreover, the delay spread of the channel filter generates interference at the ending frames which could be handled by introducing a cyclic-prefix.

The most simple example of a multi-carrier scheme is the OFDM technique, achieving high data rates while keeping orthogonal sub-carriers by setting $p(t)$ as a frequency cardinal sine filter at the price of high out-of-band power. Moreover, the transceiver complexity turns out to be very low because the transmitter performs a simple IFFT operation and the receiver implements a FFT after leaving the cyclic prefix out. For its advantages, OFDM based systems are now widely used and this technique is at the origin of most of the multi-carrier waveforms.

Derived from OFDM, the concept of Multi-Carrier FTN signaling has been introduced by John B. Anderson and F. Rusek in 2006 under the name MFTN [AR06] and detailed in 2009 [RA09b]. They proposed to extend OFDM to other Nyquist pulses such as rRC filters with bandwidth $W = (1 + \beta)T^{-1}$. In order to compensate the spectral efficiency damage introduced by the rolloff, they compress in time and also in frequency domains setting $T_s = \tau T$ and $F = \nu T^{-1}$ where $\nu \in (0, 1+\beta]$ is the frequency compression factor. Hence, as soon as we have $\nu < 1 + \beta$, the sub-carriers are not orthogonal anymore. This MFTN model combines two types of interference: ISI coming from the time compression and channel filter, and ICI generated by the frequency compression.

The first works on MFTN aimed at estimating the bi-dimensional Mazo bound, i.e. the lower compression products $\tau\nu$ yielding the same BER performance at high SNR as OFDM for a given Nyquist pulse $p(t)$ and constellation when optimally processing the interference [RA09b]. Surprisingly, it appeared that the time and frequency compression factors are almost independent. While the time-domain Mazo bound is $\tau = 0.802$ for a cardinal sine filter, the bi-dimensional compression product can be decreased down to $\tau\nu = 0.54$ for $\beta = 0.1$. This theoritical and optimistic result revealed a potential spectral efficiency gain of 85% compared to the best orthogonal scheme. Hence, MFTN signaling is nowadays a cutting edge research area and is sometimes proposed for next generation standards of digital communications [Lee+19].

Following the first propositions of MFTN signaling, some studies extended the results of other pulse shapes such as Isotropic Orthogonal Transform Algorithm (IOTA) proposing optimal time and frequency localization [DMO11]. Multiple studies also drop out the Nyquist constraint imposed to the filter such as [Pie+13; Sec+15; Mar17] yielding small improvements. Other authors try to limit the interference by optimizing the symbols' constellation as proposed in [Bei+14], or [SIN17] which uses index modulations at the price of a higher PAPR. Offset constellations can also be used to limit the interference and slightly decrease the PAPR as proposed by [Lah+17] with precoding as in [JLM19]. Nevertheless, the gain decreases when considering rich constellations, and precoding techniques suffer from high PAPR or spectrum damages. Filter optimization is a wide area of research, but its impact on the interference power at fixed spectral efficiency

is also limited. For this reason, different propositions surged to process the interference of MFTN signaling. We dig into them in the following sub-section.

B.2 System model of MFTN signaling of the literature

The MFTN system model follows the same symbol generation process as single-carrier FTN signaling. Hence, we generate iid bits $\mathbf{b}$ which are encoded and interleaved. These bits are then converted to N_s symbols $\mathbf{s}$ given a complex constellation $\mathcal{M}$.

MFTN signal shaping

We assume a MFTN signal composed of N sub-carriers separated by $F = \nu T^{-1}$ Hz, carrying K symbols per sub-carrier with duration $T_s = \tau T$ where T^{-1} represents the -3 dB bandwidth of the Nyquist filter $p(t)$. The numbers N and K satisfy $N_s = NK$ where N_s can be adjusted by padding the vector $\mathbf{s}$. The transmitted signal is expressed as follows:

$$x(t) = \sum_{k=1}^{K}\sum_{l=1}^{N} s_l^k p(t-(k-1)T_s)\,\mathrm{e}^{j2\pi(l-1)Ft} \tag{V.5}$$

$$= \sum_{k=1}^{K}\sum_{l=1}^{N} \vec{s}_l^k p_l(t-(k-1)T_s) \tag{V.6}$$

where s_l^k is the kth symbol of the lth sub-carrier, $\vec{s}_l^k = s_l^k\,\mathrm{e}^{-j2\pi\tau\nu(l-1)(k-1)}$ corresponds to the rotated symbol s_l^k, and $p_l(t) = p(t)\,\mathrm{e}^{j2\pi(l-1)Ft}$ is the filter associated to the lth sub-carrier. Using a matrix formalism is easier with the rewritten expression (V.6) instead of (V.5), and we define the $(N_s \times 1)$ symbols vector $\mathbf{s}$ organized as follows:

$$\mathbf{s} = \begin{pmatrix} \mathbf{s}_1 \\ \mathbf{s}_2 \\ \vdots \\ \mathbf{s}_N \end{pmatrix} \tag{V.7}$$

where each sub-vector $\mathbf{s}_l = [s_l^1, s_l^2, .., s_l^K]^T$ corresponds to the symbols of the lth sub-carrier. We define the rotated symbols vectors $\vec{\mathbf{s}}$ and $\vec{\mathbf{s}}_l$ organized similarly as $\mathbf{s}$ and $\mathbf{s}_l$, and we have:

$$\vec{\mathbf{s}} = \mathbf{R}\mathbf{s} \tag{V.8}$$

with $\mathbf{R} = (\mathrm{e}^{j2\pi\tau\nu(l-1)(k-1)}\,\delta_{i-j})_{i=(l-1)K+k,j}$ the $(N_s \times N_s)$ diagonal matrix aiming at rotating the symbols $\mathbf{s}$.

Following the same methods as single-carrier signaling, we consider equivalently the discrete version of $x(t)$. To do so, the signal $x(t)$ is sampled at a rate T_e^{-1} chosen to

be wider than the communication bandwidth. It yields the vector $\mathbf{x} = [x_1, x_2, ..., x_{N_x}]^T$ whose elements are expressed as:

$$x_i = x((i-1)T_e - L_\tau T_s) \tag{V.9}$$

$$= \sum_{k=1}^{K} \sum_{l=1}^{N} \vec{s}_l^k p_l((i-1)T_e - (L_\tau + k - 1)T_s) \tag{V.10}$$

Using a matrix formalism, we define the vector $\mathbf{x}$ whose expression is similar as single-carrier FTN signaling:

$$\mathbf{x} = \mathbf{P}\mathbf{U}\vec{\mathbf{s}} \tag{V.11}$$

where $\mathbf{U}$ is a $(\frac{T_s}{T_e}N_s \times N_s)$ matrix up-sampling $\vec{\mathbf{s}}$ by a factor $\frac{T_s}{T_e}$. The $(N_x \times \frac{T_s}{T_e}N_s)$ matrix $\mathbf{P}$ expressed as:

$$\mathbf{P} = \begin{pmatrix} \mathbf{P}_1 & \mathbf{P}_2 & \dots & \mathbf{P}_N \end{pmatrix} \tag{V.12}$$

where each $\mathbf{P}_l$ is a $(N_r \times \frac{T_s}{T_e}K)$ matrix generating the lth sub-carrier shaping filter defined as:

$$(\mathbf{P}_l)_{i,j} = p_l((i+j-2)T_e - L_\tau T_s) \tag{V.13}$$

At reception, we retrieve the continuous-time signal $r(t)$ subject to the AWGN component and the multipath channel. Hence, its expression is given by:

$$r(t) = (x * v)(t) + w(t) \tag{V.14}$$

which can be translated in discrete-time. For the sake of simplicity, we omit a normalized ideal anti-aliasing filter of bandwidth T_e^{-1}. The expression of the discrete-time received signal becomes:

$$\mathbf{r} = \mathbf{H}\mathbf{U}\vec{\mathbf{s}} + \mathbf{w} \tag{V.15}$$

where $\mathbf{H} = \mathbf{V}\mathbf{P}$ is a $(N_r \times \frac{T_s}{T_e}N_s)$ convolution matrix associated with $h(t) = (v * p)(t)$ representing the effects of the transmit filters and the multipath channel. In a similar way, the matrix $\mathbf{V}$ represents the $(N_r \times N_x)$ convolution matrix associated to the filter $v(t)$ over the communication bandwidth, sampled at rate T_e^{-1}.

At reception, we assume a perfect knowledge of the multipath channel coefficients. The observation model given in (V.15) is similar as the single-carrier FTN signaling one. Hence, we can directly apply the MAP, MMSE and EP receivers starting by matched filtering and down-sampling at time T_s. It yields the following signal:

$$\mathbf{y} = \mathbf{R}^\dagger\mathbf{D}\mathbf{H}^\dagger\mathbf{r} \tag{V.16}$$

where $\mathbf{D} = \mathbf{U}^\dagger$ is a $(N_s \times \frac{T_s}{T_e}N_s)$ down-sampling matrix. Note that $\mathbf{w}' = \mathbf{R}^\dagger\mathbf{D}\mathbf{H}^\dagger\mathbf{w}$ is a colored noise if $\tau \neq 1$ or $\nu \neq 1$, and $\mathbf{G} = \mathbf{D}\mathbf{H}^\dagger\mathbf{H}\mathbf{U}$ is the ambiguity function sampled at

the symbol-time T_s and frequency space F. This $(N_s \times N_s)$ matrix $\mathbf{G}$ is structured as follows:

$$\mathbf{G} = \begin{pmatrix} \mathbf{G}_{1,1} & \mathbf{G}_{1,2} & ... & \mathbf{G}_{1,N} \\ \mathbf{G}_{2,1} & \mathbf{G}_{2,2} & ... & \mathbf{G}_{2,N} \\ \vdots & \vdots & \ddots & \vdots \\ \mathbf{G}_{N,1} & \mathbf{G}_{N,N-1} & ... & \mathbf{G}_{N,N} \end{pmatrix} \tag{V.17}$$

where $\mathbf{G}_{l',l} = \mathbf{U}'^{\dagger}\mathbf{H}_{l'}^{\dagger}\mathbf{H}_l\mathbf{U}'$ can be expressed as:

$$(\mathbf{G}_{l',l})_{i,j} = \int h_{l'}^*(t)h_l(t-(j-i)T_s)\,\mathrm{d}t \tag{V.18}$$

with $\mathbf{U}'$ is a $(\frac{T_s}{T_e}K \times K)$ sub-matrix of $\mathbf{U}$ and $h_l(t) = h(t)\,\mathrm{e}^{j2\pi(l-1)Ft}$. Defining the rotated signal $\vec{\mathbf{y}} = \mathbf{R}\mathbf{y}$ and noise $\vec{\mathbf{w}} = \mathbf{R}\mathbf{w}$, (V.16) becomes:

$$\vec{\mathbf{y}} = \mathbf{G}\vec{\mathbf{s}} + \vec{\mathbf{w}}' \tag{V.19}$$

The matrix $\mathbf{G}$ characterizes the transformation applied to every rotated symbol $\vec{s}_l^k$ on the vector $\vec{\mathbf{y}}$. More precisely, a coefficient $(\mathbf{G}_{l',l})_{i,j}$ represents the quantity of $\vec{s}_l^k$ (the kth symbol of sub-carrier l) at the jth symbol time in the l'th sub-carrier of the vector $\vec{\mathbf{y}}$. For orthogonal communications, we have $(\mathbf{G}_{l-l'})_{i,j} \propto \delta_{i-j}\delta_{l-l'}$ where the term δ_{i-j} characterizes the absence of ISI and the term $\delta_{l',l}$ stands for no ICI. When we have $\nu = 1+\beta$, the communication does not generate any ICI and $\mathbf{G}$ turns out to be a block-diagonal matrix because $\mathbf{G}_{l',l} = \mathbf{0}_K$ for $l \neq l'$. For $\tau = 1$, their is no ISI and the diagonal sub-matrices $\mathbf{G}_{l,l}$ of $\mathbf{G}$ become diagonal matrices, i.e. we have $\forall l : \mathbf{G}_{l,l} \propto \mathbf{I}_K$. The spectral efficiency of such a system is the following:

$$\rho = \frac{R\log_2|\mathcal{M}|}{\tau\nu} \tag{V.20}$$

MFTN receivers of the literature

After matched-filter and down-sampling, different options are offered to retrieve the symbols information before decoding. The joint symbol estimation problem of the whole symbol vector can be theoretically handled by the MAP estimator, or the MMSE equalization. In both cases, the problem aims at maximizing the posterior distribution $p(\vec{\mathbf{s}}|\vec{\mathbf{y}})$ where $\vec{\mathbf{s}}$ is supposed to be a sequence of rotated symbols (MAP) or gaussianly distributed random variables (MMSE). However, the complexity of such algorithms is not affordable because the interference applied to each symbol depends on $K-1$ others symbols if their is no ICI and $N_s - 1$ symbols else. The corresponding FG is given in Fig. V.3.

An alternative to the MAP sequence computation is a sub-carrier MAP-based estimation which minimizes each rotated sub-sequence $\vec{\mathbf{s}}_{l'}$ probability of error instead of the

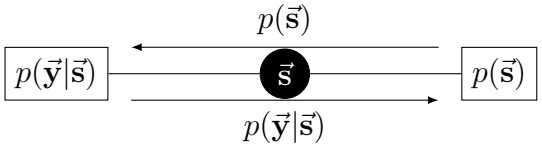

Figure V.3: Factor Graph of the sequence MAP factorization

full symbol sequence. Considering a time-domain MMSE-based equalizer, the complexity decreases from $O(N_s^3)$ to $O(N[(2L+1)K]^3)$ while remaining optimal. A common approximation proposed by [RA09b] consists in performing IC of the adjacent sub-carriers before estimating a sub-carrier l'. This amounts to consider that the observation of $\vec{\mathbf{y}}_l$ with $l \neq l'$ is not informative for $\vec{\mathbf{s}}_{l'}$: $p(\vec{\mathbf{s}}_{l'}|\vec{\mathbf{y}}_l) \propto 1$ where $\vec{\mathbf{y}}_l$ is the lth sub-vector with length N of $\vec{\mathbf{y}}$. Hence, the sub-carrier posterior distribution is approximated to the computation of $p(\vec{\mathbf{s}}_{l'}|\vec{\mathbf{y}}_{l'})$ which factorizes as follows:

$$p(\vec{\mathbf{s}}_{l'}|\vec{\mathbf{y}}_{l'}) = \sum_{\vec{\mathbf{s}}_{\sim l'}} p(\vec{\mathbf{s}}|\vec{\mathbf{y}}_{l'}) \tag{V.21}$$

$$\propto \sum_{\vec{\mathbf{s}}_{\sim l'}} p(\vec{\mathbf{y}}_{l'}|\vec{\mathbf{s}}_{l'-L}, \vec{\mathbf{s}}_{l'-L+1}, ..., \vec{\mathbf{s}}_{l'+L}) \prod_{m=1}^{N} p(\vec{\mathbf{s}}_m) \tag{V.22}$$

The factorization (V.22) is depicted in the FG of Fig. V.4 where the dashed diagonal downard messages $p(\vec{\mathbf{s}}_{l'}|\vec{\mathbf{y}}_l), l \neq l'$ have been ignored due to the approximation $p(\vec{\mathbf{s}}_{l'}|\vec{\mathbf{y}}_l) \propto 1$. The posterior sub-carrier distribution leads to computing $\vec{\mathbf{z}}_{l'}$ the l'th sub-carrier of $\vec{\mathbf{y}}$ deprived of ICI as follows:

$$\vec{\mathbf{z}}_{l'} = \vec{\mathbf{y}}_{l'} - \sum_{i=-L, i\neq 0}^{L} \mathbf{G}_{l',l'+i}\vec{\mathbf{s}}_{l'+i} \tag{V.23}$$

This simplifies the estimation of the full sequence with length N_s to N estimations of sub-sequences with length K. However, it requires to compute $\vec{\mathbf{z}}_l$ with the knowledge of the adjacent sub-carrier rotated symbols $\vec{\mathbf{s}}_{l+i}$. In practice, this rotated symbols' information is brought by the prior information of the decoder making this IC subject to error propagation. In order to limit this phenomenon, the scheduling for IC should start with processing the first and last sub-carriers before progressing toward the central sub-carriers. However, with an iterative receiver, the scheduling strategy has almost no impact on the overall performance.

The paper [RA09b] uses IC for ICI cancellation combined with N BCJR algorithms achieving a product $\tau\nu \approx 0.43$ yielding a spectral efficiency more than twice better than Nyquist signaling with almost no BER degradation. However, the huge complexity of N BCJR estimators make this solution quickly intractable for rich constellations and high spectral efficiencies. To tackle this problem, a low complexity symbol-by-symbol receiver is exposed in [BFC09] based on modeling the interference as a gaussianly distributed variable. A two-dimensional MMSE equalizer has also been proposed in [Pen+18] but it requires to inverse a $(N_s \times N_s)$ matrix, making this solution out of the low-complexity scope of this thesis. Hence, an alternative solution aiming at lowering the complexity has been proposed in [Ma+20] with similar performance, but the complexity savings are not

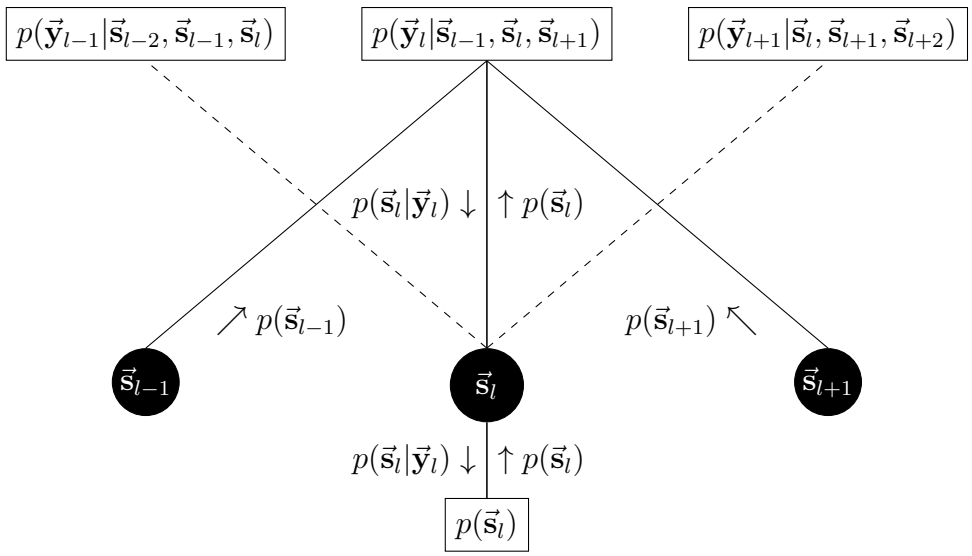

Figure V.4: Factor Graph of the approximate sub-carrier MAP factorization for $\mathbf{s}_l$ assuming $L = 1$

significant enough to be seriously considered in practice. The one dimensional MMSE equalization taking benefit of the sub-optimal IC elimination for ICI has been explored in [Tia+18] with even more performance degradation. Another algorithm based on a FG formalism has also been developed in [CFP11] with a linear complexity for single or multi-dimensional interference. Finally, a FD-MMSE equalization with cyclic-prefix insertion is considered in [Pen+17] for MFTN yielding a low-complexity algorithm, yet unable to achieve high spectral efficiencies. Following the same perspective, we propose to go further the FD-MMSE equalization by combining it with EP. This yields us to propose a new EP-based receiver combined with a new doubly-circular MFTN model, able to achieve high spectral efficiencies while maintaining a limited complexity.

B.3 Proposed Doubly-Circular MFTN signaling system model

In order to target a FD processing at reception, we adapt the commonly used MFTN system model by introducing two circularities: one in the time-domain, and another in the frequency domain.

The FD circularity is similar as in single-carrier FTN signaling. Each sub-carrier is shaped by the periodized shaping filter $\dot{p}(t)$ defined as:

$$\dot{p}(t) = \sum_{m\in\mathbb{Z}} p(t - mNT_s) \tag{V.24}$$

Hence, replacing $p(t)$ by $\dot{p}(t)$ in (V.6) yields:

$$\dot{x}(t) = \sum_{k=1}^{K}\sum_{l=1}^{N} \bar{s}_l^k \dot{p}_l(t - (k-1)T_s) \tag{V.25}$$

where $\dot{p}_l(t) = \dot{p}(t)\,\mathrm{e}^{j2\pi(l-1)Ft}$ is the periodized shaping filter frequency-shifted by $(l-1)F$ Hz. As presented hereafter, convolution with the shaping filter can then be applied in the FD with a lower complexity.

The time-domain circularity is analogous to the FD one, but performed in the time-domain. As presented before, the circularity in a given domain is obtained by sampling the corresponding signal in the dual domain, or equivalently by periodizing the signal in the actual domain. Following this logic, we chose to build the discrete signal $\ddot{\mathbf{x}}$ by sampling $\dot{x}(t)$ at rate $T_e^{-1} = NF$. Such a sampling yields aliasing as represented in Fig. V.6 compared to the classical linear MFTN signaling represented in Fig. V.5. Note that the frequency centers have been shifted to the signal's center frequency in these figures. In doubly-circular MFTN signaling, the first sub-carrier interferes with the last one, as if they where neighbors sub-carriers. The first effect is a bandwidth reduction of the full signal, and hence a spectral efficiency increase for low values of N. The second effect is that each sub-carrier is subject to the same distribution of interference, even the first and last ones.

These two circularities allow an easy and low-complexity construction of the transmitted signal $\ddot{\mathbf{x}}$ in the frequency domain. Hence, it has a length $N_{\ddot{\mathbf{x}}} = N_s\tau\nu$ and can be expressed as:

$$\ddot{\mathbf{x}} = \ddot{\mathbf{P}}\mathbf{U}\vec{\mathbf{s}} \tag{V.26}$$

where $\ddot{\mathbf{P}}$ is the $(N_{\ddot{\mathbf{x}}} \times NN_s\tau\nu)$ shaping matrix described hereafter, and $\mathbf{U}$ is the $(NN_s\tau\nu \times N_s)$ up-sampling matrix by a factor $\frac{T_s}{T_e} = N\tau\nu$. The sampling rate yields a first operational requirement of the proposed doubly-circular MFTN signaling: the factor $N\tau\nu$ is required to be an integer, which is not very restrictive in practice. The shaping matrix $\ddot{\mathbf{P}}$ is composed as follows:

$$\ddot{\mathbf{P}} = \begin{pmatrix} \ddot{\mathbf{P}}_1 & \ddot{\mathbf{P}}_2 & \dots & \ddot{\mathbf{P}}_N \end{pmatrix} \tag{V.27}$$

where each $(N_s\tau\nu \times N_s\tau\nu)$ sub-matrix $\ddot{\mathbf{P}}_l$ defined as $(\ddot{\mathbf{P}}_l)_{i,j} = \dot{p}((j-i)T_e)$ is not only Hermitian but also circulant to produce the FD circularity.

The construction of $\ddot{\mathbf{x}}$ can be performed in the FD because it can be decomposed as follows:

$$\ddot{\mathbf{x}} = \sum_{l=1}^{N} \mathbf{F}^{\dagger}_{N_{\ddot{\mathbf{x}}}} \hat{\ddot{\mathbf{x}}}_l \tag{V.28}$$

where $\hat{\ddot{\mathbf{x}}}_l$ is the FD lth sub-carrier of $\ddot{\mathbf{x}}$ which can be obtained following the process depicted in Fig. V.7. From a mathematical point of view, $\hat{\ddot{\mathbf{x}}}_l$ can be expressed as:

$$\hat{\ddot{\mathbf{x}}}_l = \mathbf{F}_{N_{\ddot{\mathbf{x}}}} \ddot{\mathbf{P}}_l \mathbf{U}' \vec{\mathbf{s}}_l \tag{V.29}$$

$$= \hat{\ddot{\mathbf{P}}}_l \mathbf{F}_{N_{\ddot{\mathbf{x}}}} \mathbf{U}' \vec{\mathbf{s}}_l \tag{V.30}$$

with $\mathbf{U}'$ the $(N_{\ddot{\mathbf{x}}} \times K)$ up-sampling matrix and $\hat{\ddot{\mathbf{P}}}_l = \mathbf{F}_{N_{\ddot{\mathbf{x}}}} \ddot{\mathbf{P}}_l \mathbf{F}^{\dagger}_{N_{\ddot{\mathbf{x}}}}$ a diagonal matrix com-

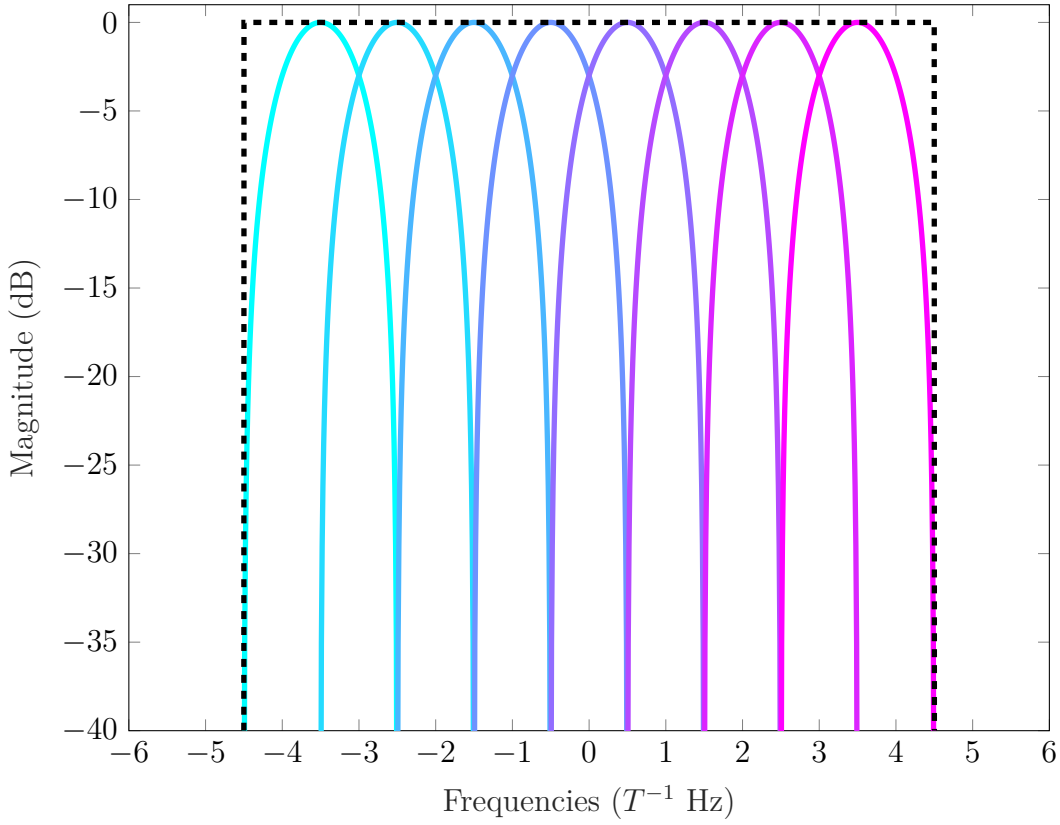

Figure V.5: FD shaping filters of linear MFTN signaling with $\beta = 1$ and $\nu = 1$

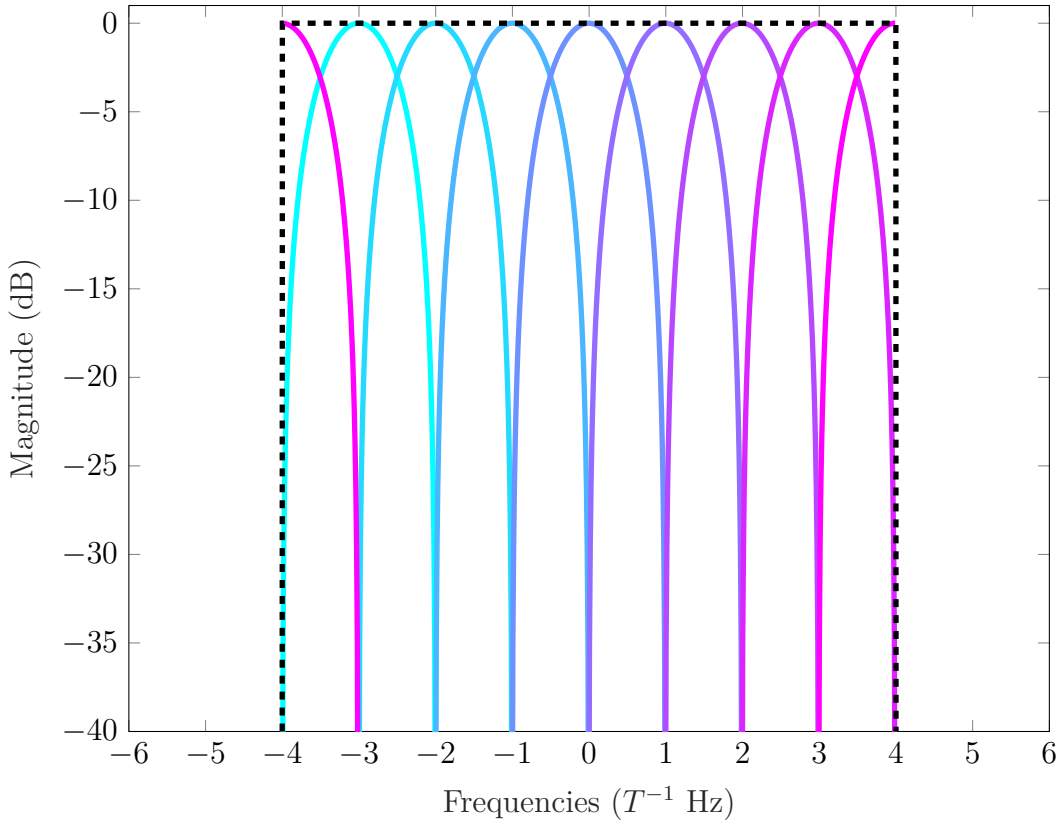

Figure V.6: FD shaping filters of doubly-circular MFTN signaling with $\beta = 1$ and $\nu = 1$

posed of the Fourier coefficients of $p_l(t)$. These Fourier coefficients are the same as those of $p(t)$, shifted by $(l-1)F$ because $P_l(f) = P(f-(l-1)F)$. Consequently, each vector $\hat{\ddot{\mathbf{x}}}_l$ is obtained by multiplying the discrete shifted frequency response $\{P_l(\frac{n-1}{KT_s})\}_{n\in[\![1,N_{\ddot{\mathbf{x}}}]\!]}$ of the filter $p(t)$ with $\mathbf{F}_{N_{\ddot{\mathbf{x}}}}\mathbf{U}'\vec{\mathbf{s}}_l$. Moreover, $\mathbf{F}_{N_{\ddot{\mathbf{x}}}}\mathbf{U}'\vec{\mathbf{s}}_l$ is nothing more than the periodization of $\mathbf{F}_N\vec{\mathbf{s}}_l$ the FT of $\vec{\mathbf{s}}_l$. The transmitted signal $\ddot{\mathbf{x}}$ is then obtained by adding up the inverse FT of each elements $\hat{\ddot{\mathbf{x}}}_l$ as given in (V.28). Finally, its continuous-time version $\ddot{x}(t)$ is defined as follows:

$$\ddot{x}(t) = \sum_{m=1}^{N_{\ddot{\mathbf{x}}}} \ddot{x}_m \Gamma\left(t-(m-1)T_e\right) \tag{V.31}$$

where $\Gamma(t)$ is an ideal and normalized filter with bandwidth T_e^{-1}.

From this general doubly-circular MFTN signaling model, we propose to limit the frequency compression factor ν. More precisely, we do not want each sub-carrier to be interfered by more than its two adjacent sub-carriers. Each sub-carrier having a bandwidth $W = \frac{1+\beta}{T}$, we must ensure that:

$$\frac{W}{2} \leq F \leq W \Longleftrightarrow 1 \geq 2 - \frac{2\nu}{1+\beta} \geq 0 \tag{V.32}$$

and we define $\Omega \in [0,1]$ the frequency overlap factor as follows:

$$\Omega = 2 - \frac{2\nu}{1+\beta} \tag{V.33}$$

For $\Omega = 1$ each sub-carrier is fully overlapped by its adjacent sub-carriers, and for $\Omega = 0$ the system model is orthogonal. A FD representation of the shaping filters for different values of Ω is given in V.8. Note that the signals are shifted by half the communication bandwidth for symmetry reasons. The spectral efficiency becomes:

$$\rho = \frac{2R\log_2|\mathcal{M}|}{\tau(1+\beta)(2-\Omega)} \tag{V.34}$$

In the following, we use either the factor ν or Ω depending on the context, but the two notations are completely equivalent.

A multipath channel is then applied to the transmitted signal, as well as an AWGN component. Hence, the received signal is expressed as:

$$\ddot{r}(t) = (\ddot{x} * v)(t) + w(t) \tag{V.35}$$

where we omit the expression of a cyclic prefix longer the channel delay spread appended to the transmit signal in order to conserve the circular property of the convolution between the global filter $\dot{h}(t) = (\dot{p} \star v)(t)$ and the symbols. At reception, the cyclic prefix is left out after a perfect synchronization and before any further processing. We developed an iterative receiver based on EP aiming at retrieving the symbols information described hereafter.

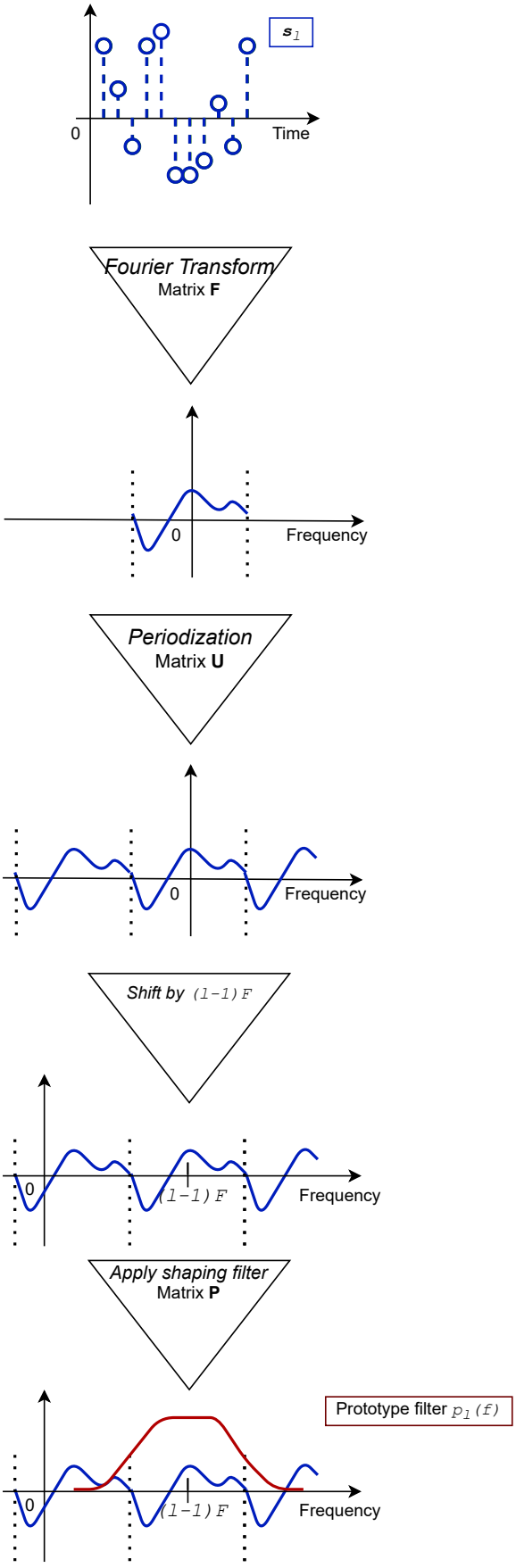

Figure V.7: FD construction of $\hat{\tilde{\mathbf{x}}}_l$

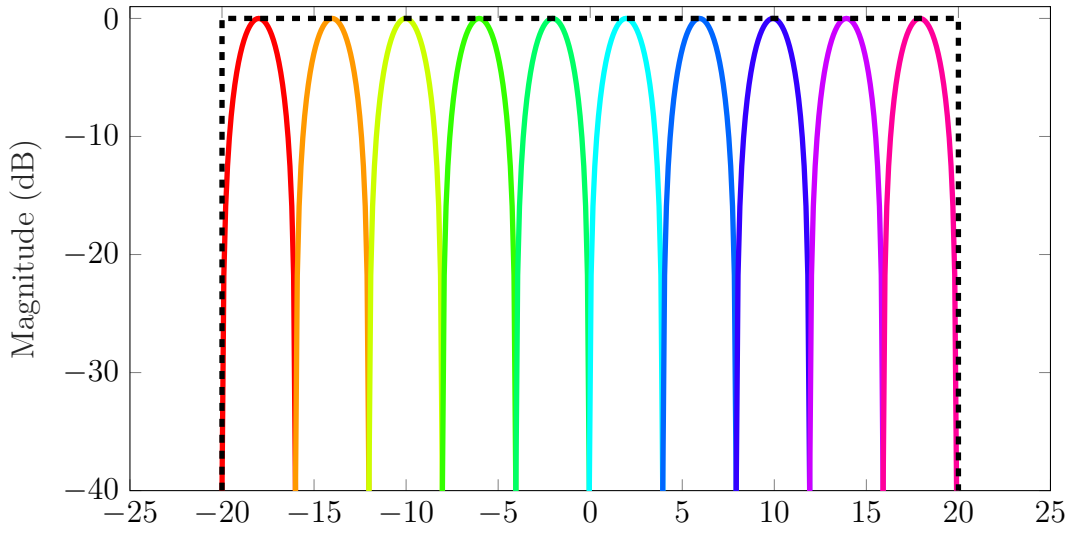

(a) $\Omega = 0\%$

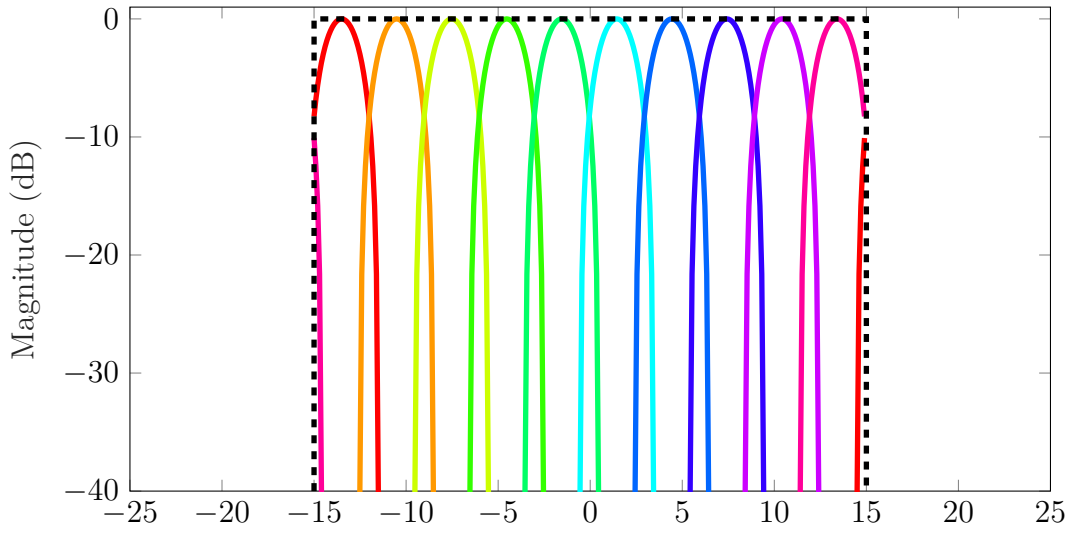

(b) $\Omega = 50\%$

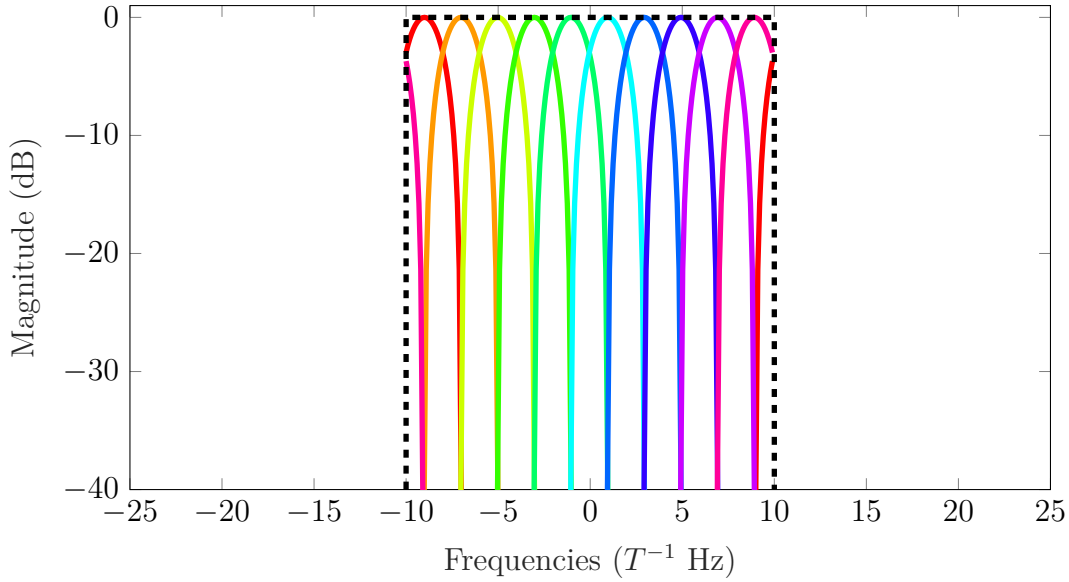

(c) $\Omega = 100\%$

Figure V.8: Shaping filters of doubly-circular MFTN signaling for $\beta = 1$ and different values of Ω

Proposed EP-based receiver for Doubly-Circular MFTN signaling

As presented previously, the discrete-time received signal sampled at rate $T_e^{-1} = NF$ is expressed as follows:

$$\ddot{\mathbf{r}} = \ddot{\mathbf{H}}\mathbf{U}\vec{\mathbf{s}} + \mathbf{w} \tag{V.36}$$

where $\ddot{\mathbf{H}} = \ddot{\mathbf{V}}\ddot{\mathbf{P}}$ is the $(N_{\ddot{\mathbf{x}}} \times N_s N\tau\nu)$ convolution matrix associated to the transmit filters and the multipath channel. In a similar way, the matrix $\mathbf{V}$ represents the $(N_{\ddot{\mathbf{x}}} \times N_{\ddot{\mathbf{x}}})$ circular matrix associated to the filter $v(t)$ sampled at rate T_e^{-1}. The discrete signal $\mathbf{r}$ is then processed by an EP-based iterative algorithm.

The matched-filtering and down-sampling operations yields:

$$\ddot{\mathbf{y}} = \mathbf{R}^\dagger \mathbf{D} \ddot{\mathbf{H}}^\dagger \ddot{\mathbf{r}} \tag{V.37}$$

where $\mathbf{w}' = \mathbf{R}^\dagger \mathbf{D} \ddot{\mathbf{H}}^\dagger \mathbf{w}$ is a colored noise if $\tau \neq 1$ or $\nu \neq 1$. The frequency shifted signals are denoted $\vec{\ddot{\mathbf{y}}} = \mathbf{R}\mathbf{y}$ and $\vec{\mathbf{w}} = \mathbf{R}\mathbf{w}$, and we have:

$$\vec{\ddot{\mathbf{y}}} = \ddot{\mathbf{G}}\vec{\mathbf{s}} + \vec{\mathbf{w}}' \tag{V.38}$$

where the $(N_s \times N_s)$ matrix $\ddot{\mathbf{G}}$ a has three block diagonals with circulant blocks:

$$\ddot{\mathbf{G}} = \begin{pmatrix} \ddot{\mathbf{G}}_{1,1} & \ddot{\mathbf{G}}_{1,2} & \mathbf{0}_K & \mathbf{0}_K & \mathbf{0}_K & \dots & \dots & \mathbf{0}_K & \ddot{\mathbf{G}}_{1,N} \\ \ddot{\mathbf{G}}_{2,1} & \ddot{\mathbf{G}}_{2,2} & \ddot{\mathbf{G}}_{2,3} & \mathbf{0}_K & \mathbf{0}_K & \dots & \dots & \mathbf{0}_K & \mathbf{0}_K \\ \mathbf{0}_K & \ddot{\mathbf{G}}_{3,2} & \ddot{\mathbf{G}}_{3,3} & \ddot{\mathbf{G}}_{3,4} & \mathbf{0}_K & \dots & \dots & \mathbf{0}_K & \mathbf{0}_K \\ \vdots & \ddots & \ddots & \ddots & \ddots & \ddots & & & \vdots \\ \vdots & & & \ddots & \ddots & \ddots & \ddots & & \vdots \\ \mathbf{0}_K & \mathbf{0}_K & \dots & \dots & \mathbf{0}_K & \ddot{\mathbf{G}}_{N-2,N-3} & \ddot{\mathbf{G}}_{N-2,N-2} & \ddot{\mathbf{G}}_{N-2,N-1} & \mathbf{0}_K \\ \mathbf{0}_K & \mathbf{0}_K & \dots & \dots & \mathbf{0}_K & \mathbf{0}_K & \ddot{\mathbf{G}}_{N-1,N-2} & \ddot{\mathbf{G}}_{N-1,N-1} & \ddot{\mathbf{G}}_{N-1,N} \\ \ddot{\mathbf{G}}_{N,1} & \mathbf{0}_K & \dots & \dots & \mathbf{0}_K & \mathbf{0}_K & \mathbf{0}_K & \ddot{\mathbf{G}}_{N-1,N} & \ddot{\mathbf{G}}_{N,N} \end{pmatrix} \tag{V.39}$$

where each $\ddot{\mathbf{G}}_{l',l} = \mathbf{U}'^\dagger \ddot{\mathbf{H}}_{l'}^\dagger \ddot{\mathbf{H}}_l \mathbf{U}'$ is a circulant matrix representing the ICI or the ISI on sub-carrier l if $l = l'$. The effect of the ICI limitation with $\Omega \in [0, 1]$ yields the sub-matrices $\ddot{\mathbf{G}}_{l',l}$ composing the matrix $\ddot{\mathbf{G}}$ to be null as soon as $|l - l'| > 1$. If there is no multipath channel, we have $\ddot{\mathbf{G}}_{l',l} = \ddot{\mathbf{G}}_{l-l'} = \mathbf{U}'^\dagger \mathbf{P}_{l'}^\dagger \mathbf{P}_l \mathbf{U}'$ and the matrix $\ddot{\mathbf{G}}$ becomes additionally block circulant (always with circulant blocks). Such a structured matrix is diagonal in the two-dimensional Fourier domain, and the proposed waveform becomes close to Orthogonal Time Frequency and Space (OTFS) signaling [Had+17].

In the general case of a multipath channel, we could apply EP with a two-dimensional equalization for both ICI and ISI processing. However, this would require the inversion of a $(N_s \times N_s)$, far beyond the targeted complexity. Hence, we apply the

FD-EP equalization on each sub-carrier after IC for ICI processing. This amounts to performing N single-carrier EP algorithms. The scheduling strategy for the sub-carrier processing has no impact on the performance, and the N sub-carriers can be computed in parallel using the symbol estimation of the previous EP iteration. This ability to process the whole sub-carriers in parallel is an important benefit offered by the EP receiver compared to the MMSE-IC equalizer. The equalization step is performed on the signals $\vec{\mathbf{z}}_{l'} = \vec{\mathbf{y}}_{l'} - \ddot{\mathbf{G}}_{l',l'-1}\vec{\mathbf{s}}_{l'-1} - \ddot{\mathbf{G}}_{l',l'+1}\vec{\mathbf{s}}_{l'+1}$ yielding:

$$\vec{\mathbf{s}}_{l'}^{\Psi} = \vec{\mathbf{s}}_{l'}^{\Phi} + \xi_{l'}^{-1}\ddot{\mathbf{\Sigma}}_{l'}^{-1}(\vec{\mathbf{z}}_{l'} - \ddot{\mathbf{G}}_{l',l'}\vec{\mathbf{s}}_{l'}^{\Phi}) \tag{V.40}$$

with the $(K \times K)$ MMSE matrix $\ddot{\mathbf{\Sigma}}_{l'} = v_{l'}^{\Phi}\ddot{\mathbf{G}}_{l',l'} + \sigma_w^2\mathbf{I}_K$ and $\xi_{l'} = (\ddot{\mathbf{\Sigma}}_{l'}^{-1}\ddot{\mathbf{G}}_{l',l'})_{1,1}$. The AWGN component can also be empowered to take into account the error coming from the IC when computing $\vec{\mathbf{z}}_l'$. This would result in considering that the ICI contribution is a circular AWGN with same variance as proposed by [CFP11].

In order to lower the computational complexity, the IC step can be performed in the FD using frequency shifts and product of diagonal matrices as presented in sub-Sec B.3. Once the ICI is removed, a single-carrier FD-EP process described in sub-Sec B.3 can be performed on $\vec{\mathbf{z}}_{l'}$ for each sub-carrier l'. It consists in performing the equalization given in (V.40) in the FD followed by a Constellation Matcher step for each symbol of the considered sub-carrier.

The proposed receiver called FD-EP for MFTN signaling has a complexity in $O(\mathcal{I}N_s\log_2(K))$ where $\mathcal{I}$ represents the number of EP iterations. Such a low-complexity process outperforms existing MFTN receivers as presented in the following sub-section.

Performance of EP-based receiver for MFTN signaling

Before evaluating the performance of the proposed EP-based receiver for MFTN signaling, we propose to present the results of existing low-complexity receivers over an AWGN channel. To do so, we consider a doubly-circular MFTN system transmitting $N_b = 4000$ useful bits. These bits are coded by a with a (7,5) convolutional code with rate $R = \frac{1}{2}$. After a random interleaver, the symbols are transmitted over $N = 10$ sub-carriers considering different constellations. The filter parameter β, the time compression factor τ and frequency overlap factor Ω are chosen to minimize the interference (ISI + ICI) on the signal $\ddot{\mathbf{y}}$ at a given $\tau\nu$ value, i.e. at fixed spectral efficiency if the constellation does not change. The minimization is performed by exploring the values $\tau \in \{0.1, 0.2, ..., 0.9\}$ and $\beta \in \{0, 0.1, ..., 1\}$. The resulting parameters are summed-up in Tab. V.1.

At the receiver, we process the received signal by the proposed FD-EP receiver and 8 turbo-iterations. Due to their intractable complexities, we did not explored the performance obtained with a BCJR for symbol processing, nor a two-dimensional MMSE equalizer processing jointly the ISI and ICI. Consequently, we compare our results to the FD-MMSE receiver developed in [Pen+17] with IC for ICI processing and cyclic prefix insertion.

Fig. V.9 shows the BER obtained considering different constellations and spectral

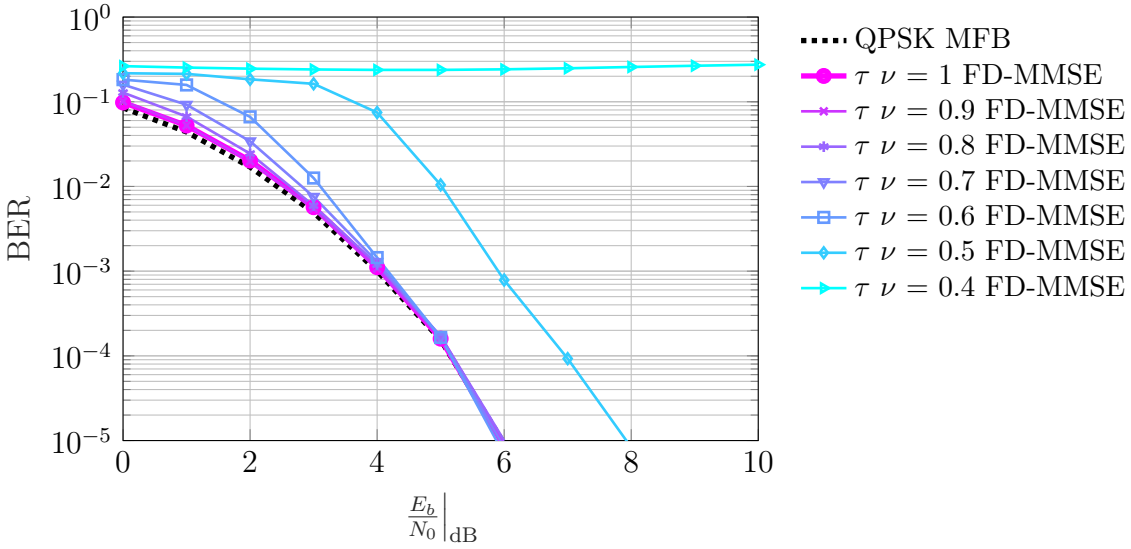

(a) QPSK

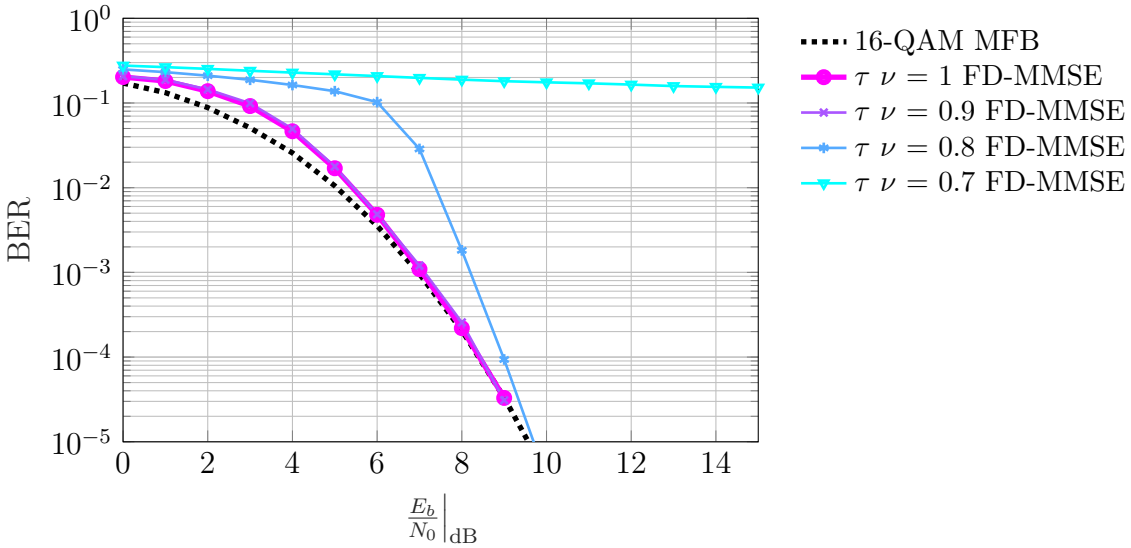

(b) 16-QAM

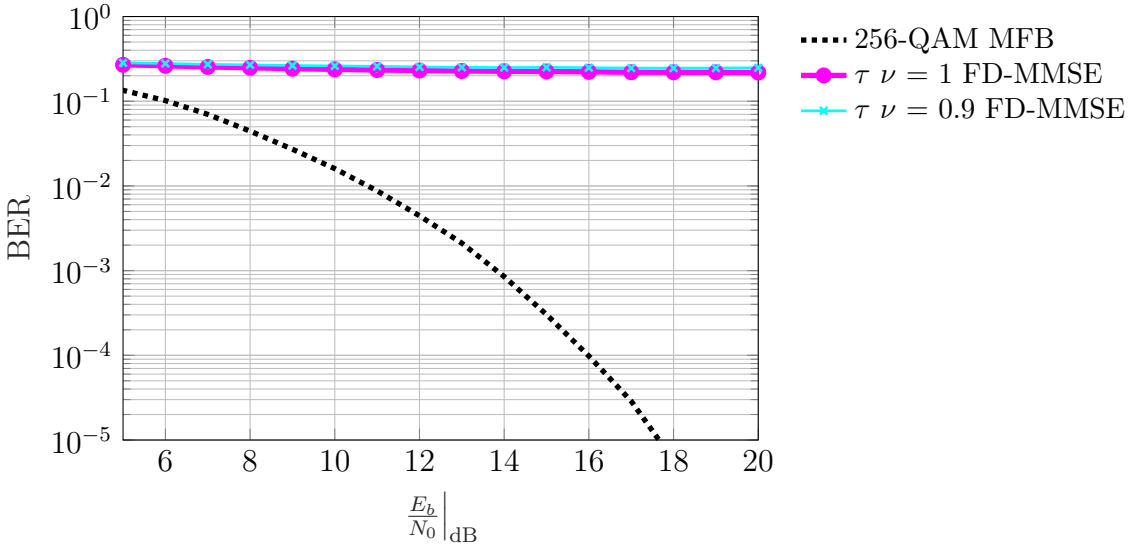

(c) 256-QAM

Figure V.9: BER of MFTN signaling for different constellations and $\tau\nu$ values

Table V.1: MFTN waveform parameters for different $\tau\nu$ values

Compression factor $\boldsymbol{\tau\nu}$	**1**	**0.9**	**0.8**	**0.7**	**0.6**	**0.5**	**0.4**
Frequency space factor $\boldsymbol{\nu}$	1.25	1	1	1	1.2	1	0.8
Time compression factor $\boldsymbol{\tau}$	0.8	0.9	0.8	0.7	0.5	0.5	0.5
Filter rolloff $\boldsymbol{\beta}$	1	0.3	0.7	1	0.9	0.7	0.5
Frequency overlap $\boldsymbol{\Omega}$	75 %	46 %	82 %	100 %	74 %	82 %	93 %

efficiencies of the existing FD-MMSE receiver. With a QPSK, the receiver completely handles the interference down to $\tau\nu = 0.6$, and shows a loss of 2 dB compared to its MFB for $\tau\nu = 0.5$. When compressing even more, it cannot remove the interference. We recall that the two-dimensional Mazo bound of such a model is $\tau\nu = 0.43$. Hence, the existing FD-MMSE for MFTN comes with a 70 % spectral efficiency gain compared to the best Nyquist scheme, but does not reach the BCJR performance. Regarding the 16-QAM constellation, the FD-MMSE removes the interference down to $\tau\nu = 0.8$ without BER damage. It represents a spectral efficiency increase of 25 % compared to Nyquist signaling. Nevertheless, for the 256-QAM the FD-MMSE is not able to handle any interference and thus does not propose any benefit compared to Nyquist signaling. To conclude, the richer the constellation, the less we can compress and the FD-MMSE offers significant spectral efficiency gains up to 3 bits/s/Hz.

In Fig. V.10 we compare the performance between Nyquist signaling, the existing FD-MMSE and the proposed FD-EP receiver at given spectral efficiencies over an AWGN channel. Considering $\rho = 2.5$ bits/s/Hz, the QPSK MFTN waveform with $\tau\nu = 0.5$ can be compared to the 64-QAM Nyquist communication. While the FD-MMSE receiver achieves 1.5 dB better than the Nyquist counterpart, the proposed FD-EP receiver performs 3.5 dB better by handling the whole interference after 3 EP iterations. In the following figure, we consider a 16-QAM MFTN signal with $\tau\nu = 0.7$, and a 64-QAM Nyquist waveform achieving $\rho = 3$ bits/s/Hz. The FD-MMSE receiver does not estimate at all the interference while our FD-EP receiver completely removes it, performing 4 dB better than Nyquist signaling. The conclusion is similar for a 256-QAM constellation achieving $\rho = 4.5$ bits/s/Hz with $\tau\nu = 0.9$. At such a very high spectral efficiency, this MFTN signaling can be compared to a 512-QAM Nyquist signal. Consequently, our EP-based receiver outperform existing solutions while maintaining a low complexity, even at very high spectral efficiencies.

Regarding the IAPR depicted in Fig. V.11, the compared waveforms are almost equivalent with IAPR(10^{-5}) $\approx$ 10 dB. Hence, we did not considered the ESNR metric because it would lead to similar results as SNR comparisons.

In the following sub-section, we confront the proposed single-carrier and multi-carrier system models to a frequency selective propagation channel.

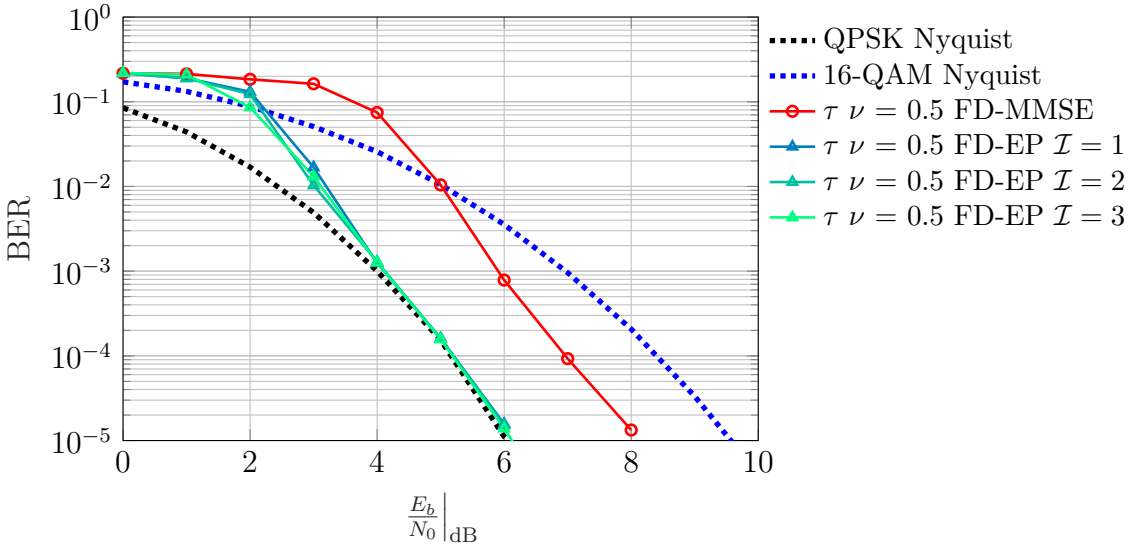

(a) $\rho = 2.5$ bits/s/Hz

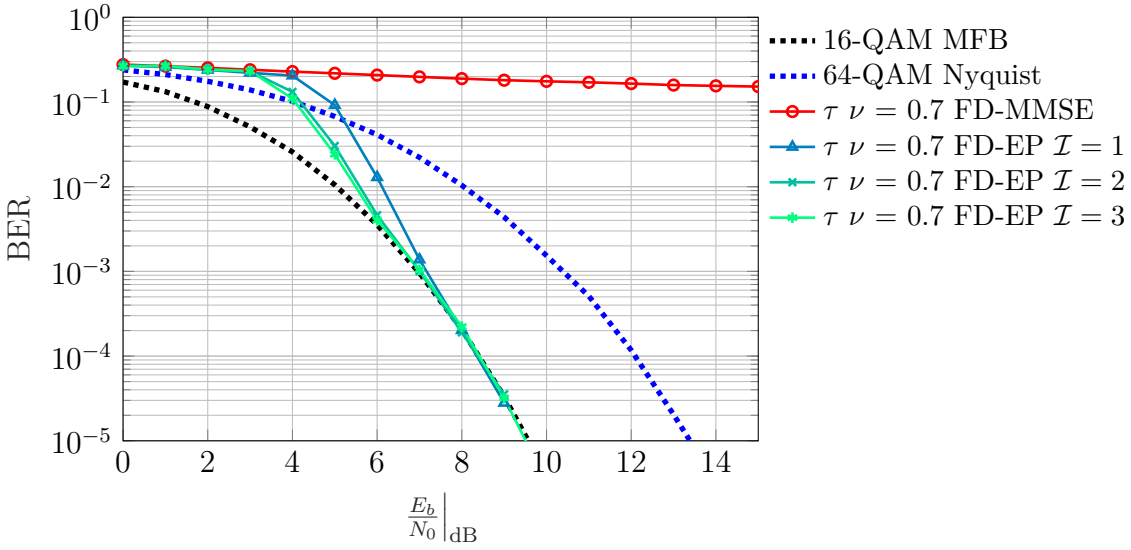

(b) $\rho = 3$ bits/s/Hz

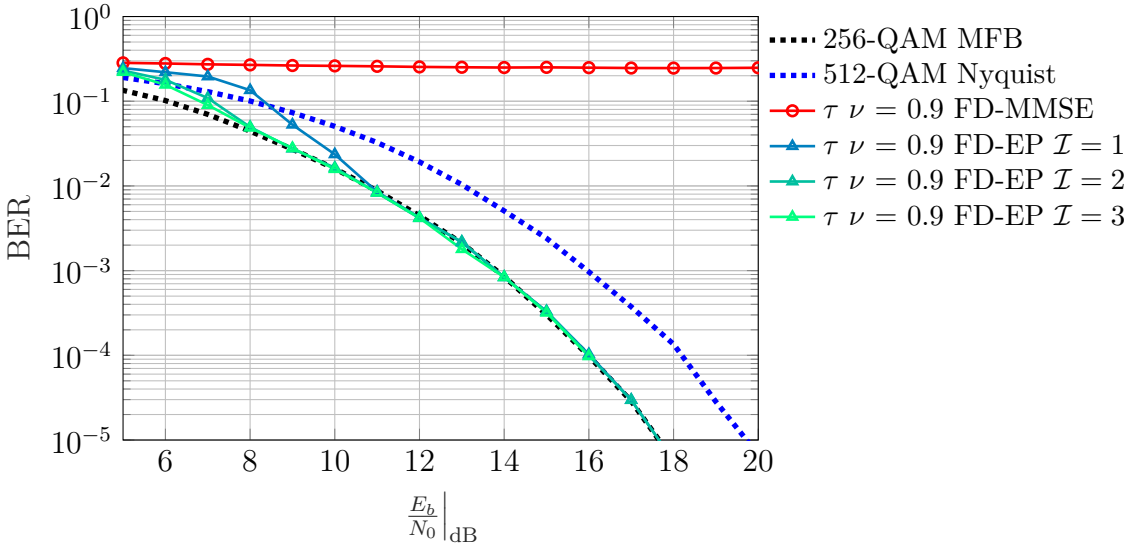

(c) $\rho = 4.5$ bits/s/Hz

Figure V.10: BER of MFTN signaling for different constellations at fixed spectral efficiency

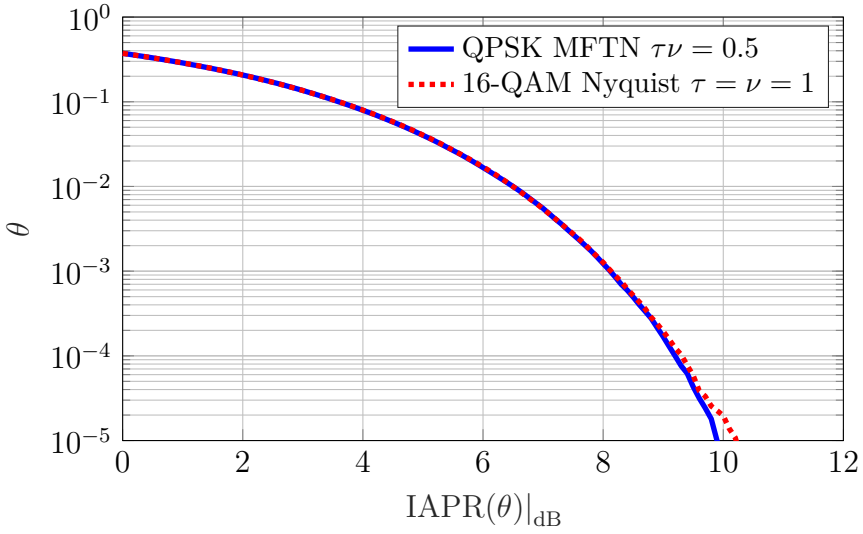

(a) $\rho = 1.5$ bits/s/Hz

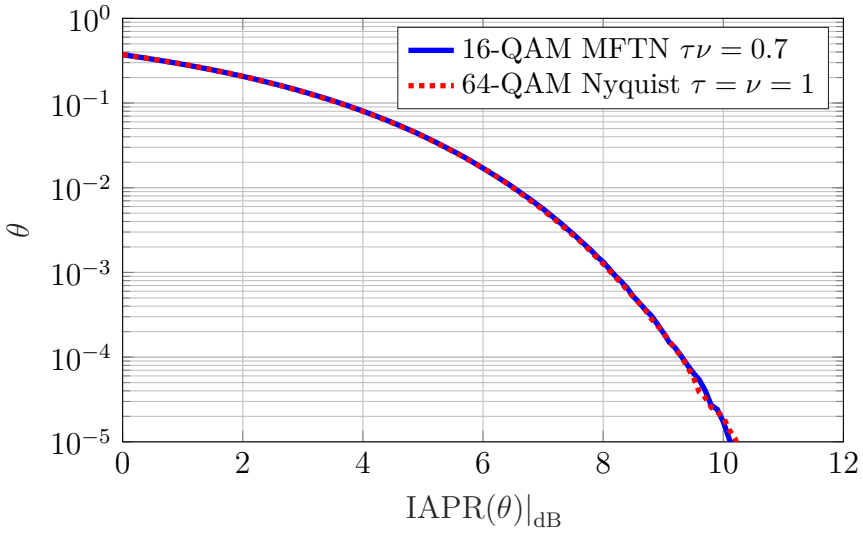

(b) $\rho = 3$ bits/s/Hz

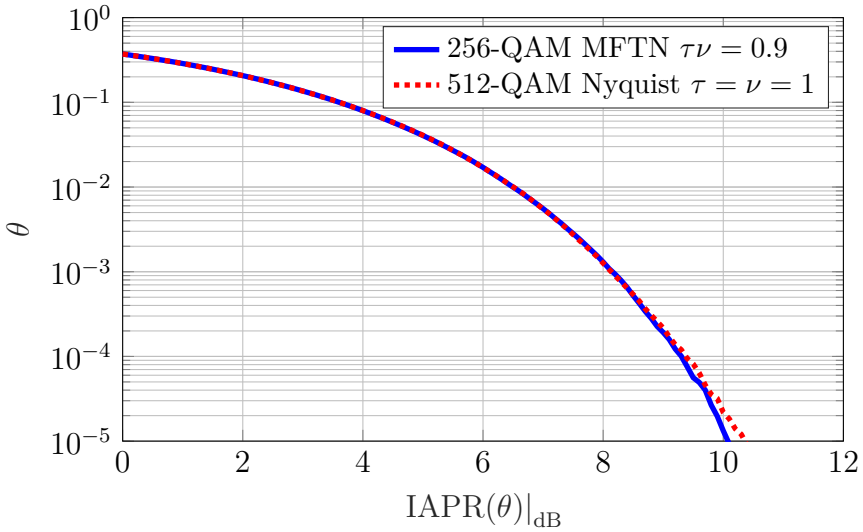

(c) $\rho = 4.5$ bits/s/Hz

Figure V.11: IAPR of MFTN signaling for different constellations at fixed spectral efficiency

C Single and Multi-Carrier comparisons with Frequency selective channels

This final sub-section is devoted to performance evaluation of Nyquist and FTN signaling with EP-based receivers in a multipath channel context. We explore different strategies, from single-carrier to multi-carrier signaling, for Nyquist and FTN signaling.

The comparisons are performed at fixed spectral efficiencies, and fixed -3 dB bandwidth over a Proakis B channel filter [Pro01] depicted in Fig. V.12 and expressed as:

$$v_B(t) = \frac{1}{\sqrt{6}} \left(\delta(t-T) + 2\delta(t) + \delta(t+T)\right) \tag{V.41}$$

Fixing the -3 dB bandwidth of the communication instead of the full bandwidth allows a fair comparison in the sense that the received SNR of single-carrier signaling is not impacted by a frequency shift of the channel filter. Indeed, if we had fixed the full bandwidth communication, we could have located the high selectivity of the Proakis B channel filter at the high frequencies of the communication benefiting to single-carrier signaling because it transmits almost no energy their.

We transmit $N_b = 8192$ useful bits encoded with a (7,5) code with rate $R = \frac{1}{2}$. The rolloff is set to $\beta = 0.33$ for single-carrier signaling, and $\beta = 1$ for multi-carrier signaling with $N = 128$ sub-carriers separated by $F = T^{-1}$ Hz (i.e. $\nu = 1$). The considered system model is CCFTN for single-carrier and doubly-circular MFTN signaling for multi-carrier. The time compression factor and constellations are given hereafter, they depend on the targeted spectral efficiency. The signals are processed at reception by the proposed FD-EP receivers with $\mathcal{I} = 3$ EP iterations and 8 turbo-iterations. The channel filter is supposed to be perfectly known.

C.1 Comparison results for different spectral efficiencies

Fig. V.13a reveals the performance obtained at $\rho = 1.5$ bits/s/Hz achieved by the colored curved. Black curves represent bounds and then do not achieve the same spectral efficiency. The time compression factor is set to $\tau = 0.5$ for CCFTN signaling, and we have $\tau\nu = \frac{2}{3}$ for MFTN. FTN signaling achieves the targeted spectral efficiency with a QPSK while Nyquist signaling achieves it with a 16-QAM. With the considered channel, MFTN signaling performs 1.5 dB better than the best multi-carrier orthogonal scheme $\tau\nu = 1$ which is, in fact, more a bound than a real scheme due to the filter side lobes. Considering single-carrier signaling, FTN signaling also outperforms the Nyquist communication by 3 dB at high SNR. Moreover, if taking into account the IAPR, the two single-carrier scheme have a IAPR 4 dB better than the multi-carrier schemes for $\theta = 10^{-5}$. Hence, single-carrier signaling outperforms multi-carrier signaling in this context.

In Fig. V.13b the spectral efficiency is set to $\rho = 3$ bits/s/Hz. For single-carrier signaling, we use a 256-QAM Nyquist and a 64-QAM FTN $\tau = 0.75$ CCFTN communica-

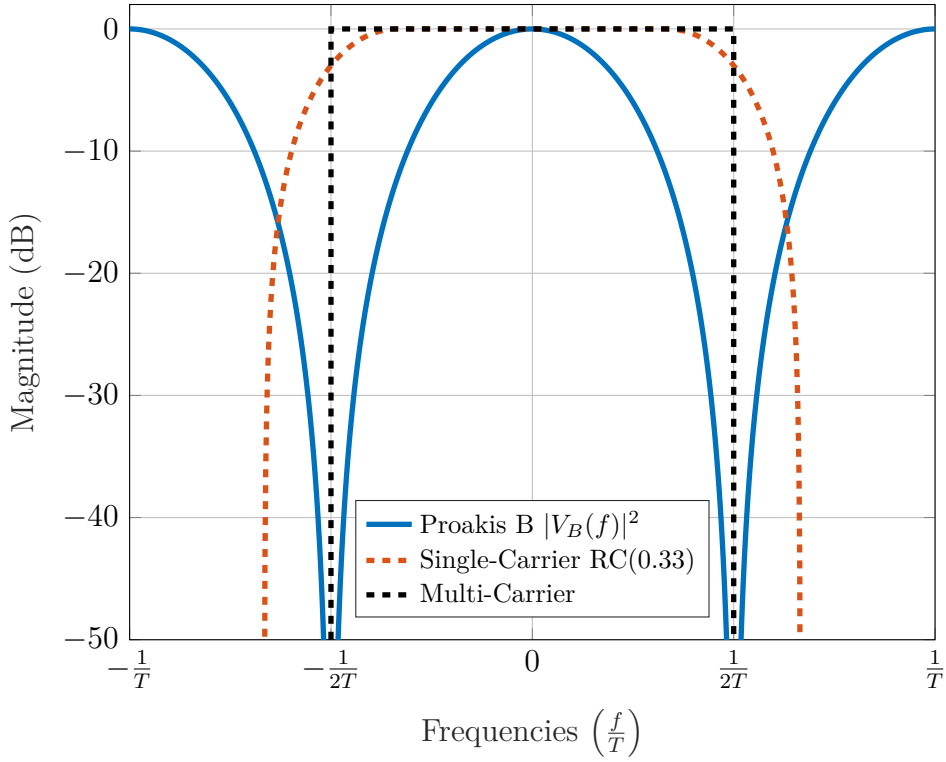

Figure V.12: Proakis B frequency representation

tions. Regarding multi-carrier schemes, the compression is set to $\tau\nu = \frac{2}{3}$ combined with a 16-QAM MFTN communication, and the orthogonal scheme uses a 64-QAM constellation. Similar conclusions can be drawn, MFTN signaling achieves 2 dB better than its orthogonal counterpart, and single-carrier CCFTN outperforms 4 dB better than single-carrier Nyquist signaling. In terms of IAPR for single-carrier, CCFTN achieves 7.5 dB while Nyquist signaling offers 7 dB. These values remain below the 10 dB of multi-carrier signaling. Moreover, multi-carrier signaling performance are below single-carrier ones.

A very high spectral efficiency of $\rho = 4$ bits/s/Hz is targeted in Fig. V.13c. The rolloff of the single-carrier 2048-QAM Nyquist communication modulation has been slightly modified from $\beta = 0.33$ to $\beta = 0.375$ in order have an integer value of bits per symbol. The single-carrier CCFTN communication uses a 256-QAM compressed by $\tau = 0.75$. For multi-carrier signaling, the orthogonal scheme supposes a 256-QAM constellation, and the MFTN signal achieves the spectral efficiency with a 64-QAM constellation compressed by $\tau\nu = 0.75$. At moderate SNR, multi-carrier performs better than single-carrier signaling. However, at high SNR, multi-carrier schemes achieve similar performance as single-carrier Nyquist signaling but worst than CCFTN. MFTN signaling shows 3 dB better than its orthogonal counterpart. The IAPR, not represented in the figure, benefits to the Nyquist single-carrier communication with 6 dB, followed by the single-carrier FTN signaling with 7.5 dB. Consequently, even at very high spectral efficiencies, single-carrier FTN signaling achieves better results than multi-carrier signaling.

C.2 General conclusions with a frequency selective channel

From the previous figures, different conclusions can be drawn. Regarding multi-carrier signaling, the proposed EP-based receiver allows MFTN to achieve better performance than an orthogonal multi-carrier scheme. The SNR gain increases with the targeted spectral efficiency even if the compression factor $\tau\nu$ comes closer to 1 due to the higher constellation density. Due to the channel frequency selectivity, the sub-carriers are subject to different gains, and the overall performance are comparable to a single-carrier communication over a Rayleigh channel yielding a lack of diversity. Moreover, the IAPR of the multi-carrier schemes is very similar and achieves 10 dB for $\theta = 10^{-5}$.

Considering single-carrier communications, even with a frequency-selective channel as the Proakis B, CCFTN is preferable than Nyquist signaling with the FD-EP receiver. At fixed spectral efficiency, the IAPR can be lowered by FTN signaling, even if it is scarcely the case for the combinations we chose in Fig. V.13.

Finally, comparing single-carrier to multi-carrier signaling demonstrates the superiority of single-carrier CCFTN signaling even if the multi-criteria benefit reduces when the targeted spectral efficiency increases. This result assumes processing the interference with EP-based receivers under complexity constraints. Furthermore, these conclusions remain subject to the considered channel code, suppose a perfect knowledge of the channel filter, and a fine time and frequency synchronization at reception.

D Conclusion

In this chapter, we exhibited the limits of EP-based receivers for single-carrier FTN communications in the presence of a Proakis C channel with very high frequency selectivity. It led us to explore different strategies based on multi-carrier signaling aiming at simplifying the equalization step of the channel filter. Moreover, MFTN signaling can also be a mean for increasing the spectral efficiency by compressing in time and frequency domains. This technique has already been studied in the literature, with different proposition at reception to handle the interference. While BCJR-based and two-dimensional MMSE equalizers are very complex, the combination of IC for ICI processing and a FD-MMSE for ISI mitigation is a low-complexity alternative which, however, require a long cyclic prefix damaging the spectral efficiency. In order to bypass this major issue, we proposed a doubly-circular system model designed based on a circular convolution without cyclic prefix. Moreover, we extended the proposed FD-EP receivers for CCFTN to our multi-carrier model. Confronting our receiver to the existing FD-MMSE solution demonstrates important benefits compared to existing solutions, and high spectral efficiency gains. After that, we introduced a frequency selective Proakis B channel filter, and compared the proposed single-carrier and multi-carrier receivers. Our simulations reveal that MFTN signaling outperforms multi-carrier orthogonal schemes, and single-carrier CCFTN offer better results than multi-carrier signaling even at high spectral efficiency for the considered channel.

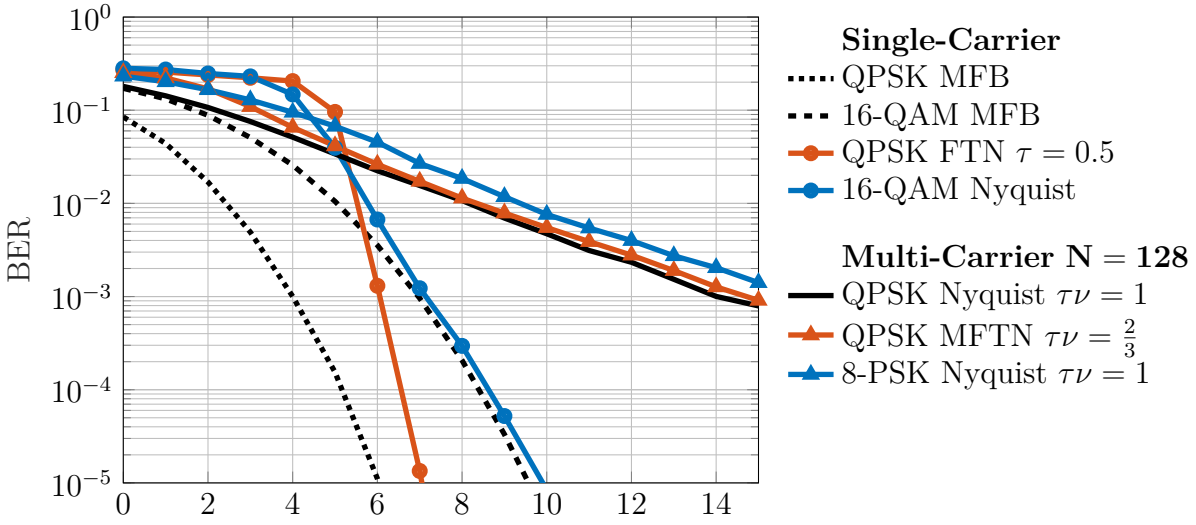

(a) $\rho = 1.5$ bits/s/Hz

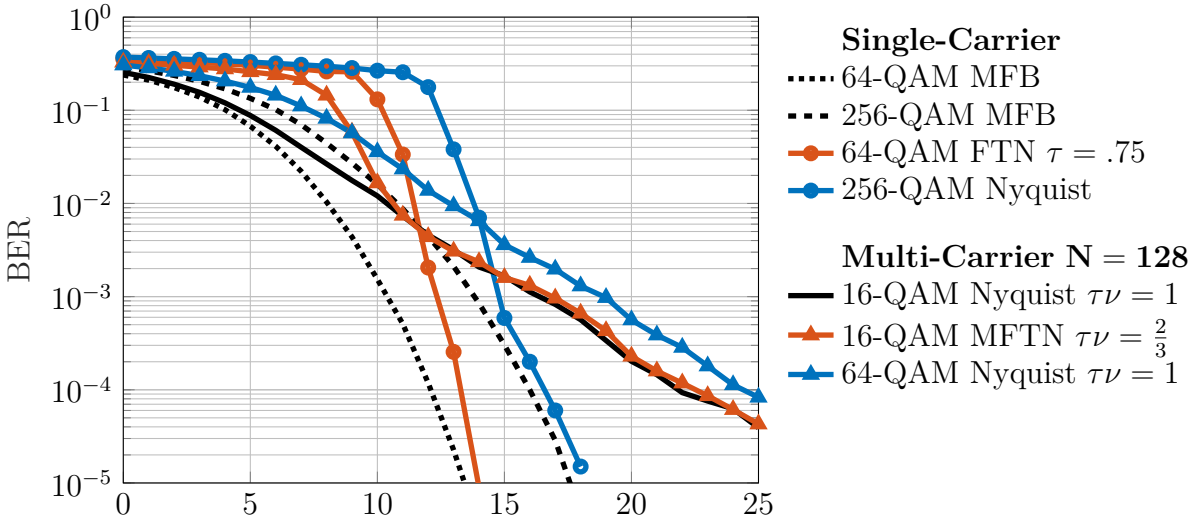

(b) $\rho = 3$ bits/s/Hz

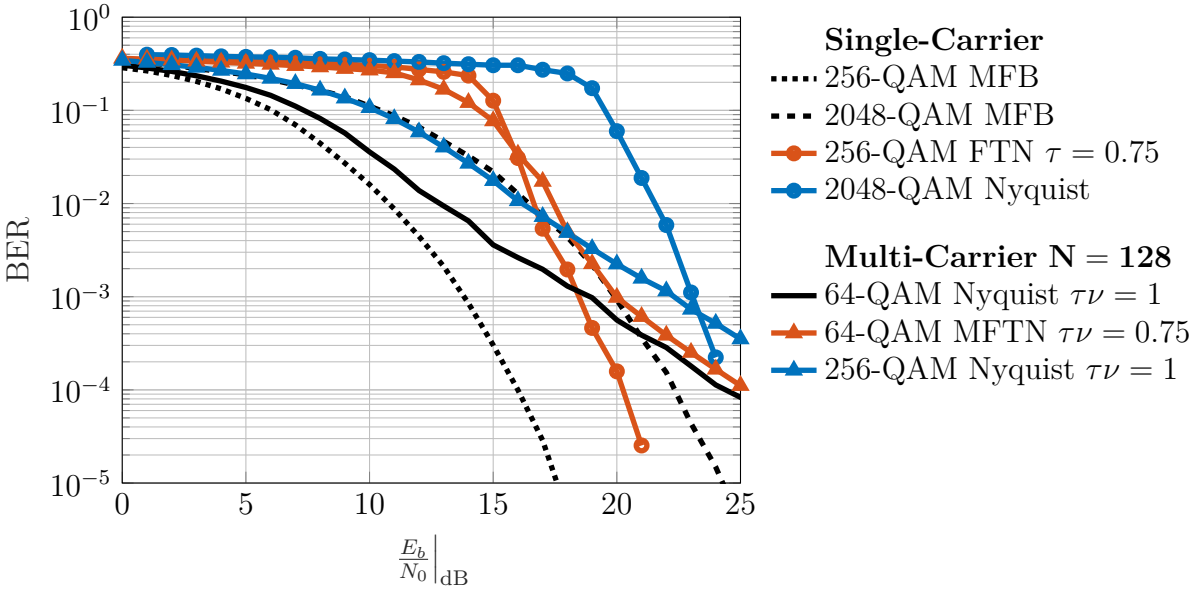

(c) $\rho = 4$ bits/s/Hz

Figure V.13: Single-Carrier and Multi-Carrier signaling over a Proakis B channel processed by a FD-EP receiver

Conclusion and Perspectives

In this thesis, we conducted a multi-criteria analysis of FTN signaling for single-carrier and multi-carrier signaling. We presented a brief historical review of various contributions which led to the actual emergence of the FTN technique, driven by the user needs and allowed by higher computational capacities. A heuristic version of the FTN technique has been introduced in DVB-S2X, where ISI is voluntarily introduced by slightly reducing the transponder bandwidth. Nevertheless, embedding FTN signaling in future communication standards struggles to convince at this point.

From this consideration, we presented two different types of single-carrier FTN signaling: linear and circular shaping. While LCFTN is widely used in the literature, CCFTN offers several important advantages: slightly higher spectral efficiency due to its lower time support, an efficient frequency-domain processing at emission, a lower latency, and it is naturally compatible with frequency-domain processings at reception without requiring any cyclic prefix. As a first step, we supposed an AWGN model to evaluate the potential of FTN signaling with an ideal model. At reception, we explored different techniques of the literature dedicated to handle the ISI with or without a channel code scheme.

The interest of FTN signaling has been then motivated with an analysis of the Shannon capacity constraining the Nyquist filters with and without time compression factor. This study shows the interest of FTN signaling as it achieves higher spectral efficiencies. Then, we focused on operational constraints and more specifically on the IAPR of Nyquist and FTN signaling. Depending on the compression factor, among others, the IAPR can vary significantly and then would lead to different power amplifier constraints at fixed transmitted average power. Hence, we proposed the ESNR metric aiming at penalizing each waveform by its associated IAPR for a given saturation probability. Moreover, comparing the IAPR at fixed spectral efficiency sometimes shows significant benefits brought by FTN compared to Nyquist signaling. Using this new metric, different communications at fixed spectral efficiencies have been compared. From a multi-criteria point of view, this evaluation benefits to FTN signaling with MMSE-based receivers if considering low order constellations (BPSK, QPSK). However, when constraining the computational complexity at reception and targeting higher spectral efficiencies, FTN signaling reaches the limits of the ISI equalization and do not offer benefits compared to Nyquist signaling. Consequently, we explored different reception strategies based on EP.

Before applying EP to the MAP optimization of the symbol sequence, we introduced EP as a general framework and we proposed a didactic rethinking of the technique. Then, we extended existing results of the literature and proposed new EP-based receiver to mitigate the ISI induced by FTN signaling. We proposed three distribution families

and different types of scheduling yielding to distinct receivers. Moreover, combining the CCFTN model with a particular Gaussian family yields an efficient frequency-domain equalization without cyclic prefix. The proposed receivers turns out to be complementary in the sense that they do not achieve the same performance nor require the same complexities. Moreover, the resulting receivers perform particularly well with rich constellations such as 16-QAM, 64-QAM and 256-QAM, and allow FTN signaling to achieve up to 5 bits/s/Hz while offering significant gains compared to Nyquist signaling.

Based on the previous works, we extended the framework of EP receivers to MFTN signaling. This is motivated by the limitations of ISI mitigation in a frequency-selective channel context combined with single-carrier FTN signaling. After presenting the commonly used MFTN system model of the literature, we studied the existing receivers. The IC for ICI processing is motivated with a bayesian approached based on FG. The ISI can then be processed by different types of receivers, such as a FD-MMSE which offers a good trade-off between BER performance and computational complexity. Nevertheless, this receiver requires a circulant shaping at emission achieved by means of a long cyclic prefix. To tackle this important drawback, we proposed a doubly-circular MFTN model benefiting from an efficient FD shaping at transmission. Moreover, we extended the concept of EP and applied it to MFTN signaling. The resulting model outperforms existing MFTN models of the literature and increases the spectral efficiency of orthogonal schemes even with rich constellations.

Finally, we confronted both single-carrier and multi-carrier FTN signaling to a multipath propagation channel, and compared it to Nyquist signaling. Considering a Proakis B channel, the proposed EP-based receivers allow FTN signaling to achieve better performance than Nyquist signaling. Nevertheless, single-carrier FTN signaling seems to be more promising than MFTN signaling, even though the difference tends to decrease at high spectral efficiencies. The benefit of single-carrier FTN is moreover empathized when considering IAPR gains yielding a multi-criteria point of view.

Multiple studies can be conducted to push further the analysis and the potential of FTN signaling. A non-exhaustive list is given hereafter:

1. Convergence analysis of EP receivers for FTN signaling: we started a study to understand and predict the convergence of EP receivers in a similar way as EXIT charts or MSE charts [TBH02; AAND09].

2. Extension to (MU-)MIMO: MIMO systems are at the heart of several wireless communication standards. The extension of FTN signaling have already been proposed [Lee+19; Guo+19], the addition of EP-based receivers could be particularly interesting.

3. Given that FTN signaling does not take advantage of the Nyquist criterion, non-Nyquist low-pass filters can be used for signal shaping. Several studies evaluated the performance of FTN signaling with existing filters [Le+14]. Moreover, filters maximizing the achievable spectral efficiency under complexity constraints for BCJR-based receivers have been proposed [MRC13], while other authors developed filters minimizing the MSE at reception after matched-filter and down-sampling [Mar17].

Combining these filters with the proposed EP-based receiver could yield higher spectral efficiency gains. Nevertheless, the non-linear structure of EP makes the optimization criteria for the filter design particularly complex. Hence, this study partially cross-matches the first enumerated point.

4. In the multi-criteria study based on the ESNR metric, we measured the IAPR at the power-amplifier output. Hoewever, we did not assume any technique to lower the IAPR. Taking into account such techniques could benefit to FTN signaling [Wen+19].

5. Extension of the results to different channel codes, non time and frequency synchronized signals, miss-estimated channel models. Even though our conclusions are optimistic for FTN to achievement high spectral efficiencies, the results are subject to the particular models and idealistic assumptions we made so far. Extending the results to other channel models, with longer delay spread, time-variant filters with time selectivity should be addressed to draw firmer conclusions. Moreover, multiple operational constraints need to be introduced in the communication, each of them representing a wide area of research.

Appendix A

Derivation of the averaged CCDF of the IAPR

The definition of $x(t)$ yields the following expression of $\Upsilon_x(\gamma)$:

$$\Upsilon_x(\gamma) = \lim_{N_s \to +\infty} \frac{1}{N_s} \sum_{n=1}^{N_s} R((s_n)_n) \tag{A.1}$$

where $R((s_n)_n) = \frac{1}{T_s} \int_{nT_s}^{(n+1)T_s} \mathbb{1}(|x(t)|^2 > \gamma P_x) \mathrm{d}t$. The ergodicity theorem for Markov chains gives:

$$\Upsilon_x(\gamma) = \mathbb{E}_\sigma \left[R(\sigma) \right] \tag{A.2}$$

where σ is a state composed of $2(L_\tau + 1)$ symbols which fully characterize $x(t)$ for $t \in [nT_s, (n+1)T_s]$. The expression of $\Upsilon_x(\gamma)$ becomes:

$$\begin{aligned}
\Upsilon_x(\gamma) &= (\log_2 |\mathcal{M}|)^{-2(L_\tau+1)} \sum_{\sigma \in \mathcal{M}^{2(L_\tau+1)}} R(\sigma) && \text{(A.3)} \\
&= (\log_2 |\mathcal{M}|)^{-2(L_\tau+1)} \sum_{\sigma \in \mathcal{M}^{2(L_\tau+1)}} \frac{1}{T_s} \int_0^{T_s} \mathbb{1}(|x(t)|^2 > \gamma P_x) \mathrm{d}t && \text{(A.4)} \\
&= \frac{1}{T_s} \int_0^{T_s} \mathbb{P}(|x(t)|^2 > \gamma P_x) \mathrm{d}t && \text{(A.5)} \\
&= \frac{1}{T_s} \int_0^{T_s} \tilde{\Upsilon}_x(t, \gamma) \mathrm{d}t && \text{(A.6)}
\end{aligned}$$

Therefore, $\Upsilon_x(\gamma)$ corresponds to the averaged IAPR CCDF over a cyclostationarity period.

Appendix B

KL Divergence minimization for the FD-EP receiver

We suppose a multivariate distribution $p(\mathbf{s})$ on a $(N \times 1)$ random vector $\mathbf{s}$ with mean vector $\mathbf{x}$ and covariance matrix $\mathbf{V} = (v_{i,j})_{i,j \in [\![1,N]\!]}$. The projection of $p(\mathbf{s})$ on $\mathcal{N}_{\mathrm{C}}$ yields the pdf $q(\mathbf{s}) = \mathcal{N}_{\mathrm{C}}(\mathbf{s} : \boldsymbol{\mu}, v\mathbf{I}_N)$ minimizing the KL divergence:

$$D_{\mathrm{KL}}(p||q) = \int p(\mathbf{s}) \log\left(p(\mathbf{s})\right) \, \mathrm{d}\mathbf{s} + \frac{N}{2}\log(2\pi v) + \frac{1}{2v}\sum_{i=1}^{N}\left(|\mu_i|^2 - 2\Re(\mu_i^* x_i) + v_{i,i} + |x_i|^2\right)$$

The minimization of $D_{\mathrm{KL}}(p||q)$ is performed by computing its first derivatives:

$$\begin{aligned} \forall i \in [\![1, N]\!] : \frac{\partial D_{\mathrm{KL}}(p||q)}{\partial \mu_i} &= 0 \Leftrightarrow \mu_i = x_i \\ \frac{\partial D_{\mathrm{KL}}(p||q)}{\partial v} &= 0 \Leftrightarrow v = \frac{1}{N}\sum_{i=1}^{N} v_{i,i} \end{aligned}$$

Consequently, the KL minimization of $p(\mathbf{s})$ with respect to $q(\mathbf{s})$ leads to a moment-matching for the mean vector $\boldsymbol{\mu}$, and v is given by averaging the diagonal variance terms of $\mathbf{s}$. Hence we have:

$$q(\mathbf{s}) = \mathcal{N}_{\mathrm{C}}\left(\mathbf{s} : \mathbf{x}, (\frac{1}{N}\sum_{i=1}^{N} v_{i,i})\mathbf{I}_N\right) \tag{B.1}$$

Appendix C

MAP estimation with Gaussian prior estimates leads to a MMSE equalizer

The expression of the Gaussian priors pdfs $\Phi_l(s_i)$ are expressed as follows:

$$\prod_{i=1}^{N_s} \Phi_l(s_i) = \prod_{i=1}^{N_s} \mathcal{N}_{\mathrm{C}}(s_i : s_i^{\Phi_{l-1}}, v_i^{\Phi_{l-1}}) = \mathcal{N}_{\mathrm{C}}(\mathbf{s} : \mathbf{s}^{\Phi_{l-1}}, \mathbf{V}^{\Phi_{l-1}}) \tag{C.1}$$

where $\mathbf{s}^{\Phi_{l-1}} = [s_1^{\Phi_{l-1}}, ..., s_{N_s}^{\Phi_{l-1}}]^T$ and $\mathbf{V}^{\Phi_{l-1}} = \mathrm{diag}([v_1^{\Phi_{l-1}}, ..., v_{N_s}^{\Phi_{l-1}}])$ is a diagonal covariance matrix reflecting an independence assumption on the symbols. The channel model expression gives:

$$\begin{aligned}\tilde{\Psi}(s_n) &\propto \int_{\mathbf{s}_{\sim n} \in \mathbb{C}^{N_s-1}} p(\mathbf{r}|\mathbf{s}) \prod_{i=1}^{N_s} \Phi_{l-1}(s_i)\, \mathrm{d}\mathbf{s}_{\sim n} \\ &\propto \int_{\mathbf{s}_{\sim n}} \mathcal{N}_{\mathrm{C}}(\mathbf{r} : \mathbf{H}\mathbf{U}\mathbf{s}, \sigma_w^2 \mathbf{I}_{N_r}) \mathcal{N}_{\mathrm{C}}(\mathbf{s} : \mathbf{s}^{\Phi_{l-1}}, \mathbf{V}^{\Phi_{l-1}})\, \mathrm{d}\mathbf{s}_{\sim n}\end{aligned} \tag{C.2}$$

Using the analytical expressions of the involved Gaussian distributions, (C.2) becomes

$$\begin{aligned}\tilde{\Psi}_l(s_n) &\propto \int_{\mathbf{s}_{\sim n}} \exp\left(-\sigma_w^{-2}(\mathbf{r} - \mathbf{H}\mathbf{U}\mathbf{s})^\dagger(\mathbf{r} - \mathbf{H}\mathbf{U}\mathbf{s}) - (\mathbf{s} - \mathbf{s}^{\Phi_{l-1}})^\dagger (\mathbf{V}^{\Phi_{l-1}})^{-1}(\mathbf{s} - \mathbf{s}^{\Phi_{l-1}})\right) \mathrm{d}\mathbf{s}_{\sim n} \\ &\propto \int_{\mathbf{s}_{\sim n}} \exp\left(-\mathbf{s}^\dagger(\sigma_w^{-2}\mathbf{G} + (\mathbf{V}^{\Phi_{l-1}})^{-1})\mathbf{s} + 2\Re(\mathbf{s}^\dagger[\sigma_w^{-2}\mathbf{y} + (\mathbf{V}^{\Phi_{l-1}})^{-1}\mathbf{s}^{\Phi_{l-1}}])\right) \mathrm{d}\mathbf{s}_{\sim n}\end{aligned} \tag{C.3}$$

where $\mathbf{y} = \mathbf{D}\mathbf{H}^\dagger\mathbf{r}$ is the received signal after matched filtering and down-sampling, and $\mathbf{G} = \mathbf{D}\mathbf{H}^\dagger\mathbf{H}\mathbf{U}$ is the aliased and down-sampled Nyquist filter. The integrand of (C.3) can now easily be identified to a new Gaussian distribution:

$$\tilde{\Psi}_l(s_n) \propto \int_{\mathbf{s}_{\sim n}} \mathcal{N}_{\mathrm{C}}(\mathbf{s} : \mathbf{s}^{\tilde{\Psi}_l}, \mathbf{V}^{\tilde{\Psi}_l})\, \mathrm{d}\mathbf{s}_{\sim n} \tag{C.4}$$

where $\mathbf{s}^{\tilde{\Psi}_l}$ and $\mathbf{V}^{\tilde{\Psi}_l}$ are given by:

$$\begin{aligned}\mathbf{s}^{\tilde{\Psi}_l} &= \mathbf{V}^{\tilde{\Psi}_l}(\sigma_w^{-2}\mathbf{y} + (\mathbf{V}^{\Phi_{l-1}})^{-1}\mathbf{s}^{\Phi_{l-1}}) \\ \mathbf{V}^{\tilde{\Psi}_l} &= (\sigma_w^{-2}\mathbf{G} + (\mathbf{V}^{\Phi_{l-1}})^{-1})^{-1}\end{aligned}$$

Some mathematical developments give:

$$\mathbf{V}^{\tilde{\Psi}_l} = \sigma_w^2(\mathbf{V}^{\Phi_{l-1}}\mathbf{G} + \sigma_w^2\mathbf{I}_{N_s})^{-1}\mathbf{V}^{\Phi_{l-1}}$$

Using $\mathbf{A}(\mathbf{B}\mathbf{A} + \mathbf{I}_{N_2})^{-1} = (\mathbf{A}\mathbf{B} + \mathbf{I}_{N_1})^{-1}\mathbf{A}$ for any $(N_1 \times N_2)$ matrix $\mathbf{A}$ and $(N_2 \times N_1)$ matrix $\mathbf{B}$ (the proof is trivial if $\mathbf{A}$ is invertible and $N_1 = N_2$, for a more general case see the Woodburry Identity) and setting $\mathbf{A} = \mathbf{V}^{\Phi_{l-1}}$ and $\mathbf{B} = (\mathbf{V}^{\Phi_{l-1}}\mathbf{G} + \sigma_w^2\mathbf{I}_{N_s})^{-1}$, we have:

$$\mathbf{V}^{\tilde{\Psi}_l} = \sigma_w^2\mathbf{V}^{\Phi_{l-1}}\boldsymbol{\Sigma}_l^{-1}$$

where $\boldsymbol{\Sigma}_l = \mathbf{G}\mathbf{V}^{\Phi_{l-1}} + \sigma_w^2\mathbf{I}_{N_s}$ is the MMSE matrix. The expression of $\mathbf{s}^{\tilde{\Psi}_l}$ is the following:

$$\begin{aligned}\mathbf{s}^{\tilde{\Psi}_l} &= \sigma_w^2\mathbf{V}^{\Phi_{l-1}}\boldsymbol{\Sigma}_l^{-1}(\sigma_w^{-2}\mathbf{y} + (\mathbf{V}^{\Phi_{l-1}})^{-1}\mathbf{s}^{\Phi_{l-1}}) \\ &= \mathbf{V}^{\Phi_{l-1}}\boldsymbol{\Sigma}_l^{-1}(\mathbf{y} + \sigma_w^2(\mathbf{V}^{\Phi_{l-1}})^{-1}\mathbf{s}^{\Phi_{l-1}}) \\ &= \mathbf{V}^{\Phi_{l-1}}\boldsymbol{\Sigma}_l^{-1}(\mathbf{y} + (\boldsymbol{\Sigma}_l(\mathbf{V}^{\Phi_{l-1}})^{-1} - \mathbf{G})\mathbf{s}^{\Phi_{l-1}}) \\ &= \mathbf{s}^{\Phi_{l-1}} + \mathbf{V}^{\Phi_{l-1}}\boldsymbol{\Sigma}_l^{-1}(\mathbf{y} - \mathbf{G}\mathbf{s}^{\Phi_{l-1}})\end{aligned}$$

The multivariate distribution $\mathcal{N}_{\mathrm{C}}(\mathbf{s} : \mathbf{s}^{\tilde{\Psi}_l}, \mathbf{V}^{\tilde{\Psi}_l})$ is then characterized by:

$$\begin{cases} \mathbf{s}^{\tilde{\Psi}_l} = \mathbf{s}^{\Phi_{l-1}} + \mathbf{V}^{\Phi_{l-1}}\boldsymbol{\Sigma}_l^{-1}(\mathbf{y} - \mathbf{G}\mathbf{s}^{\Phi_{l-1}}) \\ \mathbf{V}^{\tilde{\Psi}_l} = \sigma_w^2\mathbf{V}^{\Phi_{l-1}}\boldsymbol{\Sigma}_l^{-1} \end{cases}$$

Finally, the marginalization of (C.4) gives:

$$\tilde{\Psi}_l(s_n) \propto \int_{\mathbf{s}_{\sim n}} \mathcal{N}_{\mathrm{C}}(\mathbf{s} : \mathbf{s}^{\tilde{\Psi}_l}, \mathbf{V}^{\tilde{\Psi}_l})\,\mathrm{d}\mathbf{s}_{\sim n} = \mathcal{N}_{\mathrm{C}}(s_n : s_n^{\tilde{\Psi}_l}, v_n^{\tilde{\Psi}_l}) \tag{C.6}$$

where we recall that $\mathbf{V}^{\Phi_{l-1}}$ is a diagonal matrix and the distribution $\tilde{\Psi}_l(s_n)$ is given by:

$$\begin{cases} s_n^{\tilde{\Psi}_l} = \mathbf{e}_n^\dagger\mathbf{s}^{\tilde{\Psi}_l} = s_n^{\Phi_{l-1}} + v_n^{\Phi_{l-1}}\mathbf{f}_{n,l}^\dagger(\mathbf{y} - \mathbf{G}\mathbf{s}^{\Phi_{l-1}}) & \text{(C.7a)} \\ v_n^{\tilde{\Psi}_l} = \mathbf{e}_n^\dagger\mathbf{V}^{\tilde{\Psi}_l}\mathbf{e}_n = v_n^{\Phi_{l-1}}(1 - v_n^{\Phi_{l-1}}\xi_{n,l}) & \text{(C.7b)} \end{cases}$$

where $\mathbf{f}_{n,l} = {\boldsymbol{\Sigma}_l}^{-1}\mathbf{e}_n$ represents the MMSE filter, and $\xi_{n,l} = \mathbf{f}_{n,l}^\dagger\mathbf{G}\mathbf{e}_n$.

Bibliography

[AAND09] Alexandre Graell i Amat, Charbel Abdel Nour, and Catherine Douillard. "Serially concatenated continuous phase modulation for satellite communications". In: *IEEE Transactions on Wireless Communications* 8.6 (2009), pp. 3260–3269. DOI: 10.1109/TWC.2009.081051.

[AMJ14] M. J. Abdoli, Ming Jia, and Jianglei Ma. "Turbo-coded single-carrier faster-than-Nyquist transmission". In: *2014 IEEE 15th International Workshop on Signal Processing Advances in Wireless Communications (SPAWC)*. June 2014, pp. 170–173. DOI: 10.1109/SPAWC.2014.6941377.

[AR06] J. B. Anderson and F. Rusek. "Improving OFDM: Multistream Faster-than-Nyquist Signaling". In: *4th International Symposium on Turbo Codes Related Topics; 6th International ITG-Conference on Source and Channel Coding*. 2006, pp. 1–5.

[AR07] J. B. Anderson and F. Rusek. "Optimal Side Lobes under Linear and Faster-than-Nyquist Modulation". In: *2007 IEEE International Symposium on Information Theory*. June 2007, pp. 2301–2304. DOI: 10.1109/ISIT.2007.4557168.

[ARO13] J. B. Anderson, F. Rusek, and V. Owall. "Faster-Than-Nyquist Signaling". In: *Proceedings of the IEEE* 101.8 (Aug. 2013), pp. 1817–1830. DOI: 10.1109/JPROC.2012.2233451.

[Bah+74] L. Bahl, J. Cocke, F. Jelinek, and J. Raviv. "Optimal decoding of linear codes for minimizing symbol error rate (Corresp.)" In: *IEEE Transactions on Information Theory* 20.2 (Mar. 1974), pp. 284–287. ISSN: 0018-9448. DOI: 10.1109/TIT.1974.1055186.

[Bei+14] B. F. Beidas, R. I. Seshadri, M. Eroz, and L. Lee. "Faster-than-Nyquist Signaling and Optimized Signal Constellation for High Spectral Efficiency Communications in Nonlinear Satellite Systems". In: *2014 IEEE Military Communications Conference*. 2014, pp. 818–823. DOI: 10.1109/MILCOM.2014.142.

[BFC09] A. Barbieri, D. Fertonani, and G. Colavolpe. "Time-frequency packing for linear modulations: spectral efficiency and practical detection schemes". In: *IEEE Transactions on Communications* 57.10 (2009), pp. 2951–2959. DOI: 10.1109/TCOMM.2009.10.080200.

[BGT93] C. Berrou, A. Glavieux, and P. Thitimajshima. "Near Shannon limit error-correcting coding and decoding: Turbo-codes. 1". In: *Proceedings of ICC '93 - IEEE International Conference on Communications*. Vol. 2. 1993, 1064–1070 vol.2.

[Cai+19] Biao Cai, AiJun Liu, Chao Gao, and Xiaohu Liang. "PAPR Reduction of Multicarrier Faster-than-Nyquist Signaling by PTS Based on Tree". In: *Journal of Physics: Conference Series*. Vol. 1345. 4. IOP Publishing. 2019, p. 042009.

[CB05] G. Colavolpe and A. Barbieri. "On MAP symbol detection for ISI channels using the Ungerboeck observation model". In: *IEEE Communications Letters* 9.8 (2005), pp. 720–722. DOI: 10.1109/LCOMM.2005.1496594.

[CF14] Giulio Colavolpe and Tommaso Foggi. "Time-Frequency Packing for High-Capacity Coherent Optical Links". In: *IEEE Transactions on Communications* 62.8 (2014), pp. 2986–2995. DOI: 10.1109/TCOMM.2014.2339321.

[CFP11] G. Colavolpe, D. Fertonani, and A. Piemontese. "SISO Detection Over Linear Channels With Linear Complexity in the Number of Interferers". In: *IEEE Journal of Selected Topics in Signal Processing* 5.8 (2011), pp. 1475–1485. DOI: 10.1109/JSTSP.2011.2168943.

[CFR01] Giulio Colavolpe, Gianluigi Ferrari, and Riccardo Raheli. "Reduced-state BCJR-type algorithms". In: *IEEE J. Sel. Areas Commun.* 19 (2001), pp. 848–859.

[Cha+15] D. Chang, O. Omomukuyo, O. Dobre, R. Venkatesan, and P. Gillard. "A faster-than-Nyquist PDM-16QAM scheme enabled by Tomlinson-Harashima precoding". In: *2015 17th International Conference on Transparent Optical Networks (ICTON)*. July 2015, pp. 1–4. DOI: 10.1109/ICTON.2015.7193359.

[CL91] Cheng-Kun Wang and Lin-Shan Lee. "Practically realizable digital transmission significantly below the Nyquist bandwidth". In: *IEEE Global Telecommunications Conference GLOBECOM '91: Countdown to the New Millennium. Conference Record*. 1991, 1187–1191 vol.2.

[Col11] G. Colavolpe. "Faster-than-Nyquist and beyond: How to improve spectral efficiency by accepting interference Giulio Colavolpe". In: *2011 37th European Conference and Exhibition on Optical Communication*. Sept. 2011, pp. 1–25.

[DMM09] David L Donoho, Arian Maleki, and Andrea Montanari. "Message-passing algorithms for compressed sensing". In: *Proceedings of the National Academy of Sciences* 106.45 (2009), pp. 18914–18919.

[DMO11] D. Dasalukunte, S. Mehmood, and V. Owall. "Complexity analysis of IOTA filter architectures in faster-than-Nyquist multicarrier systems". In: *2011 NORCHIP*. 2011, pp. 1–4. DOI: 10.1109/NORCHP.2011.6126704.

[Dou+95a] Catherine Douillard, Michel Jézéquel, Claude Berrou, Département Electronique, Annie Picart, Pierre Didier, and Alain Glavieux. "Iterative correction of intersymbol interference: Turbo-equalization". In: *European transactions on telecommunications* 6.5 (1995), pp. 507–511.

[Dou+95b] Catherine Douillard, Michel Jézéquel, Claude Berrou, Département Electronique, Annie Picart, Pierre Didier, and Alain Glavieux. "Iterative correction of intersymbol interference: Turbo-equalization". In: *European Transactions on Telecommunications* 6.5 (1995), pp. 507–511. DOI: 10.1002/ett.4460060506. eprint: https://onlinelibrary.wiley.com/doi/pdf/10.1002/ett.4460060506. URL: https://onlinelibrary.wiley.com/doi/abs/10.1002/ett.4460060506.

[ETS] EN ETSI. "302 307-2 Digital Video Broadcasting (DVB)". In: *Second generation framing structure, channel coding and modulation systems for Broadcasting, Interactive Services, News Gathering and other broadband satellite applications* ().

[FA97] V. Franz and J. B. Anderson. "Reduced-search BCJR algorithms". In: *Proceedings of IEEE International Symposium on Information Theory.* June 1997, p. 230. DOI: 10.1109/ISIT.1997.613145.

[FM76] D. Falconer and F. Magee. "Evaluation of Decision Feedback Equalization and Viterbi Algorithm Detection for Voiceband Data Transmission - Part II". In: *IEEE Transactions on Communications* 24.11 (Nov. 1976), pp. 1238–1245. ISSN: 0090-6778. DOI: 10.1109/TCOM.1976.1093243.

[For72] G. Forney. "Maximum-likelihood sequence estimation of digital sequences in the presence of intersymbol interference". In: *IEEE Transactions on Information Theory* 18.3 (1972), pp. 363–378.

[For73] G. D. Forney. "The viterbi algorithm". In: *Proceedings of the IEEE* 61.3 (Mar. 1973), pp. 268–278. DOI: 10.1109/PROC.1973.9030.

[Fra+02] C. Fragouli, N. Al-Dhahir, S. N. Diggavi, and W. Turin. "Prefiltered space-time M-BCJR equalizer for frequency-selective channels". In: *IEEE Transactions on Communications* 50.5 (May 2002), pp. 742–753. ISSN: 0090-6778. DOI: 10.1109/TCOMM.2002.1006556.

[GP93] D. R. Gimlin and C. R. Patisaul. "On minimizing the peak-to-average power ratio for the sum of N sinusoids". In: *IEEE Transactions on Communications* 41.4 (1993), pp. 631–635. DOI: 10.1109/26.223788.

[Guo+19] Mengqi Guo, Yaojun Qiao, Ji Zhou, Xizi Tang, Jia Qi, Shuangyue Liu, Xuekai Xu, and Yueming Lu. "ICI Cancellation Based on MIMO Decoding for FTN Non-Orthogonal FDM Systems". In: *Journal of Lightwave Technology* 37.3 (2019), pp. 1045–1055. DOI: 10.1109/JLT.2018.2885791.

[Had+17] R. Hadani, S. Rakib, M. Tsatsanis, A. Monk, A. J. Goldsmith, A. F. Molisch, and R. Calderbank. "Orthogonal Time Frequency Space Modulation". In: *2017 IEEE Wireless Communications and Networking Conference (WCNC).* 2017, pp. 1–6. DOI: 10.1109/WCNC.2017.7925924.

[Haj90] D. Hajela. "On computing the minimum distance for faster than Nyquist signaling". In: *IEEE Transactions on Information Theory* 36.2 (1990), pp. 289–295.

[Har28] Ralph VL Hartley. "Transmission of information 1". In: *Bell System technical journal* 7.3 (1928), pp. 535–563.

[HH89] J. Hagenauer and P. Hoeher. "A Viterbi algorithm with soft-decision outputs and its applications". In: *1989 IEEE Global Telecommunications Conference and Exhibition 'Communications Technology for the 1990s and Beyond'*. Nov. 1989, 1680–1686 vol.3. DOI: 10.1109/GLOCOM.1989.64230.

[Jan+17] M. Jana, A. Medra, L. Lampe, and J. Mitra. "Pre-Equalized Faster-Than-Nyquist Transmission". In: *IEEE Transactions on Communications* 65.10 (Oct. 2017), pp. 4406–4418. DOI: 10.1109/TCOMM.2017.2704609.

[JLM19] M. Jana, L. Lampe, and J. Mitra. "Precoded Time-Frequency-Packed Multicarrier Faster-than-Nyquist Transmission". In: *2019 IEEE 20th International Workshop on Signal Processing Advances in Wireless Communications (SPAWC)*. 2019, pp. 1–5. DOI: 10.1109/SPAWC.2019.8815431.

[JY04] Jae-Hyok Lee and Yong-Hwan Lee. "Design of multiple MMSE subequalizers for faster-than-Nyquist-rate transmission". In: *IEEE Transactions on Communications* 52.8 (Aug. 2004), pp. 1257–1264. DOI: 10.1109/TCOMM.2004.833009.

[KFL01] F. R. Kschischang, B. J. Frey, and H. . Loeliger. "Factor graphs and the sum-product algorithm". In: *IEEE Transactions on Information Theory* 47.2 (Feb. 2001), pp. 498–519. ISSN: 0018-9448. DOI: 10.1109/18.910572.

[Lah+17] N. Lahbabi, H. Lin, C. A. Nour, C. Douillard, and P. Siohan. "An enhanced coding strategy for FTN-OFDM/OQAM transceiver design". In: *2017 IEEE International Conference on Communications (ICC)*. 2017, pp. 1–6. DOI: 10.1109/ICC.2017.7997300.

[Le+14] C. Le, M. Schellmann, M. Fuhrwerk, and J. Peissig. "On the practical benefits of faster-than-Nyquist signaling". In: *2014 International Conference on Advanced Technologies for Communications (ATC 2014)*. Oct. 2014, pp. 208–213. DOI: 10.1109/ATC.2014.7043385.

[Lee+19] Byungju Lee, Junghyun Kim, Hyojin Lee, Byonghyo Shim, Younsun Kim, and Juho Lee. "Towards Faster-Than-Nyquist Transmission for Beyond 5G Wireless Communications". In: *ICC 2019 - 2019 IEEE International Conference on Communications (ICC)*. 2019, pp. 1–6. DOI: 10.1109/ICC.2019.8762037.

[LG03] A. D. Liveris and C. N. Georghiades. "Exploiting faster-than-Nyquist signaling". In: *IEEE Transactions on Communications* 51.9 (Sept. 2003), pp. 1502–1511. DOI: 10.1109/TCOMM.2003.816943.

[LGL01] C. Laot, A. Glavieux, and J. Labat. "Turbo equalization: adaptive equalization and channel decoding jointly optimized". In: *IEEE Journal on Selected Areas in Communications* 19.9 (2001), pp. 1744–1752. DOI: 10.1109/49.947038.

[Liu+18] AiJun Liu, Siming Peng, Li Song, Xiaohu Liang, KE Wang, and Qingshuang Zhang. "Peak-to-average power ratio of multicarrier faster-than-Nyquist signals: distribution, optimization and reduction". In: *IEEE Access* 6 (2018), pp. 11977–11987.

[LM12] Edward A Lee and David G Messerschmitt. *Digital communication*. Springer Science & Business Media, 2012.

[Luc+16] J. Lucciardi, N. Thomas, M. Boucheret, C. Poulliat, and G. Mesnager. "Trade-off between spectral efficiency increase and PAPR reduction when using FTN signaling: Impact of non linearities". In: *2016 IEEE International Conference on Communications (ICC)*. May 2016, pp. 1–7. DOI: 10.1109/ICC.2016.7510842.

[Ma+20] Y. Ma, F. Tian, N. Wu, B. Li, and X. Ma. "A Low-Complexity Receiver for Multicarrier Faster-Than-Nyquist Signaling Over Frequency Selective Channels". In: *IEEE Communications Letters* 24.1 (2020), pp. 81–85. DOI: 10.1109/LCOMM.2019.2950320.

[Mar17] Alexandre Marquet. "Transmission au delà de la cadence de Nyquist sur canal radiomobile". PhD thesis. Université Grenoble Alpes, 2017.

[Maz75] J. E. Mazo. "Faster-than-Nyquist signaling". In: *The Bell System Technical Journal* 54.8 (Oct. 1975), pp. 1451–1462. ISSN: 0005-8580. DOI: 10.1002/j.1538-7305.1975.tb02043.x.

[Med+17] Yahia Medjahdi, Sylvain Traverso, Robin Gerzaguet, Hmaied Shaiek, Rafik Zayani, David Demmer, Rostom Zakaria, Jean-Baptiste Doré, Mouna Ben Mabrouk, Didier Le Ruyet, et al. "On the road to 5G: Comparative study of physical layer in MTC context". In: *IEEE Access* 5 (2017), pp. 26556–26581.

[Min+05] Tom Minka et al. *Divergence measures and message passing*. Tech. rep. Technical report, Microsoft Research, 2005.

[ML88] J. E. Mazo and H. J. Landau. "On the minimum distance problem for faster-than-Nyquist signaling". In: *IEEE Transactions on Information Theory* 34.6 (1988), pp. 1420–1427.

[MOP94] H. Meyr, M. Oerder, and A. Polydoros. "On sampling rate, analog prefiltering, and sufficient statistics for digital receivers". In: *IEEE Transactions on Communications* 42.12 (1994), pp. 3208–3214. DOI: 10.1109/26.339842.

[MP01] T. Minka and Thomas P. "Expectation Propagation for Approximate Bayesian Inference". In: *Proceedings of the Seventeenth Conference on Uncertainty in Artificial Intelligence*. UAI'01. Morgan Kaufmann Publishers Inc., 2001, pp. 362–369. ISBN: 1-55860-800-1. URL: http://dl.acm.org/citation.cfm?id=2074022.2074067.

[MRC13] Andrea Modenini, Fredrik Rusek, and Giulio Colavolpe. "Optimal Transmit Filters for ISI Channels under Channel Shortening Detection". In: *IEEE Transactions on Communications* 61.12 (2013), pp. 4997–5005. DOI: 10.1109/TCOMM.2013.110813.130385.

[Nyq24] Harry Nyquist. "Certain factors affecting telegraph speed". In: *Transactions of the American Institute of Electrical Engineers* 43 (1924), pp. 412–422.

[Nyq28] H. Nyquist. "Certain Topics in Telegraph Transmission Theory". In: *Transactions of the American Institute of Electrical Engineers* 47.2 (1928), pp. 617–644.

[PA12] Adnan Prlja and John B Anderson. "Reduced-complexity receivers for strongly narrowband intersymbol interference introduced by faster-than-Nyquist signaling". In: *IEEE Transactions on Communications* 60.9 (2012), pp. 2591–2601.

[PAR08] A. Prlja, J. B. Anderson, and F. Rusek. "Receivers for Faster-than-Nyquist signaling with and without turbo equalization". In: *2008 IEEE International Symposium on Information Theory*. July 2008, pp. 464–468. DOI: 10.1109/ISIT.2008.4595029.

[PC95] B. Picinbono and P. Chevalier. "Widely linear estimation with complex data". In: *IEEE Transactions on Signal Processing* 43.8 (Aug. 1995), pp. 2030–2033. DOI: 10.1109/78.403373.

[Pen+17] S. Peng, A. Liu, H. Fang, K. Wang, and X. Liang. "Turbo Frequency Domain Equalization and Detection for Multicarrier Faster-Than-Nyquist Signaling". In: *2017 IEEE Wireless Communications and Networking Conference (WCNC)*. 2017, pp. 1–6. DOI: 10.1109/WCNC.2017.7925577.

[Pen+18] S. Peng, A. Liu, X. Liu, K. Wang, and X. Liang. "MMSE Turbo Equalization and Detection for Multicarrier Faster-Than-Nyquist Signaling". In: *IEEE Transactions on Vehicular Technology* 67.3 (2018), pp. 2267–2275. DOI: 10.1109/TVT.2017.2767035.

[Pie+13] A. Piemontese, A. Modenini, G. Colavolpe, and N. S. Alagha. "Improving the Spectral Efficiency of Nonlinear Satellite Systems through Time-Frequency Packing and Advanced Receiver Processing". In: *IEEE Transactions on Communications* 61.8 (2013), pp. 3404–3412. DOI: 10.1109/TCOMM.2013.070213.130064.

[Pie+13] Amina Piemontese, Andrea Modenini, Giulio Colavolpe, and Nader S Alagha. "Improving the spectral efficiency of nonlinear satellite systems through time-frequency packing and advanced receiver processing". In: *IEEE Transactions on Communications* 61.8 (2013), pp. 3404–3412.

[Pro01] J.G. Proakis. *Digital Communications*. McGraw-Hill series in electrical and computer engineering : communications and signal processing. McGraw-Hill, 2001. ISBN: 9780071181839. URL: https://books.google.fr/books?id=aUp2QgAACAAJ.

[RA07] F. Rusek and J. B. Anderson. "Maximal Capacity Partial Response Signaling". In: *2007 IEEE International Conference on Communications*. 2007, pp. 821–826. DOI: 10.1109/ICC.2007.140.

[RA09a] F. Rusek and J. B. Anderson. "Constrained Capacities for Faster-Than-Nyquist Signaling". In: *IEEE Transactions on Information Theory* 55.2 (Feb. 2009), pp. 764–775. ISSN: 0018-9448. DOI: 10.1109/TIT.2008.2009832.

[RA09b] F. Rusek and J. B. Anderson. "Multistream Faster than Nyquist Signaling". In: *IEEE Transactions on Communications* 57.5 (2009), pp. 1329–1340. DOI: 10.1109/TCOMM.2009.05.070224.

[Rap91] Christoph Rapp. "Effects of HPA-nonlinearity on a 4-DPSK/OFDM-signal for a digital sound broadcasting signal". In: *ESASP* 332 (1991), pp. 179–184.

[RCS15] Fredrik Rusek, Giulio Colavolpe, and Carl Erik W Sundberg. "40 years with the Ungerboeck model: A look at its potentialities [lecture notes]". In: *IEEE Signal Processing Magazine* 32.3 (2015), pp. 156–161.

[RLP07] F. Rusek, M. Loncar, and A. Prlja. "A Comparison of Ungerboeck and Forney Models for Reduced-Complexity ISI Equalization". In: *IEEE GLOBECOM 2007 - IEEE Global Telecommunications Conference*. Nov. 2007, pp. 1431–1436. DOI: 10.1109/GLOCOM.2007.275.

[RP12] Fredrik Rusek and Adnan Prlja. "Optimal Channel Shortening for MIMO and ISI Channels". In: *IEEE Transactions on Wireless Communications* 11.2 (2012), pp. 810–818. DOI: 10.1109/TWC.2011.121911.110809.

[RSF19] S. Rangan, P. Schniter, and A. K. Fletcher. "Vector Approximate Message Passing". In: *IEEE Transactions on Information Theory* 65.10 (2019), pp. 6664–6684. DOI: 10.1109/TIT.2019.2916359.

[Rus07] Fredrik Rusek. *Partial response and faster-than-Nyquist signaling*. Lund University, 2007.

[SA11] M. Senst and G. Ascheid. "How the Framework of Expectation Propagation Yields an Iterative IC-LMMSE MIMO Receiver". In: *2011 IEEE Global Telecommunications Conference - GLOBECOM 2011*. Dec. 2011, pp. 1–6. DOI: 10.1109/GLOCOM.2011.6133608.

[Sal73] J. Salz. "Optimum mean-square decision feedback equalization". In: *The Bell System Technical Journal* 52.8 (Oct. 1973), pp. 1341–1373. DOI: 10.1002/j.1538-7305.1973.tb02023.x.

[San+17] I. Santos, J. J. Murillo-Fuentes, R. Boloix-Tortosa, E. Arias-de-Reyna, and P. M. Olmos. "Expectation Propagation as Turbo Equalizer in ISI Channels". In: *IEEE Transactions on Communications* 65.1 (2017), pp. 360–370. DOI: 10.1109/TCOMM.2016.2616141.

[San+18] I. Santos, J. J. Murillo-Fuentes, E. Arias de Reyna, and P. M. Olmos. "Turbo EP-Based Equalization: A Filter-Type Implementation". In: *IEEE Transactions on Communications* 66.9 (Sept. 2018), pp. 4259–4270. ISSN: 0090-6778. DOI: 10.1109/TCOMM.2018.2832202.

[SC05] M. Sikora and D. J. Costello. "A new SISO algorithm with application to turbo equalization". In: *Proceedings. International Symposium on Information Theory, 2005. ISIT 2005.* 2005, pp. 2031–2035.

[Sec+15] M. Secondini, T. Foggi, F. Fresi, G. Meloni, F. Cavaliere, G. Colavolpe, E. Forestieri, L. Potí, R. Sabella, and G. Prati. "Optical Time–Frequency Packing: Principles, Design, Implementation, and Experimental Demonstration". In: *Journal of Lightwave Technology* 33.17 (2015), pp. 3558–3570. DOI: 10.1109/JLT.2015.2443876.

[Sha48] Claude E Shannon. "A mathematical theory of communication". In: *The Bell system technical journal* 27.3 (1948), pp. 379–423.

[SIN17] S. Sugiura, T. Ishihara, and M. Nakao. “State-of-the-Art Design of Index Modulation in the Space, Time, and Frequency Domains: Benefits and Fundamental Limitations”. In: *IEEE Access* 5 (2017), pp. 21774–21790. DOI: 10.1109/ACCESS.2017.2763978.

[SL96] Shlomo Shamai and Rajiv Laroia. “The intersymbol interference channel: Lower bounds on capacity and channel precoding loss”. In: *IEEE Transactions on Information Theory* 42.5 (1996), pp. 1388–1404.

[SMFO15] I. Santos, J. J. Murillo-Fuentes, and P. M. Olmos. “Block expectation propagation equalization for ISI channels”. In: *2015 23rd European Signal Processing Conference (EUSIPCO)*. Aug. 2015, pp. 379–383. DOI: 10.1109/EUSIPCO.2015.7362409.

[Sug13] S. Sugiura. “Frequency-Domain Equalization of Faster-than-Nyquist Signaling”. In: *IEEE Wireless Communications Letters* 2.5 (Oct. 2013), pp. 555–558. ISSN: 2162-2337. DOI: 10.1109/WCL.2013.072313.130408.

[TBH02] M. Tüchler, S. Ten Brink, and J. Hagenauer. “Measures for Tracing Convergence of Iterative Decoding Algorithms”. In: *in Proc. 4th IEEE/ITG Conf. on Source and Channel Coding*. 2002, pp. 53–60.

[Tia+18] F. Tian, Y. Feng, Y. Ma, and N. Wu. “Gaussian Message Passing based Receiver for Multicarrier Faster-Than-Nyquist Signaling”. In: *2018 10th International Conference on Wireless Communications and Signal Processing (WCSP)*. 2018, pp. 1–6. DOI: 10.1109/WCSP.2018.8555919.

[TKS02] Michael Tuchler, Ralf Koetter, and Andrew C Singer. “Turbo equalization: principles and new results”. In: *IEEE transactions on communications* 50.5 (2002), pp. 754–767.

[TPB16] R. Tajan, C. Poulliat, and M. Boucheret. “Circular Faster Than Nyquist: Transmitter and iterative receiver design”. In: *2016 9th International Symposium on Turbo Codes and Iterative Information Processing (ISTC)*. Sept. 2016, pp. 241–245. DOI: 10.1109/ISTC.2016.7593113.

[Tra16] S. Traverso. “A Family of Square-Root Nyquist Filter With Low Group Delay and High Stopband Attenuation”. In: *IEEE Communications Letters* 20.6 (2016), pp. 1136–1139.

[TS11] M. Tüchler and A. C. Singer. “Turbo Equalization: An Overview”. In: *IEEE Transactions on Information Theory* 57.2 (2011), pp. 920–952.

[TSK02] M. Tuchler, A. C. Singer, and R. Koetter. “Minimum mean squared error equalization using a priori information”. In: *IEEE Transactions on Signal Processing* 50.3 (Mar. 2002), pp. 673–683. ISSN: 1053-587X. DOI: 10.1109/78.984761.

[Tuf68] D. W. Tufts. “On "Sampling, data transmission, and the Nyquist rate" and adaptive communication using randomly time-varying channels”. In: *Proceedings of the IEEE* 56.5 (May 1968), pp. 889–889. DOI: 10.1109/PROC.1968.6437.

[Ung74] Gottfried Ungerboeck. "Adaptive maximum-likelihood receiver for carrier-modulated data-transmission systems". In: *IEEE Transactions on Communications* 22.5 (1974), pp. 624–636.

[Vit67a] A. Viterbi. "Error bounds for convolutional codes and an asymptotically optimum decoding algorithm". In: *IEEE Transactions on Information Theory* 13.2 (Apr. 1967), pp. 260–269. DOI: 10.1109/TIT.1967.1054010.

[Vit67b] A. Viterbi. "Error bounds for convolutional codes and an asymptotically optimum decoding algorithm". In: *IEEE Transactions on Information Theory* 13.2 (1967), pp. 260–269.

[Wan+17] H. Wang, A. Liu, X. Liang, S. Peng, and K. Wang. "Linear precoding for Faster-than-Nyquist signaling". In: *2017 3rd IEEE International Conference on Computer and Communications (ICCC)*. Dec. 2017, pp. 52–56. DOI: 10.1109/CompComm.2017.8322513.

[Wen+19] Shan Wen, Guanghui Liu, Qiang Chen, Huiyang Qu, Yanyan Wang, and Pan Zhou. "Optimization of Precoded FTN Signaling with MMSE-Based Turbo Equalization". In: *ICC 2019 - 2019 IEEE International Conference on Communications (ICC)*. 2019, pp. 1–6. DOI: 10.1109/ICC.2019.8761120.

[Wu+17] N. Wu, W. Yuan, Q. Guo, and J. Kuang. "A Hybrid BP-EP-VMP Approach to Joint Channel Estimation and Decoding for FTN Signaling over Frequency Selective Fading Channels". In: *IEEE Access* 5 (2017), pp. 6849–6858. DOI: 10.1109/ACCESS.2017.2702571.

[XCW09] P. Xiao, R. A. Carrasco, and I. J. Wassell. "Generalized Equalization Algorithm Utilizing Improper ISI". In: *IEEE Transactions on Vehicular Technology* 58.2 (Feb. 2009), pp. 788–799. DOI: 10.1109/TVT.2008.927727.

[Yu+14] J. Yu, J. Park, F. Rusek, B. Kudryashov, and I. Bocharova. "High Order Modulation in Faster-Than-Nyquist Signaling Communication Systems". In: *2014 IEEE 80th Vehicular Technology Conference (VTC2014-Fall)*. Sept. 2014, pp. 1–5. DOI: 10.1109/VTCFall.2014.6965997.

[Şa+18] S. Şahin, A. M. Cipriano, C. Poulliat, and M. Boucheret. "Iterative Equalization With Decision Feedback Based on Expectation Propagation". In: *IEEE Transactions on Communications* 66.10 (Oct. 2018), pp. 4473–4487. ISSN: 0090-6778. DOI: 10.1109/TCOMM.2018.2843760.